Regulation of dynamic front-rear cell polarity by the Frz chemosensory system in *Myxococcus xanthus*

Dissertation

zur Erlangung des akademischen Grades

des Doktors der Naturwissenschaften

(Dr. rer. nat.)

dem Fachbereich Biologie

der Philipps-Universität Marburg

Vorgelegt von

Franziska Müller

Aus Marburg (Wehrda)

Marburg an der Lahn, 2023

Die vorliegende Dissertation wurde von Oktober 2019 bis Oktober 2023 am Max-Planck-Institut für terrestrische Mikrobiologie unter der Leitung von Prof. Dr. Lotte Søgaard-Andersen angefertigt.

Vom Fachbereich Biologie der Philipps-Universität Marburg (Hochschulkennziffer 1180) als Dissertation angenommen am:

27.10.2023

Erstgutachter(in): Prof. Dr. Lotte Søgaard-Andersen

Zweitgutachter(in): Prof. Dr. Martin Thanbichler

Weitere Mitglieder der Prüfungskommission:

Prof. Dr. Victor Sourjik

Prof. Dr. Hans-Ulrich Mösch

Tag der Disputation: 12.02.2024

Die während der Promotion erzielten Ergebnisse wurden zum Teil in folgenden Originalpublikationen veröffentlicht:

A miniTurbo-based proximity labeling protocol to identify conditional protein interactomes *in vivo* in *Myxococcus xanthus*
Herfurth M., **Müller F.**, Søgaard-Andersen L., Glatter T.
STAR Protocols 2023, https://doi.org/10.1016/j.xpro.2023.102657 (accepted)

Let the sunshine in.

Table of Contents

Abbreviations

aa	amino acid
ABC	ammonium bicarbonate
ATP	adenosine triphosphate
BPS	biosurfactant polysaccharide
c-di-GMP	cyclic dimeric guanosine monophosphate
DMSO	dimethyl sulphoxide
DNA	desoxyribonucleic acid
EDTA	ethylenediaminetetraacetic acid
EPS	exopolysaccharide
FHA	forkhead-associated
GAP	GTPase-activating protein
GDP	guanosine diphosphate
GEF	Guanine nucleotide exchange factor
GOF	gain of function
GTP	guanosine triphosphate
GYF	glycine-tyrosine-phenylalanine
HPS	hormogonium polysaccharide
IAA	isoamyl alcohol
IM	inner membrane
LC-MS	liquid chromatography-mass spectrometry
LFQ	label-free quantification
LOF	loss of function
LPS	lipopolysaccharide
MCP	methyl-accepting chemotaxis protein
OM	outer membrane
ON	over night
P	phosphate
PMF	proton motive force
RR	response regulator
SDC	sodium deoxycholate
SDS	sodium dodecyl sulfate
sfGFP	duperfolder GFP
T4P	type IVa pili
TCEP	tris-(2-carboxyethyl)-phosphine hydrochloride

TFA	trifluoroacetic acid
TM	transmembrane
TPR	tetratricopeptide repeat
tRNA	transfer ribonucleic acid
WT	wildtype

Abstract

Bacterial cells are spatiotemporally highly organized, with proteins localizing to distinct subcellular regions. The rod-shaped *Myxococcus xanthus* cells move across surfaces with defined front-rear polarity. This polarity is determined by the small Ras-like GTPase MglA that localizes to the leading cell pole in its GTP-bound form. The nucleotide-bound form of MglA and its localization are regulated by the remaining five proteins of the polarity module. All six proteins of the polarity module localize asymmetrically to the cell poles. Occasionally, cells invert polarity and, in parallel, reverse their direction of movement. The Frz chemosensory system triggers the inversion of cell polarity and, therefore, cellular reversals. The two output response regulators of the Frz system, FrzX and FrzZ, localize to the lagging and leading cell poles, respectively, in their phosphorylated form, targeting the proteins of the polarity module and, thereby jointly causing an inversion of the polarity of these proteins. However, the molecular mechanism that bridges FrzX and FrzZ and the proteins of the polarity module are poorly understood.

Here, we addressed this question, focusing on FrzZ. Using a biotin-based proximity labeling approach, we identify PixA as a strong candidate for directly interacting with phosphorylated FrzZ. Epistasis analyses support that FrzZ and PixA regulate reversals in the same output branch of the Frz system, and PixA inhibits reversals. In this branch, FrzZ~P induces reversals by inhibiting PixA, thereby relieving the PixA-mediated inhibition of reversals. PixA localized weakly at the lagging pole between reversals. Strikingly, Frz signaling altered PixA localization to the pole. Genetic analyses suggest that FrzZ inhibits lagging pole localization of PixA. During Frz signaling, FrzZ~P “pulls” PixA to the leading pole, while FrzX~P “pushes off” PixA at the lagging pole. Elevated levels of PixA resulted in increased lagging pole localization of PixA and strong reduction of reversals. Altogether, our findings support a model in which PixA inhibits reversals at the lagging cell pole while FrzX~P and FrzZ~P, in a “push and pull” mechanism, relocate PixA from the lagging to the leading pole, thereby allowing a reversal to occur.

In proximity labelling approaches, we identified the response regulator PglH as a potential interaction partner of PixA, FrzX, and MglA. A Δ*pglH* mutant had a hyper-reversing phenotype, suggesting that PglH is a strong candidate for also being involved in regulating leading-lagging cell polarity in *M. xanthus.*

Zusammenfassung

Bakterienzellen sind räumlich und zeitlich hoch organisiert. Dabei lokalisieren Proteine in bestimmten subzellulären Regionen. Das stäbchenförmige Bakterium *Myxococcus xanthus* bewegt sich auf Oberflächen mit definierter Vorder-Rück-Polarität. Diese Polarität wird durch die Ras-ähnliche GTPase MglA bestimmt, welche in ihrer GTP-gebundenen Form zum vorderen Zellpol lokalisiert. Die Nukleotid-gebundene Form von MglA und deren Lokalisation werden von insgesamt fünf weiteren Proteinen des Polaritätsmoduls reguliert. Diese insgesamt sechs Proteine lokalisieren asymmetrisch an den Zellpolen. Gelegentlich invertieren Zellen ihre Polarität, um ihre Bewegungsrichtung zu ändern. Diese Umpolung der Zellpolarität wird durch das Frz-Chemosensory-System ausgelöst. Die beiden Output-Regulatoren FrzX und FrzZ lokalisieren, wenn sie phosphoryliert sind, an dem hinteren oder vorderen Zellpol, wo sie die Proteine des Polaritätsmoduls anvisieren, um deren Polariät zu invertieren. Allerdings sind die molekularen Mechanismen, die FrzX und FrzZ mit den Proteinen des Polaritätsmoduls verknüpfen, immer noch unzureichend verstanden. In der vorliegenden Studie wird diese Fragestellung mit einem Fokus auf FrzZ untersucht.

Mit Hilfe einer biotinbasierten Proximity-Labelling Methode, konnten wir PixA als einen vielversprechenden Kandidaten für eine direkte Interaktion mit phosphoryliertem FrzZ identifizieren. Epistase-Experimente unterstützen die Hypothese, dass FrzZ und PixA im selben Pfad des Frz Systems agieren, um Zellumkehrungen zu regulieren, wobei PixA diese hemmt. In diesem Pfad induziert FrzZ~P Zellumkehrungen, indem es PixA hemmt und dadurch die von PixA vermittelte Hemmung von Zellumkehrungen aufhebt. In Zellen, die sich in eine Richtung fortbewegen, lokalisiert PixA instabil am hinteren Zellpol. Bemerkenswerterweise ändern Signale des Frz-Systems diese Lokalisation. Genetische Analysen untermauern, dass FrzZ PixA Lokalisation am hinteren Pol hemmt. Während der Frz Signalweiterleitung „zieht“ FrzZ~P PixA zum vorderen Pol. Gleichzeitig „schiebt“ FrzZ~P PixA weg vom hinteren Pol. Erhöhte Mengen von PixA führen zu vermehrter Lokalisation von PixA am hinteren Zellpol und einer starken Reduzierung von Zellumkehrungen. Insgesamt unterstützen unsere Ergebnisse ein Modell, bei dem PixA Zellumkehrungen am hinteren Zellpol hemmt, während FrzZ~P und FrzX~P in einem „Push and Pull“ Mechanismus PixA vom hinteren zum vorderen Zellpol relokalisieren und so Zellumkehrungen ermöglichen.

In Proximity-Labelling Experimenten, konnte der Response Regulator PglH als potenzieller Interaktionspartner von PixA, FrzX und MglA identifiziert werden. Eine Δ*pglH* Mutante, zeigte einen hyper-zellumkehrenden Phänotyp. Dies weist darauf hin, dass PglH ein vielversprechender Kandidat ist, welcher ebenfalls an der Regulation der Vorder-Rück-Polarität in *M. xanthus* beteiligt sein könnte.

1 Introduction

In the realm of life, bacteria are considered relatively simple organisms. However, they can perform a multitude of complex actions. They can detect and move toward nutrients. They differentiate into different cell types depending on their environment. And they can work together to act as one entity. But how can these complex behaviors arise?

In the past 30 years, our understanding of bacteria fundamentally changed as new methods enabled the investigation of their intracellular processes. One of the key findings emerging from this work is that bacterial cells are spatially highly organized, with proteins localizing to specific regions within the cell. This asymmetric localization of proteins is referred to as cell polarity and plays a vital role in critical processes such as cell division, organelle localization, and motility (Treuner-Lange & Søgaard-Andersen, 2014). Generally, cell polarity is highly regulated in space and time. Changes in cell polarity can occur in a cell cycle-dependent manner as well as in response to external cues. The response to external cues requires coordinated rearrangements of cellular processes and is implemented by sensing external stimuli and translating them into a cellular response using signal transduction networks. To understand how bacteria can deploy intricate behaviors, we must understand how cell polarity is regulated.

1.1 Cell polarity and motility

Cell polarity is crucial for many processes in eukaryotes and bacteria, including cell migration. This introduction will focus on polarizing motility systems. Bacteria can harbor various motility systems to move on surfaces or swim in liquids. These systems include flagella, Type IVa pili (T4P), and gliding motility. For all these systems, polarity plays a crucial role since the correct positioning of motility systems within the cell and their spatiotemporal activity must be correct to ensure optimal locomotion.

1.1.1 Flagella

Flagellar motility is the best-studied mode of movement in bacteria and is used for swimming in liquids or swarming on surfaces. It depends on the flagellar supracomplex consisting of the filament, the basal body, and the flagellar hook, which connects the filament with the basal body (Figure 1 A). The filament rotates, powered by the flagellar motor that is part of the basal body, leading to the motion of the bacterium. Most flagella can rotate in a clockwise or counterclockwise direction, and switches in rotation are often induced via chemosensory

systems to ensure the directed movement of cells (Thormann *et al.*, 2022). Chemosensory systems controlling flagellar motility are described in 1.2.1.1. Their number can range from one flagellum to several hundred, depending on the organism, and their localization can be restricted to the cell pole(s) or found along the entire cell body. Flagellar patterns include monotrichious with one single flagellum (*Caulobacter*, *Vibrio*), amphitrichious with one flagellum at each pole (*Campylobacter*), lophotrichious with multiple flagella at one pole (*Helicobacter*), and peritrichous with flagella evenly distributed over the entire surface of the cell (*Escherichia coli*, *Bacillus subtilis*) (Figure 1 B).

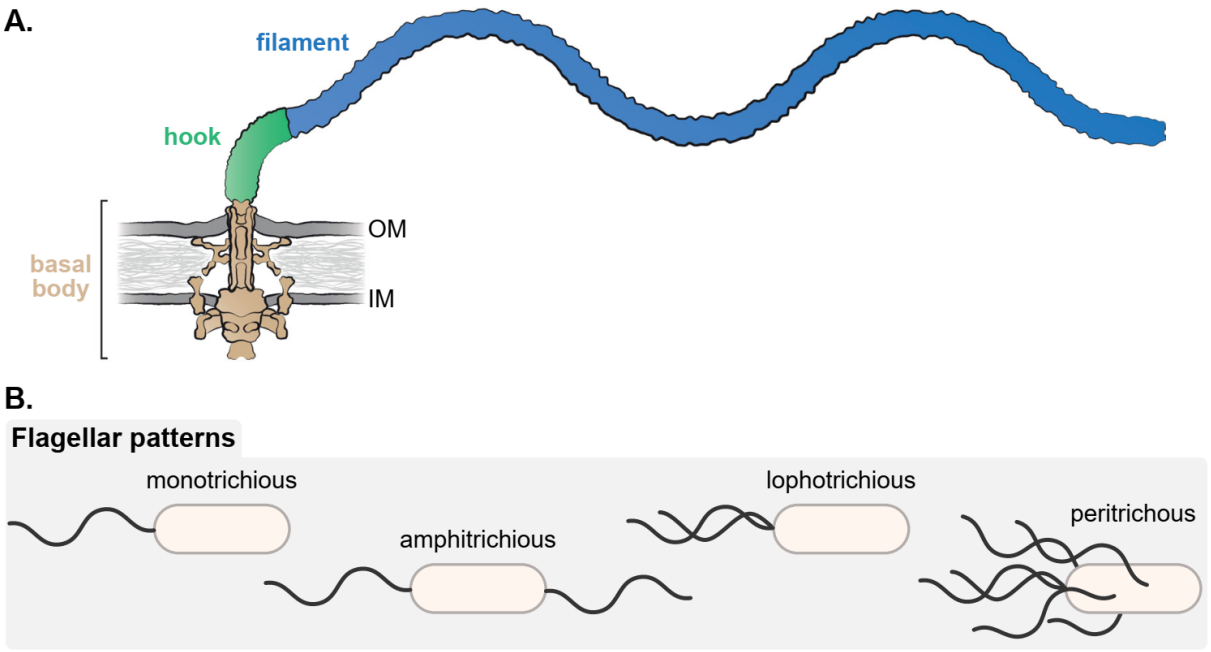

Figure 1: **Composition and localization of bacterial flagella.** (A) Schematic of the bacterial flagellum consisting of three parts: the filament (blue), the hook (green) and the basal body (brown). Figure modified from Thormann *et al.*, 2022. (B) Simplified depiction of flagella localization. Flagella are shown as thick black lines.

Bacteria such as *E. coli* have a peritrichous flagellation pattern (Smith, 1954). Despite extensive studies of peritrichous flagellated organisms, it is still not understood how correct flagella number and precise position are established. However, it is suspected that the flagellation pattern arises through a stochastic nucleation pattern (random), which depends on the localization of the ancestor cell flagellar systems (Schuhmacher *et al.*, 2015).

The GTPase FlhF and the ParA/MinD-like ATPase FlhG are needed for corrected flagella number and positioning, respectively, in several species. Their action can regulate different flagellar patterns like monotrichious flagellation in, e.g., *Vibrio cholerae* or *Pseudomonas aeruginosa*, the amphitrichious pattern in *Campylobacter jejuni*, lophotrichious flagella in

Helicobacter pylori, and peritrichous flagella in, e.g., *B. subtilis* (Kazmierczak & Hendrixson, 2013). The exact mechanism of the FlhFG system is not fully understood. A working hypothesis describes FlhF as targeting a polar determinant (a landmark protein or potentially lipid composition within the cell) and bringing the first building block to the future flagellum site, thereby serving as a positive regulator for flagellar synthesis. FlhG arrives at the basal body of the flagellum last and concludes its assembly. FlhG then assists the association of the flagellar motor switch proteins FliM/FliN, which control the direction of flagella rotation, with the basal body. FlhG is suggested to act as a negative regulator that controls flagella number since lack of FlhG leads to hyper-flagellation (Schuhmacher *et al.*, 2015). In addition, FlhF and FlhG have been suggested to interact with each other in some systems. The exact mechanism of how this system works is not understood. The polar target of FlhF and FlhG and, by this, the structure setting up polarity in the forementioned organisms is mostly unknown. However, it is known that the polar landmark protein HubP organizes cell polarity in *V. cholerae*. In addition to its interaction with FlhG, it positions other cellular components. First, HubP interacts with the ParA1 ATPase involved in the segregation of chromosome 1 (Yamaichi *et al.*, 2012). Furthermore, it anchors the ParA/MinD-like ATPase ParC to the cell pole, positioning chemotaxis arrays (Yamaichi *et al.*, 2012).

C. crescentus cells are highly asymmetric. During cell division, the cell differentiates into a “stalked” cell, with a stalk at the old pole that attaches the cell to a surface and into a “swarmer” cell possessing a single flagellum. In the “swarmer” cell, the landmark protein TipN positions the flagellum (Lam *et al.*, 2006, Huitema *et al.*, 2006). TipN localizes to the division plane and remains there after division, providing a molecular marker defining the new cell pole of a cell and, by this, the location for the flagellum to be formed during the subsequent cell division (Huitema *et al.*, 2006). During cell differentiation, the second messenger cyclic dimeric guanosine monophosphate (c-di-GMP) establishes cell polarity with the stalked cell having higher levels of c-di-GMP and the swarmer cell having lower levels of c-di-GMP (Christen *et al.*, 2010). Upon cell differentiation of the “stalked” cell, TipN recruits the flagellum assembly regulator TipF (Huitema *et al.*, 2006). TipF is a receptor of the second messenger c-di-GMP, and is stabilized when bound to c-di-GMP. When the c-di-GMP level rises upon differentiation, TipF accumulates and initiates flagellar assembly (Davis *et al.*, 2013). For this, it recruits PflI, which facilitates flagellar placement, and FliF and FliG, which are part of the flagellar base (Davis *et al.*, 2013).

1.1.2 Type IVa pili

Type IV pili are thin appendages that function in motility, DNA uptake, adhesion and microcolony formation. Bacteria can move on surfaces using T4P via cycles of extension, attachment to the surface, and retraction (Merz *et al.*, 2000). They are polymers of major pilin subunits. In order to extend and retract, the major pilin subunits are rapidly polymerized and depolymerized, respectively, which is powered by the T4P machinery. The T4P machinery consists of several interconnected ring-like structures that span the cell envelope. It harbors an outer membrane (OM) secretin surrounded by secretin-associated proteins. This OM pore complex is connected to an alignment complex that reaches from the periplasm to the cytoplasm. An inner membrane (IM) platform protein facilitates the incorporation of major pilin subunits into the T4P. ATPases bind to the machinery's cytoplasmic components and power the pilus's extension and retraction. T4P can also harbor minor pilins, which are suggested as a priming complex for pilus assembly and forming a tip complex (Figure 2 A) (Craig *et al.*, 2019). T4P, similar to flagella, can exhibit various localization patterns. The machinery can be present at both poles while pili are active at both poles, as in *Thermosynechochoccus vulcanus,* or only active at one pole at a time, such as in *P. aeruginosa* or *M. xanthus*. Additionally, T4P can form at the lateral axis of the cell (*Acinetobacter baylyi*) or along the entire cell body but are only asymmetrically active (*Synechocystis*) (Figure 2 B).

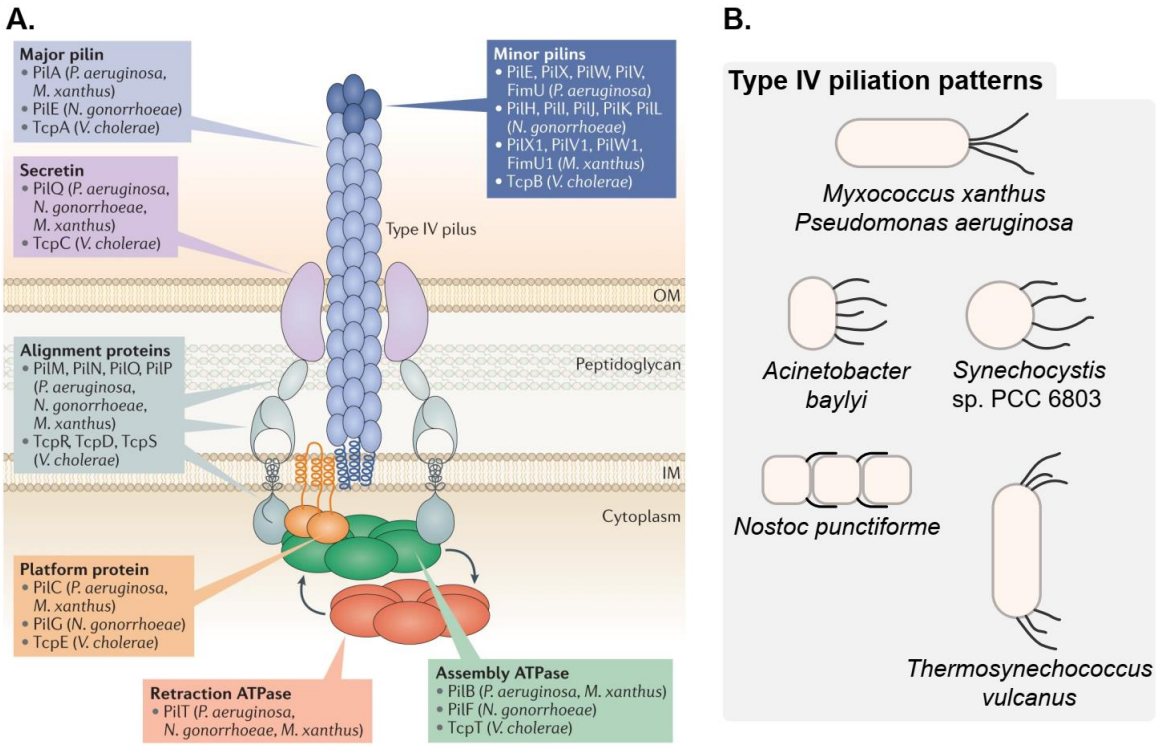

Figure 2: **Composition and localization of T4P.** (A) Schematic of the T4P machinery. Figure from Craig *et al*., 2019. (B) Simplified depiction of T4P localization. Top view of cells moving on a surface from left to right. T4P are shown as thin black lines.

The mechanisms of how T4P machineries are placed have been studied in a few organisms. In *M. xanthus*, the T4P machinery is assembled outside-in*,* with OM secretin PilQ being the first component of machinery assembly (Friedrich *et al.*, 2014). Recently, it was suggested that PilQ might bind to septal and polar peptidoglycan and then recruits the protein Tgl, which stimulates the multimerization of PilQ. This leads to the assembly of new T4P machines at the nascent and new cell poles, ultimately leading to the known bipolar localization of the machineries (Herfurth *et al.*, 2023b). In *P. aeruginosa*, the key components of the T4P machine are recruited to the future cell division site in nascent cells, leading to daughter cells inheriting T4P machineries at both poles. The localization of T4P machineries depends on PilQ and the IM protein FimV and their ability to bind peptidoglycan (Wehbi *et al.*, 2011, Carter *et al.*, 2017). Additionally, PilQ localization to midcell depends on the presence of FimV, suggesting that FimV acts as a polar landmark protein (Carter *et al.*, 2017). In *A. baylyi*, the T4P machinery localizes in a line along the long cell axis. In this organism, the protein FimV (a homolog of the *P. aeruginosa* FimV) is the localization determinant of the T4P machineries. However, it is still unclear how FimV localizes to the lateral axis and how the dynamics of T4P are regulated (Ellison *et al.*, 2022).

In addition to machinery placement, the activity of T4P is spatiotemporally regulated. In *M. xanthus,* the extension and retraction ATPases PilB and PilT, drive the extension and retraction of the pilus powered by ATP hydrolysis. Two polarity systems determine their localization. One consists of the bactofilin BacP and the GTPase SofG, and one called the polarity module, which ultimately lead to T4P being active at the leading cell pole. T4P motility and the polarity modules of *M. xanthus* are described in detail in 1.3. Similarly, the dynamic activity of the T4P machineries is controlled by the extension ATPase PilB and the retraction ATPase PilT in *P. aeruginosa* (Burrows, 2012). However, *P. aeruginosa* harbors a second retraction ATPase, PilU, whose function is PilT-dependent (Adams *et al.*, 2019). In this organism, the c-di-GMP-binding protein FimX and PilB positively depend on each other regarding their localization, and the presence of FimX increased PilB-dependent T4P assembly by a yet unknown mechanism (Jain *et al.*, 2017). The Chp chemosensory system enables dynamic polarization of T4P in *P. aeruginosa* (described in 1.2.1.2). Chemosensory systems are regulating T4P activity in other organisms, too. In the spherical cyanobacterium *Synechocystis*, T4P machines are distributed throughout the whole cell body (Bhaya *et al.*, 2000). T4P are spatially regulated via phototaxis by a chemosensory system, which activates T4P in order for cells to move. *Nostoc punctiforme* T4P machineries are arranged in bipolar rings in each cell of the filamentous cyanobacterium. The ATPases PilB and PilT are localized

statically at each cell pole, but pili form only at the leading pole of each cell (Khayatan *et al.*, 2015). It is suggested that the SMC (Structural Maintenance of Chromosomes) protein HmpF, which is part of the Hmp chemosensory system, activates PilB at the leading cell pole to achieve polar activation of the motility machines (Cho *et al.*, 2017). In *T. vulcanus,* pili are localized at both poles of a laterally moving cell. In this organism, T4P are asymmetrically activated on one side of the rod depending on positive (movement towards green light) and negative (movement away from additional blue light) phototaxis. It was suggested that regulation of this short-axis cell polarity involved light-dependent changes in the cellular concentration of c-di-GMP (Nakane *et al.*, 2022). The studied chemosensory systems regulating T4P are described in detail in 1.2.1.2.

1.1.3 Gliding

Organisms do not always rely on external appendages to move but can move independently on hard surfaces via gliding motility. Polarized gliding mechanisms have been described for *M. xanthus* and mycoplasma species (Figure 3).

Gliding motility of *M. xanthus* is based on Agl-Glt motor complexes, which form at the leading cell pole and become fixed to the substratum as focal adhesion complexes, which propel the forward movement of the cell. The small Ras-like GTPase MglA defines the leading cell pole by interacting with effectors of the gliding machinery and being an integral part of them. Gliding motility function and regulation are discussed in 1.3.1.1 and 1.3.2.

Mycoplasma pneumonia, *Mycoplasma mobile,* and other polarized mycoplasma species form attachment organelles at one pole (usually the leading cell pole) required for attachment to host cells and gliding motility (Balish, 2006). These organelles contain a cytoskeletal structure and adhesins, by which the cell moves, that are concentrated at this terminal organelle (Balish, 2006, Biberfeld & Biberfeld, 1970, Nakane & Miyata, 2007). The cues that localize the attachment organelle assembly are not understood.

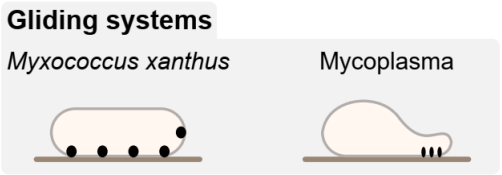

Figure 3: **Gliding systems.** Simplified depiction of gliding structures. Side view of cells moving on a surface from left to right. Motility structures are shown as black structures.

1.2 Signal transduction networks

Signal transduction networks are frequently formed by two-component systems found in all domains of life. Its core consists of a receptor, often a membrane-localized sensor histidine kinase, and its associated response regulator (RR) (Kirby, 2009). The receptor domain typically senses an external signal, such as nutrients, toxic substances or light. After activation, the histidine kinase uses ATP to autophosphorylate on a conserved His residue. Then the phosphoryl group is transferred to a conserved Asp within the receiver domain of the RR. The RR then regulates downstream processes, e.g., gene expression, secondary messenger synthesis, or protein-protein interactions (Stock *et al.*, 2000). These two-component systems can act independently or be modular and be incorporated in, among others, chemosensory-type systems. These chemosensory systems are diverse and can be grouped into 19 major groups: 17 groups controlling flagellar motility, one group controlling T4P-based motility, and one group controlling alternative cellular functions (Wuichet & Zhulin, 2010).

1.2.1 Chemosensory systems

The best-understood chemosensory system is the chemotaxis machinery (i.e., Che system) in *E. coli* (Figure 4). It regulates flagellar motility and causes changes in the flagellar rotation from counterclockwise to clockwise upon a stimulus, causing the cell to change from a “run” motion used for directed movement to a “tumble” to reorient the cell (Larsen *et al.*, 1974).

Several chemoreceptor sensor proteins called methyl-accepting chemotaxis proteins (MCPs) transduce inputs for chemotaxis. The prototypical MCP possesses two transmembrane regions that create a periplasmic loop, which binds to a ligand. Additionally, it has a cytoplasmic region comprising a HAMP domain (Histidine kinases, Adenylate cyclases, Methyl accepting proteins and Phosphatases), methylation helices, and the highly conserved domain that regulates kinase activity (Kirby, 2009). Following a stimulus or ligand-binding event, the signal is transduced across the cytoplasmic membrane, resulting in a conformational change in the HAMP domain that triggers the rotation of downstream elements, including the highly conserved domain (Khursigara *et al.*, 2008). In the *E. coli* Che system, this domain interacts with the CheA histidine kinase via the coupling protein CheW (Gegner *et al.*, 1992). CheA autophosphorylates on a conserved His and transfers the phosphoryl group to the single-domain RR CheY (Hess *et al.*, 1988a, Hess *et al.*, 1987). Next, CheY~P diffuses from the receptor/kinase complex to its target proteins FliM/FliN (Welch *et al.*, 1993, Sarkar *et al.*, 2010). FliM/FliN then affect the rotation of the *E. coli* flagellar motor from counterclockwise to clockwise, causing “tumbling” and reorientation of the cell (Sarkar *et al.*, 2010). Additionally, the methylesterase CheB and the methyltransferase CheR modify the activity of the

chemoreceptors and form an adaption of the system (Goy *et al.*, 1977). CheR methylates specific residues on MCPs, while CheB removes them after being phosphorylated by CheA (Springer & Koshland, 1977, Stock & Koshland, 1978, Lupas & Stock, 1989). Thus, CheR and CheB constitute a feedback mechanism that resets MCPs to a pre-stimulus state, allowing MCPs to monitor environmental changes constantly. Furthermore, the phosphatase CheZ controls the amount of CheY~P by accelerating dephosphorylation (Hess *et al.*, 1988b).

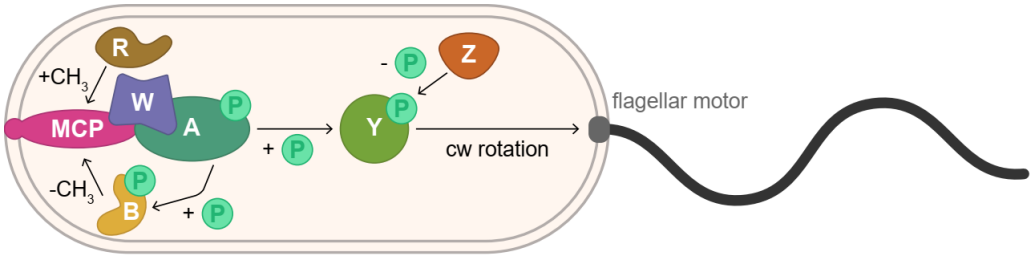

Figure 4: **The Che system of *E. coli*.** After an input signal, CheA autophosphorylates and transfers the phosphoryl group to CheY. CheY~P then interacts with flagellar motor proteins, changing the rotation of the flagellum to clockwise (cw). Phosphate is depicted as P. Arrows represent a modification of proteins (+CH_3: methylation, -CH_3: demethylation, +P: phosphorylation, -P dephosphorylation). Che proteins are labeled with their corresponding letters. The thick black line represents a flagellum.

1.2.1.1 Regulation of flagellar motility by chemosensory systems

Chemosensory systems controlling flagellar motility in other bacteria are at their core similar to the *E. coli* Che system but show alterations.

B. subtilis regulates flagellar motion by an opposing mechanism to *E. coli*. Here, activating the system by attractants activates CheA~P, which then phosphorylates CheY. CheY~P binds to the flagellar motor, leading to a run instead of the tumbling behavior seen for *E. coli* (Rao *et al.*, 2008, Bischoff *et al.*, 1993). Signaling is then altered via three systems. First, the methyltransferase CheR and the methylesterase CheB promote adaption to repellents and attractants, respectively (Kirsch *et al.*, 1993a, Kirsch *et al.*, 1993b). Second, the two phosphatases, FliY and CheC, regulate the hydrolysis of CheY~P to CheY (Szurmant *et al.*, 2004). The latter is suggested to function with the protein CheD in a negative feedback loop with CheY~P to inhibit kinase activity of CheA (Rosario & Ordal, 1996). Finally, the CheW-like receiver domain hybrid protein CheV is involved in adapting to the chemoattractant asparagine (Karatan *et al.*, 2001).

In *P. aeruginosa* the Che system controls the singular flagellum. In contrast to *E. coli*, the change from counterclockwise to clockwise rotation of the flagellum leads to a straight backward movement in a “run-and-reverse-turn” (Cai *et al.*, 2016). In addition, a pause phase correlated with turn angle sizes (Cai *et al.*, 2016). Homologs of *E. coli* CheA, CheW, CheY,

CheZ, CheB, and CheR are essential for *P. aeruginosa* chemotaxis but their exact function has yet to be completely determined (Masduki *et al.*, 1995, Kato *et al.*, 1999).

Rhodobacter sphaeroides has two complete sets of flagellar genes, *fla1,* and *fla2*, of which only the *fla1* genes are expressed constitutively to form a single flagellum under laboratory conditions (Poggio *et al.*, 2007). Furthermore, cells possess three gene clusters encoding three chemosensory systems, of which clusters two and three regulate the flagellar motor by turning the rotation “on” or “off”. Both systems are needed for chemotaxis. Proteins of cluster two localize to the cell pole together with transmembrane chemoreceptors (Wadhams *et al.*, 2003). In this system, $CheA_2$ is autophosphorylated (Porter & Armitage, 2002) and phosphorylates all six known CheYs of *R. sphaeroides in vitro* (Porter & Armitage, 2002). Proteins of cluster three form a cytoplasmic cluster together with cytoplasmic chemoreceptors (Wadhams *et al.*, 2003). Here, the two histidine kinases $CheA_3$ and $CheA_4$, which are unable to autophosphorylate, form a complex in which the kinase domain of $CheA_4$ phosphorylates $CheA_3$ (Porter & Armitage, 2004). $CheA_3$~P was shown to phosphorylate the RRs $CheY_1$ and $CheY_6$ *in vitro* (Porter & Armitage, 2004). The combined output is then required to control the Fla1 flagella. For this, $CheY_6$ can stop the flagellar motor, but $CheY_3$ or $CheY_4$ are also needed for functioning chemotaxis (Porter *et al.*, 2006). *In vitro,* studies suggest that they bind to the motor switch protein FliM (Ferre *et al.*, 2004).

The legume symbiont *Sinorhizobium meliloti* uses eight chemoreceptors, of which some were shown to be involved in chemotaxis toward the plant (Webb *et al.*, 2016). *S. meliloti* possesses two single-domain RRs. $CheY_2$ is the primary regulator of flagellar rotation, while $CheY_1$ modulates the activity of $CheY_2$ by acting as a phosphate sink (Sourjik & Schmitt, 1996, Sourjik & Schmitt, 1998). In addition to the core chemosensory genes *cheA*, *cheW*, *cheB*, and *cheR*, the three additional genes *cheD*, *cheS*, and *cheT* are found in the chemotaxis operon. CheS enhances the phosphate transfer from CheA~P to $CheY_1$ by increasing the binding affinity of the two proteins (Dogra *et al.*, 2012). The roles of CheD and CheT remain to be elucidated.

Interestingly, *Azospirillum brasilense* harbors two distinct chemotaxis pathways that control flagellar motility. The Che1 system regulates changes in swimming speed, while the Che4 system controls the frequency of swimming reversals (Mukherjee *et al.*, 2016). Two RRs, CheY6 and CheY7, encoded by genes outside the chemotaxis clusters, seem to be part of the Che1 and Che4 pathways, respectively (Mukherjee *et al.*, 2019).

Additionally, other bacteria control flagellar motion via a chemosensory system, e.g., *V. cholerae*, which encodes three chemosensory clusters, of which cluster two is involved in regulating chemotaxis under standard conditions (Gosink *et al.*, 2002).

1.2.1.2 Regulation of type IV pili-dependent motility by chemosensory systems

In *P. aeruginosa,* the Chp system regulates motility via T4P on solid surfaces. The organism deploys mechanotaxis by sensing T4P surface attachment at one pole (Kühn *et al.*, 2021). The MCP PilJ senses structural changes in the T4P and interacts with the monomer unit PilA via its periplasmic region, followed by transduction of the signal by a CheW-like protein called PilI. The signal is then transduced from PilJ to the histidine kinase ChpA (Persat *et al.*, 2015). The Chp system harbors two CheY-like RRs, PilG and PilH. PilG is required for a functioning Chp system by being important for pilus extension (Darzins, 1993). Phosphorylation of PilG leads to protein polarization, stimulating forward motion by regulating the extension ATPase PilB and thereby creating a positive feedback loop between surface sensing by T4P and activating T4P extension (Kühn *et al.*, 2021, Kühn *et al.*, 2023). In addition, PilG is suggested to regulate the activation of the adenylate cyclase CyaB, which controls cyclic adenosine monophosphate (cAMP) levels, which are critical for virulence gene regulation (Fulcher *et al.*, 2010). The second RR, PilH, has been proposed to act as a phosphate sink to limit signaling or as a RR that controls T4P retraction (Bertrand *et al.*, 2010, Fulcher *et al.*, 2010). Recently, it was suggested that PilH inhibits the polarization of PilB by breaking the local positive feedback established by PilG, and this allows the cell to reverse when the signal changes (Kühn *et al.*, 2021, Kühn *et al.*, 2023). This system also encodes another CheW-like protein, ChpC, which is not essential for motility but is involved in response to host-derived signals, which increase motility (Nolan *et al.*, 2020).

The two cyanobacteria *N. punctiforme* and *Synechocystis* sp. PCC 6803 also harbour chemosensory systems for regulating T4P-based motility via phototaxis (Campbell *et al.*, 2015, Bhaya *et al.*, 2001, Yoshihara & Ikeuchi, 2004). In *Synechocystis*, the blue-light sensor PixD regulates negative phototaxis, which is used for directed movement away from a light source (Okajima *et al.*, 2005). PixD forms a complex with the CheY-like RR PixE (Tanaka *et al.*, 2012). Upon exposure to blue light, PixE dissociates from the complex and interacts with PilB to change the direction of phototaxis from positive to negative (Jakob *et al.*, 2020). In *N. punctiforme*, the Hmp chemosensory system was suggested to control the polarity of T4P and sense light indirectly by sensing changes in the proton motive force (PMF) (Harwood *et al.*, 2021). It consists of CheA, CheW, CheY homologs, and an MCP that are important for polarity but do not affect piliation (Risser *et al.*, 2014). The system harbors the additional component HmpF, whose unipolar localization leads to the activation of T4P at the leading pole (Cho *et al.*, 2017, Harwood *et al.*, 2021). The Ptx chemosensory system senses light directly through GAF domains and directs phototaxis (Campbell *et al.*, 2015).

1.3 *Myxococcus xanthus*

The Gram-negative bacterium *M. xanthus* is a model organism for social behavior in bacteria. *M. xanthus* exhibits a complex life cycle as a response to environmental changes. In the presence of nutrients, cells grow, divide, and move as predatory swarms (Zusman *et al.*, 2007). In the absence of nutrients, *M. xanthus* cells form fruiting bodies in which cells differentiate into environmentally resistant myxospores; in addition cells develop into peripheral rods or lyse (O'Connor & Zusman, 1991, Wireman & Dworkin, 1977). This multicellular behavior must be highly regulated by, i.a., regulating the motility of *M. xanthus* in order for cells to act collectively to expand out of colonies, form rippling waves needed for efficient predation, and aggregate to fruiting bodies (Figure 5).

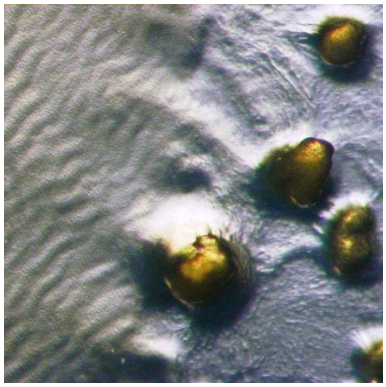

Figure 5: *M. xanthus* cells organize into rippling waves (left). In areas without nutrients, *M. xanthus* cells self-organize into fruiting bodies (right). [Zalman Vaksman and Heidi Kaplan, University of Texas Medical School, https://doi.org/10.1371/image.pcbi.v08.i09.g001]

1.3.1 The two motility systems of *M. xanthus*

M. xanthus does not swim but instead moves on surfaces via two genetically distinct motility systems (i.e., T4P-dependent and gliding motility) that are essential for the bacterium's complex life cycle and are favored depending on the surface cells are moving on. Cells primarily move as single cells through gliding motility on hard, dry surfaces, while T4P-dependent motility is preferred on soft, wet surfaces when moving in groups (Konovalova *et al.*, 2010, Hodgkin & Kaiser, 1979).

1.3.1.1 Gliding Motility

In *M. xanthus*, gliding motility, also called adventurous (A-) motility, is used by single cells that rotate along their longitudinal axis without using surface appendages. Cells leave behind a

slime trail composed of diverse substances, such as polysaccharides and OM vesicles, that other cells are suggested to follow (Ducret *et al.*, 2012, Ducret *et al.*, 2013a). The IM motor, formed by the AglQRS proteins, utilizes PMF to power the gliding machinery. The AglQRS complex forms a membrane-spanning macromolecular system together with the Glt complex consisting of 11 Glt proteins (GltA-K) called the Agl-Glt complex, which is connected to a cytoplasmic subcomplex comprised of the proteins AglZ, MglA, and MreB (Islam & Mignot, 2015). MglA interacts with AglZ, and MreB (Yang *et al.*, 2004, Mauriello *et al.*, 2010, Treuner-Lange *et al.*, 2015). Initially, it was proposed that MreB forms a track on which complexes move along the cell (Mauriello *et al.*, 2010). However, because MreB was suggested not to form a helical filament but rather patches or short filaments, MreB may form a cytosolic scaffold for protein assembly (Errington, 2015, Islam & Mignot, 2015) (Figure 6 left).

Motor complexes are assembled at the leading cell pole, and after engaging with OM components form the Agl/Glt complex, this complex becomes fixed to the substrate, resulting in a distribution of so-called focal adhesion complexes along the cell body that propel the screw-like movement of the cell (Faure *et al.*, 2016). Complexes are disassembled when reaching the lagging pole, while new complexes are formed at the leading cell pole (Treuner-Lange *et al.*, 2015) (Figure 6 right).

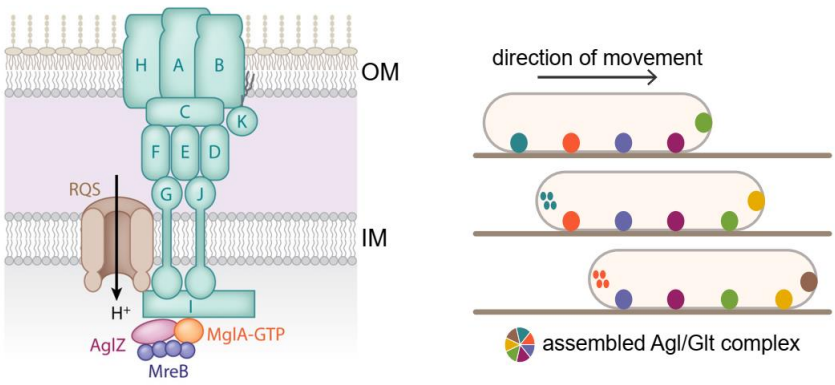

Figure 6: **Gliding motility in *M. xanthus*.** (Left) Model of the *M. xanthus* gliding motility machinery spanning the outer (OM) and inner membrane (IM). Agl and Glt proteins are in brown and aqua, respectively. Agl and Glt proteins are labeled with their corresponding letters. Figure modified from Schumacher & Søgaard-Andersen, 2017. (Right) The gliding motor complexes are assembled at the leading cell pole. They stay fixated on the substratum as focal adhesion complexes and disassemble at the lagging cell pole.

1.3.1.2 T4P-dependent motility

T4P-dependent motility is generally characterized by the movement of groups of cells and is stimulated by cell-cell proximity. This type of motility is also called social (S-) motility and

requires T4P, the two secreted polysaccharides exopolysaccharide (EPS) and biosurfactant polysaccharide (BPS), and lipopolysaccharide (LPS) O-antigen to function correctly (Konovalova *et al.*, 2010, Li *et al.*, 2003). Additionally, the second messenger, c-di-GMP, influences T4P-dependent motility (Skotnicka *et al.*, 2016a).

In the rod-shaped cells of *M. xanthus*, T4P are located at the leading cell pole. The pilus machinery comprises proteins encoded in the *pil* locus, gene clusters for minor pilins and PilY1, and the peptidoglycan-binding protein TsaP (Wall & Kaiser, 1999, Siewering *et al.*, 2014). PilA is the major pilin. PilQ and TsaP form a pore in the OM through which the pilus extends (Chang *et al.*, 2016, Siewering *et al.*, 2014). PilP is part of the mid-periplasmic ring and directly interacts with PilQ (Chang *et al.*, 2016, Friedrich *et al.*, 2014). It is suggested to be important for linking other components to the OM complex and their stability (Friedrich *et al.*, 2014). PilN and PilO are located in the IM and interact with PilP to form the alignment complex in the lower periplasmic ring (Friedrich *et al.*, 2014, Chang *et al.*, 2016). PilM forms the cytoplasmic ring of the T4P machinery (Chang *et al.*, 2016). In a recent model, PilC forms dimers that build the cytoplasmic dome of the pilus machinery. The ATPases PilB and PilT create the energy for extension and retraction of the pilus fiber, respectively (Chang *et al.*, 2016). PilY1 and the four minor pilins PilX, PilV, PilQ, and FimU form a complex, which is part of the T4P machinery and the extended pilus. It is proposed that this complex primes pilus assembly and caps the T4P (Friedrich *et al.*, 2014, Chang *et al.*, 2016, Treuner-Lange *et al.*, 2020).

EPS is important for T4P motility. Cells lacking EPS do not cohere and are not able to agglutinate and show reduced T4P-dependent motility (Perez-Burgos *et al.*, 2020). EPS is part of the extracellular matrix of *M. xanthus* (Behmlander & Dworkin, 1994, Sutherland & Thomson, 1975). It is synthesized via a Wzx/Wzy-dependent pathway (Perez-Burgos *et al.*, 2020, Islam *et al.*, 2020). Apart from the EPS biosynthetic machinery, several regulatory genes of EPS production have been identified whose molecular function still needs to be elucidated. An extensively studied system of EPS regulation is the Dif chemosensory system, described in detail in 1.3.3. Recently, a third cell-surface polysaccharide was identified, which is involved in motility. The biosurfactant polysaccharide (BPS) is also synthesized via a Wzx/Wzy-dependent pathway and is thought to stimulate T4P-dependent motility by reducing surface tension (Islam *et al.*, 2020, Perez-Burgos *et al.*, 2020). Additionally, cells lacking BPS have defects in development (Islam *et al.*, 2020).

The LPS of *M. xanthus* consists of joined molecules of O-antigen and a lipid A-core (Fink & Zissler, 1989). Mutants defective in LPS O-antigen (e.g., mutants lacking components of the ABC-transporter involved in the transport of O-antigen molecules from the cytoplasm to the

periplasm) have defects in T4P-dependent motility, gliding, and development (Bowden & Kaplan, 1998, Perez-Burgos *et al.*, 2019).

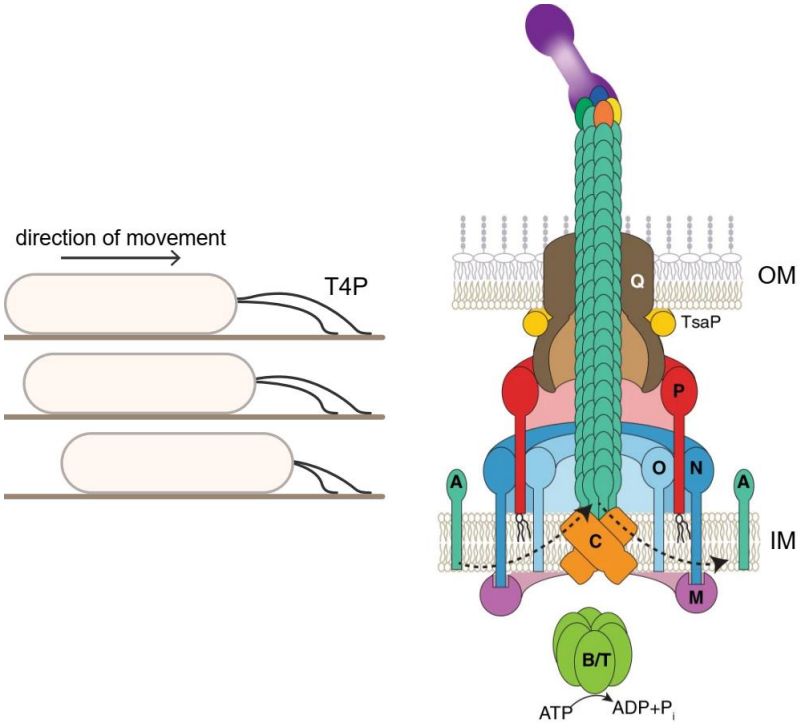

Figure 7: **T4P-dependent motility in *M. xanthus*.** (Left) T4P assemble at the leading cell pole, attach to a surface, and retract, by which the cell moves forward. (Right) Model of the *M. xanthus* T4P machinery spanning the outer (OM) and inner membrane (IM). Pil and minor pilin proteins are labeled with their corresponding letters. Figure was modified from Treuner-Lange *et al.*, 2020.

1.3.2 Cell polarity in *M. xanthus*

Both motility systems in *M. xanthus* show a front-rear polarity with T4P assembling at the leading cell pole and gliding motility complexes forming at the leading pole and disassembling at the lagging cell pole. This front-rear polarity is established by the polarity module (Figure 8). Another module containing SofG is needed for the proper localization of the two ATPases, PilB and PilT. In addition, the PilZ proteins PlpA, PixA, and PixB also impact cell polarity, but their molecular mechanisms remain elusive (Kuzmich *et al.*, 2021, Pogue *et al.*, 2018).

The key protein of the polarity module is the small Ras-like GTPase MglA that is essential for both motility systems (Hartzell & Kaiser, 1991). Small Ras-like GTPases depend on their ability to bind nucleotides for their function, switching between “on” and “off” states when bound to GTP or GDP, respectively (Vetter & Wittinghofer, 2001). In their active GTP-bound state, they can interact with effectors. GTPases have low intrinsic rates of GTP hydrolysis and GDP/GTP exchange and rely on regulating proteins for their function. Guanine nucleotide exchange

factors (GEFs) stimulate the exchange of GDP to GTP, while GTPase activating proteins (GAPs) stimulate GTP hydrolysis (Bos et al., 2007).

The nucleotide exchange by MglA from GDP to GTP, and therefore its change from inactive to active form, is stimulated by the proteins RomR and RomX, which form a GEF complex. In this complex, RomX interacts with MglA to promote nucleotide exchange, while RomX's GEF activity is stimulated when complexed with RomR (Szadkowski *et al.*, 2019). MglB is a GAP that stimulates the low intrinsic GTPase activity of MglA (Zhang *et al.*, 2010, Leonardy *et al.*, 2010). Recently, the protein RomY was identified as a co-GAP that forms a low-affinity complex with MglB and stimulates its GAP activity (Figure 8 A) (Szadkowski *et al.*, 2022). Together with MglC, which regulates polarity by forming a complex with RomR and MglB, these proteins form the polarity module (McLoon *et al.*, 2016, Carreira *et al.*, 2023).

The proteins of the polarity module interact in a highly intricate manner to bring about their asymmetric polar localization (Figure 8 B). RomR is the base of the polarity network and promotes the polar localization of itself and the other components (Carreira *et al.*, 2020). The RomR/MglC/MglB complex establishes a positive feedback for their polar accumulation (Carreira *et al.*, 2023). Additionally, RomR recruits RomX, while high concentrations of MglB recruit RomY. The RomR/RomX complex promotes while the MglB/RomY complex inhibits MglA-GTP polar accumulation (Szadkowski *et al.*, 2019, Szadkowski *et al.*, 2022, Zhang *et al.*, 2010, Leonardy *et al.*, 2010). The accumulation of MglA-GTP inhibits the RomR/MglC/MglB positive feedback by interfering with the interaction of MglC and MglB (Carreira *et al.*, 2020, Carreira *et al.*, 2023).

The interactions of the polarity module give rise to a bipolar asymmetric localization of MglC, as well as of the GEF and GAP complexes with a larger cluster at the lagging cell pole (Figure 8 C). Nonetheless, based on this model, GAP activity dominates at the lagging cell pole, while GEF activity is predominant at the leading cell pole, resulting in MglA-GTP localizing to the leading cell pole (Carreira *et al.*, 2020).

MglA-GTP is thought to directly or indirectly recruit critical proteins of the two motility systems at the leading cell pole. In contrast, the inactive MglA-GDP form localizes diffusely throughout the cytoplasm (Leonardy *et al.*, 2010, Zhang *et al.*, 2010). MglA-GTP interacts with the gliding motility proteins AglZ and MreB to stimulate the formation of focal adhesion complexes and is also an integral part of these complexes (Figure 6) (Treuner-Lange *et al.*, 2015). Furthermore, the proteins RomR and RomX are incorporated into the Agl-Glt complexes (Szadkowski *et al.*, 2019). Recently, the protein GltJ was proposed to recruit MglA-GTP and AglZ to stimulate focal adhesion assembly (Mignot *et al.*, 2023). Furthermore, MglA is required for the correct localization of the extension and retraction ATPases of the T4P machine, PilB, and PilT,

respectively (Bulyha *et al.*, 2013, Berleman *et al.*, 2011). MglA-GTP interacts with SgmX, which is then recruited to the pole by the polar beacon protein FrzS (Bautista *et al.*, 2023). Here, SgmX stimulates the polar accumulation of PilB (Potapova *et al.*, 2020, Mercier *et al.*, 2020).

The small GTPase SofG and the bactofilin BacP form another important module for T4P-dependent motility. BacP localizes as subpolar patches, and one of these patches is used as a landmark for SofG, which forms a single cluster that shuttles in one subpolar region. In the current model, BacP and SofG stimulate the accumulation of PilB and PilT at one pole by transporting them to or retaining them at the pole. PilB and PilT are then sorted to opposite poles by the polarity module (Bulyha et al., 2013).

The front-rear polarity of *M. xanthus* is not fixed but is periodically inverted, resulting in cells reversing their direction of movement (Blackhart & Zusman, 1985). During such a reversal event, all proteins of the polarity module switch poles, and, therefore, the former lagging cell pole becomes the new leading cell pole. These reversals are triggered by a signal from the Frz chemosensory system (described in 1.3.3.1).

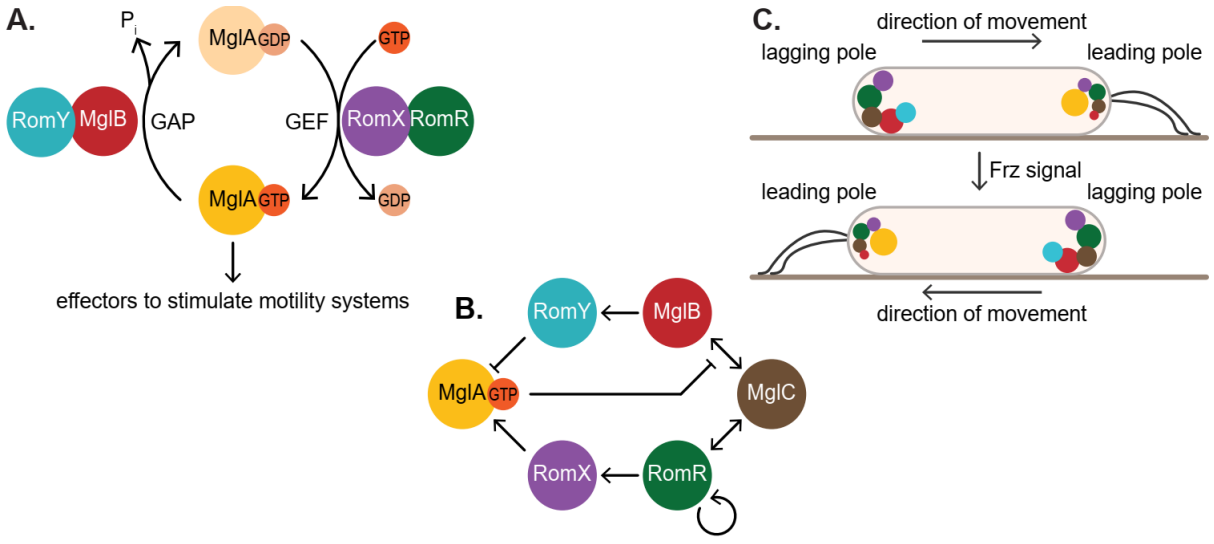

Figure 8: **The polarity module of *M. xanthus***. **(A)** The MglA GTPase cycle. **(B)** Schematic of interactions between the polarity proteins. **(C)** Schematic of polarity protein localization in a cell with T4P at the leading cell pole. Circle sizes indicate the amount of protein at the pole. Color code as in A and B.

1.3.3 Chemosensory systems of *M. xanthus*

The genome of *M. xanthus* contains eight clusters of chemotaxis-like genes that form eight chemosensory-like systems, which are homologous to the Che system of *E. coli*. These systems are involved in different cellular functions, which will be described below.

The first chemosensory system described in *M. xanthus* was the Frz system, which regulates cellular reversals by inducing the polarity switch and is described in detail in 1.3.3.1.

The Dif (defective in fruiting/fibrils) chemosensory system is essential for development and EPS synthesis (Yang et al., 1998b). It consists of six chemotaxis proteins, which seem to be involved in the chemotactic response of *M. xanthus* to phosphatidylethanolamine (PE) (Kearns *et al.*, 2000, Bonner *et al.*, 2005). The MCP DifA is a transmembrane protein and is suggested to transduce a signal through its C-terminal domain because a chimera of the *E. coli* nitrate sensor NarX and the C-terminus of DifA led to EPS production only in the presence of nitrate (Xu *et al.*, 2005). The signal is transduced to the histidine kinase DifE (CheA), via the CheW coupling protein DifC that was shown to interact with DifA and DifE in a yeast two-hybrid system (Yang & Li, 2005). DifE autophosphorylates and can then phosphorylate the system's two RR, DifD and EpsW (Black *et al.*, 2010, Black *et al.*, 2015). The orphan RR EpsW~P is a positive regulator of EPS production and is considered an intermediate step in a phosphorelay instead of the terminal output of the Dif system (Black *et al.*, 2015). DifD negatively affects EPS production since deleting *difD* results in the overproduction of EPS. The same is true for the deletion of *difG,* which encodes for a CheC homologous phosphatase (Black & Yang, 2004). DifG accelerated dephosphorylation of DifD~P, which is suggested to act as a phosphate sink for DifE (Black *et al.*, 2010, Black *et al.*, 2006). The molecular mechanism by which the Dif system regulates EPS synthesis is still unknown.

While the first two chemosensory systems, the Frz and the Dif system, have been extensively studied, the function of the other systems is less clear, and only four of the remaining six systems have been analyzed experimentally.

The Che3 chemosensory system is involved in development. The *che3* gene cluster encodes two MCPs, a CheW, a hybrid CheA, a CheB, and a CheR, but no CheY homolog. The lack of the two MCPs or the CheA led to early aggregation and overexpression of developmentally regulated genes (Kirby & Zusman, 2003). It was further discovered that the system, together with an additional kinase, CrdS, phosphorylates the transcriptional activator called CrdA that regulates developmental gene expression (Kirby & Zusman, 2003, Willett & Kirby, 2011).

The *che4* gene cluster encodes an MCP, two CheW, a hybrid CheA-CheY, a RR, and a CheR homolog. Deleting the complete operon or the RR in a strain that could only move through T4P-dependent motility led to enhanced swarming. These strains were not able to aggregate or sporulate. On the other hand, swarming was reduced when the MCP was deleted, enhancing sporulation. This defect was suggested to be caused by a defective correlation between velocity and reversal frequency (Vlamakis *et al.*, 2004).

The Che7 chemosensory system consists of a CheY, CheA, CheW, MCP, CheB, and a CheR homolog. Additionally, the HEAT-repeat containing protein Cpc7 was identified. The lack of proteins of this system led to defects in aggregation but no defect in sporulation. Furthermore, it was found that CheY7 interacted with Cpc7, which regulates development (Darnell *et al.*, 2014).

No publication covers the Che6 chemosensory system, but it was suggested to be involved in T4P assembly (Zusman *et al.*, 2007). The functions of the Che5 and the Che8 chemosensory system remain to be elucidated.

1.3.3.1 The Frz chemosensory system

The Frz chemosensory system is also called the polarity inversion module and triggers the inversion of the polarity axis in *M. xanthus* cells during reversals (Figure 9) (McBride *et al.*, 1989, Blackhart & Zusman, 1985). It was first discovered in mutants defective in fruiting body formation that formed frizzy filament-like aggregates (Blackhart & Zusman, 1985).

The specific signals that the Frz system senses to induce reversals are still unknown, but isoamyl alcohol (IAA) and dimethyl sulphoxide (DMSO) activate the Frz system by supposedly acting as repellents. At the same time, it has been proposed that the intercellular C-signal, EPS, and other complex substrates may regulate Frz signaling as attractants (Shi *et al.*, 1993, McBride *et al.*, 1992, Søgaard-Andersen & Kaiser, 1996, Zhou & Nan, 2017).

The core of the Frz system consists of the cytoplasmic MCP FrzCD, the CheA-type histidine kinase FrzE with a C-terminal CheY receiver domain ($FrzE^{CheY}$), and the CheW homolog FrzA, which are all essential for signaling (Bustamante *et al.*, 2004). FrzCD localizes in multiple nucleoid-associated clusters with FrzA and FrzE (Kaimer & Zusman, 2016). Recently, it was shown that the CheW-like protein FrzB interacts with FrzCD and is involved in the formation and distribution of these clusters (Guiseppi *et al.*, 2019). FrzCD possesses an N-terminal domain of unknown function that does not seem necessary for sensing signals and a conserved C-terminal module for signal recognition and transduction (Bustamante *et al.*, 2004). Its activity is modulated by methylation by the methyltransferase FrzF (homologous to CheR) and the methylesterase FrzG (homologous to CheB) (McCleary *et al.*, 1990, Bustamante *et al.*, 2004, McBride *et al.*, 1992, Astling *et al.*, 2006, Scott *et al.*, 2008). When FrzCD is active, FrzE autophosphorylates on a conserved His residue (H49) (McCleary & Zusman, 1990). This interaction is mediated by FrzA (Kaimer & Zusman, 2016). FrzE then phosphorylates at least three RRs on Asp residues: $FrzE^{CheY}$ (D709), FrzZ (D52, D220), and FrzX (D53) at conserved residues (Guzzo *et al.*, 2018, Inclan *et al.*, 2007, Kaimer & Zusman, 2016). $FrzE^{CheY}$ is proposed to act as a phosphate sink, preventing noisy activation of the

system at low stimulation levels (Kaimer & Zusman, 2016). FrzZ consists of two CheY-like RR domains and is not essential but important for reversals (Guzzo *et al.*, 2015, Bustamante *et al.*, 2004). It is phosphorylated at two residues, with D52 being the preferred target residue (Kaimer & Zusman, 2013, Inclan *et al.*, 2007). Phosphorylation of FrzZ is independent of cell movement and directly correlates with the reversal frequency (Kaimer & Zusman, 2013). The second output response regulator, FrzX, was suggested to be the CheY-like phosphorylation-dependent trigger for a reversal event (Guzzo *et al.*, 2018).

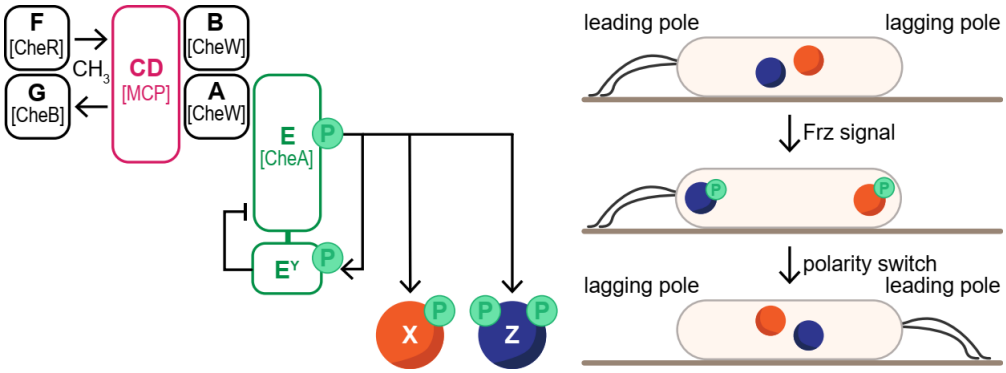

Figure 9: **The Frz pathway.** Schematic of the Frz pathway (left). Frz proteins are labeled with their corresponding letters. Phosphorylation of protein (domains) is indicated with P. Localization of FrzX and FrzZ (right). Upon Frz signaling, FrzX (orange) and FrzZ (blue) localize to the lagging and leading cell poles, leading to a polarity switch.

Upon phosphorylation, FrzX~P and FrzZ~P localize to the lagging cell pole and the leading cell pole, depending on MglB or MglA, respectively (Figure 9) (Guzzo *et al.*, 2018, Kaimer & Zusman, 2013). This triggers the switch of polarity. Among the proteins of the polarity module that have been analyzed in detail during reversals, MglA-GTP detaches first from the old leading cell pole, a process that is thought to be stimulated by FrzZ~P, and then localizes to the old lagging cell pole, defining it as the new leading cell pole. For this to occur, FrzX~P is thought to change the balance between RomR/RomX and MglB/RomY GEF and GAP activities at the lagging cell pole. MglA and MglB colocalize for up to 30s until MglB relocalizes to the opposite pole (Guzzo *et al.*, 2018). RomR has the slowest switching dynamics and is the last polarity module protein to relocalize fully. The exact molecular mechanisms of this switch are still not understood. Guzzo et *al.*, 2018 suggested that the system functions as a gated relaxation oscillator with RomR defining a refractory period insensitive to Frz signaling, which FrzX~P ultimately triggers. Alternatively, three additional switching mechanisms have been proposed: the reset switch, the prime-release switch, and the push switch (Tostevin *et al.*, 2021). In the reset switch the system gradually relaxes towards a symmetric configuration when a signal is applied. When it is removed, the system becomes polarized again but settles

into the opposite configuration. Similarly, the polarity reversion occurs after removing the signal as the “release phase” in a prime-release mechanism. However, in this mechanism, when the signal is applied in the “prime phase”, the system reaches a new bistable steady state, which is still polarized. Lastly, in a push switch mechanism, the switch begins immediately when the signal is applied and subsequently remains stably polarized in the opposite orientation (Tostevin *et al.*, 2021). Carreira *et al.*, 2020 suggest that a spatial toggle switch dynamically regulates front-rear polarity consisting of the interconnected polarity module and the Frz system, with stable polarized phases between switching events.

2 Scope of this study

M. xanthus harbors two polarized motility systems activated by the small Ras-like GTPase MglA. MglA’s GTP-bound state is controlled by the proteins of the polarity module, whose interactions lead to an equilibrium state, which ultimately leads to the polarity axis of a forward-moving cell. For *M. xanthus* cells to change their direction of movement, the polarity axis has to be inverted.

This inversion occurs after a signal of the Frz system leads the two response regulators, FrzZ and FrzX, to localize to the leading and lagging cell poles, respectively, in their phosphorylated form. The interactions and molecular mechanism of the switch are not understood.

In this study, we investigated the interactions underlying the switch in polarity using three approaches. First, in a candidate approach, we performed quantitative live-cell imaging to investigate the dependencies of the localization of both response regulators on the polarity module proteins. Second, we identified new potential interaction partners using proximity labeling. Third, we used bioinformatics analyses to identify proteins possibly involved in polarity regulation.

3 Results

Since this study focuses on the function of the two RRs of the Frz system, we first established the phenotypes of *frz* mutants, which will be used in the following to confirm published data. For this, we constructed in-frame deletion mutants of *frzE*, *frzZ*, *frzX*, a double in-frame deletion mutant of *frzZ* and *frzX*, as well as a gain of function (GOF) mutant using the *frzCD*$^{\Delta 6\text{-}153}$ allele (from here on *frzCD*^{GOF}). In order to assess the reversal phenotypes of these strains, we performed single-cell motility assays (Figure 10 A). Timelapse recordings of cells moving on 0.5 % CTT 1.5 % agarose were recorded for 20 min in 30 s intervals. These movies were then analyzed for single cells' directional changes (reversals) per 20 min.

A Δ*frzE* mutant has inactive Frz signaling since the signal can no longer be transduced to the RRs, leading to a loss of function (LOF) of the Frz system (Bustamante *et al.*, 2004). This results in cells reversing with a lower frequency compared to wildtype (WT) (Figure 10 A). A *frzCD*^{GOF} was used for cells with constantly active Frz signaling of the Frz system and was constructed based on its severe hyperreversing phenotype (Bustamante *et al.*, 2004). This led to cells with higher reversal frequencies compared to WT (Figure 10 A). Similar to a Δ*frzE* deletion, the proper transduction of the Frz signal is lost in cells lacking one or the other of the two RRs (Inclan *et al.*, 2007, Guzzo *et al.*, 2018). This led to hyporeversing cells similar to a Δ*frzE* mutant (Figure 10 A). The same phenotype was observed in a Δ*frzZ*Δ*frzX*, leading to a reversal frequency similar to that of the Δ*frzE* mutant but significantly lower than in strains lacking only a single RR (Figure 10 A). We conclude that FrzZ and FrzX are equally important for reversals.

These reversal defects led to distinct motility phenotypes in colony-based motility assays that favor T4P-dependent or gliding motility (Figure 10 B). A WT colony had characteristic flares at the colony edge on 0.5 % agar, which favors T4P-dependent motility. On 1.5 % agar favoring gliding motility, a WT colony expanded and had slime trails and single cells at the colony edge. The hyporeversing Δ*frzE*, Δ*frzZ*, Δ*frzX*, and Δ*frzZ*Δ*frzX* mutants had reduced colony expansion and short, less defined flares at the colony edge than WT on 0.5 % agar. On 1.5 % agar, the colonies had an increased amount of slime trails and single cells at the colony edges. The hyperreversing *frzCD*^{GOF} mutant had no colony expansion on 0.5 % and only little spreading on 1.5 % agar on which a single layer of spreading cells and single cells were visible (Figure 10 B).

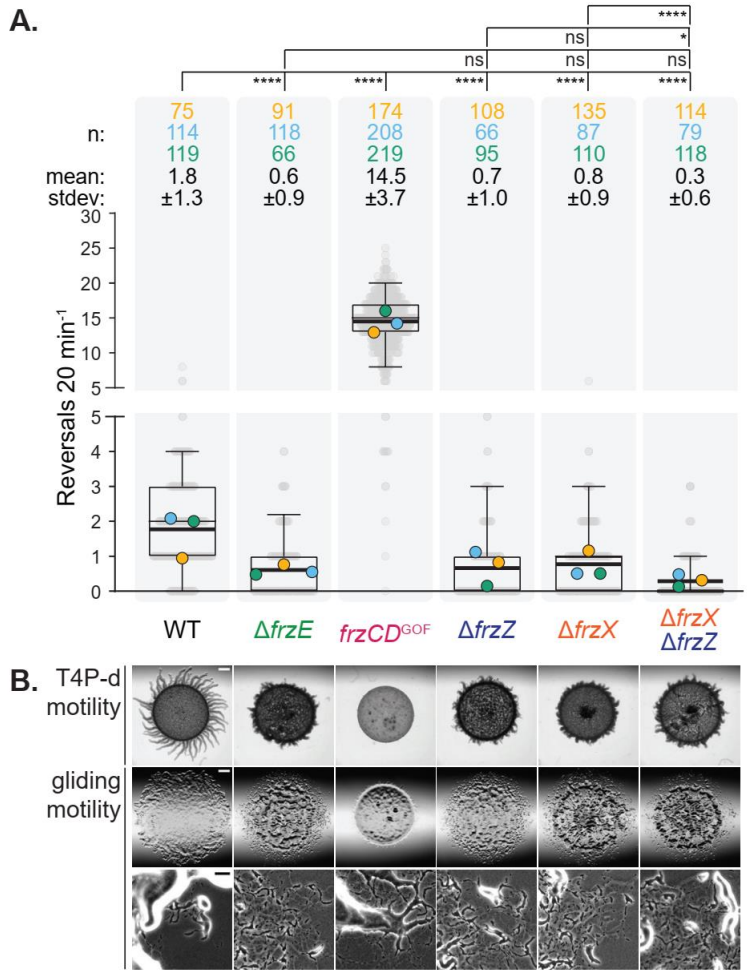

Figure 10: **Reversal phenotypes of *frz* mutants used in this study**. **(A)** Single-cell gliding reversal assay on 0.5 % CTT 1.5% agarose. Boxplots show the number of reversals per cell per 20 min. Each dot in the scatterplot represents the number of reversals of one cell. Boxes enclose the 25th and 75th percentile. Whiskers enclose the 5th and 95th percentile. The median is shown as a thin line in the box. The mean of each replicate is shown as a symbol in orange, blue, and green. The mean based on all three experiments is shown as a thick black line. Y-axis is divided into two segments for better visibility of hyporeversing strains. The number of trajectories analyzed per replicate (n) and mean reversal frequencies for each strain are shown above the graph. Kruskal-Wallis test was used for statistical analysis. “ns”, not significant (p>0.05); “*”, p≤0.05; and “****”, p<0.0001. **(B)** Motility assay. T4P-dependent motility was tested on 0.5 % agar. Gliding motility was tested on 1.5 % agar. Scale bars from top to bottom: 1 mm, 1 mm, and 50 µm.

3.1 How does FrzZ induce a switch in polarity?

First, we aimed to elucidate the function of FrzZ at the leading cell pole in stimulating the polarity switch. Phosphorylation is important for the localization of FrzZ to the leading pole (Kaimer & Zusman, 2013, Guzzo *et al.*, 2018). To verify this observation, we constructed strains expressing *frzZ-mVenus* from its native site in otherwise WT, a Δ*frzE,* and a *frzCD*^{GOF} strain. The fusion protein accumulated in the three strains detected by immunoblot analysis using α-GFP antibodies but showed degradation at a size of ~50 kDa, which cannot be assigned (Figure 11 A and B).

The fluorescent fusion protein was functional as strains expressing *frzZ-mVenus* resembled their corresponding parent strains in a motility assay (Figure 11 C). WT and the WT expressing *frzZ-mVenus* formed flares at the colony edges on agar favoring T4P-dependent motility and slime trails and single cells at the colony edges on agar favoring gliding motility. The hyporeversing Δ*frzE* mutants showed less colony expansion and frizzy colony edges on 0.5 % agar. On 1.5 % agar, the colonies showed an increased amount of slime trails and single cells at the colony edges. The hyperreversing *frzCD*$^{\Delta 6\text{-}153}$ mutants showed no colony expansion on 0.5 % and only little spreading on 1.5 % agar.

The localization of FrzZ-mVenus was assessed by fluorescence microscopy. For this, we used a fluorescence quantification pipeline to determine the presence and intensity of polar clusters. Briefly, exponentially growing cells were placed on chitosan-coated slides for 1 h and then imaged in snapshots or as moving cells in time-lapse recordings. In time-lapse recordings, cells were prepared as described and recorded for 5 min with images captured every 20 s. Cell masks were determined using oufti and then used to quantify fluorescence microscopy images using a custom MATLAB script. In this pipeline, the polar regions are defined as the parts of a cell within a distance of 10 pixels, corresponding to 0.65 µm, from a tip of a cell. The cytoplasmic region includes all pixels of the cell with the exception of the polar regions. A pole was considered to have a polar cluster if a contiguous set of at least three pixels above the threshold intensity was found in the polar region.

FrzZ-mVenus in an otherwise WT strain localized mostly diffusely in the cytoplasm, with only a few cells having a polar cluster (Figure 12 A). This polar localization depended on the activation state of the Frz system, as described previously (Kaimer & Zusman, 2013, Guzzo *et al.*, 2018). In a Δ*frzE* mutant in which FrzZ is not phosphorylated, polar cluster formation was lost, as previously reported (Kaimer & Zusman, 2013). Also as previously reported (Kaimer & Zusman, 2013, Guzzo *et al.*, 2018), cluster formation was stimulated in frequency and intensity in the *frzCD*^{GOF} mutant in which FrzZ is constantly phosphorylated (Figure 12 A and C, data is also plotted as scatterplots in Supplementary Figure 3). To determine at which pole FrzZ-mVenus localized, we performed time-lapse fluorescence microscopy. As previously reported (Kaimer & Zusman, 2013, Guzzo *et al.*, 2018), clusters localized to the leading cell pole in WT while no clusters were observed in the Δ*frzE* mutant (Figure 12 A). In a *frzCD*^{GOF} mutant FrzZ-mVenus clusters localized to the leading cell pole and could also be bipolar in few frames close to reversals (Figure 12 A). In this *frzCD*^{GOF} strain, clusters were visible in the majority of frames. In the WT strain, FrzZ-mVenus clusters localized to the leading cell pole unstably between reversals and before a reversal.

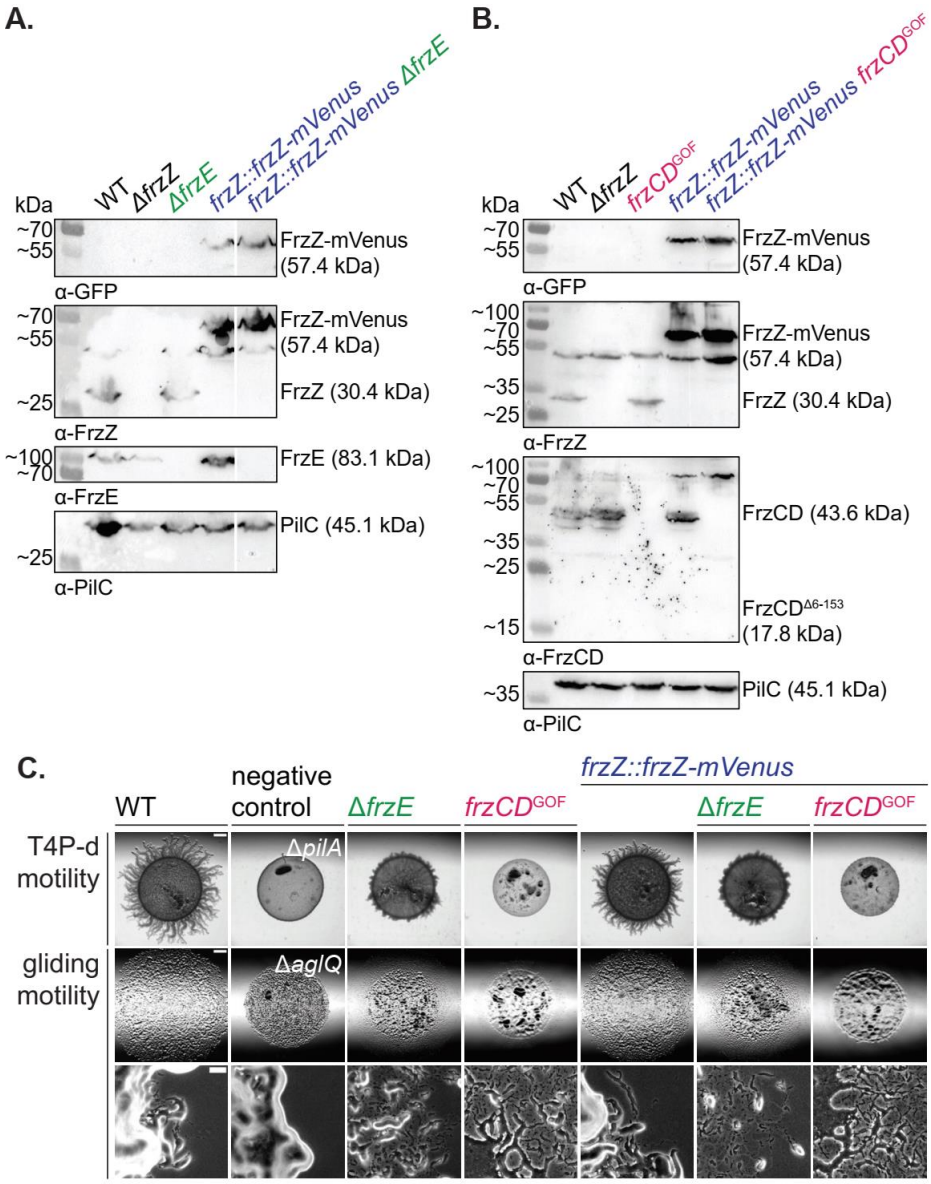

Figure 11: Immunoblot analysis of cell lysates of exponentially grown cells expressing *frzZ-mVenus* from the native site in otherwise WT, *ΔfrzE* **(A)** and *frzCD*^{GOF} **(B)** strains using α-GFP, α-FrzZ , α-FrzE, and α-FrzCD; and α-PilC antibodies as a loading control. Cell lysate from the same number of cells was loaded per lane. **(C)** Motility assay of *frzZ-mVenus* mutants in WT, Δ*frzE*, and *frzCD*^{GOF} backgrounds. T4P-dependent motility was tested on 0.5 % agar. Gliding motility was tested on 1.5 % agar. Scale bars from top to bottom: 1 mm, 1 mm, and 50 µm. One representative clone of each strain is shown.

3.1.1 MglA is important but not essential for the polar localization of FrzZ

FrzZ is suggested to interact with FrzE over the nucleoid where FrzE localizes in clusters. After phosphorylation, FrzZ~P dissociates from FrzE and localizes to the leading cell pole, where it eventually (directly or indirectly) interacts with proteins of the polarity module and to

induce a switch in polarity (Kaimer & Zusman, 2016). FrzZ localization was previously shown to depend on MglA, the protein defining front-rear polarity (Kaimer & Zusman, 2013). To gain further insight into how FrzZ localizes to the leading pole, we quantified polar fluorescence as described and quantified the localization of FrzZ-mVenus in WT and in the *frzCD*^{GOF} mutant in the absence of each individual protein of the polarity module. To this end, we again used cells expressing *frzZ-mVenus* from the native site in a WT and a *frzCD*^{GOF} strains and combined them with in-frame deletions of the *mglA*, *mglB*, *romR*, *romX*, *romY,* and *mglC*. Δ*mglA*, Δ*mglB,* and Δ*romR* strains showed distinct motility phenotypes in the WT and *frzCD*^{GOF} strains, while Δ*romX*, Δ*romY,* and Δ*mglC* strains were stimulated by Frz signaling and showed the *frz*^{GOF} phenotype described above (Supplementary Figure 2). All strains accumulated FrzZ-mVenus but showed degradation at a size of ~50 kDa, which cannot be assigned (Supplementary Figure 1). Additionally *frzZ-mVenus* mutants in Δ*mglA*, Δ*mglB*, and Δ*romR* strains showed low levels of free mVenus.

As previously published, the polar localization of FrzZ-mVenus was abolished in a Δ*mglA* strain (Figure 12 B upper panel) (Kaimer & Zusman, 2013). In agreement with published reports and FrzZ depending on MglA for polar localization, cluster frequency was increased in a Δ*mglB* strain, in which MglA localization is increased and more bipolar (Leonardy *et al.*, 2010, Kaimer & Zusman, 2013, Carreira *et al.*, 2020, Zhang *et al.*, 2010). Conversely, polar FrzZ-mVenus localization was reduced in Δ*romX* and Δ*mglC* strains, in which MglA polar localization is decreased (Szadkowski *et al.*, 2019, Carreira *et al.*, 2023). Surprisingly, polar cluster frequency decreased in the Δ*romY* strain in which MglA localizes as in the Δ*mglB* strain (Szadkowski *et al.*, 2022). In contrast, FrzZ-mVenus polar localization was increased in a Δ*romR* strain where the polar localization of MglA is highly reduced (Keilberg *et al.*, 2012) (Figure 12 B upper panel and C, data is also plotted as scatterplots in Supplementary Figure 3).

FrzZ-mVenus localization was also tested in a *frzCD*^{GOF} strain (in which the amount of FrzZ~P and its polar localization is increased) in the absence of each individual polarity protein. Without MglA, FrzZ-mVenus localization to the pole was strongly reduced, but polar localization was still detected in a small fraction of cells (Figure 12 B lower panel and C). Moreover, cytoplasmic clusters in subpolar or more midcell regions oscillated along the cell body in a few cells (Figure 12 D). In Δ*romR*, Δ*romX*, and Δ*mglC* strains, FrzZ-mVenus localization was similar or slightly decreased compared to the *frzCD*^{GOF} strain. In the absence of the GAP proteins MglB and RomY, bipolar localization of FrzZ-mVenus was increased (Figure 12 B lower panel and C, data is also plotted as scatterplots in Supplementary Figure 3).

These observations support that MglA is important for polar FrzZ localization. However, MglA is not essential because FrzZ can still localize to a pole in a small fraction of cells in the Δ*mglA frzCD*^{GOF} mutant. Also, in a Δ*romR* and Δ*romX* mutants, in which MglA is mostly diffused, FrzZ-mVenus polar localization is even increased compared to otherwise WT, arguing against the importance of MglA for polar localization of FrzZ-mVenus. Finally, FrzZ-mVenus accumulated in cytoplasmic clusters in the absence of MglA in the *frzCD*^{GOF} strain. Because this candidate approach did not result in a clear candidate for recruiting FrzZ-mVenus to the leading pole, we decided to use alternative strategies to identify FrzZ interaction partners.

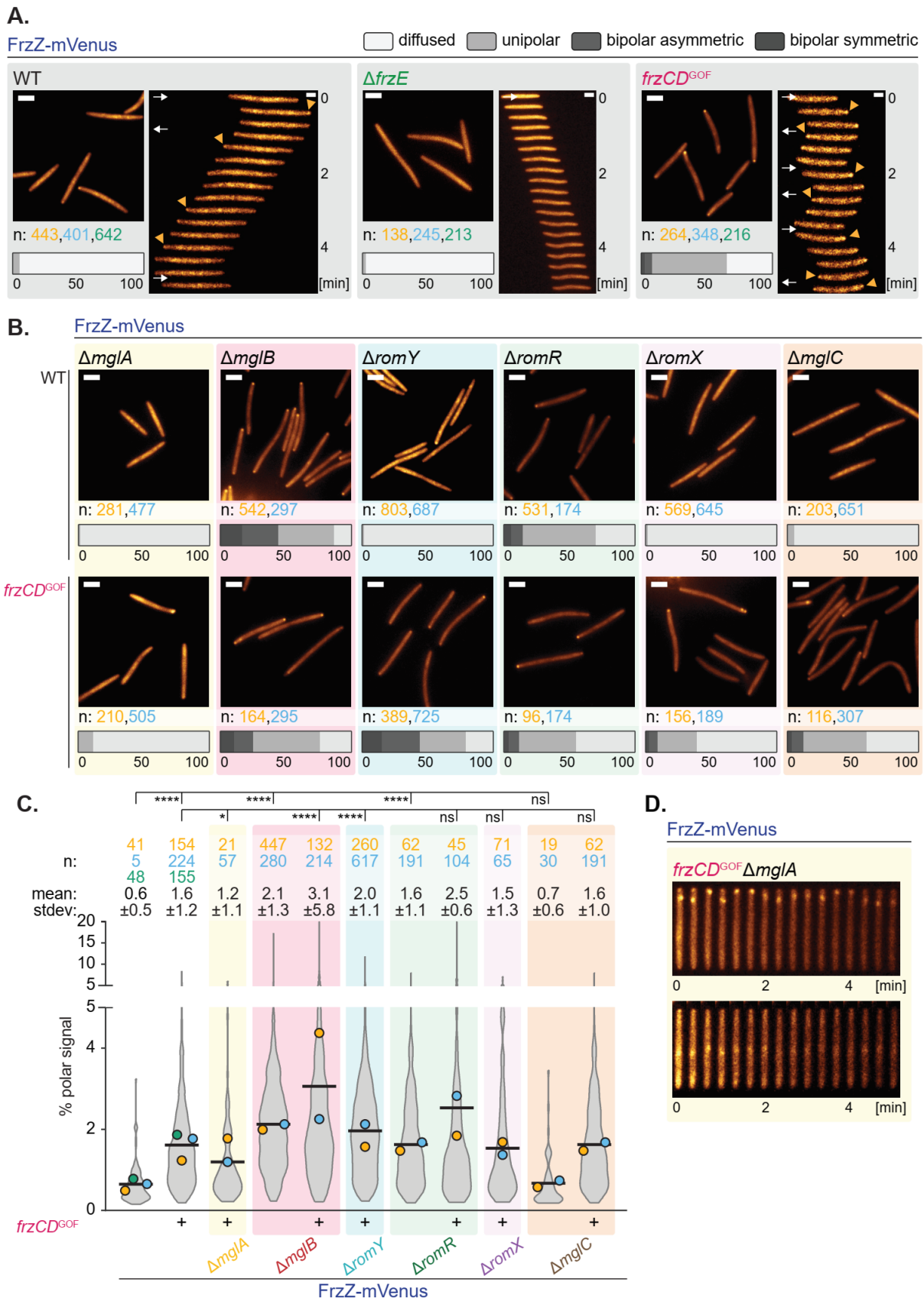

Figure 12: **Localization of FrzZ-mVenus in polarity module mutants.** Fluorescence microscopy analysis of *frzZ::frzZ-mVenus* in *frz* mutants **(A)** and polarity mutants **(B)**. Cells were analyzed for the presence of polar localization. Pictures show representative cells of each strain in exponential growth phase. Cells were imaged on chitosan-coated slides in MC7 buffer after incubation for 1 h. Number of

cells analysed for each replicate (n) is shown below microscopy images in orange, blue and green. The polar regions are defined as the parts of a cell within a distance of 0.65 µm, from a tip of a cell. A pole was considered to have a polar cluster if a contiguous set of at least three pixels above the threshold intensity was found in the polar region. Horizontal bars show the percentage of cells with a polar and diffuse localization pattern according to the color code. Scale bar, 2 µm. In (A), straightened timelapse montages of a representative cell for each strain. Yellow arrows indicate the appearance of a cluster, white arrows indicate direction of movement. Images were recorded every 20 s. All experiments were performed with strains expressing *frzZ-mVenus* from the native site. **(C)** Violin plots show the percentage of the total polar fluorescence signal in cells with FrzZ-mVenus polar cluster(s). Note that the violin plots only include cells having a polar clusters. The means from three replicates are shown as symbols in orange, blue, and green. The average mean based on all three replicates is shown as black line. The number of trajectories analyzed per replicate (n) and mean polar signal with standard deviation for each strain are shown above the graph. Kruskal-Wallis test was used for statistical analysis. “ns”, not significant ($p>0.05$); “*“, $p<0.05$; and “****” $p<0.0001$. **(D)** Straightened timelapse montages of representative cells showing dynamic cytoplasmic clusters. Images were recorded every 20 s.

3.1.2 FrzZ and PixA localize in proximity of each other in a *frzCD*^{GOF} mutant

We performed Co-Immunoprecipitation experiments to identify interaction partners of FrzZ. To this end, we used FrzZ-mVenus as our bait protein in Δ*frzE* and *frzCD*^{GOF} strains. Gratifyingly, FrzZ-mVenus was enriched in samples of both backgrounds, while FrzE was enriched in samples of a *frzCD*^{GOF} strain (data not shown). However, we did not identify additional potential targets, suggesting that the interaction of FrzZ at the pole might be too transient or that active FrzZ~P is dephosphorylated too quickly for interaction partners to be identified using Co-Immunoprecipitation experiments.

Therefore, we opted for a second method: Proximity labeling. In the past ten years, proximity-dependent biotinylation techniques have expanded the ability to study protein associations ranging from weak and transient to stable protein interactions (May & Roux, 2019). In the BioID method, a promiscuous biotin ligase catalyzes the biotinylation of Lys residues on proteins within a distance of approximately 10 nm upon activation by biotin. The pool of biotinylated proteins is then enriched by a pull-down method using streptavidin-coated beads and subsequently identified via mass spectrometry after tryptic digest (Figure 13) (May & Roux, 2019). This method is well established and widely used in, e.g., mammalian cells, plant protoplasts, parasites, mice, or yeast but only scarcely used to decode bacterial protein interactomes (May & Roux, 2019, Kimmel *et al.*, 2022, D'Costa *et al.*, 2019, Santin *et al.*, 2018). Here, we first established biotin ligase miniTurbo-based proximity labeling in *M. xanthus*, a through directed evolution engineered variant leading to higher efficiency of the method compared to the original BioID method (described in 5.6.5) (Branon *et al.*, 2018).

Figure 13: Overview of the biotin ligase miniTurbo-based proximity labeling method. A miniTurbo fusion protein biotinylates proteins in close proximity. Proteins are enriched using Streptavidin beads. After processing, isolated proteins are identified via mass spectrometry.

The *frzZ-miniTurbo* allele was integrated at the native site in *frzCD*^{GOF} and Δ*frzE* strains. These two strains result in high levels of FrzZ~P or no FrzZ~P, respectively (Kaimer & Zusman, 2013). As a negative control, a *miniTurbo-FLAG* allele was expressed under the control of the native *frzZ* promoter from the Mx8 *attB* site to have the same level of the two miniTurbo variants. *miniTurbo-flag* was also expressed in a *frzCD*^{GOF} and a Δ*frzE* background to compare with the corresponding *frzZ-miniTurbo* strains. All four strains had the expected motility phenotypes documenting that FrzZ-MiniTurbo-FLAG is active and also showed accumulation of the miniTurbo variants (Figure 14 A-C). Experiments were performed using cells attached to a surface.

A total of 1538 proteins were identified in the biotinylated samples, among which seven were significantly enriched in the FrzZ-miniTurbo samples compared to the negative control after applying a threshold (log_2ratio>3; p-value<0.005) (Figure 14 D, Table 1). Gratifyingly, FrzZ (1 (number refers to numbering in Fig. 14D)) was enriched in both the *frzCD*^{GOF} and the Δ*frzE* strain. The same was true for miniTurbo (2), suggesting that it is more stably accumulating or has easier access to the beads when fused to FrzZ. Moreover, FrzE, which phosphorylates FrzZ, was enriched in the *frzCD*^{GOF} strain, providing strong evidence that the method can successfully identify FrzZ interaction partner(s). We observed that the PilZ-domain protein Mxan_0961 (3) and the hypothetical protein Mxan_1142 annotated as Plectin1 (4) were enriched in both strains. Deletion of *mxan_0961* did not result in an aberrant phenotype in motility or development (Kuzmich *et al.*, 2021). Excitingly, we observed that PixA (Mxan_1087) (6) was only enriched in the *frzCD*^{GOF} strain, suggesting that FrzZ is in close proximity to PixA in its phosphorylated form. Proteins of the polarity module were not significantly enriched in proximity labeling experiments.

PixA is a PilZ-RR protein and was previously shown to be involved in regulating the reversal frequency (Kuzmich *et al.*, 2021).

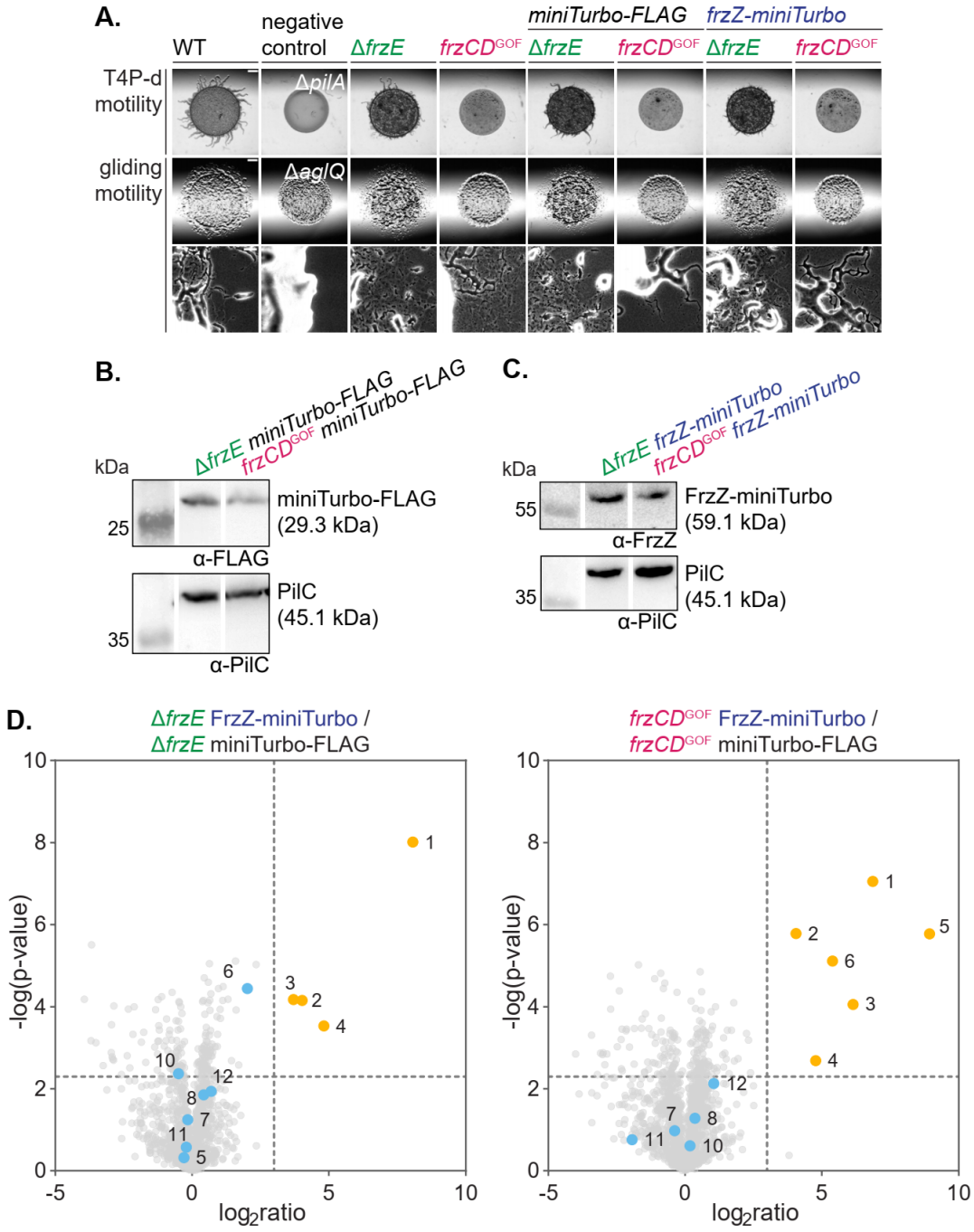

Figure 14: **Proximity labeling using FrzZ-miniTurbo. (A)** Motility assay of mutants expressing *miniTurbo-flag* from the Mx8 *attB* site and *frzZ-miniTurbo* from the native site in a Δ*frzE and frzCD*^{GOF} strains. T4P-dependent motility was tested on 0.5 % agar. Gliding motility was tested on 1.5 % agar. Scale bars from top to bottom: 1 mm, 1 mm, and 50 µm. (**B & C**) Immunoblot analysis of cell lysates of exponentially grown cells expressing *miniTurbo-FLAG* from the Mx8 *attB* site **(B)** and *frzZ-miniTurbo* from the native site **(C)** in a Δ*frzE and frzCD*^{GOF} mutant using α-FLAG or α-FrzZ and α-PilC antibodies as a loading control Cell lysate from the same number of cells was loaded per lane. **(D)** Biotinylated proteins enriched by FrzZ-miniTurbo. Δ*frzE* FrzZ-miniTurbo was compared to Δ*frzE* miniTurbo-FLAG (left) and *frzCD*^{GOF} FrzZ-miniTurbo was compared to *frzCD*^{GOF} miniTurbo-FLAG (right). The X-axis represents the $\log_2$ratio of normalized values of the individual protein. The Y-axis represents the statistical significance of the corresponding targets. Dashed lines represent the threshold ($\log_2$ratio>3; -log(p-value)>-Log(0.005)). Orange points represent significantly enriched proteins. Blue points represent proteins of interest that were not significantly enriched. Numbers correspond to proteins listed in Table 1.

Table 1: **Pulled down biotinylated proteins in the proximity of FrzZ [1].**

		Δ*frzE*		*frzCD*^{GOF}	
No.	**Protein**	**log2ratio**	**-log(p-value)**	**log2ratio**	**-log(p-value)**
1	FrzZ	8.07	8.01	6.86	7.05
2	miniTurbo	4.02	4.15	4.05	5.78
3	MXAN_0961	3.71	4.18	6.14	4.06
4	MXAN_1142	4.81	3.53	4.78	2.69
5	FrzE	-0.29	0.32	8.94	5.43
6	PixA	2.02	4.44	5.39	5.11
7	MglA	-0.16	1.25	-0.38	0.98
8	MglB	0.42	1.85	0.36	1.28
9	MglC	-	-	-	-
10	RomR	-0.49	2.37	0.18	0.61
11	RomX	-0.21	0.58	-1.94	0.76
12	RomY	0.70	1.94	1.05	2.13

To further support that PixA and FrzZ~P are in close proximity, we performed the inverse experiment. For this, we constructed strains expressing *pixA-miniTurbo-FLAG* from the *18-19* site under the control of the vanillate promoter because an endogenous fusion was not functional (data not shown). The fusion protein was expressed in Δ*pixA*, Δ*frzE*Δ*pixA*, and *frzCD*^{GOF}Δ*pixA* backgrounds to elucidate its interactions at different activity levels of Frz signaling. As a negative control, *sfGFP-miniTurbo-FLAG* was expressed from the *18-19* site under the control of the vanillate promoter in WT, Δ*frzE*, and *frzCD*^{GOF} backgrounds. The vanillate concentration was adjusted by assessing the functionality of different PixA-miniTurbo-FLAG levels in a motility assay (Figure 15 A). To this end, WT and *frzCD*^{GOF} strains were spotted onto 0.5 % CTT 0.5 % agar plates supplemented with 0, 5, 10, and 20 µM vanillate. At a concentration of 10 µM vanillate, a Δ*pixA* strain expressing *pixA-miniTurbo-FLAG* showed WT-like flares, and a *pixA-miniTurbo-FLAG frzCD*^{GOF}Δ*pixA* strain showed the distinct Frz GOF phenotype. With 20 µM vanillate added, both strains exhibited a frizzy colony morphology suggesting that these strains accumulate increased levels of PixA (see 3.1.3). The colony morphology of strains expressing *sfGFP-miniTurbo-FLAG* did not change with increasing vanillate concentrations. 10 µM vanillate was added ON to induce the expression of miniTurbo proteins and led to similar accumulation levels. sfGFP-miniTurbo-FLAG showed degradation into miniTurbo-FLAG (Figure 15 B). Induction using biotin and subsequent experimental steps were performed as for FrzZ-miniTurbo experiments.

In order to identify significantly enriched proteins, strains expressing *pixA-miniTurbo-FLAG* in WT, Δ*frzE* and *frzCD*^{GOF} backgrounds were compared with their corresponding *sfGFP-*

[1] No. refers to the individual target number depicted in Figure 14 D. Black text indicates proteins enriched above the set threshold. Grey text indicates proteins enriched below the threshold.

miniTurbo-FLAG control strain. In these proximity labeling experiments, a total of 2158 proteins were identified, of which 84 were found to be significantly enriched after applying a threshold (log_2ratio>3; p-value<0.005) (

Supplementary Table 1). Of these 84 proteins, we found eight particularly interesting (Figure 15 C, Table 2).

The bait protein PixA (1) was enriched in WT and *frzCD*^{GOF}, while it was not significantly enriched (but close to the set threshold) in a Δ*frzE* background. Importantly, FrzZ (5) was enriched in WT and *frzCD*^{GOF} but not in the *ΔfrzE* backgrounds, confirming the link between the two proteins and supporting that phosphorylated FrzZ and PixA interact more strongly than non-phosphorylated FrzZ and PixA. PglH (2) was highly enriched all backgrounds, and is a RR-PATAN domain protein previously shown to be involved in regulating the reversal frequency (Yu & Kaiser, 2007) (this protein will be discussed in more details in 3.4). Mxan_5199 (3) is a Forkhead-associated (FHA)/GGDEF domain protein. FHA proteins are protein-protein interaction domains specific for phosphoproteins with a preference for phospho-threonines (Almawi *et al.*, 2017). Generally, GGDEF proteins are diguanylate cyclases (Ryjenkov *et al.*, 2005). In a previous study, deletion of *mxan_5199* did not lead to a defect in T4P-dependent motility, gliding motility, or development (Skotnicka *et al.*, 2016a, Skotnicka *et al.*, 2016b). PilS2 (4) is a transmembrane protein containing a HAMP, histidine kinase, and ATPase domain. *pilS2* is encoded in the *pil* locus and the deletion of *pilS2* did not lead to a motility defect (Bretl *et al.*, 2016). Mxan_5812 (6) is a leucine-rich repeat protein with no annotated domains (https://www.uniprot.org/uniprotkb/Q1D074/entry). Proteins with these repeats are particularly suitable for protein-protein interactions (Kobe & Kajava, 2001). Mxan_6866 (7) is a histidine kinase with two PAS domains, generally involved in signal sensing (https://www.ebi.ac.uk/interpro/protein/UniProt/Q1CX90/) (Taylor & Zhulin, 1999). RomY (8) is the co-GAP of the polarity module, which regulates the GTP-bound state of MglA (Szadkowski *et al.*, 2022). Please note that Mxan_6866 and RomY were not significantly enriched in a previous experiment using PixA-miniTurbo-FLAG (data not shown).

Interestingly, (almost all) enriched proteins of interest were found in all three analyzed strains, suggesting that some interaction partners of PixA could be independent of the activity of Frz signaling. Importantly, FrzZ was enriched when Frz signaling was active and FrzZ could be phosphorylated, confirming our previous findings. PglH is an exciting candidate since it was already found to be involved in the regulation of reversals. Although tempting, it is unclear if PixA closes the gap between Frz signaling and the polarity module via a potential interaction with RomY since it was not enriched in a previous proximity labeling experiment.

These proximity labeling experiments gave us strong evidence that FrzZ and PixA interact and that this interaction might depend on active Frz signaling.

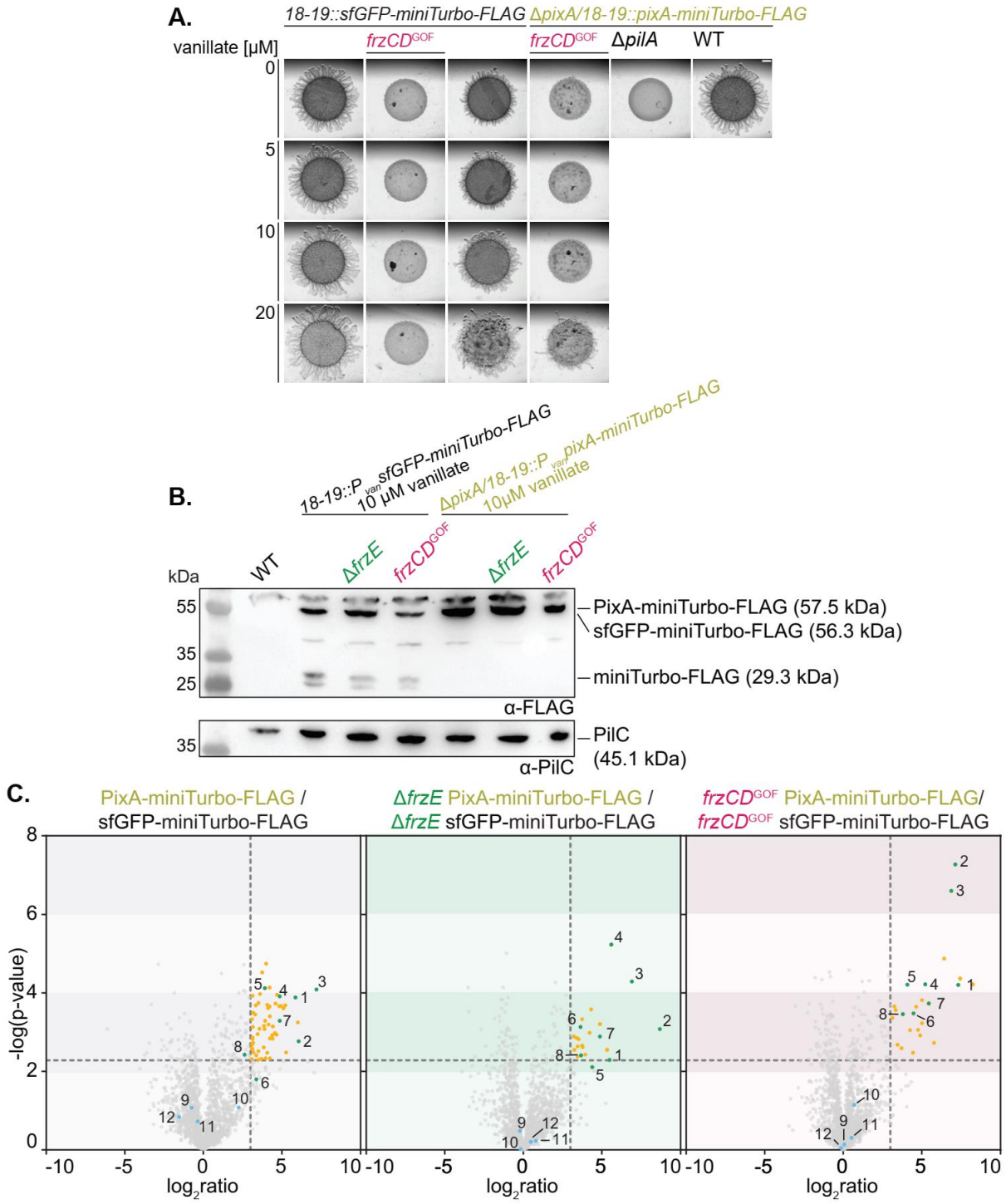

Figure 15: **Proximity labeling using PixA-miniTurbo-FLAG. (A)** Motility assay assessing phenotypes of mutants expressing different levels of *sfGFP-miniTurbo-FLAG* and *pixA-miniTurbo-FLAG* in WT and *frzCD*^{GOF} backgrounds from the *18-19* site expressed under the control of the vanillate promoter. 0, 5, 10, and 20 μM vanillate were added to 0.5 % agar to test T4P-dependent motility. Scale bar, 1 mm. **(B)** Immunoblot analysis of cell lysates of exponentially grown cells expressing *sfGFP-miniTurbo-FLAG* from the *18-19* site and *pixA-miniTurbo-FLAG* from the native site in a WT, Δ*frzE and frzCD*^{GOF} mutant using α-FLAG and α-PilC antibodies as a loading control. Cell lysate from the same number of cells was loaded per lane. It was tested for the presence of sfGFP-miniTurbo-FLAG (56.3 kDa) (29.3 kDa),

PixA-miniTurbo-FLAG (57.5 kDa), and PilC (45.1 kDa). **(C)** Volcano plots of pulled-down biotinylated proteins in the proximity of PixA. PixA-miniTurbo-FLAG was compared to sfGFP-miniTurbo-FLAG (left), Δ*frzE* PixA-miniTurbo-FLAG was compared to Δ*frzE* sfGFP-miniTurbo-FLAG (middle), and *frzCD*^{GOF} PixA-miniTurbo-FLAG was compared to *frzCD*^{GOF} sfGFP-miniTurbo-FLAG (right). The X-axis represents the log_2ratio of normalized values of the individual protein. The Y-axis represents the statistical significance of the corresponding targets. Dashed lines represent the threshold (log_2ratio>3; -log(p-value)>-Log(0.005)). Orange points represent significantly enriched proteins. Green points represent proteins of interest that were statistically significantly enriched. Blue points represent proteins of the Frz system. Numbers correspond to proteins listed in Table 2.

Table 2: **Interesting candidates of pulled-down biotinylated proteins in the proximity of PixA [2].**

		WT		Δ*frzE*		*frzCD*^{GOF}	
No.	**Protein**	**log2ratio**	**-log(p-value)**	**log2ratio**	**-log(p-value)**	**log2ratio**	**-log(p-value)**
1	PixA	5.85	3.89	5.49	2.29	7.31	4.20
2	PglH	6.07	2.77	8.69	3.08	7.13	7.27
3	Mxan_5199	7.20	4.09	6.91	4.29	6.88	6.60
4	PilS2	4.86	3.91	5.60	5.23	5.21	4.22
5	FrzZ	3.91	4.12	4.38	2.11	4.08	4.21
6	Mxan_5812	3.37	1.80	3.64	3.13	4.47	3.48
7	Mxan_6866	4.86	3.29	4.87	2.89	5.44	3.73
8	RomY	2.63	2.43	3.67	2.41	3.80	3.46
9	FrzE	1.69	2.24	-0.41	0.36	2.61	3.16
10	FrzCD	-0.75	1.08	-0.22	0.48	0.07	0.14
11	FrzX	2.26	1.08	-0.16	0.02	0.70	1.15
12	FrzA	-0.36	0.73	0.80	0.23	0.52	0.30
13	FrzG	-1.54	0.84	0.48	0.21	-0.13	0.05

3.1.3 PixA is epistatic to FrzZ

PixA was reported to inhibit reversals, while FrzZ~P promotes reversals (Kuzmich *et al.*, 2021, Inclan *et al.*, 2007).

To investigate the relation between PixA and the Frz system, we performed epistasis analyses using the reversal frequency as a readout. For this, we introduced the Δ*pixA* mutation into the following *frz* mutants: Δ*frzZ*, Δ*frzX*, Δ*frzZ*Δ*frzX*, Δ*frzE*, *frzCD*^{GOF}. Moreover, we generated strains that overexpress *pixA-FLAG* in otherwise WT and in a *frzCD*^{GOF} mutant.

We confirmed that the Δ*pixA* strain has a hyperreversing phenotype that could be complemented by ectopically expressing *pixA-FLAG* under the control of its native promoter from the Mx8 *attB* site (Figure 16 A) (Kuzmich *et al.*, 2021). Moreover, a strain ectopically expressing *pixA-FLAG* under the control of the strong *pilA* promoter accumulated PixA-FLAG

[2] No. refers to the individual target number depicted in Figure 15 C. Black text indicates proteins enriched above the set threshold. Grey text indicates proteins enriched below the threshold.

at a higher level compared to the *P*$_{nat}$*pixA-FLAG* strain, and these cells were hyporeversing (Figure 16 A and B).

As described above and consistent with published data (Inclan *et al.*, 2007, Guzzo *et al.*, 2018, Blackhart & Zusman, 1985), cells of Δ*frzZ*, Δ*frzX,* Δ*frzZ*Δ*frzX*, and Δ*frzE* mutants were hyporeversing (Figure 16 A). Importantly, the Δ*frzZ*Δ*pixA* strain was hyperreversing and not significantly different from the Δ*pixA* mutant, demonstrating that PixA is epistatic to FrzZ. By contrast, Δ*frzX*Δ*pixA*, Δ*frzZ*Δ*frzX*Δ*pixA*, and Δ*frzE*Δ*pixA* all had a significantly decreased reversal frequency compared to the Δ*pixA* mutant and a significantly increased reversal frequency compared to the corresponding *frz* mutants (Figure 16 A). These observations support that (i) PixA acts downstream of FrzZ in the same pathway; (ii) PixA and FrzX act in independent pathways; and (iii) PixA can inhibit reversals in the absence of FrzX and FrzZ.

We then investigated the role of PixA in the *frzCD*^{GOF} strain. As described above, the *frzCD*^{GOF} strain is hyperreversing (Bustamante *et al.*, 2004). The reversal frequency of the *frzCD*^{GOF}Δ*pixA* mutant was not significantly different from that of the *frzCD*^{GOF} mutant. However, when *pixA-FLAG* was overexpressed, the reversal frequency was significantly reduced compared to the *frzCD*^{GOF} strain, showing that a high level of PixA can reduce Frz-dependent reversals.

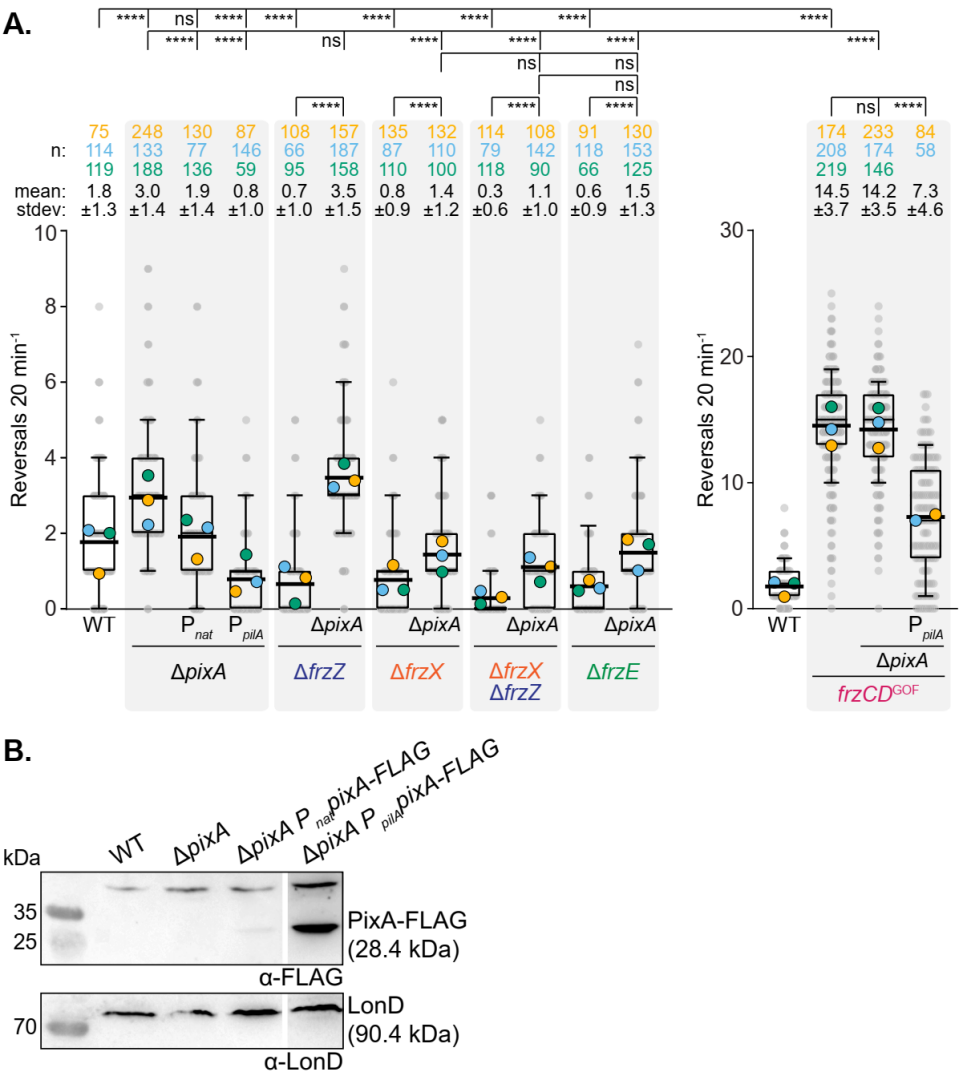

Figure 16: **Reversal assay of Δ*pixA frz* mutants. (A)** Single-cell gliding reversal assay on 0.5 % CTT 1.5% agarose of Δ*pixA frz* mutants. Boxplots show the measured reversal frequency monitored as the number of directional changes per 20 min. Each dot in the scatterplot represents the reversal frequency of one cell. Boxes enclose the 25th and 75th percentile. Whiskers enclose the 5th and 95th percentile. The median is shown as a thin line in the box. The overall mean is shown as thick black line. The mean of each replicate is shown as a symbol in orange, blue, and green. The number of trajectories analyzed per replicate (n) and mean reversal frequencies for each strain are shown above the graph. Kruskal-Wallis test was used for statistical analysis. "ns", non-significant (p>0.05); and "****, p<0.0001. The Left and right plots were separated for better visibility of single points of the left plot. Note the different y-axis dimensions. WT on the right is the same as shown on the left and shown for comparison. WT and *frz* mutant reversals are the same as in Figure 10 and are shown for comparison. **(B)** Immunoblot analysis of lysates of exponentially grown cells using α-FLAG and α-LonD antibodies as a loading control. WT was used as a control. Cell lysate from the same number of cells was loaded per lane.

Our data suggest a pathway in which PixA inhibits reversals, and FrzZ~P inhibits PixA activity, ultimately leading to a reversal (Figure 17 A). This pathway is supported by the following observations: First, PixA is epistatic to FrzZ; second, PixA inhibits reversals in the absence of FrzZ and FrzX; third, during high Frz activity with high levels of FrzZ~P, lack of PixA does not have an effect on the reversal frequency, while an excess of PixA-FLAG does. Moreover, our

data support that FrzX stimulates reversals independently of PixA, suggesting that the Frz signal is transduced via two pathways (Figure 17 B). One depends on FrzZ and PixA, and one depends on FrzX.

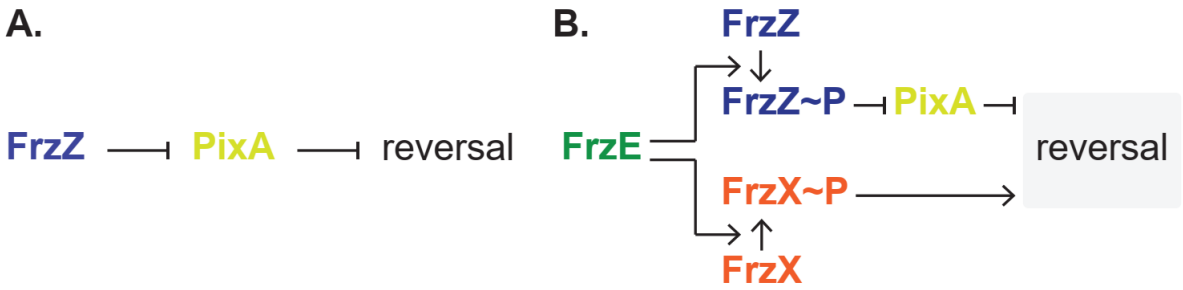

Figure 17: **PixA acts in the FrzZ branch of the Frz output pathway.** (A) PixA inhibits reversal and is inhibited by FrzZ, which causes a switch in polarity. (B) The two pathways of Frz signaling.

3.1.4 PixA stimulates the polar localization of FrzZ-mVenus

So far, we have established that PixA is epistatic to FrzZ and in our model, FrzZ-P targets PixA to inhibit it from repressing reversals. To further understand the interaction between the Frz system and PixA, we asked whether PixA has an impact on FrzZ localization. To this end, we introduced the *pixA* deletion into the WT and the *frzCD*^{GOF} strains expressing *frzZ-mVenus* endogenously. FrzZ-mVenus accumulated in all tested strains (Figure 18 A). As previously described (Kuzmich *et al.*, 2021), in motility assays, the hyperreversing phenotype of a Δ*pixA* mutant resulted in shorter flares on 0.5 % agar and reduced colony expansion on 1.5 % agar, (Figure 18 B). As expected based on our previous observations, a *frzCD*^{GOF} Δ*pixA* mutant showed the same phenotype as a *frzCD*^{GOF} mutant.

When analyzing fluorescence microscopy images for polar clusters, we observed that the frequency of cells with a polar FrzZ-mVenus in the Δ*pixA* strain was decreased compared to an otherwise WT strain (Figure 18 C). Also, in the *frzCD*^{GOF}Δ*pixA* mutant, the frequency of cells with a polar cluster was lower than in the *frzCD*^{GOF} mutant (Figure 18 C). Furthermore, the polar signal in cells with clusters was decreased in a Δ*pixA frzCD*^{GOF} mutant compared to the polar signal of FrzZ-mVenus in a *frzCD*^{GOF} strain containing PixA, suggesting that less FrzZ is localizing to the pole (Figure 18 D, data is also plotted as scatterplots in Supplementary Figure 3). Clusters in a *frzCD*^{GOF}Δ*pixA* mutant could still localize to the leading cell pole (Figure 18 C).

This data suggests that PixA, although not essential, enhances FrzZ localization to the pole.

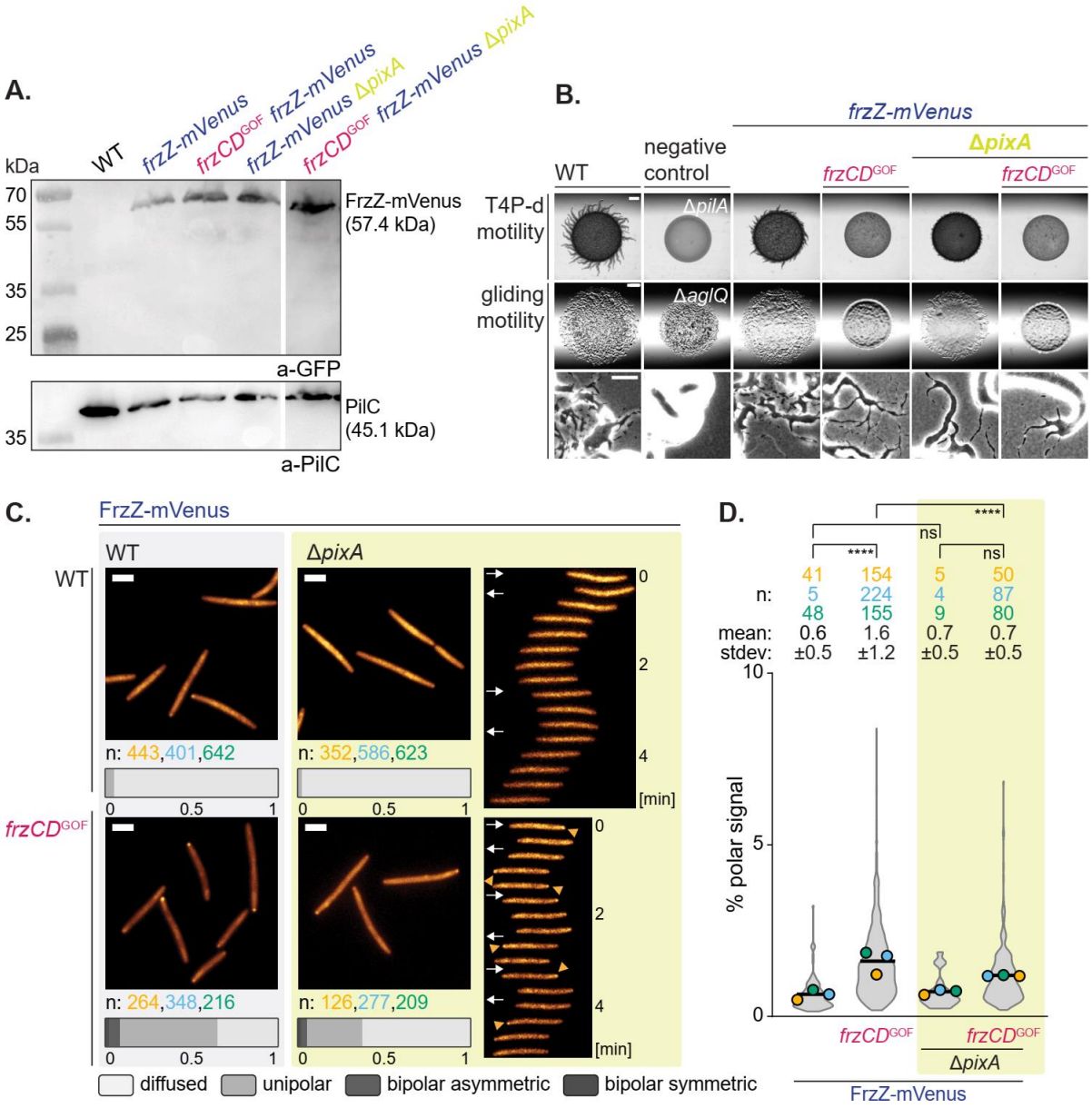

Figure 18: **Localization of FrzZ-mVenus in the absence of PixA. (A)** Immunoblot analysis of lysates of exponentially grown cells using α-GFP and α-PilC antibodies as a loading control. WT was used as a control. Cell lysate from the same number of cells was loaded per lane.**(B)** Motility assay of *frzZ::frzZ-mVenus* Δ*pixA* mutants. T4P-dependent motility was tested on 0.5 % agar. Gliding motility was tested on 1.5 % agar. Scale bars from top to bottom: 1 mm, 1 mm, and 50 µm. **(C)** Fluorescence microscopic analysis of FrzZ-mVenus in the absence of PixA. Images show representative cells of each strain in the exponential growth phase. Cells were imaged on chitosan-coated slides in MC7 buffer after incubation for 1 h. Number of cells analyzed for each replicate (n) is shown below microscopy pictures in orange, blue, and green. The polar regions are defined as the parts of a cell within a distance of 0.65 µm, from a tip of a cell. A pole was considered to have a polar cluster if a contiguous set of at least three pixels above the threshold intensity was found in the polar region. Horizontal bars show the percentage of cells with a polar and diffuse localization pattern according to the color code. Scale bar, 2 µm. Straightened timelapse montages of a representative cell for strains lacking PixA. Yellow arrows indicate the appearance of a cluster, white arrows indicate direction of movement. Images were taken every 20 s. Pictures and analysis of cells expressing *frzZ-mVenus* in the presence of PixA are the same as in Figure 12 A and included for comparison. **(D)** Violin plots show the percentage of the total polar fluorescence signal in cells with FrzZ-mVenus polar cluster(s). Note that the violin plots only include cells having polar clusters. The means from three replicates are shown as symbols in orange, blue, and green. The average mean based on all three replicates is shown as black line.The number of trajectories

analyzed per replicate (n) and mean polar signal with standard deviation for each strain are shown above the graph. Kruskal-Wallis test was used for statistical analysis. “ns”, not significant (p>0.05); “*” p<0.05; and “****” p<0.0001.

3.1.5 PixA localizes to the pole depending on the Frz system

In order to elucidate the connection between PixA and the Frz system, we determined the localization of PixA. To this end, we constructed strains expressing *pixA-mVenus* from its native site in WT, Δ*frzE*, *frzCD*^{GOF}, Δ*frzZ*, Δ*frzX*, Δ*frzZ* Δ*frzX*, *frzCD*^{GOF} Δ*frzZ*, *frzCD*^{GOF} Δ*frzX*, and *frzCD*^{GOF} Δ*frzX* Δ*frzZ* strains. The PixA-mVenus fusion accumulated in all strains (Supplementary Figure 4 A). Additionally, a low level of free mVenus and a degradation product that cannot be assigned were visible. The *pixA::pixA-mVenus* strain had a significantly higher reversal frequency than the WT but significantly lower than the Δ*pixA* mutant, documenting that the fusion is partially active (Supplementary Figure 4 B). In motility assays, this reversal phenotype most likely led to the differences observed between *pixA-mVenus* Δ*frzZ* and *pixA-mVenus frzCD*^{GOF} Δ*frzX* mutant strains compared to their parent Δ*frzZ* and *frzCD*^{GOF} Δ*frzX* strain, respectively. In a motility assay, the remaining *pixA-mVenus frz* mutants had the same phenotype as their parent strain (Supplementary Figure 4 C).

When analyzing the localization of PixA-mVenus, we found a primarily diffuse localization in the cytoplasm, with approximately 20 % of cells having a faint polar cluster (Figure 19 A, data is also plotted as scatterplots in Supplementary Figure 5). Upon further observation using time-lapse microscopy, we found that these clusters could localize to leading or lagging cell poles. Furthermore, the pole PixA-mVenus localized to, was correlated with reversals frequencies. In WT cells reversing less frequently and moving in one direction only, PixA-mVenus localized to the lagging cell pole, while in WT cells that reversed more frequently, PixA-mVenus localized to the leading cell pole. Clusters at the lagging cell pole appeared between reversals, while clusters at the leading cell pole were visible between reversals and in frames close to a reversal of a cell. However, PixA-mVenus localizing to the leading cell pole was not essential for reversals (Figure 19 A).

We then tested if proteins of the Frz system were responsible for this difference in PixA-mVenus localization (Figure 19 B and C). In a Δ*frzE* mutant, PixA-mVenus cluster frequency and intensity were increased compared to WT. In this mutant, clusters localized exclusively to the lagging cell pole. In a *frzCD*^{GOF} strain, cluster frequency and intensity were also increased compared to WT. Strikingly, they localized to the leading cell pole. To test if this localization change was caused by the two known outputs of the Frz system, we examined the localization of PixA-mVenus in the absence of FrzZ and/or FrzX (Figure 19 B and C). Remarkably, cluster frequency and intensity increased even more in a Δ*frzZ* mutant than in a Δ*frzE* mutant.

Clusters localized to the lagging cell pole. These lagging cell pole clusters localized for more consecutive frames to the pole than in WT and Δ*frzE* strains. In contrast, the lack of FrzX only slightly affected PixA localization concerning cluster intensity but not frequency. The latter finding was further supported as cells lacking FrzX and FrzZ had a PixA-mVenus localization phenotype similar to the Δ*frzZ* mutant with increased cluster frequency and intensity. Furthermore, clusters localized stably at the lagging cell pole.

Since PixA-mVenus localized to the leading cell pole in a *frzCD*^{GOF} mutant, we investigated if FrzZ~P and/or FrzX~P is needed to relocate PixA to this pole (Figure 19 B and C). Indeed, in a *frzCD*^{GOF} Δ*frzZ* mutant, clusters were no longer localizing to the leading but exclusively to the lagging cell pole. Surprisingly, we observed decreased cluster frequency and intensity in such cells compared to the Δ*frzZ* mutant. This suggests that PixA-mVenus is somewhat excluded from the lagging cell pole in a *frzCD*^{GOF} mutant. We then tested PixA-mVenus localization in a *frzCD*^{GOF} Δ*frzX* mutant since FrzX~P localizes to the lagging cell pole (Guzzo *et al.*, 2018). Interestingly, in such a strain, clusters were able to localize to the leading cell pole, but the number of cells with a bipolar signal was increased compared to all other examined strains. This suggests that FrzX~P inhibits PixA lagging pole localization. PixA-mVenus showed a similar localization pattern in the *frzCD*^{GOF} Δ*frzX* Δ*frzZ* mutant compared to the Δ*frzX* Δ*frzZ* mutant (although polar signal intensity was slightly increased in the latter strain) in which PixA localized stably to the lagging cell pole. This suggests that the impact of active Frz signaling on PixA is transmitted via the two RRs FrzZ and FrzX.

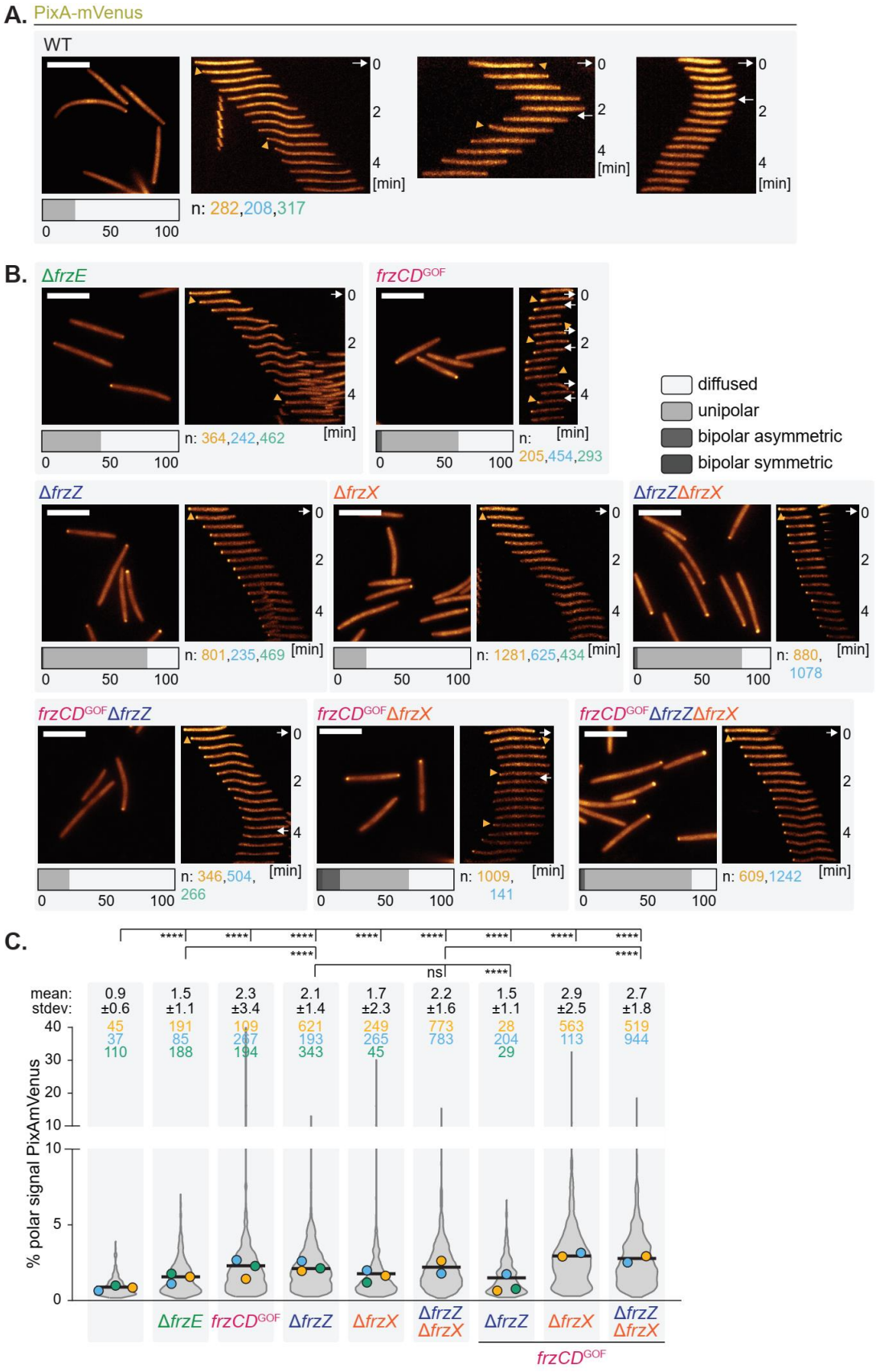

Figure 19: **Localization of PixA-mVenus in *frz* mutants.** Fluorescence microscopic analysis of a *pixA::pixA-mVenus* strain **(A)** and *pixA::pixA-mVenus frz* mutant strains **(B)**. Cells were analyzed for the presence of polar localization. Pictures show representative cells of each strain in exponential growth phase. Cells were imaged on chitosan-coated slides in MC7 buffer after incubation for 1.5 h.

Number of cells analyzed for each replicate (n) is shown below microscopy images in orange, blue and green. The polar regions are defined as the parts of a cell within a distance of 0.65 µm, from a tip of a cell. A pole was considered to have a polar cluster if a contiguous set of at least three pixels above the threshold intensity was found in the polar region. Horizontal bars show the percentage of cells with a polar and diffuse localization pattern according to the color code. Scale bar, 5 µm. Straightened timelapse montages of a representative cell for each strain. Yellow arrows indicate the appearance of a cluster, white arrows indicate direction of movement. Images were recorded every 20 s. **(C)** Violin plots show the percentage of the total polar fluorescence signal in cells with PixA-mVenus polar cluster(s). Note that the violin plots only include cells having polar clusters. The means from all replicates are shown as symbols in orange, blue, and green. The average mean based on all three replicates is shown as black line.The number of trajectories analyzed per replicate (n) and mean polar signal with standard deviation for each strain are shown above the graph. Kruskal-Wallis test was used for statistical analysis. “ns”, not significant (p>0.05); and “****”, p<0.0001.

In summary, PixA is a dynamically localized protein predominantly localizing in the cytoplasm. The protein can localize as clusters to leading and lagging cell poles, and this altering localization was influenced by proteins of the Frz system (Figure 20). Specifically, FrzZ has a strong inhibitory effect on PixA lagging cell pole localization. FrzZ~P is needed for leading cell pole localization, while FrzX~P inhibits PixA lagging cell pole localization. Furthermore, at least one other protein or cue is involved in PixA polar localization in order for it to target the pole, because it was able to localize to the pole in all tested mutants.

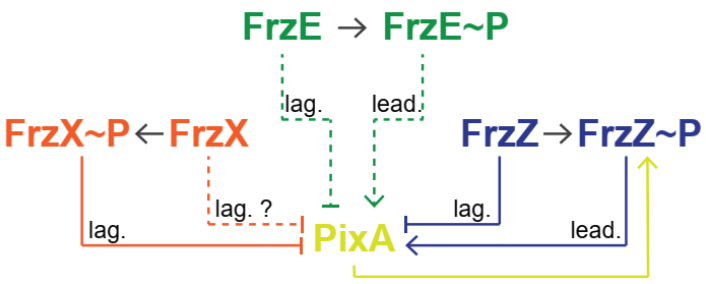

Figure 20: **The Frz system impacts localization of PixA.** Arrows indicate stimulation. T-bars indicate inhibition. Dashed lines indicate possibly indirect relations.

3.1.6 PixA localizes to the lagging pole when overexpressed

As previously described, a mutant that accumulates high levels of PixA-FLAG is hyporeversing. In addition, PixA localization correlated with the activity of the Frz system which regulates reversals. Therefore, we determined the localization of elevated levels of PixA-mVenus to test if a change in localization could lead to the reversal phenotype observed previously.

To this end, we constructed strains expressing *pixA-mVenus* from the Mx8 *attB* site under the control of the strong *pilA* promoter and the putative native promoter as a control. As expected from previous experiments, PixA-mVenus accumulated at elevated levels when expressed

from the *pilA* promoter, while the protein synthesized under the control of the native promoter accumulated at similar levels to the endogenous fusion (Figure 21 A). As described for the PixA-mVenus fusion synthesized from the native site (Supplementary Figure 4 B), the PixA-mVenus fusion was partially functional because the reversal frequency of the P_{nat}*pixA-mVenus* mutant was significantly higher than WT but significantly lower than a Δ*pixA* mutant. Nevertheless, the reversal frequency of a P_{pilA}*pixA-mVenus* mutant was significantly decreased compared to the P_{nat}*pixA-mVenus* mutant (Figure 21 B), showing the same trend as observed before (Figure 16 A).

A strain expressing *pixA-mVenus* from Mx8 *attB* site under the control of the native promoter had a similar localization of PixA-mVenus as the strain in which the protein was expressed from the native site, i.e. the majority of protein localizing diffusely in the cytoplasm while a few cells had weak polar clusters, although, in this case, the cluster frequency was slightly increased compared to the fusion expressed from the native site (Figure 21 C & D, data is also plotted as scatterplots in Supplementary Figure 6 A). As observed previously for the native fusion, clusters localized to the lagging pole when cells were moving unidirectionally or to the leading cell pole when cells were reversing (Figure 21 C). Cells with an elevated level of PixA-mVenus also had most of the protein diffusely in the cytoplasm. Clusters were found more frequently and were of slightly higher intensities than the former strain with native levels of PixA-mVenus (Figure 21 C & D, data is also plotted as scatterplots in Supplementary Figure 6 A). Additionally, clusters localized exclusively at the lagging cell pole and were visible for more consecutive frames than observed for native levels of PixA-mVenus (Figure 21 C).

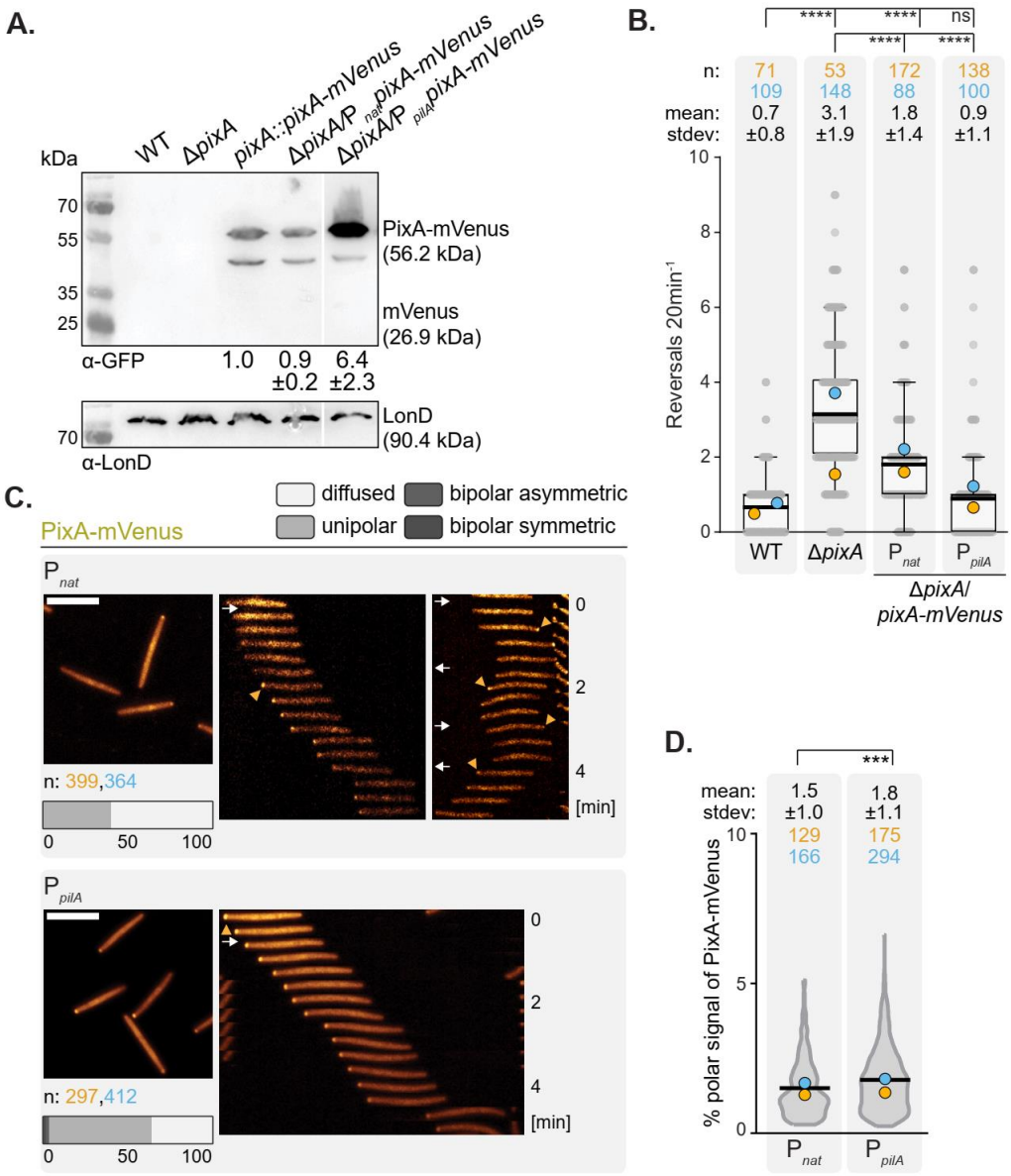

Figure 21: **Localization of elevated levels of PixA-mVenus. (A)** Immunoblot analysis of cell lysates of exponentially grown cells using α-GFP and α-LonD antibodies as a loading control. WT and Δ*pixA* strains were used as a control. Cell lysate from the same number of cells was loaded per lane. Numbers below show the mean accumulation level of PixA-mVenus relative to the *pixA::pixA-mVenus* strain calculated from three biological replicates. **(B)** Single-cell gliding reversal assay on 0.5 % CTT 1.5% agarose. Boxplots show the number of reversals per cell per 20 min. Each dot in the scatterplot represents the number of reversals of one cell. Boxes enclose the 25th and 75th percentile. Whiskers enclose the 5th and 95th percentile. The median is shown as a thin line in the box. The mean of each replicate is shown as a symbol in orange and blue. The mean based on all two experiments is shown as a thick black line. The number of trajectories analyzed per replicate (n) and mean reversal frequencies for each strain are shown above the graph. Kruskal-Wallis test was used for statistical analysis. “ns”, not significant (p>0.05); and “****”, p<0.0001. **(C)** Fluorescence microscopic analysis of *attB::pixA-mVenus* strains. Cells were analyzed for the presence of polar localization. Pictures show representative cells of each strain in exponential growth phase. Cells were imaged on chitosan-coated slides in MC7 buffer after incubation for 1.5 h. Number of cells analyzed per replicate (n) is shown below microscopy images in orange, blue and green. The polar regions are defined as the parts of a cell within a distance of 0.65 µm, from a tip of a cell. A pole was considered to have a polar cluster if a contiguous set of at least three pixels above the threshold intensity was found in the polar region. Horizontal bars show the percentage of cells with a polar and diffuse localization pattern according to the color code. Scale bar, 5 µm. Straightened timelapse montages of a representative cell for each strain. Yellow

arrows indicate the appearance of a cluster, white arrows indicate direction of movement. Images were recorded every 20 s. **(D)** Violin plots show the percentage of the total polar fluorescence signal in cells with PixA-mVenus polar cluster(s). Note that the violin plots only include cells having polar clusters The means from two replicates are shown as symbols in orange and blue. The average mean based on all two replicates is shown as black line. The number of trajectories analyzed per replicate (n), and the mean polar signal for each strain are shown above the graph. Kruskal-Wallis test was used for statistical analysis. "***", $p<0.001$.

3.1.7 The D180 residue of PixA is needed for localization to the pole

It was previously shown that a mutation of the potentially phosphorylated D180 residue in the receiver domain of PixA affected its functionality (Kuzmich *et al.*, 2021). A D180N substitution, did not cause a motility phenotype, while a D180E substitution that potentially mimics the phosphorylated state, had a Δ*pixA* phenotype (Kuzmich *et al.*, 2021). We sought to elucidate how these substitutions affect PixA localization.

To this end, we constructed strains expressing *pixA*^{D180N}*-mVenus* or *pixA*^{D180E}*-mVenus* from the native site. Both variants accumulated at similar levels to the endogenous PixA-mVenus fusion used before and showed the same degradation product and low levels of free mVenus (Figure 22 A).

In a reversal assay, we found that both, the *pixA::pixA*^{D180N}*-mVenus* and *pixA::pixA*^{D180E}*-mVenus* mutant, had a Δ*pixA* hyperreversing phenotype compared to a *pixA::pixA-mVenus* strain. This was in contrast to published results for *pixA::pixA*^{D180N}*-mVenus* (Kuzmich *et al.*, 2021). Previously, it was reported that Frz signaling can be activated by the short-chain alcohol isoamyl alcohol (IAA) (McBride *et al.*, 1992). This activation was observed by an increased reversal frequency of WT upon the addition of 0.075 % IAA (Figure 22 B). All three strains, the Δ*pixA* deletion and the two point mutants, still responded to the activation of Frz signaling by IAA, as shown by an increase in the reversal frequency (Figure 22 B).

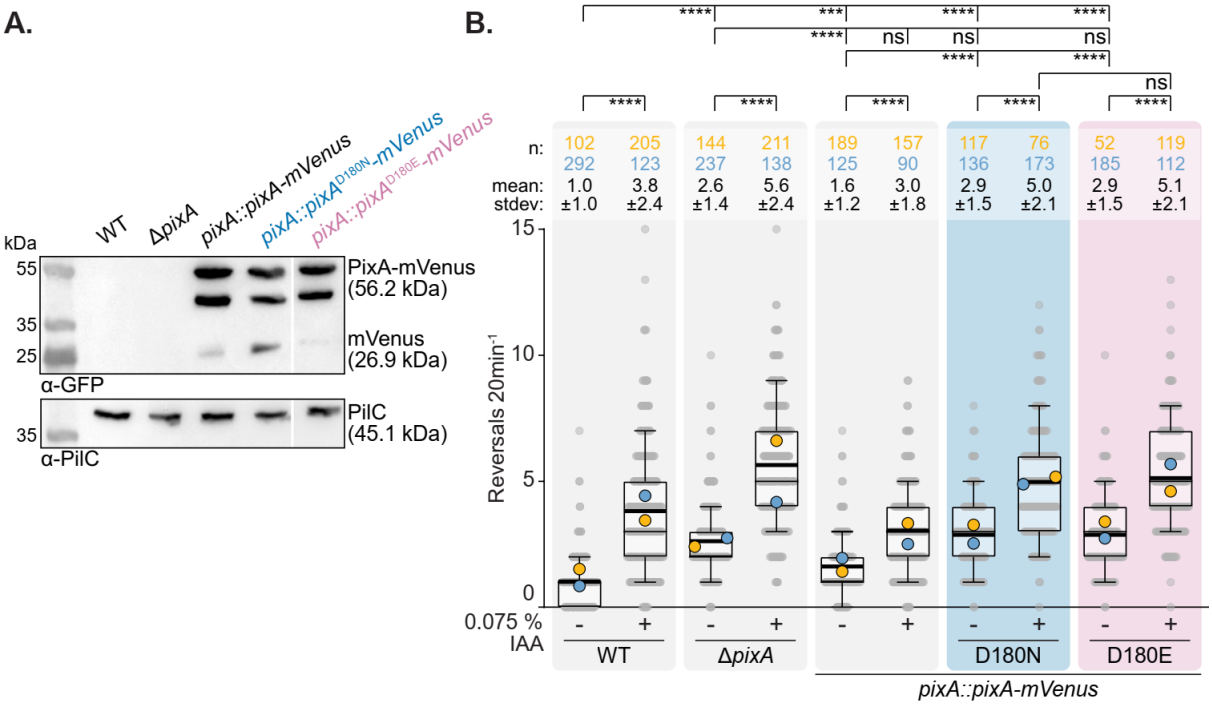

Figure 22: **Reversal phenotype of *pixA-mVenus* D180 point mutants**. **(A)** Immunoblot analysis of cell lysates of exponentially grown using α-GFP and α-PilC antibodies as a loading control. WT and Δ*pixA* strains were used as a control. Cell lysate from the same number of cells was loaded per lane **(B)** Single-cell gliding reversal assay on 0.5 % CTT 1.5% agarose. Boxplots show the number of reversals per cell per 20 min. Each dot in the scatterplot represents the number of reversals of one cell. Boxes enclose the 25th and 75th percentile. Whiskers enclose the 5th and 95th percentile. The median is shown as a thin line in the box. The mean of each replicate is shown as a symbol in orange and blue. The mean based on all two experiments is shown as a thick black line. The number of trajectories analyzed per replicate (n) and mean reversal frequencies for each strain are shown above the graph. Kruskal-Wallis test was used for statistical analysis. “ns”, not significant (p>0.05); “***”, p<0.001; and “****” indicates p<0.0001.

We then quantified the fluorescent polar signal of the two variants. In the absence of IAA, the two fluorescent fusion proteins did not generate polar clusters and had a diffuse localization in all cells. In contrast, most of PixA-mVenus localized diffusely along the cell body, with 38 % of cells showing a unipolar cluster, which was increased compared to previously observed results (Figure 23 A). As observed in reversal assays, cells of the two *pixA-mVenus* point mutants still reversed without PixA-mVenus localizing to the pole (Figure 22 B, Figure 23 A). When activating Frz signaling using 0.075 % IAA, PixA-mVenus localized to the poles more frequently and with higher intensity than in the absence of IAA (as previously observed in a *frzCD*^{GOF} mutant) (Figure 23 A and B). Clusters were localized to the leading cell pole (Figure 23 A). Interestingly, PixA^{D180N}-mVenus did not localize to a pole in the presence of IAA, while PixA^{D180E}-mVenus localized to the leading pole when Frz signaling was activated by IAA (Figure 23 A). These clusters were less intense than those of the WT protein in the presence of IAA (Figure 23 B, data is also plotted as scatterplots in Supplementary Figure 6 B).

In summary, PixA^{D180N}-mVenus and PixA^{D180E}-mVenus are non-functional variants. Even though PixA^{D180E}-mVenus still localized to the leading cell pole when Frz signaling was activated, its reversal frequency was the same as observed for a PixA^{D180N}-mVenus mutant that showed diffuse localization under both tested conditions.

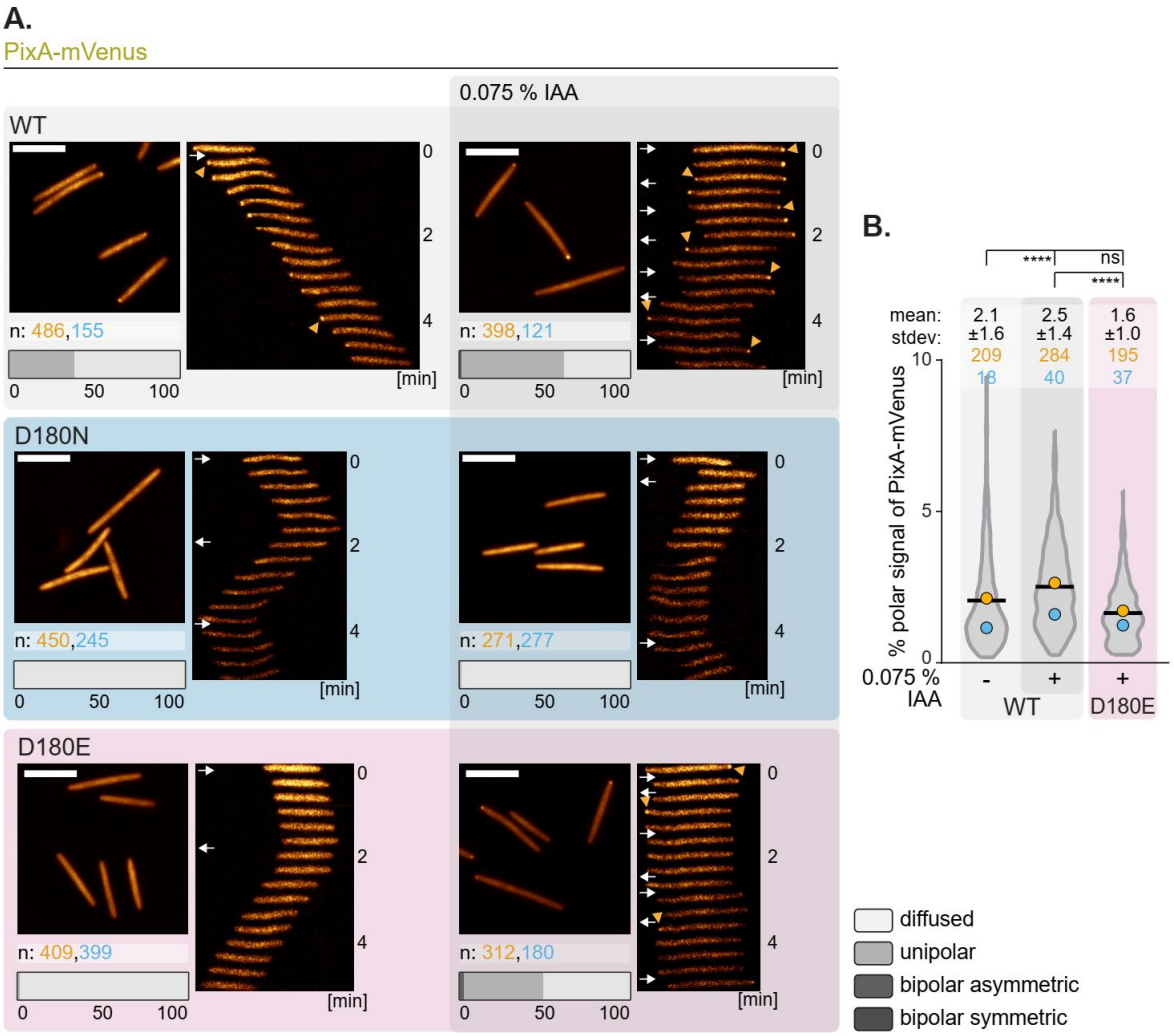

Figure 23: **Localization of PixA-mVenus D180 point mutations. (A)** Fluorescence microscopic analysis of *pixA*$^{D180N/E}$*-mVenus* mutants. Cells were analyzed for the presence of polar localization. Pictures show representative cells of each strain in exponential growth phase. Cells were imaged on chitosan-coated slides in MC7 buffer after incubation for 1.5 h. Number of cells analyzed per replicate (n) is shown below microscopy images in orange and blue. The polar regions are defined as the parts of a cell within a distance of 0.65 µm, from a tip of a cell. A pole was considered to have a polar cluster if a contiguous set of at least three pixels above the threshold intensity was found in the polar region. Horizontal bars show the percentage of cells with a polar and diffuse localization pattern according to the color code. Scale bar, 5 µm. Straightened timelapse montages of a representative cell for each strain. Yellow arrows indicate the appearance of a cluster, white arrows indicate direction of movement. Images were recorded every 20 s. **(B)** Violin plots show the percentage of the total polar fluorescence signal in cells with PixA-mVenus polar cluster(s). Note that the violin plots only includecells having polar clusters. The means from two replicates are shown as symbols in orange and blue. The average mean based on all two replicates is shown as black line. The graph shows the number of trajectories analyzed per replicate (n) and mean polar signal for each strain. Kruskal-Wallis test was used for statistical analysis. “ns”, not significant (p>0.05); and “****”, p<0.0001.

3.1.8 Polar localization of PixA is decreased in a Δ*mglA* mutant

PixA leading cell pole localization was abolished in the absence of FrzZ, suggesting that PixA is brought to the leading cell pole by FrzZ in a *frzCD*^{GOF} strain. Additionally, PixA-mVenus and FrzZ-mVenus polar localization were similar and PixA and FrzZ were found in close proximity of each other in a *frzCD*^{GOF} strain, suggesting that they colocalize in such a background (Figure 24). We suspect that PixA-mVenus should follow FrzZ in other mutants. Following this hypothesis, MglA would be important for PixA-mVenus leading cell pole localization. Hence, we investigated if the polar localization of PixA-mVenus was affected in a Δ*mglA* strain in which FrzZ could no longer localize efficiently to the pole (3.1.1). For this purpose, we constructed a strain expressing *pixA-mVenus* from its native site in a *frzCD*^{GOF}Δ*mglA* background.

In fluorescence microscopy analyses, we found that PixA-mVenus polar cluster formation was decreased in a *frzCD*^{GOF} Δ*mglA* strain compared to a *frzCD*^{GOF} strain. In time-lapse movies, PixA localized in dynamic cytoplasmic clusters in some cells in subpolar or midcell regions. This is similar to the FrzZ-mVenus clusters visible in a *frzCD*^{GOF} Δ*mglA* background (Figure 24), suggesting that PixA follows FrzZ in such a strain.

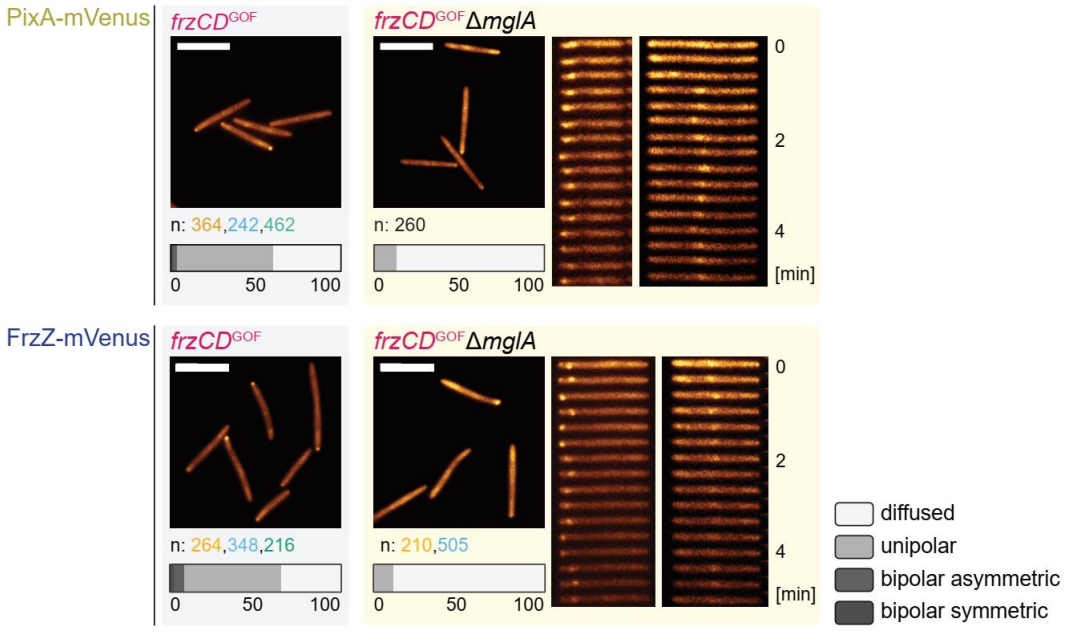

Figure 24: **Localization of PixA-mVenus in the absence of MglA in a *frzCD*^{GOF} background.** Fluorescence microscopic analysis of a *frzCD*^{GOF} Δ*mglA pixA::pixA-mVenus* strain. Cells were analyzed for the presence of polar localization. Pictures show representative cells of each strain in exponential growth phase. Cells were imaged on chitosan-coated slides in MC7 buffer after incubation for 1.5 h. Number of cells analyzed for each replicate (n) is shown below microscopy images in orange, blue and green. The polar regions are defined as the parts of a cell within a distance of 0.65 µm, from a tip of a cell. A pole was considered to have a polar cluster if a contiguous set of at least three pixels above the threshold intensity was found in the polar region. Horizontal bars show the percentage of cells with a

polar and diffuse localization pattern according to the color code. Scale bar, 5 µm. Straightened timelapse montages show representative cells. Images were recorded every 20 s. Strains expressing *pixA-mVenus* in a *frzCD*^{GOF} background and *frzZ-mVenus* strains are described above and shown for ease of comparison.

3.2 How does FrzX induce a switch in polarity?

We then aimed to elucidate the function of FrzX at the lagging cell pole in stimulating the polarity switch. Phosphorylation is important for the localization of FrzX to the lagging pole (Guzzo *et al.*, 2018). To this end, we performed fluorescence microscopy analyses of strains expressing *sfGFP-frzX* from its native site in otherwise WT, Δ*frzE*, and *frzCD*^{GOF} strains. The fusion protein accumulated in the three strains detected by immunoblot analysis using α-GFP antibodies but showed degradation into sfGFP (Figure 25 A). The fluorescent fusion protein was fully functional as strains expressing *sfGFP-frzX* resembled their corresponding parent strains in a motility assay (Figure 25 B)

The localization of sfGFP-FrzX was assessed by fluorescence microscopy as described above. sfGFP-FrzX shows a mostly diffuse localization along the cell body in all tested strains (Figure 26 A). In a WT background and in a Δ*frzE* mutant, polar clusters of sfGFP-FrzX were not observed (please note that up to approximately 4 % of cells are assigned with false-positive polar localization due to the faint signal of FrzX). Polar clusters were only visible at high signaling levels in a *frzCD*^{GOF} mutant (Figure 26 A). The polar accumulation of sfGFP-FrzX was even stronger stimulated by the addition of IAA in a WT background (Supplementary Figure 9 A). To determine at which pole sfGFP-FrzX localized, we performed time-lapse fluorescence microscopy. As previously observed in snapshots, no clusters were observed in otherwise WT and Δ*frzE* strains. In a *frzCD*^{GOF} mutant, sfGFP-FrzX clusters localized to the lagging cell pole (Figure 26 A).

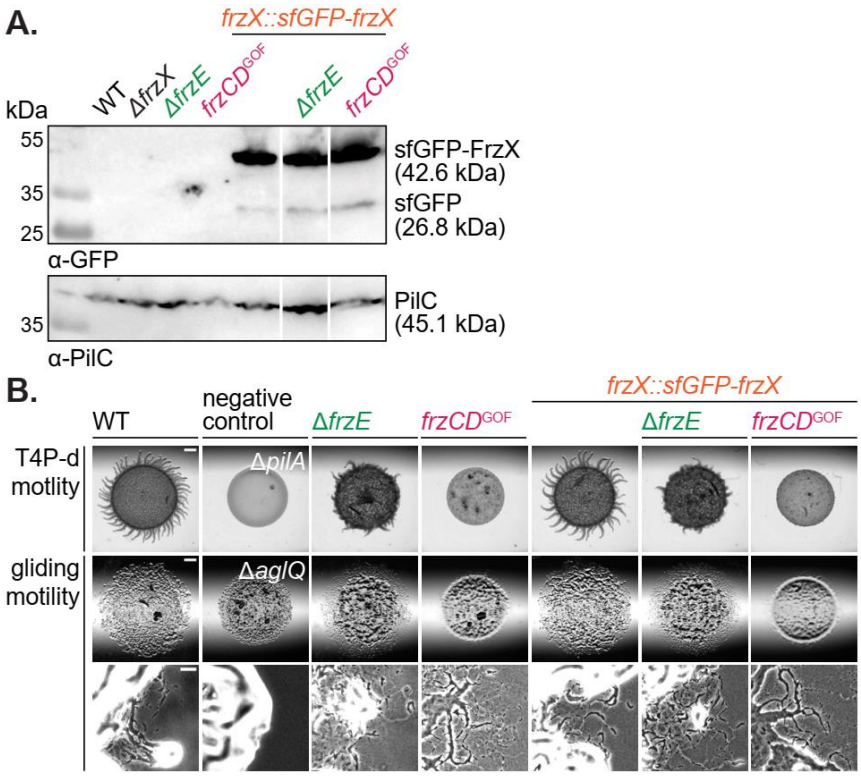

Figure 25: **(A)** Immunoblot analysis of cell lysates of exponentially grown cells expressing *sfGFP-FrzX* from its native site in otherwise WT, *ΔfrzE,* and *frzCD*^{GOF}strains using α-GFP; and α-PilC antibodies as a loading control. Cell lysate from the same number of cells was loaded per lane. **(B)** Motility assay of *sfGFP-frzX* mutants in WT, Δ*frzE*, and *frzCD*^{GOF} backgrounds. T4P-dependent motility was tested on 0.5 % agar. Gliding motility was tested on 1.5 % agar. Scale bars from top to bottom: 1 mm, 1 mm, and 50 µm. One representative clone of each strain is shown.

3.2.1 FrzX localizes to the lagging cell pole depending on RomY

FrzX might interact with the polarity proteins in order to induce the polarity switch and it was already suggested that the polar localization of FrzX depends on MglB, while its polar accumulation was slightly decreased in a Δ*mglA* deletion and is unaffected in a Δ*romR* mutant (Guzzo *et al.*, 2018). Carreira *et al.*, 2020 found that polar localization of MglB is increased in a Δ*mglA* mutant, while it was strongly decreased in a Δ*romR* mutant. Following this model, polar FrzX localization should be increased in a Δ*mglA* mutant and strongly decreased in a Δ*romR* mutant, if polar localization only depended on MglB. This is in contrast to what was observed by Guzzo *et al.*, 2018.

In order to gain further insight about the interaction of FrzX with the polarity proteins, we created mutants expressing *sfGFP-frzX* from its native site in WT and *frzCD*^{GOF} strains and combined them with in-frame deletions of *mglA*, *mglB*, *romR*, *romX*, *romY,* and *mglC*. All strains accumulated sfGFP-FrzX (Supplementary Figure 7 B). Δ*mglA*, Δ*mglB,* and Δ*romR* strains showed their distinct motility phenotypes in the WT and *frzCD*^{GOF} background, while Δ*romX*, Δ*romY,* and Δ*mglC* strains were stimulated by Frz signaling and showed a *frz*^{GOF}

phenotype described above, as was already observed for strains expressing *frzZ-mVenus* (Supplementary Figure 9).

When analyzing fluorescent microscopy for the localization of sfGFP-FrzX in polarity mutants, we found that generally, no clusters were visible, as was previously observed for an otherwise WT strain (Supplementary Figure 9 B). In a *frzCD*^{GOF} Δ*mglB strain,* sfGFP-FrzX clusters disappeared as previously published (Guzzo *et al.*, 2018). Additionally, we observed that polar localization was lost in a *frzCD*^{GOF} Δ*romY* strain. The polar cluster formation of RomY depends on MglB, suggesting that FrzX localizes to the pole depending on RomY rather than MglB (Szadkowski *et al.*, 2022). In a *frzCD*^{GOF} Δ*mglA* strain, polar localization of sfGFP-FrzX was slightly increased. Deletion of *mglA* also leads to increased polar accumulation of MglB (Carreira *et al.*, 2020). RomY, on the other hand, is only slightly affected by the loss of MglA (Szadkowski *et al.*, 2022) suggesting that MglB might still affect FrzX localization. We found that the Δ*mglC*, mutation, which leads to decreased polar MglB (Carreira *et al.*, 2023), resulted in decreased polar localization of sfGFP-FrzX. Interestingly, polar cluster localization of sfGFP-FrzX was increased in Δ*romR* and Δ*romX* mutants. In the absence of RomR polar localization, RomY is decreased (Szadkowski *et al.*, 2022). A Δ*romX* mutation results in more unipolar localization of MglB (Szadkowski *et al.*, 2019). In these strains, sfGFP-FrzX did not follow MglB localization. Cluster intensities in *frzCD*^{GOF} Δ*mglA*, Δ*romR,* Δ*romX*, and Δ*mglC* strains did not change compared to the *frzCD*^{GOF} mutant (Figure 26 B). The same trend was observed in *sfGFP-frzX* strains with activated Frz signaling by adding 0.075 % IAA, although cluster frequency was generally higher (Supplementary Figure 9 B).

These results partially support that FrzX targets RomY at the lagging pole but also show that the GEF complex proteins RomR and RomX have a negative impact on FrzX polar localization. The latter finding is similar to what was observed before for FrzZ (3.1.1). Altogether, it is not clear how FrzX targets the lagging pole.

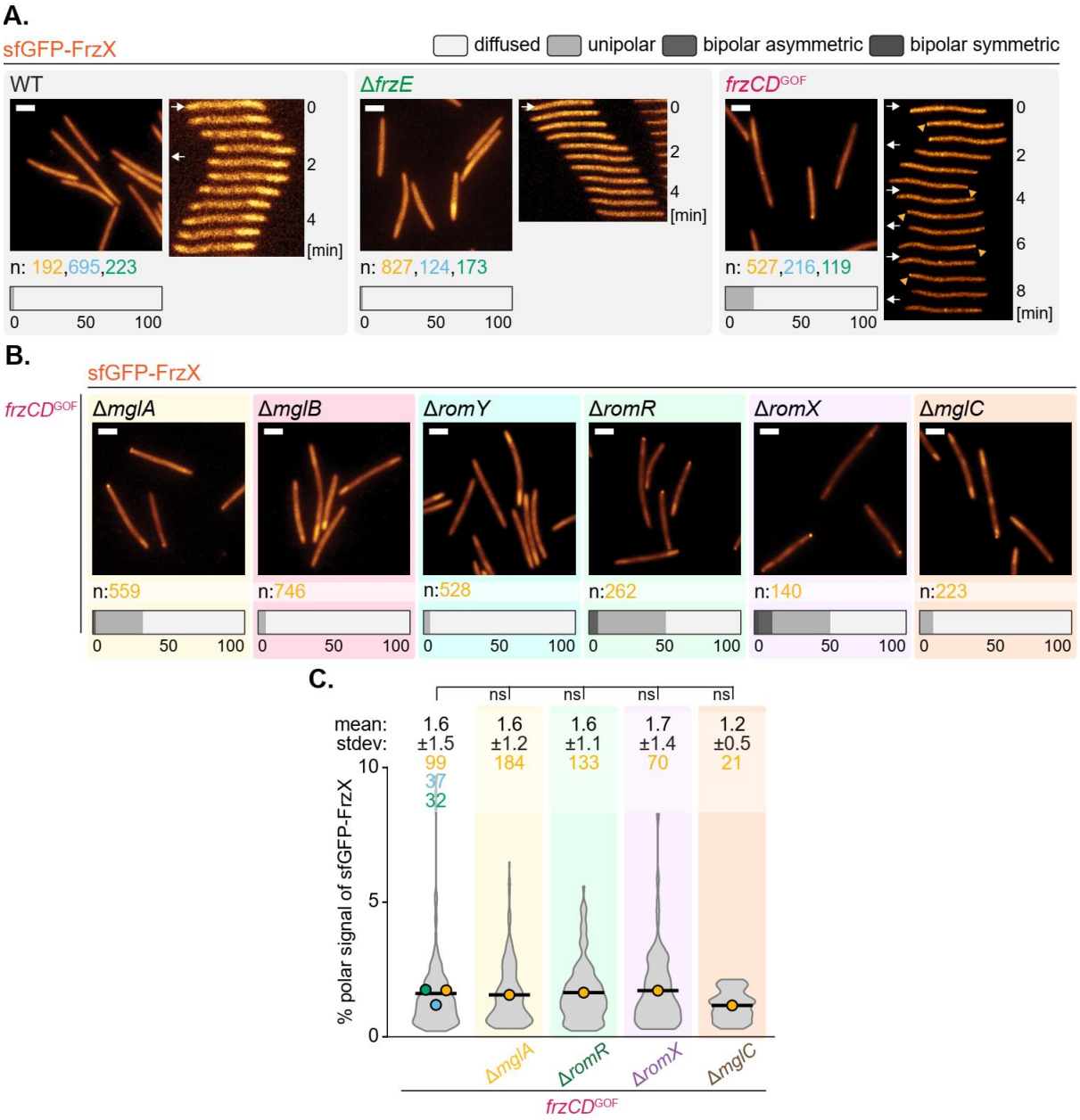

Figure 26: **Localization of sfGFP-FrzX in polarity module mutants.** Fluorescence microscopy analysis of *frzX::sfGFP-frzX* strains in WT, Δ*frzE*, and *frzCD*^{GOF} background **(A)** and in *frzCD*^{GOF} polarity mutants **(B)**. Cells were analyzed for the presence of polar localization. Pictures show representative cells of each strain in exponential growth phase. Cells were imaged on chitosan-coated slides in MC7 buffer for 1.5 h. Number of cells analyzed per replicate (n) is shown below microscopy pictures in orange, blue and green. The polar regions are defined as the parts of a cell within a distance of 0.65 µm, from a tip of a cell. A pole was considered to have a polar cluster if a contiguous set of at least three pixels above the threshold intensity was found in the polar region. Horizontal bars show the percentage of cells with a polar and diffuse localization pattern according to the color code. Scale bar, 2 µm. Straightened timelapse montages of a representative cell for each strain. **(C)** Violin plots show the percentage of the total polar fluorescence signal in cells with sfGFP-FrzX polar cluster(s). Note that the violin plots only include cells having a polar clusters. The means from three replicates are shown as symbols in orange, blue, and green. The average mean based on all replicates is shown as black line. The graph shows the number of cells analyzed per replicate (n), the mean polar signal, and the standard deviation for each strain.

3.2.2 FrzX localizes in close proximity to PglH in a *frzCD*^{GOF} mutant

In order to identify novel interaction partners of FrzX at the lagging cell pole, we performed proximity labeling (3.1.2).

An endogenous *FLAG-miniTurbo-frzX* fusion was expressed in a *frzCD*^{GOF} and a Δ*frzE* background, in which FrzX localized to the lagging cell pole or diffusely, respectively. As a negative control, *sfGFP-miniTurbo-FLAG* was expressed from the *18-19* site under the control of the inducible vanillate promoter in a *frzCD*^{GOF} and a Δ*frzE* background to compare with the corresponding *FLAG-miniTurbo-frzX* strains.

When optimizing the vanillate concentration to control the accumulation of FLAG-minTurboID-FrzX, we found that similar levels of the two proteins detected via immunoblot analysis lead to much higher biotinylation levels of the *FLAG-miniTurbo-frzX* strain than for the control, suggesting that sfGFP-miniTurbo-FLAG was easier detected by α-FLAG antibodies or that the control protein is less active (data not shown). In order to obtain similar amounts of biotinylated proteins as in the *FLAG-miniTurbo-frzX* strains, the controls were induced using 5 µM vanillate ON, which led to similar levels of biotinylation (Figure 27 B). All four strains had the expected motility phenotypes, documenting that FLAG-miniTurbo-FrzX is active (Figure 27 A).

In total, 958 proteins were identified in this experiment, of which four were found to be significantly enriched after applying a threshold (Log_2ratio>3; p-value<0.005) (Figure 27 C, Table 3). FrzX (1) was enriched in both backgrounds. In a *frzCD*^{GOF} strain, PglH (2) was significantly enriched, while it was not enriched in a Δ*frzE* strain. Additionally, Mxan_2752 (3), a glycine-tyrosine-phenylalanine (GYF) domain protein often involved in protein-protein interactions, and KynA (4), a tryptophane dioxygenase, were significantly enriched in the Δ*frzE* background. Of note, FrzE (5), which we would have expected to find enriched in the *frzCD*^{GOF} strain, PixA (6), and the proteins of the polarity module (7-12) were either not detected or not significantly enriched in either background.

This experiment introduces PglH as a potential interaction partner for FrzX at the lagging cell pole, since it was found in the *frzCD*^{GOF} background. Interestingly, this protein was also enriched in a proximity labelling experiment using PixA as a bait.

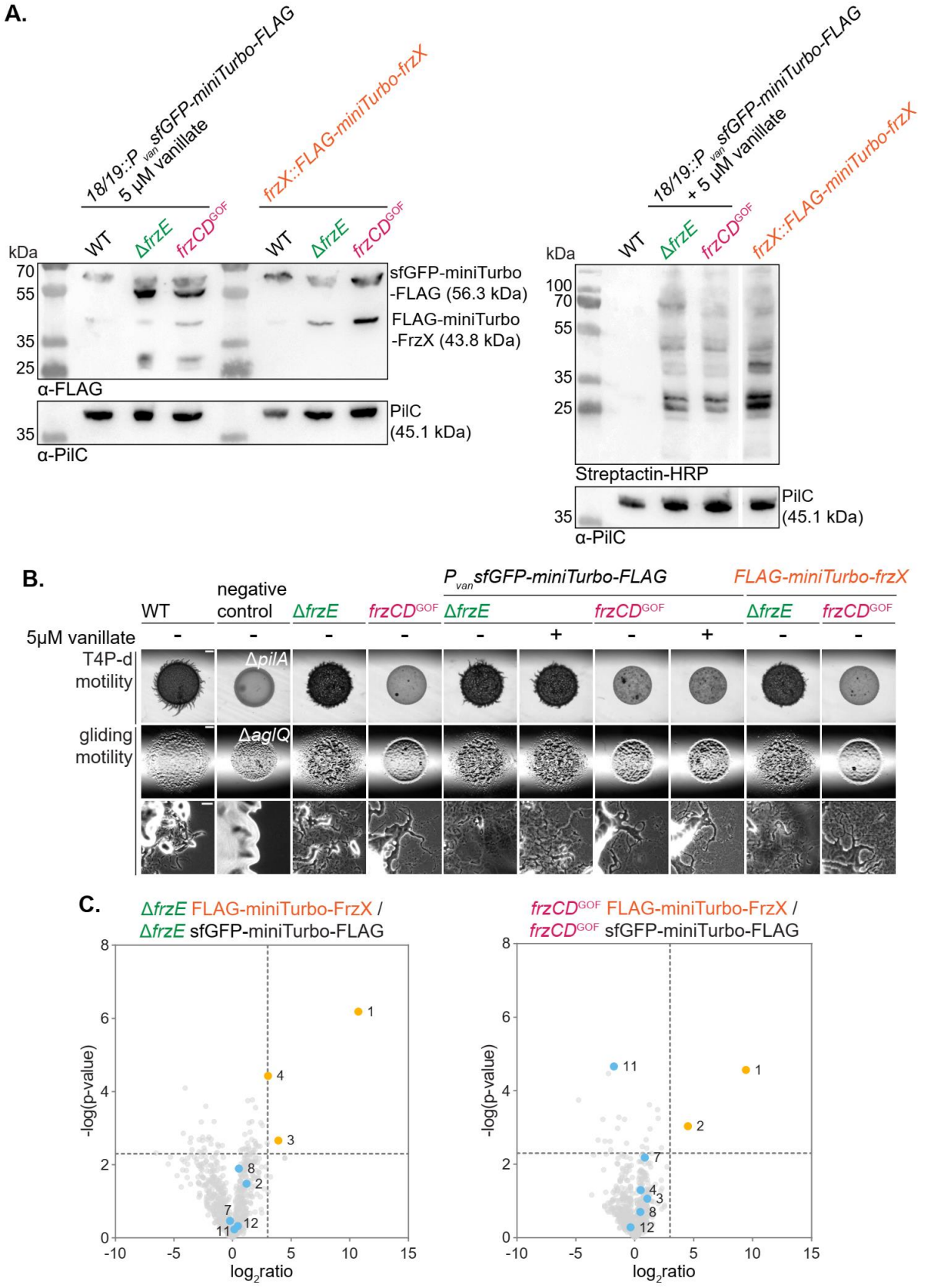

Figure 27: **Proximity labeling using FLAG-miniTurbo-FrzX. (A)** Immunoblot analysis of cell lysates of exponentially grown cells expressing *sfGFP-miniTurboI-FLAG* from the *18-19* site and *FLAG-miniTurbo-frzX* from the native site in a *ΔfrzE and frzCD*^{GOF} mutant using α-FLAG or Streptactin-HRP and α-PilC antibodies as a loading control. Its was tested for accumulation levels of sfGFP-miniTurbo-

FLAG fusions (left) and biotinylation levels (right). Cell lysate from the same number of cells was loaded per lane. **(B)** Motility assay of mutants expressing *sfGFP-miniTurbo-FLAG* from the *18-19* site and *FLAG-miniTurbo-frzX* from the native site in Δ*frzE and frzCD*^{GOF} strains. T4P-dependent motility was tested on 0.5 % agar. Gliding motility was tested on 1.5 % agar. Scale bars from top to bottom: 1 mm, 1 mm, and 50 µm. **(C)** Biotinylated proteins enriched by FLAG-miniTurbo-FrzX. Δ*frzE* FLAG-miniTurbo-FrzX was compared to Δ*frzE* sfGFP-miniTurbo-FLAG (left) and *frzCD*^{GOF} FLAG-miniTurbo-FrzX was compared to *frzCD*^{GOF} sfGFP-miniTurbo-FLAG (right). The X-axis represents the log_2ratio of normalized values of the individual protein. The Y-axis represents the statistical significance of the corresponding targets. Dashed lines represent the threshold (log_2ratio>3; -log(p-value)>-Log(0.005)). Orange points represent significantly enriched proteins. Blue points represent proteins of interest that were not statistically significantly enriched. Numbers correspond to proteins listed in Table 3.

Table 3: **Pulled down biotinylated proteins in the proximity of FrzX[3].**

		ΔfrzE		*frzCD*^{GOF}	
No.	**Protein**	**log2ratio**	**-log(p-value)**	**log2ratio**	**-log(p-value)**
1	FrzX	10.73	6.19	9.44	4.57
2	PglH	1.19	1.48	4.51	3.03
3	Mxan_2752	3.91	2.66	1.08	1.07
4	KynA	3.04	4.43	0.51	1.30
5	FrzE	-	-	-	-
6	PixA	-	-	-	-
7	MglA	-0.21	0.46	0.87	2.18
8	MglB	0.54	1.90	0.48	0.70
9	MglC	-	-	-	-
10	RomR	-	-	-	-
11	RomX	0.15	0.24	-1.77	4.66
12	RomY	0.45	0.32	-0.35	0.28

3.3 MglA localizes in the proximity of known interaction partners and novel interaction candidates

MglA is the key protein defining polarity in *M. xanthus*. Furthermore, it is the first protein among the analized polarity module proteins to switch polarity during a reversal (Leonardy *et al.*, 2010, Guzzo *et al.*, 2018, Zhang *et al.*, 2010). In order to further look into the polarity switch, we performed proximity labeling to identify interaction partners of MglA that could be important for this process.

A strain expressing *mglA-miniTurbo-FLAG* from its native site was used to identify proteins in close proximity to MglA, while a strain expressing *sfGFP-miniTurbo-FLAG* from the *18-19* site under the control of the vanillate promoter was used as a negative control. In a motility assay,

[3] No. refers to the individual target number depicted in Figure 27 C. Black text indicates proteins enriched above the set threshold. Grey text indicates proteins enriched below the threshold.

the control strain was fully functional as it resembled the WT phenotype, while the strain expressing *mglA-miniTurbo-FLAG* was only partially functional since colony morphology resembled a frizzy phenotype rather than WT (Figure 28 A). This phenotype was similar to the one exhibited by a strain expressing a *mglA-mVenus* fusion from the native site, which was used in previous studies (Szadkowski *et al.*, 2019), so we decided to proceed with this strain. The vanillate concentration used for induction of *sfGFP-miniTurbo-FLAG* was determined by immunoblot analysis (Figure 28 B). To this end, the expression of *sfGFP-miniTurbo-FLAG* was induced with 0, 5, 10, 50, and 100 µM of vanillate ON in exponentially growing cells. The accumulation levels of sfGFP-miniTurbo-FLAG in these samples were then compared to the accumulation of MglA-miniTurbo-FLAG. The addition of 5-10 µM vanillate leads to a similar accumulation of the two proteins. Subsequently, 5 µM of vanillate was used to induce the control in proximity labeling experiments.

In total, 1614 proteins were identified, of which 44 were significantly enriched above a set threshold (Log_2ratio>2; p-value<0.05, as used in (Herfurth *et al.*, 2023a)) in the sample accumulating MglA-miniTurbo-FLAG. Of these 44 proteins, 29 were particularly interesting (Figure 28 C, Table 4, Supplementary Table 2). First, we found MglA (1), the bait protein, not to be significantly enriched but close to our set threshold. Second, we detected several characterized proteins already shown to interact with MglA, thus, documenting that this experimental approach can identify MglA-interacting proteins. Of these proteins, we identified the GAP protein MglB (2) (Zhang *et al.*, 2010, Leonardy *et al.*, 2010), the gliding motility proteins AglZ (4) and GltJ (5) (Yang *et al.*, 2004, Mignot *et al.*, 2023, Mauriello *et al.*, 2010) and the T4P-dependent motility regulators FrzS (6) and SgmX (7) (Mercier *et al.*, 2020, Potapova *et al.*, 2020, Bautista *et al.*, 2023). Third, we identified RomR (3), which is part of the GEF complex regulating MglA but was not shown to interact with MglA directly (Szadkowski *et al.*, 2019).

In addition to these proteins known to be associated with MglA, we found three additional proteins annotated as proteins that could be involved in T4P-dependent motility (8-10). The three most enriched proteins are Mxan_1142 (11), ValS (12), and Mxan_4627 (13). Mxan_1142 is annotated as Plectin 1, a cytoskeletal linker protein that interacts with components of the three major cytoskeleton-forming systems in eukaryotes (actin/myosin filaments, intermediate filaments, microtubules) (https://www.uniprot.org/uniprotkb/Q1DD71/entry, July 2023) (Steinböck & Wiche, 1999). ValS (Mxan_4460) is annotated as Valine-tRNA ligase, which attaches valine to its cognate tRNA (Berg *et al.*, 1961). Interestingly, *valS* is encoded downstream of *romR* (*mxan_4461*) but has not yet been considered to be involved in cell polarity due to its annotation (Leonardy *et al.*, 2007). Mxan_4627 (13) contains a MshEN domain, and TPR repeats (https://www.ebi.ac.uk/interpro/protein/UniProt/Q1D3I0/) (Wang *et*

al., 2016). TPR repeats often mediate protein-protein interactions (Zeytuni & Zarivach, 2012). MshEN domains can function as c-di-GMP receptors (Wang *et al.*, 2016). Interestingly, we found four significantly enriched MshEN proteins (13-16). FrgA (14) was suggested to be part of Frz signaling because lack of FrgA resulted in frizzy aggregates as observed for strains lacking Frz proteins (Cho *et al.*, 2000). FrgA was, like Mxan_4627, not predicted to bind c-di-GMP (Wang *et al.*, 2016). Mxan_4666 (15) and Mxan_4436 (16) were both predicted to bind c-di-GMP (Wang *et al.*, 2016). Deletion or overexpression of Mxan_4666 did not lead to a defect in motility or development (unpublished data, Ozan Ertekin), while only overexpression and not deletion of Mxan_4436 led to a motility defect and delayed fruiting body formation (Bernhardt, 2022). In addition to the MshEN proteins, we found three proteins containing a RR and a PATAN domain (17-19). Several so-called PatA-type regulators are involved in T4P motility (Han *et al.*, 2022). Two of them, SgnC (17) and PglH (18) have been shown to be involved in motility (Youderian & Hartzell, 2006, Yu & Kaiser, 2007). In addition to these three RR proteins, we found three proteins involved in signaling (20-22), of which the hybrid sensor histidine kinase NmpS (20) acts in the NmpRSTU signaling pathway, which is suggested to regulate *pilR* expression in response to oxygen levels which in turn regulates *pilA* expression (Bretl *et al.*, 2018). The serine/threonine kinase Mxan_3202 (22) was enriched, as well as Mxan_3203 (23), which is annotated as an FHA domain protein that recognizes phosphothreonines (Almawi *et al.*, 2017). Three proteins containing TPR repeats (24-26) and two containing a J domain and TPR repeats (27-28) were enriched. The J domain is characteristic for the DnaJ-family of chaperones that typically interact with DnaK-like chaperones via this domain to maintain protein homeostasis (Schroder *et al.*, 1993, Cyr *et al.*, 1994). Interestingly, we also found a protein annotated as a DnaK-like protein (29). Lastly, we found the secretion pathway A protein Mxan_5765 (30), encoded next to the known interactor SgmX (Potapova *et al.*, 2020).

To summarize, our results confirmed known interactors of MglA from *in vitro* studies in *vivo*. Additionally, we found proteins known to be involved in motility that were not previously associated with MglA. They are interesting candidates to study in context with MglA to extend our understanding of MglA function further. In the context of polarity switching, two proteins stand out. First, Mxan_1142, was also found in proximity labeling experiments with FrzZ. Second, PglH was also found in proximity labeling experiments using FrzX and PixA.

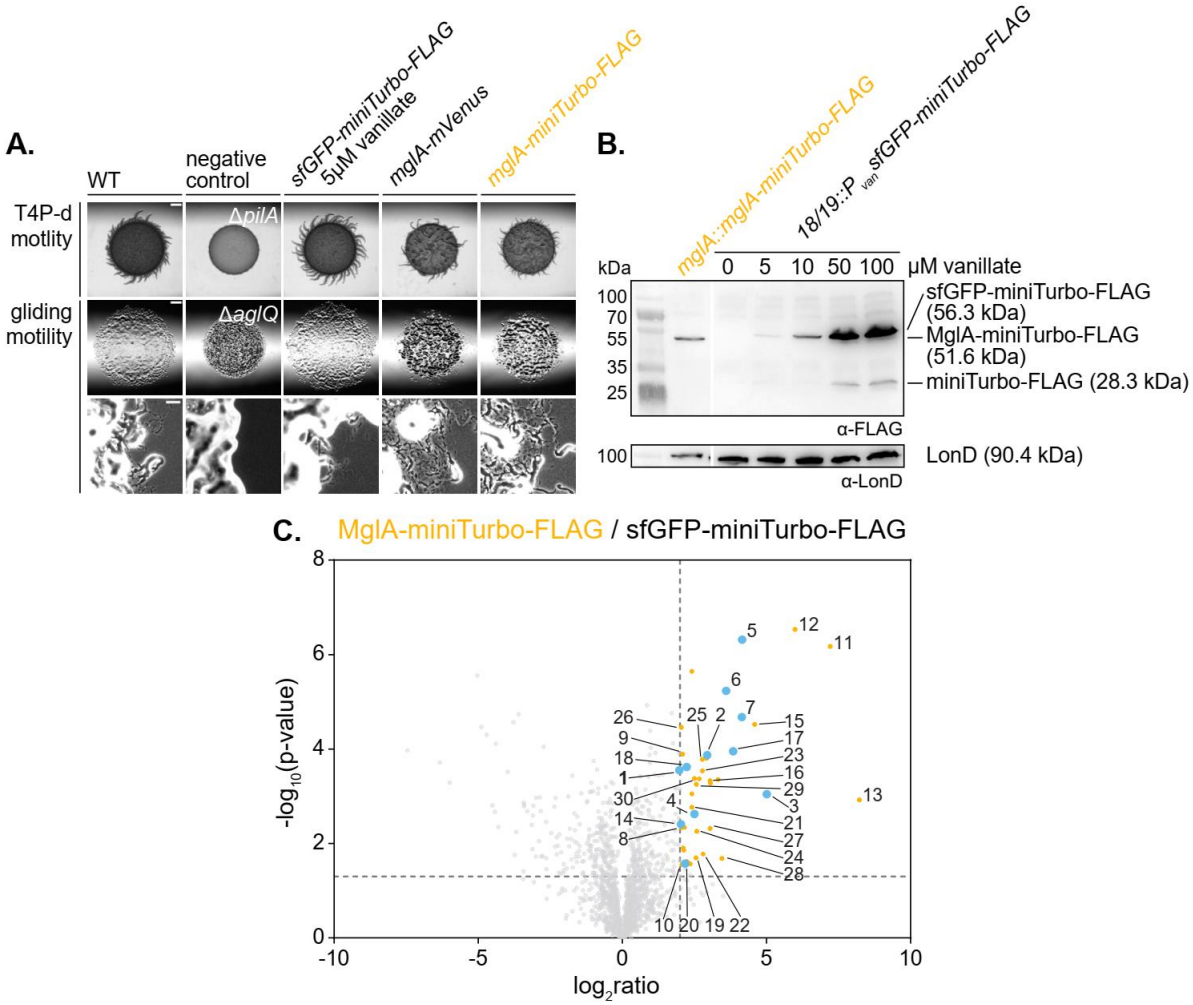

Figure 28: **Proximity labeling using MglA-miniTurbo-FLAG. (A)** Motility assay to test the functionality of a mutant expressing *sfGFP-miniTurbo-FLAG* from the *18-19* site expressed under the control of the vanillate promoter and a mutant expressing *mglA-miniTurbo-FLAG* from the native site. T4P-dependent motility was tested on 0.5 % agar. Gliding motility was tested on 1.5 % agar. 5 µM vanillate was added to plates on which the *sfGFP-miniTurbo-FLAG* was spotted. Scale bars from top to bottom: 1 mm, 1 mm, and 50 µm. **(B)** Induction test of the *sfGFP-miniTurbo-FLAG* strain using immunoblot analysis mutant using α-FLAG and α-LonD antibodies as a loading control. Cell lysate from the same number of cells was loaded per lane. sfGFP-miniTurbo-FLAG was induced using 0, 5, 10, 50, an 100 µM vanillate and accumulation was compared to MglA-miniTurbo-FLAG. **(C)** Pulled down biotinylated proteins in the proximity of MglA. MglA-miniTurbo-FLAG was compared to sfGFP-miniTurbo-FLAG. The X-axis represents the log_2ratio of normalized values of the individual protein. The Y-axis represents the statistical significance of the corresponding targets. Dashed lines represent the threshold (log_2ratio>2; -log(p-value)>-Log(0.05)). Orange points represent significantly enriched proteins. Blue points represent proteins that have been published to be involved in motility. Numbers correspond to proteins listed in Table 1.

Table 4: **Interesting candidates of pulled-down biotinylated proteins in the proximity of MglA [4].**

No.	Protein	log2ratio	-log(p-value)	pot. Function
1	MglA	1.98	3.56	bait
2	MglB	2.95	3.87	polarity module

[4] No. refers to the individual target number depicted in Figure 28 C. Blue indicates proteins that have been published to be involved in motility.

3	RomR	5.02	3.04	
4	AglZ	2.51	2.62	gliding motility
5	GltJ	4.17	6.32	
6	FrzS	3.60	5.23	
7	SgmX	4.15	4.68	
8	Mxan_6705 (PilT)	2.00	2.44	T4P-d motility
9	Mxan_1995 (PilT)	2.09	3.89	
10	Mxan_3083	2.07	1.55	
11	MXAN_1142	7.21	6.18	Plectin
12	ValS	6.00	6.53	tRNA-ligase
13	MXAN_4627	8.23	2.92	
14	FrgA	2.03	2.41	MshEN
15	MXAN_4666	4.59	4.52	
16	MXAN_4436	3.05	3.33	
17	SgnC	3.86	3.95	
18	PglH	2.24	3.62	RR-PATAN
19	MXAN_5052	2.25	1.61	
20	NmpS	2.19	1.57	
21	MXAN_6865	2.42	2.77	signaling
22	MXAN_3202	2.56	1.69	
23	MXAN_3203	2.78	3.54	FHA
24	MXAN_1423	2.58	2.26	
25	MXAN_1948	2.78	3.78	TPR
26	MXAN_1942	2.05	4.46	
27	MXAN_1145	3.05	2.32	J-TPR
28	MXAN_2049	3.47	1.69	
29	MXAN_5804	2.57	3.25	DnaK
30	MXAN_5765	2.50	3.37	secretion pathway A protein

3.4 PglH regulates reversals

PglH was enriched in proximity labeling experiments with MglA, PixA, and FrzX, making this protein a highly promising candidate to be involved in polarity switching. Interestingly, PglH was previously identified in a study of transposon insertion mutants with defective gliding motility (Yu & Kaiser, 2007). Specifically, a *pglH* insertion mutant had twice the reversal frequency of a WT strain moving by gliding motility (Yu & Kaiser, 2007).

We constructed an in-frame deletion of *pglH* and tested the Δ*pglH* mutant for its motility behavior. Indeed, the Δ*pglH* mutant had shorter flares than WT on 0.5 % agar, favoring T4P-dependent motility (Figure 29 A). On agar favoring gliding motility, a Δ*pglH* colony showed single cells at the colony edge while the expansion was slightly reduced compared to WT. Next, we performed single-cell motility assays on 0.5 % CTT 1.5 % agarose (Figure 29 B). We

found that the reversal frequency of the Δ*pglH* mutant was increased compared to WT, confirming the results of previous studies (Yu & Kaiser, 2007).

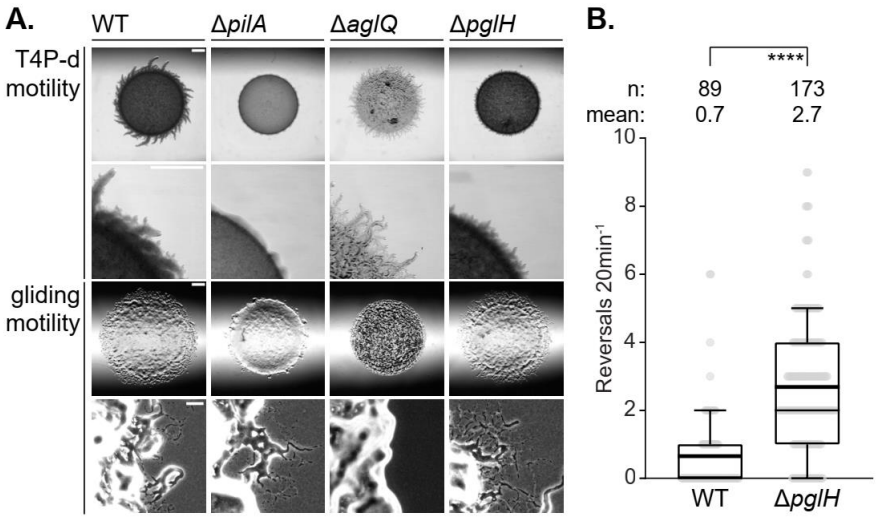

Figure 29: **A Δ*pglH* mutant shows an aberrant reversal phenotype. (A)** Motility assay of a Δ*pglH* mutant. T4P-dependent motility was tested on 0.5 % agar. Gliding motility was tested on 1.5 % agar. Scale bars from top to bottom: 1 mm, 0.5 mm,1 mm, and 50 µm. **(B)** Single-cell gliding reversal assay on 0.5 % CTT 1.5% agarose of Δ*pglH*. Boxplots show the measured reversal frequency monitored as the number of directional changes per 20 min. Each dot in the scatterplot represents the reversal frequency of one cell. Boxes enclose the 25th and 75th percentile. Whiskers enclose the 5th and 95th percentile. The median is shown as a thin line in the box. The mean is shown as thick black line. The number of trajectories analyzed (n) and mean reversal frequencies for each strain are shown above the graph. Kruskal-Wallis test was used for statistical analysis. "****", p<0.0001.

When analyzing the genomic neighborhood of *pglH*, we found the J-TPR protein *mxan_2049* encoded upstream of *pglH*, which was enriched in the proximity labeling experiment using MglA-miniTurbo-FLAG as bait (3.3). Downstream, a tRNA (*mxan_2051*), a ribosomal RNA small subunit methyltransferase A (*mxan_2052*), a protein of unknown function (*mxan_2023*), a deoxynucleoside kinase protein (*mxan_2054*), and PanB, which is a hydroxymethyltransferase involved in pantothenate biosynthesis in *E. coli* (*mxan_2055*) were encoded (Figure 30 A) (Jones *et al.*, 1993).

PglH is a 927 aa protein with several annotated domains (https://www.ebi.ac.uk/interpro/protein/UniProt/Q1DAP4/, August 2023). From aa 1 to 121, a RR domain is annotated. From aa 138 to 318, a domain related to proteins classified as GAPs containing a PATAN domain is found based on PANTHER classification (https://www.pantherdb.org/panther/family.do?clsAccession=PTHR36304, October 2023). The PATAN domain is located from aa 141 to 237 within the GAP-related domain. Proteins containing a PATAN domain are often associated with helix-turn-helix (HTH) and RR domains and interact with the T4P-pilus motor in *Synechocystis* to control motility (Han *et al.*, 2022, Makarova *et al.*, 2006). From aa 698 to 715, a transmembrane (TM) helix is found (Figure 30 B). Cytoplasmic vs. periplasmic

localization predictions were inconclusive since different algorithms gave different results (Supplementary Figure 10 A & B). No signal peptide is predicted for PglH (Supplementary Figure 10 B & C).

Homologs of PglH were found in all Myxococcota and RR, PATAN and the GAP-related domain where highly conserved (Figure 32, Supplementary Figure 11).

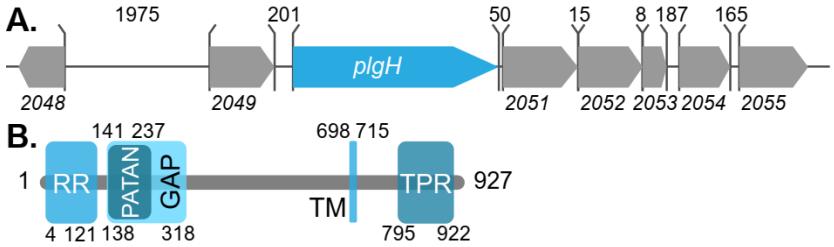

Figure 30: **Bioinformatic analysis of PglH.** (A) The genomic neighborhood of *pglH* with nearby genes. The numbers below indicate *mxan* numbers of neighboring genes. Numbers on top display distances between genes in base pairs. Genes are shown as arrows. Arrows indicate the orientation of encoded genes. Grey arrows display genes next to *pglH*. The genomic region was created using KEGG. (B) Conserved regions in PglH. Numbers indicate aa positions.

3.5 Five response regulators are involved in Frz signaling

Interestingly, five proteins with in total six RR domains have been identified to be involved in switching polarity. The dual RR protein FrzZ harbors two of these domains, while the remaining four are found in FrzX, the histidine kinase FrzE, PixA and PglH. We performed bioinformatic analyses to gain insights into their similarities and differences.

We found they all possess the phosphorylatable Asp, as well as, most other residues important for phosphotransfer (Figure 31 A)(Bourret, 2010).

We build a maximum likelihood tree of the RR domains of homologs among Myxococcota using RaxML to unravel their phylogeny (Stamatakis, 2014) (Figure 31 B). We used the RR domain of the protein CtrA, which can bind to DNA and regulate the cell cycle in *C. crescentus*, to root the tree (Reisenauer *et al.*, 1999). By this, we made the following conclusions: First, the RR domains of the Frz proteins and PixA are more closely related to each other than to PglH. Second, the RR domains of the Frz proteins are more closely related to each other than to PixA. Third, the RR domains of FrzZ and FrzX are more closely related to each other than to FrzE. Fourth, the first RR domain of FrzZ, which is more critical for its function (Kaimer & Zusman, 2013), and FrzX are more closely related to each other than to the second RR domain of FrzZ. Fifth, the RR domains of FrzX homologs in *Chondromyces crocatus* and *Sandracinus amyloticus* did not cluster with their homologs.

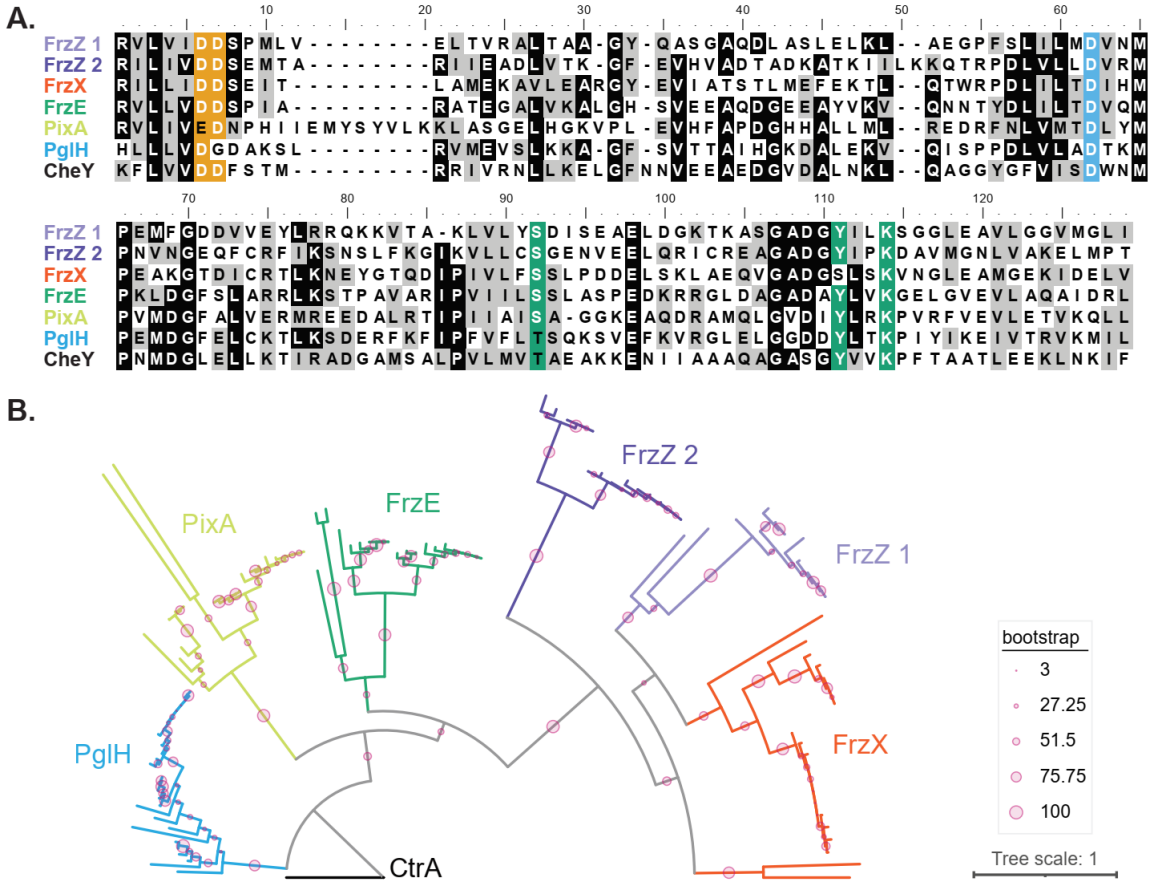

Figure 31: **Bioinformatic analysis of RR domains of FrzZ, FrzX, FrzE, PixA, and PglH. (A)** Alignment of RR domains with the RR domain of CheY. The numbers on top indicate aa residues. Black and grey backgrounds indicate identical and similar aa residues, respectively. Orange indicates aa residues important for binding of the divalent metal ion. Blue indicates the aa residue important for binding the divalent metal ion and the phosphorylation site. Green indicates residues important for signal transduction. **(B)** Maximum-likelihood phylogenetic tree of the RR domains of FrzZ. FrzX, FrzE, PixA, PglH, and their respective homologs found in Myxococcota. Homologs were identified using a reciprocal BlastP method using Kegg. Colors indicate domains of homologous proteins. Bootstrap values are shown as circles (see legend).

It was suggested that one step in the diversification of the Frz primary pathway to regulate two motility systems instead of one was brought about by the addition of FrzZ (Guzzo *et al.*, 2015). We investigated the conservation of FrzZ, FrzX, PixA, and PglH in fully sequenced genomes to try to place them in this evolutionary scheme, in which T4P systems were found more widespread, while the Agl-Glt gliding motility machinery is only present in Cystobacterinae (Guzzo *et al.*, 2015). To this end, we identified orthologs using a reciprocal BlastP method with KEGG (Figure 32). Similar to FrzZ, FrzX and PixA are mostly conserved in Cystobacterinae. As previously published (Guzzo *et al.*, 2015), FrzE showed broader conservation among Pseudomonadota, Cyanobacteria, and a few representatives of various bacterial phyla. PglH

was found in all fully sequenced Myxococcota. It is also frequently found in Pseudomonadota and, i.e., some Mycoplasmatota, Actinomycetota, and Cyanobacteria.

In summary, PglH is found in a broader range of organisms than FrzZ, FrzX, and PixA, which are also more closely related to each other than to PglH.

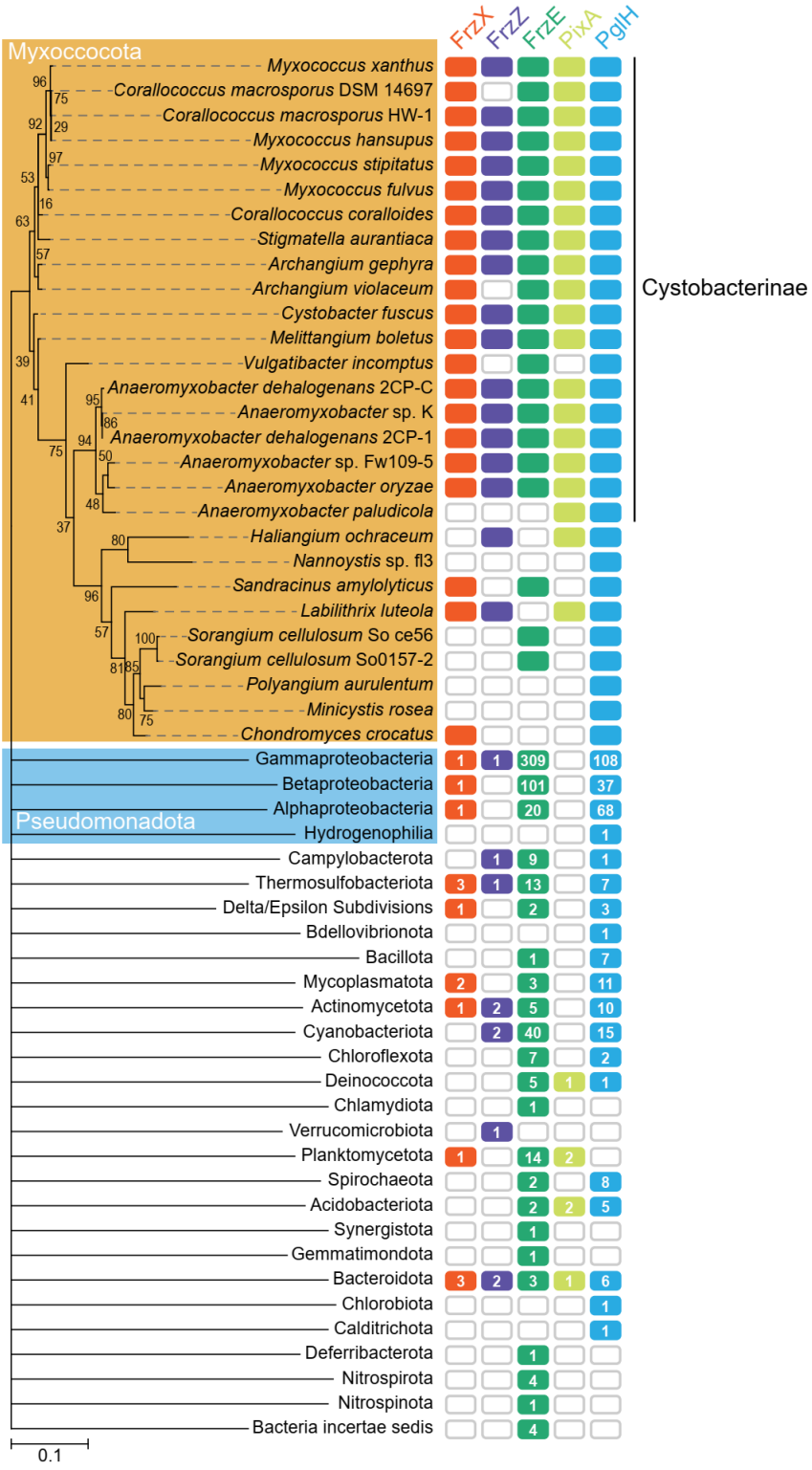

Figure 32: **Conservation of FrzZ, FrzX, FrzE, PixA, and PglH in bacteria with fully sequenced genomes.** 16S rRNA tree of Myxococcota with fully sequenced genomes (left). The phylum pseudomonadota is divided into classes since Myxococcota used to belong to this phylum. Other phyla are not shown with their phylogenic relations. If homolog(s) were found, boxes are colored. The number of homologs found in pseudomonadota classes and other phyla are indicated with numbers. Homologs were identified via a reciprocal BlastP method using KEGG.

3.6 Bioinformatics approach

As an alternative to the candidate approach and proximity labeling, we performed bioinformatic analysis to identify new interaction partners of the Frz proteins. Interestingly, while the *frzX* gene is not part of the *frz* operon in *M. xanthus,* all Frz homologs are encoded in one cluster in *Anaeromyxobacter* species (Guzzo *et al.*, 2018). Therefore, we followed the same principle to identify other interesting candidates. When searching for orthologs of full-length Frz proteins via KEGG (https://www.kegg.jp/), we found (most of them) encoded in a *frz* cluster in several species of Myxococcota (Figure 33 A). The cluster is conserved in closely related species but has a different order and is incompletely conserved in the more distantly related species. Noteworthy, *Corallococcus macrosporus* DSM 14697 and *Sandracinus amyloticus* did not encode a homolog of *frzZ*. *Vulgatibacter incomptus*, *Archangium violaceum*, *Minicystis rosea*, *Sorangium cellulosum* So ce56, *Sorangium cellulosum* So0157-2, and *Chondromyces crocatus* encode for a RR found by blast search but not by reciprocal blast. We found that *frzX* was encoded in the *frz* cluster in *V. incomptus* in addition to *Anaeromyxobacter* species. These species have genomes approximately half the size of *M. xanthus*. We investigated the genomic neighborhood of the *frz* gene cluster in these organisms to find other proteins possibly involved in Frz signaling with a different position in the *M. xanthus* genome.

V. incomptus encode genes with homologs in *M. xanthus* that are involved in fatty acid uptake (Bhat *et al.*, 2014), resistance against cheaters in development, a TypeIII-B CRISPR system (Bernal-Bernal *et al.*, 2018) or annotated as being involved in glucose metabolism, or breakdown of antibiotics (Supplementary Table 3). The genomic neighborhood of all *Anaeromyxobacter* species is listed in Supplementary Table 4. Especially *A. dehalogenans* 2CP-C showed an interesting genomic neighborhood (Figure 33 B). Downstream of the *frz* cluster, genes putatively involved in pyrimidine metabolism and glycogen breakdown are found. Upstream of the *frz* cluster, another putative *che* system is encoded. Between genes of this system and the *frz* homologs, four genes are found. Among them, two (*adeh_0607* and *adeh_0608*) are close to the genes homologous to the *frz* system. No *M. xanthus* homologs were found using reciprocal blast but only one-way hits. Nevertheless, blast searches revealed

that Mxan_1131 and Mxan_1106 were the closest homologs of Adeh_0607 and *Adeh_0608*, respectively.

Interestingly, homologs of Mxan_1106 and Mxan_1131 were only found in Myxococcales encoding for a FrzZ homolog and were not found in *C. macrosporus* DSM 14697 and *S. amyloticus* (Figure 33 A). This co-occurrence suggests that they might be linked to FrzZ. Additionally, Mxan_1106 was already described as regulating T4P-dependent motility and named SgmC (social gliding motility protein C) (Youderian & Hartzell, 2006). These observations make these two proteins attractive candidates to analyze further for their involvement in Frz signaling.

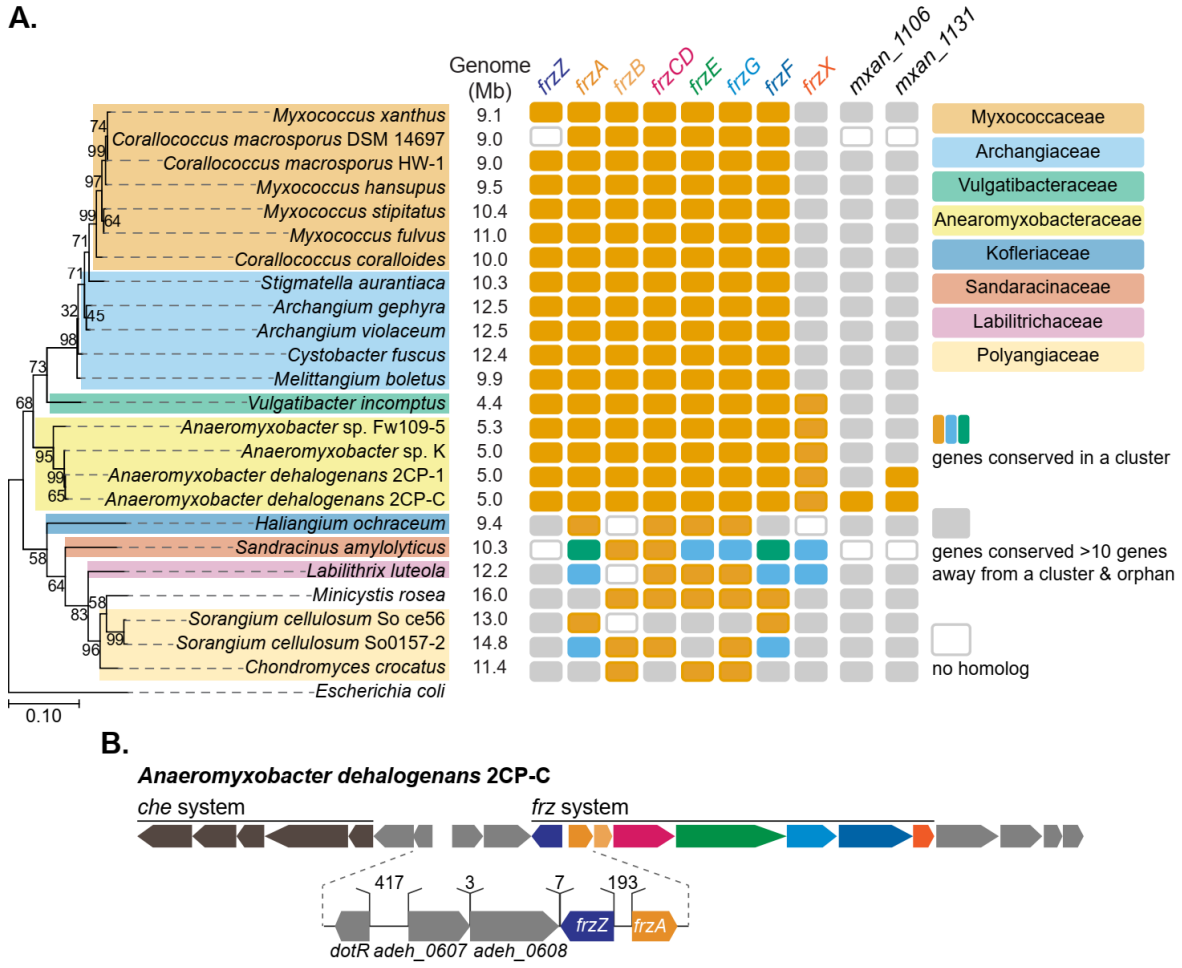

Figure 33: **Conservation of the *frz* cluster. (A)** Conservation of the *frz* cluster in Myxococcales with fully sequenced genomes. 16S rRNA tree of *Myxococcales* with fully sequenced genomes (left). Genome size and family are indicated. Ten genes were considered the maximum distance for a gene to be in a cluster. Genes found in the same cluster (within a distance of <10 genes) are marked with the same color. Light gray indicates a conserved gene found somewhere else on the genome (>10 genes away from a cluster); a white box indicates that no homolog is found.Homologs and genome regions were created using KEGG. **(B)** Genomic region of *frz* homologs found in *A. dehalogenans* 2CP-C. Colorful genes indicate homologous genes of the *frz* system. Brown genes indicate genes encoding a possible *che* system. Zoomed in the region shows the genomic neighborhood upstream of the *frz*

cluster. Numbers on top display base pair distances between genes. Genes are shown as arrows, and arrows indicate the orientation of encoded genes. The genomic region was created using KEGG.

3.6.1 Characterization of SgmC

Among the identified candidates, we studied the function of the previously identified SgmC protein, which is 892 aa long and contains several conserved domains (Figure 34 A). From aa 243 to 398 a PATAN domain is annotated, which is generally involved in the regulation of motility (Makarova *et al.*, 2006, Han *et al.*, 2022, Jakob *et al.*, 2020). Two intrinsically disordered regions (IDR) were found from aa 166 to 224, and 480 to 664. IDRs are involved in protein-protein interactions and phase separation, in which proteins containing such domains assemble into membrane-less organelles (Banani *et al.*, 2017). From aa 684 to 755, a J domain is encoded. DnaJ is a chaperone that can work together with DnaK and GrpE in diverse cellular processes like protein folding, refolding, disaggregation, and protein transfer to cellular compartments (Balchin *et al.*, 2016, Cyr *et al.*, 1994). At the C-terminus (aa 772 to 878), a TPR region with two repeats is found, often involved in mediating protein-protein interactions (Zeytuni & Zarivach, 2012).

When analyzing the genomic neighborhood of *sgmC* using KEGG (https://www.genome.jp/kegg/pathway.html July 2021), we found genes encoding for hypothetical proteins (*mxan_1109-mxan_1107,mxan_1104*), a potentially RNA-binding TIGR00253 family protein (*mxan_1105*), and an amidophosphoribosyltransferase (*mxan_1103*). Proteins of the genes of the genomic neighborhood (except *mxan_1109*) and *sgmC* were conserved among fully sequenced Myxococcales (time of analysis: July 2021). In more distantly related species, *sgmC* was encoded with only *mxan_1105* or orphan of its original cluster (Figure 34 C).

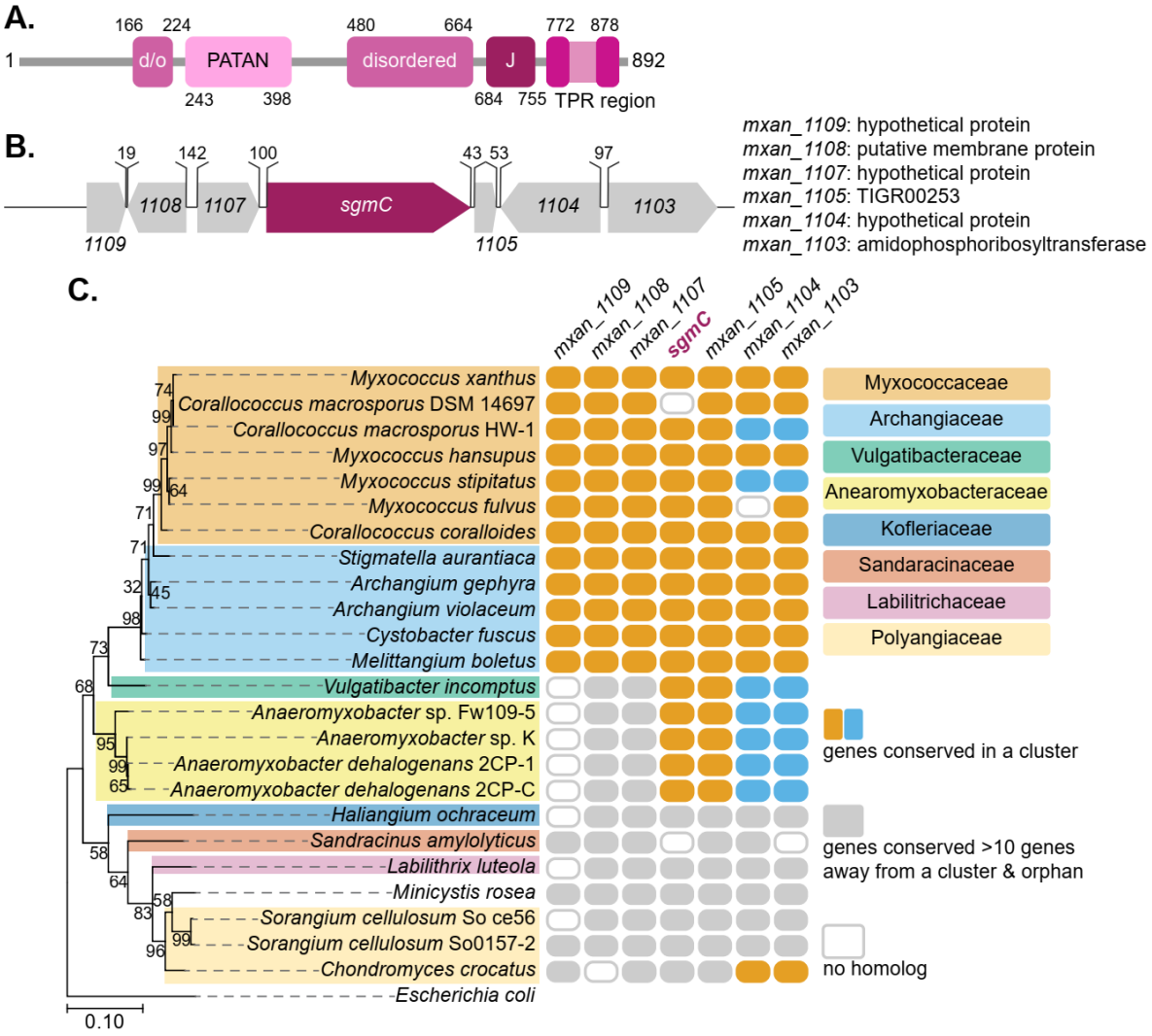

Figure 34: **Bioinformatic analysis of SgmC. (A)** Conserved regions in SgmC. Regions were obtained using InterPro (https://www.ebi.ac.uk/interpro/protein/UniProt/Q1DDA7/ May 2023). Numbers indicate aa positions. **(B)** The genomic neighborhood of *sgmC* with nearby proteins. Numbers on top display distances between genes. Genes are shown as arrows. Arrows indicate the orientation of encoded genes. Grey arrows display genes next to sgmC. The genomic region was created using KEGG. **(C)** Conservation of the *sgmC* genomic region in Myxococcales with fully sequenced genomes. 16S rRNA tree of *Myxococcales* with fully sequenced genomes (left). Families are indicated. Ten genes were considered the maximum distance for a gene to be in a cluster. Genes found in the same cluster (within a distance of <10 genes) are marked with the same color. Light gray indicates a conserved gene found somewhere else on the genome (>10 genes away from a cluster); a white box indicates no homolog is found. Homologs and genome regions were created using KEGG.

3.6.1.1 SgmC is important for both motility and EPS accumulation

To find out more about the function of SgmC, we constructed an in-frame deletion mutant (Δ*sgmC*). Since SgmC was previously described as important for T4P-dependent motility and involvement with the Frz system seems likely, we performed a motility assay (Figure 35 A upper panels).

Instead of the characteristic flares observed for WT on 0.5 % agar favoring T4P-dependent motility, a Δ*sgmC* strain showed altered motility behavior since cells formed a halo with undefined edges. On 1.5 % agar favoring gliding motility, the colony of an Δ*sgmC* mutant spread less than WT and showed more single cells and slime trails at the colony edges. This phenotype neither resembled the negative controls Δ*aglQ* or Δ*pilA* nor a Δ*frzE* mutant or a *frzCD*^{GOF} mutant strain.

Mutants lacking EPS have a smooth colony surface, similar the Δ*sgmC* colony. Therefore, we tested EPS accumulation using Trypan Blue and Congo Red, which bind EPS, leading to the colonies' blue/green or red color, respectively (Figure 35 A lower panels). Interestingly, the Δ*sgmC* mutant did not bind EPS, similar to deletion mutants that cannot synthesize EPS (i.e., Δ*epsZ* and Δ*difE*). EPS is vital for functioning T4P-dependent motility in *M. xanthus*, so lack of EPS may lead to the motility defects observed. In fact, an Δ*sgmC* colony looked similar to an Δ*epsZ* mutant, which lacks the first protein of EPS synthesis on 0.5 % agar (Perez-Burgos *et al.*, 2020). However, an Δ*epsZ* strain spread more and showed fewer single cells than a Δ*sgmC* strain. DifE is the histidine kinase of the Dif chemosensory system, which regulates EPS production (Yang *et al.*, 1998). Deleting *difE* led to a more uneven colony surface phenotype and a higher degree of spreading than a Δ*epsZ* or Δ*sgmC* mutant on both agar conditions (Figure 35 A upper panels). The observed phenotype was complemented by ectopically expressing *sgmC* under the control of its putative native promoter (Figure 35 B).

These results suggest that SgmC has a distinct function in motility regulation since its deletion phenotype does not resemble any other *M. xanthus* motility mutant reported so far.

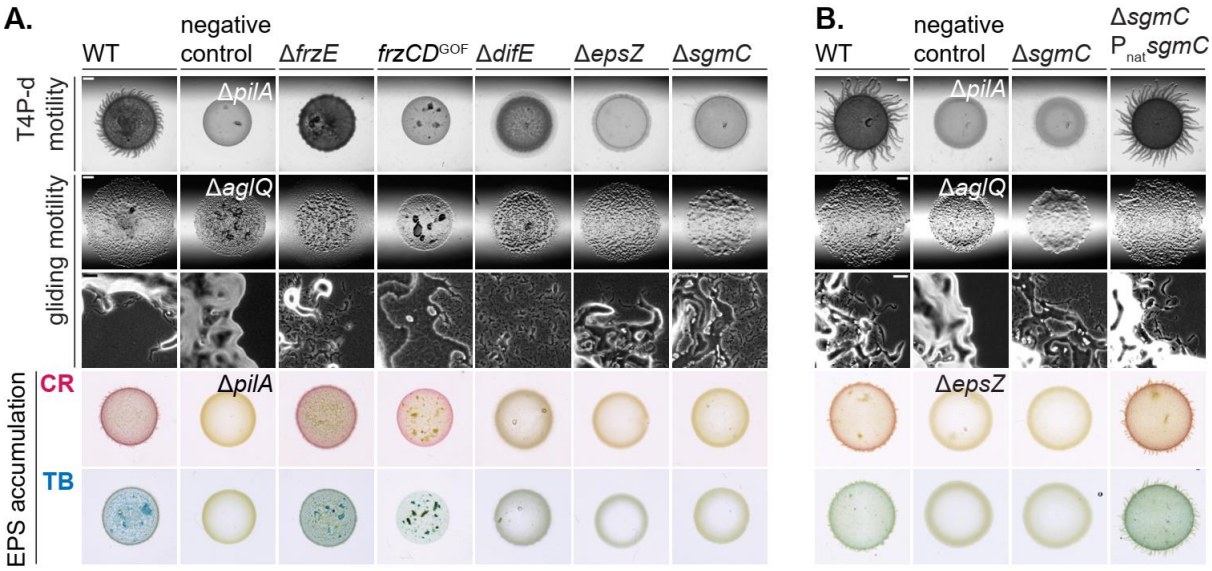

Figure 35: **A Δ*sgmC* mutant has a motility and EPS defect.** Motility assay and EPS accumulation assay of a Δ*sgmC* mutant **(A)** and a Δ*sgmC* P$_{nat}$*sgmC* mutant **(B)**. T4P-dependent motility was tested

on 0.5 % agar. Gliding motility was tested on 1.5 % agar. EPS accumulation was tested on 0.5 % agar containing 20 µg/ml Congo Red or 10 µl/ml Trypan Blue. Scale bars from top to bottom: 1 mm, 1 mm and 50 µm. One representative clone of each strain is shown.

Motility can be affected in different ways. Among others, the reversal frequency can be affected.

Since SgmC might be connected to the Frz system, we tested the reversal frequency of the Δ*sgmC* strain by performing a single cell motility assay on TPM 1.5 % agar (Figure 36 A). Δ*sgmC* cells reversed with a reversal frequency similar to that of WT. When activating the Frz system by the addition of 0.075 % IAA, WT reversals were increased. Cells of the Δ*sgmC* mutant also showed an increase in reversal frequency upon adding IAA. However, this increase was lower than observed for WT, suggesting that SgmC could be involved in controlling reversal frequency.

EPS synthesis and T4P assembly have been shown to regulate each other (Perez-Burgos *et al.*, 2020). The protein StkA negatively regulates EPS and is thought to link T4P machinery and EPS synthesis (Moak *et al.*, 2015). Because of this a lack of *stkA* can rescue the EPS defect of a Δ*pilA* strain but not a Δ*difA* strain in which the Dif system is non-functional. Similar effects can be achieved by adding 0.3 % IAA to 0.5 % agar containing Trypan Blue or Congo Red (personal communication María Pérez Burgos). In order to determine if SgmC acts up- or downstream of the EPS-regulating Dif system, we performed such an assay (Figure 36 B). As expected, the lack of EPS accumulation of a Δ*pilA* could be rescued by adding IAA. The same was observed for an *sgmC* deletion mutant, while mutants of the Dif system (Δ*difE)* or EPS synthesis (Δ*epsZ*) were still not accumulating EPS. This suggests that SgmC is acting upstream of the Dif system.

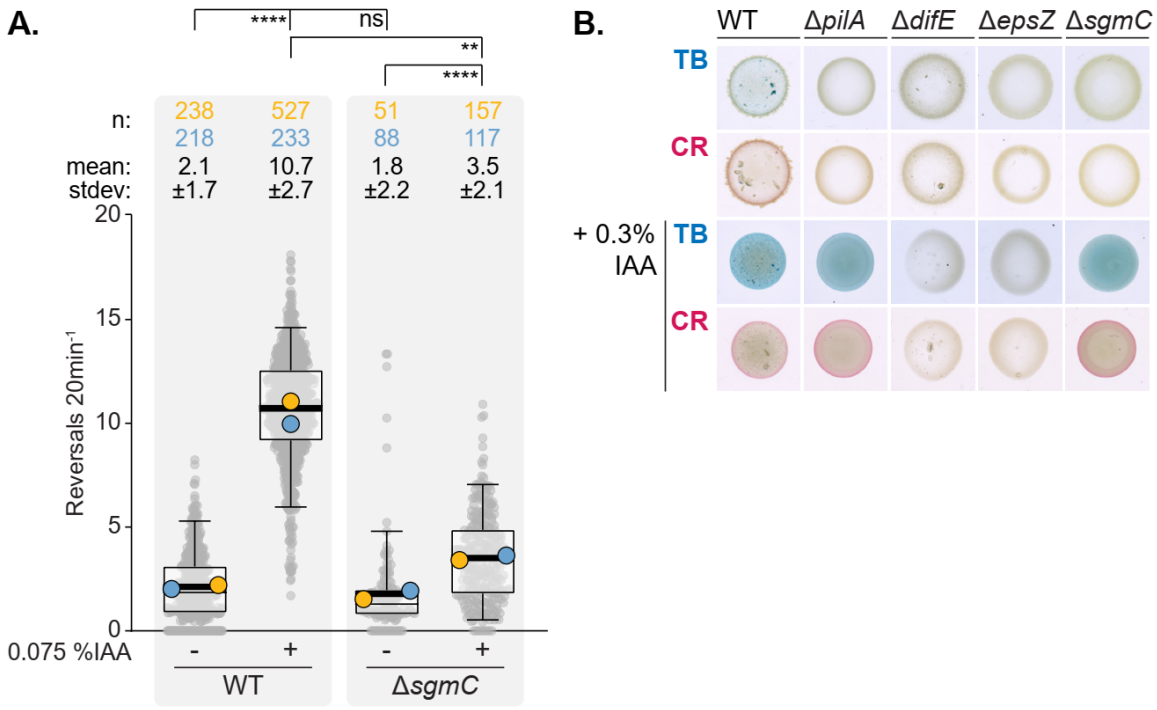

Figure 36: **SgmC acts upstream of the Dif system, leading to a decreased reversal frequency. (A)** Single-cell gliding reversal assay on TPM 1.5% agarose of Δ*sgmC*. Boxplots show the measured reversal frequency monitored as the number of directional changes per 20 min. Each dot in the scatterplot represents the reversal frequency of one cell. Boxes enclose the 25th and 75th percentile. Whiskers enclose the 5th and 95th percentile. The median is shown as a thin line in the box. The mean of each replicate is shown as a symbol in orange, blue, and green. The mean based on all three experiments is shown as a thick black line. The number of trajectories analyzed (n) and mean reversal frequencies for each strain are shown above the graph. Kruskal-Wallis test was used for statistical analysis. “ns”, non-significant ($p>0.05$); “**” indicates $p<0.01$; and “****” indicates $p<0.0001$. **(B)** EPS accumulation assay in the absence and presence of 0.3 % IAA. EPS accumulation was tested on 0.5 % agar containing 20 µg/ml Congo Red or 10 µl/ml Trypan Blue. A representative clone of each strain is shown.

3.6.2 Characterization of Mxan_1131

The second identified protein that might be connected to the Frz system is Mxan_1131. When searching for conserved domains of the 570 aa long protein using Interpro (https://www.ebi.ac.uk/interpro/protein/UniProt/Q1DD82/ July 2021), we find a RDD domain with three transmembrane regions at the C-terminus from aa 420 to 562. RDD domains which are transmembrane regions that contain one arginine and two aspartates, which are highly conserved. Additionally, two disordered regions were found from aa 56 to 312 and from 328 to 380, which might be involved in protein-protein interactions (Figure 37 A) (Banani *et al.*, 2017). Interestingly, analysis of the genomic context of *mxan_1131* using KEGG (https://www.genome.jp/kegg/pathway.html July 2021) showed that *mxan_1131* was found in a gene cluster with three genes encoding the previously described proteins FrgA, FrgB, and FrgC (Figure 37 B) (Cho *et al.*, 2000). Partial deletion of *frgA* led to frizzy aggregates in

development assays reminiscent of the frizzy phenotype. In contrast, insertion in *frgB* and *frgC* did not lead to an aberrant phenotype in development. It was suggested that FrgA might generate extracellular signal molecules needed for aggregation upon starvation (Cho *et al.*, 2000). In the meantime, it could be confirmed that a *frgA* in-frame deletion strain showed a motility defect (Schmidt, 2022). However, cells were hyperreversing and did not show a Frz LOF phenotype. Deletion of *mxan_1131* was also suggested to have a motility defect (Schmidt, 2022). In addition, Mxan_1131 was enriched in proximity labeling experiments using DmxA, while FrgA was enriched in the context with MglA (unpublished data Marco Herfurth & Maria Pérez Burgos). Deletion of the diguanylate cyclase DmxA leads to a hyperreversing phenotype, and it is suggested to regulate cell polarity during cell division (unpublished data Marco Herfurth & Maria Pérez Burgos). Furthermore, Mxan_1131 was found to localize to the septum (unpublished data Marco Herfurth & Maria Pérez Burgos). These data suggest that Mxan_1131 might be involved in regulating polarity during cell division.

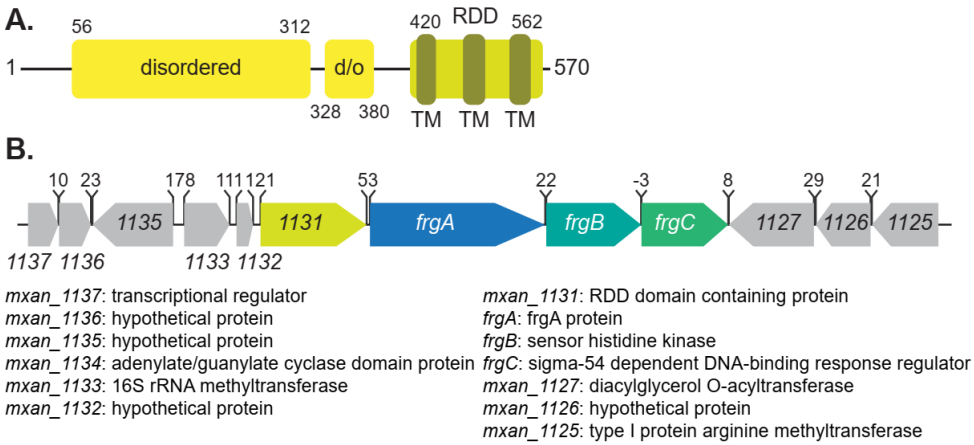

Figure 37: **Bioinformatic analysis of Mxan_1131. (A)** Conserved regions in Mxan_1131. Regions were obtained using InterPro (https://www.ebi.ac.uk/interpro/protein/UniProt/Q1DD82/ May 2023). Numbers indicate aa positions. **(B)** The genomic neighborhood of mxan_1131. Numbers on top display distances between genes. Genes are shown as arrows. Arrows indicate the orientation of encoded genes. Grey arrows display genes next to *mxan_1131, frgA, frgB, and frgC*. The genomic region was created using KEGG.

4 Discussion

M. xanthus cells move, utilizing two different motility systems, T4P-dependent, and gliding motility, exhibiting a front-rear polarity. The proteins of the polarity module establish this front-rear polarity, with the small Ras-like GTPase MglA being the main polar stimulator for both motility systems. The regulators RomR/RomX (GEF) and MglB/RomY (GAP) localize asymmetrically to both poles, but GAP activity dominates over GEF at the lagging cell pole due to the co-GAP RomY. At the leading cell pole, GEF activity dominates over GAP activity. This spatially restricts MglA-GTP localization and, therefore, functioning motility systems to the leading cell pole. However, *M. xanthus* cells can change their direction of movement in a reversal, requiring a preceding polarity switch for the motility systems to follow. The switch in polarity is induced by the Frz chemosensory system with its two response regulators, FrzX and FrzZ, that localize to lagging and leading cell pole after phosphorylation, respectively. These two proteins likely disrupt the balance of the polarity proteins at both poles to trigger the switch, but the precise molecular mechanism is poorly understood.

4.1 How does FrzZ induce a switch in polarity?

As previously shown, FrzZ localizes to the leading cell pole depending on MglA, which is thought to stimulate the dissociation of MglA (Kaimer & Zusman, 2013). Nevertheless, FrzZ-mVenus localized to the poles in a small fraction of cells without MglA when Frz signalling was enhanced, suggesting hat MglA might not be the only or the direct polar determinant of FrzZ but is still in line with the idea that MglA stimulates polar localization of FrzZ. This possibility is further substantiated by FrzZ-mVenus localizing in dynamic cytoplasmic clusters in a few cells in a *frzCD*^{GOF} Δ*mglA* background. Furthermore, our expanded candidate approach revealed that FrzZ did not follow MglA in every mutant we constructed, supporting the idea of an additional polar determinant. Of note, FrzZ localization in Δ*mglB* and Δ*romR* strains were similar in WT and *frzCD*^{GOF} strains, showing that polar localization of FrzZ did not depend on the level of Frz signaling in these strains. Thus suggests that the localization of FrzZ might be partially independent of phosphorylation and at least partially independent of the known polarity module components.

In search of a direct target of FrzZ, we first conducted Co-Immunoprecipitation experiments, which did not lead to new findings. FrzZ~P is the active variant needed for polar localization and is the form that can interact with its polar target. Previous studies showed that the half-life of phosphorylated FrzZ is limited (Kaimer & Zusman, 2013). Also, the interactions of FrzZ~P at the pole might be transient. This could explain the unsuccessful attempts using this method.

For these reasons, we tried to elucidate the interaction partners of FrzZ using biotinylation-based proximity labeling with which transient interactions can be detected *in vivo* (May & Roux, 2019). Using this approach, we found PixA in close proximity to FrzZ in a *frz*^{GOF} strain, in which FrzZ polar localization is increased. This finding was confirmed in the vice versa experiment in which we found FrzZ in close proximity to PixA in WT and *frz*^{GOF} strains. PixA is a PilZ-RR protein that was previously described to regulate reversals negatively (Kuzmich *et al.*, 2021).

We confirmed the observation that PixA inhibits reversals and expanded on this finding by showing that an increased amount of PixA within the cell leads to a decrease in reversal frequency. Furthermore, we found this inhibition was partially independent of the Frz system, because lack of PixA led to increased reversal frequency in *ΔfrzE and ΔfrzZ ΔfrzX* strains in which Frz signaling is inactive. However, this increase in reversal frequency did not reach the hyperreversing frequency of a *ΔpixA* mutant. PixA was epistatic to FrzZ, suggesting that FrzZ functions via PixA and that PixA acts downstream of FrzZ. In a model, FrzZ~P stimulates reversals by inhibiting PixA, leading to a switch in polarity (Figure 38 A). This inhibition seems to depend on the ratio of FrzZ~P to PixA since deleting *pixA* in a *frzCD*^{GOF} strain did not have an effect, while an excess of PixA-FLAG overcame the inhibition by Frz signaling, resulting in a decreased reversal frequency during high signaling levels. The addition of IAA leads to lower activity of the Frz system compared to a *frzCD*^{GOF}. *ΔpixA* cells showed a higher reversal frequency compared to WT in the presence of IAA, further supporting our hypothesis that inhibition of PixA depends on the level of active Frz signaling. Furthermore, we found that FrzX stimulates reversals independent of PixA, suggesting that after phosphorylation by FrzE, the Frz system functions via two pathways: FrzZ~P and PixA, and FrzX~P, which stimulates reversals independently of these two proteins (Figure 38 A).

We found PixA to be dynamically localized in the cell, with most of the protein localizing diffusely along the cell body. However, a fraction of PixA accumulated in clusters at the pole(s). PixA localized to either the lagging cell pole between reversals or to the leading cell pole between reversals or close to a reversal. This localization correlated with reversal frequency. Without Frz signaling, in a Δ*frzE* strain, where cells persistently move in one direction, PixA localizes more frequently to the pole and exclusively to the lagging cell pole. During high signaling levels, in a *frzCD*^{GOF} strain, at which cells reverse constantly, PixA localized to the leading cell pole. However, cells were able to reverse without a PixA cluster at the leading cell pole suggesting that leading cell pole localization is not essential for reversals.

Focusing on the connection between FrzZ and PixA, we came up with the following model (Figure 38 B): PixA occasionally localizes to the lagging cell pole in cells moving in one direction, inhibiting Frz-independent reversals. In this state, FrzZ prevents PixA from localizing stably to the lagging cell pole, and, therefore, polarity switching. FrzX might also have an

effect, although it would only be minor based on our results. When a Frz signal is sensed, FrzZ and FrzX are phosphorylated. FrzZ~P “pulls” PixA to the leading cell pole. FrzZ and PixA depended on each other for proper relocalization because PixA enhanced FrzZ localization to the leading cell pole. For the relocalization, PixA might be phosphorylated. The two proteins localize to the leading cell pole depending on MglA, although this might not be their sole target. At the same time, FrzX~P “pushes” PixA from the lagging cell pole. This is likely an indirect effect of FrzX~P targeting the lagging cell pole to induce the polarity switch via a different mechanism because FrzX functions independently of PixA.

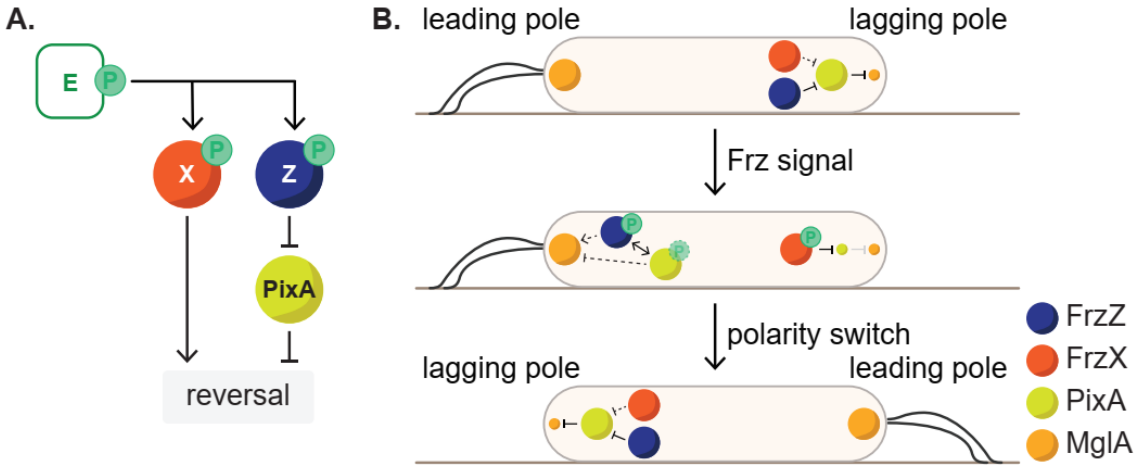

Figure 38: **(A)** Schematic of the Frz pathway including PixA. Frz proteins are labeled with their corresponding letters. Phosphorylation of protein (domains) is indicated with P. **(B)** Dynamic localization of PixA during reversals**.** Schematic cells with localization of FrzZ, FrzX, PixA, and MglA. Phosphorylation of protein (domains) is indicated with P. Arrows indicate stimulation. T-bars indicate inhibition. Dashed lines indicate unconfident relations. Grey lines indicate loss of function.

Several lines of evidence suggest that PixA inhibits Frz-independent reversals when localizing at the lagging cell pole. First, PixA inhibits reversals partially independent of Frz signaling because PixA acts downstream of FrzZ. Second, an increased amount of PixA at the lagging cell pole correlates with lower reversal frequencies. In a strain in which PixA was overexpressed, cells reversed less, and the protein localized more frequently to the lagging pole. Similarly, lagging cell pole localization was increased in Δ*frzE,* Δ*frzZ*, Δ*frzZ* Δ*frzX* strains that show a hyporeversing phenotype. Third, loss of PixA at the lagging cell pole correlates with increased reversal frequencies. This is true for a hyperreversing Δ*pixA* strain. Additionally, PixA$^{D180N/E}$ mutants that failed to localize to the lagging cell pole showed a LOF phenotype and hyperreversed.

FrzZ inhibits PixA at the lagging cell pole, since lagging cell pole localization was strongly increased in Δ*frzZ* and Δ*frzZ* Δ*frzX* strains. This increase was higher than observed for a Δ*frzE*

strain, suggesting that FrzZ inhibits PixA lagging cell pole localization independent of phosphorylation.

When phosphorylated, FrzZ~P takes PixA to the leading cell pole. This is supported by the finding that PixA did not localize to the leading cell pole in *frzCD*^{GOF} Δ*frzZ* and *frzCD*^{GOF} Δ*frzZ* Δ*frzX* strains. Additionally, PixA followed FrzZ localization in a *frzCD*^{GOF} Δ*mglA,* leading to drastically decreased polar localization at the leading cell pole. At the same time, the absence of PixA reduced FrzZ leading cell pole localization, suggesting a mutual dependency.

Our data suggest that the aspartate residue is important for the polar localization of PixA. A D180N (non-phosphorylatable) PixA variant did not localize to the lagging or leading cell pole, while a D180E (potentially phosphomimicking) PixA variant was only able to localize to the leading cell pole in a *frz*^{GOF} background, suggesting that PixA might be phosphorylated to localize to the leading cell pole.

Several lines of evidence suggest that FrzX~P inhibits lagging cell pole localization of PixA. First, lagging cell pole localization was decreased in a *frzCD*^{GOF} Δ*frzZ,* in which FrzX~P localizes to the lagging cell pole (Guzzo *et al.*, 2018), compared to a Δ*frzZ* strain. Second, in a *frzCD*^{GOF} Δ*frzX* strain in which FrzZ~P takes PixA to the leading cell pole, bipolar localization was increased.

In our aim to solve the question of how FrzZ induces a switch in polarity, we found that it acts via PixA. So far, our results show that PixA function at the lagging cell pole is important for the unidirectional movement of the cell. The polar target of PixA, however, remains to be identified. FrzZ inhibits PixA at the lagging cell pole which could be needed to enforce responsiveness to Frz signaling to respond to environmental changes by inhibiting stable accumulation of PixA. On a molecular level, PixA might inhibit the accumulation of MglA-GTP at the lagging cell pole. This is supported by the finding that MglA localized more bipolarly in the absence of PixA (Kuzmich *et al.*, 2021), which could explain the increased reversal frequency of a Δ*pixA* strain. This could be achieved by either promoting GAP activity or decreasing GEF activity to exclude MglA-GTP from the lagging cell pole. It was published that FrzZ leading cell pole localization is needed for fully functioning reversal regulation (Kaimer & Zusman, 2013). From our data, we know that PixA at the leading cell pole is not essential for reversals since cells without a leading cell pole cluster reversed. It is tempting to assume that PixA at the leading cell pole would have a similar function as at the lagging cell pole, thereby excluding MglA-GTP from this pole to ensure proper regulation of reversals. So far, we could not answer the question of whether FrzZ~P pulling PixA to the leading cell pole is beneficial for polarity switch. A PixA^{D180E} variant localized to the leading cell pole but had a Δ*pixA* (LOF) phenotype.This could imply that for a polarity switch to happen, it is only important to remove PixA from the lagging cell

pole. Alternatively, PixA must be dephosphorylated again when reaching the leading cell pole to function correctly. Further studies need to be conducted to decipher the exact function of PixA and FrzZ at the leading cell pole. Either way, the action of the two proteins lead to MglA-GTP dissociating from the pole, which starts the polarity switch. An interesting candidate to study leading cell pole localization of FrzZ, could be the Plectin Mxan_1142 which was enriched in close proximity of FrzZ and MglA.

4.2 How does FrzX induce a switch in polarity?

FrzX localizes to the lagging pole, depending on the activation state of the Frz system (Guzzo *et al.*, 2018). FrzX localizes to the lagging cell pole and is suggested to shift the balance of dominating GAP to GEF activities at the lagging cell pole to induce the switch in polarity (Guzzo *et al.*, 2018, Carreira *et al.*, 2020). Based on our previously described Frz pathways, FrzX has a function independent of PixA and FrzZ since it stimulated reversals in the absence of PixA (Figure 38 A). Because of this, FrzX~P “pushing” PixA from the lagging cell pole is likely indirect. As shown by Guzzo *et al.,* 2018, MglB was essential for polar accumulation of FrzX. In our extended candidate approach, we found that localization of FrzZ likely does not depend directly on MglB but rather on RomY, because polar localization was lost in a Δ*romY* strain. RomY is the co-GAP of the polarity module and forms a low affinity complex with MglB to stimulate its GAP activity (Szadkowski *et al.*, 2022). It is suggested that RomY ensures that the GAP activity is constrained to the lagging cell pole where it dominates over GEF activity thereby setting up the front-rear polarity with MglA-GTP at the leading cell pole (Szadkowski *et al.*, 2022). If FrzX stimulates reversals via RomY it might inhibit RomY’s function. This would lower the GAP activity and thereby shift dominating GAP to dominating GEF activity, allowing MglA-GTP to accumulate at the future leading cell pole (Figure 39). FrzX did not always follow RomY, suggesting it is not the sole polar determinator of polar FrzX accumulation. Furthermore, we confirmed that polar localization of FrzX depended on its phosphorylation in all tested strains, since we observed polar clusters at high signaling levels. This is in contrast to FrzZ that showed increased polar localization in Δ*mglB* and Δ*romR* strains independent of signaling levels.

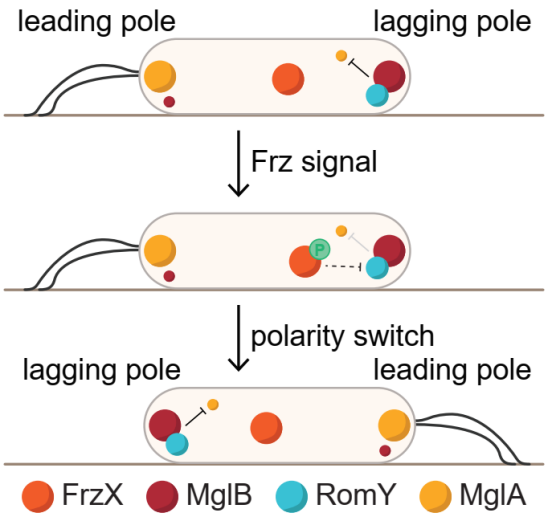

Figure 39: **Possible working model for function of FrzX.** Schematic cell with localization of FrzX, MglB, RomY, and MglA. Phosphorylation of protein is indicated with P. T-bars indicating inhibition. Dashed lines indicate unconfident relations. Grey lines indicate loss of function.

4.3 Regulation of dynamic cell polarity by the Frz system

Chemosensory systems most prominently regulate motility by flagella but are also involved in regulating T4P-dependent motility, development, biosynthesis, biofilm formation, and other cellular processes (Gumerov *et al.*, 2021). They all share conserved proteins but have modular adaptions for optimal function. The Frz system transmits the signal for switching polarity via two RRs, FrzX and FrzZ. A third RR, PixA, was identified to be part of the Frz system in this study. The RR domain of FrzE domain acts as a phosphate sink to prevent noisy activation of signaling (Kaimer & Zusman, 2016).

Other chemosensory systems also harbor several RRs to ensure ideal signal transmission and responsiveness. Similar to the function of $FrzE^{CheY}$, an additional CheY acts as a phosphate sink to regulate the rotation of the flagellum in *S. meliloti* (Sourjik & Schmitt, 1996, Kaimer & Zusman, 2016). In *R. sphaeroides*, several RRs that bind the motor switch are needed to regulate flagellar motility (Porter *et al.*, 2006). Furthermore, T4P-dependent motility in *P. aeruginosa* is controlled by the Chp system and its two RRS PilG and PilH. PilG is suggested to stimulate forward motion while PilH breaks the positive feedback of PilG to allow reversals (Kühn *et al.*, 2021, Kühn *et al.*, 2023).

The Frz pathway is especially interesting because FrzX and FrzZ act together for a tight regulation of reversals but are localized spatially separated to opposite poles. Additionally, it does not regulate motility directly but cell polarity, simultaneously promoting T4P-dependent and gliding motility activity. Intriguingly, this process does likely not solely depend on proteins of the polarity module. Both FrzX and FrzZ polar localization was increased in a Δ*romR*

mutant, in which polar localization of all polarity module proteins is severly decreased (Carreira *et al.*, 2020, Szadkowski *et al.*, 2019, Szadkowski *et al.*, 2022, Carreira *et al.*, 2023). In this study we identified PixA as a new player in Frz signaling that inhibits Frz-independent reversals. Similar to PilG in *P. aeruginosa*, PixA is suggested to ensure forward motion by preventing Frz-independent reversals. Like PilH, FrzZ might ensure responsiveness to Frz chemosensory signaling (Kühn *et al.*, 2023). However, the mechanism of the Frz pathway comprising FrzZ and PixA seems to work different from the Chp system. First, PixA can inhibit reversals independent of Frz signaling and there is no indication that FrzE phosphorylates PixA in contrast to the Chp system in which ChpA phosphorylates PilG and PilH. Second, PixA works in a linear pathway with FrzZ while PilG and PilH have separated functions in Chp signaling (Kühn *et al.*, 2023). Along the same lines, FrzZ targets PixA instead of altering the activity of the chemosensory system to ensure responsiveness as suggested for PilH (Kühn *et al.*, 2023). In addition to our new findings, FrzX~P is stimulating Frz-dependent reversals. For polarity and its switching to function correctly, the combined action of these proteins is needed because reversal frequency was even more decreased in a strain lacking both *frzX* and *frzZ* compared to single deletion strains of the two RRs.

It was suggested that the Frz signaling pathway has a modular structure that evolved to adapt regulation of polarity switching of two instead of one motility systems, when the gliding machinery was acquired in addition to the T4P machinery (Guzzo *et al.*, 2015). Downstream of the polarity module, the addition of AglZ added a connection point between MglA and the gliding machinery. Upstream, FrzZ was implemented into the pathway for optimal signal transmission to the polarity module (Guzzo *et al.*, 2015). Using bioinformatics analyses, we found that not only FrzZ is conserved primarily among bacteria that have T4P-dependent and gliding motility machines, but also FrzX and PixA, suggesting that they emerged at the same time and are also part of the adaption to regulate two motility systems.

In our quest to resolve the molecular mechanism leading to a polarity switch, we also searched for proteins found in proximity to MglA. This was done because FrzZ and FrzX, based on our results, are likely not directly targeting proteins of the polarity module, and we tried to find potential other regulators of MglA. This assay enriched known interactors regulating T4P-dependent motility (FrzS, SgmX) and gliding motility (AglZ, GltJ). Furthermore, we found RomR. Next to proteins that were already associated with MglA, we found a range of proteins that were already found to be involved in motility but also yet unknown potential interaction partners. Studies on these proteins and their connection to MglA could expand our knowledge of how MglA sets up the intricate polarity of *M. xanthus* cells. In this proximity labeling experiment, we also identified the RR-PATAN protein PglH. Interestingly, PglH was also

enriched in proximity labeling experiments using FrzX and PixA, making it a protein of interest for switching polarity.

Like a transposon-insertion mutant, gene deletion of *pglH* led to a hyperreversing phenotype (Yu & Kaiser, 2007). This suggests that PglH might be regulating polarity. Indeed, proteins possessing a combination of RR and PATAN domains were already shown to regulate polarity in cyanobacteria. PixE of *Synechocystis* sp. PCC 6803 directly regulates phototaxis negatively in response to blue light. Under blue light conditions, PixE diffuses from its complex with the blue light receptor PixD and interacts with the T4P extension ATPase PilB1, which is suggested to lead to an activation of pili at the lagging pole or an inactivation at the leading pole (Jakob *et al.*, 2020). More recently, it was shown that PixE and other cyanobacterial RR-PATAN proteins interacted with PilB via their PATAN domain, suggesting that this might be a general output (Han *et al.*, 2022). Additionally, PATAN proteins were occasionally encoded next to homologs of MglA and MglB, suggesting PATAN proteins' connection to polarity (Wuichet & Søgaard-Andersen, 2014, Makarova *et al.*, 2006). This was substantiated by our results from proximity labeling experiments using MglA as bait, in which we identified three RR-PATAN proteins (PglH, SgnC, and Mxan_5052). This makes PglH an interesting candidate that might be the bridge between the Frz system and MglA/the polarity module.

In a hypothetical scenario, PglH inhibts reversals. Since we found PglH in proximity of MglA, this could be achieved via inhibition of MglA accumulation at the pole. Furthermore, the PATAN domain of PglH is embedded within a domain related to proteins classified as GAPs containing a PATAN domain. PixA, which also inhibits reversals and was found in the proximity of PglH when it localized to lagging and the leading cell pole, would work with PglH for its proper function. Upon Frz signaling, FrzX~P, found in proximity to PglH when localizing to the lagging cell pole, would target PglH at the lagging pole, impairing its function. FrzZ~P takes PixA from the lagging to the leading cell pole. PglH would get further impaired by losing its partner at the lagging cell pole and/or possibly gaining its assistance at the leading cell pole (Figure 40). These actions would then lead to MglA-GTP dissociating from the leading cell pole and accumulating at the lagging cell pole, which causes a reversal. To support this hypothesis, many questions need to be answered: Can a Δ*pglH* mutant be complemented? Is PglH the final output of the Frz system? What is the subcellular localization of PglH? Does deletion of *pglH* affect the localization of MglA, PixA, and FrzX, and how are they connected? If PglH affects the localization of MglA, is it acting upstream of or with the polarity module proteins? Is the action of PixA needed at the leading cell pole for MglA to dissociate and how is PixA connected to PglH?

Additionally, Mxan_2049 could be a protein that functions together with PglH since it is found next to *pglH* on the genome and was also found in proximity labeling using MglA.

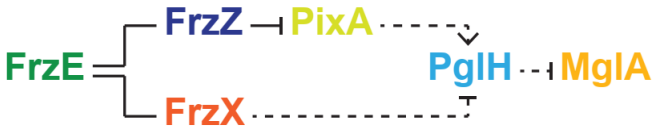

Figure 40: **A potential pathway to stimulate reversals, including PglH.** Arrows indicate stimulation. T bars indicate inhibition. Dashed lines indicate hypothetical relations.

PglH is conserved in a broader range of bacterial species, which do not harbour a gliding motility machinery (Luciano *et al.*, 2011). Suppose subsequent studies reveal PglH to be involved in polarity regulation via the predicted Frz pathway. In that case, it might have emerged before an adaption of the system was needed and would have been involved in controlling the polarity of one motility system. This hypothesis must be sustained by in-depth bioinformatics analyses, elucidating the cooccurrence of PglH, the Frz core proteins, the polarity module, and motility machinery proteins.

In our third approach to elucidate the switch in polarity using bioinformatics analysis, we identified the two proteins SgmC and Mxan_1131. SgmC regulates EPS synthesis, while Mxan_1131 might be involved in regulating cell polarity. Even though they might not be directly linked to translating the Frz signal via the response regulators FrzZ and FrzX, both might play important roles in motility regulation.

Even though this study could not fully clarify the exact molecular mechanism of the polarity switch in *M. xanthus*, we expanded our knowledge by adding one new and one potential novel player of Frz signaling. We also opened further questions, which bring us closer to understanding how the complex motility behavior, which is crucial for the population's survival, arises.

5 Material & Methods

5.1 Chemicals, Equipment and Software

All reagents, enzymes, and kits used in this study with their suppliers are listed in Table M 1, Table M 2, and Table M 3, respectively. Technical equipment with suppliers is listed in Table M 4. Software and its suppliers used are listed in Table M 5.

Table M 1: Reagents

Reagent	**Supplier**
Chemicals	Carl Roth GmbH + Co. KG (Karslruhe) Merck KGaA (Darmstadt)
Media components, agar	Carl Roth GmbH + Co. KG (Karslruhe) Fisher Scientific GmbH (Schwerte)
Oligonucleotides	Eurofins Genomics (Ebersberg)
Quick-Load® Purple 1 kb Plus DNA Ladder	New England Biolabs (Frankfurt a.M.)
PageRuler™ Plus Prestained Protein Ladder	Thermo Fisher Scientific™, Dreieich
Gel Loading Dye, Purple (6X)	New England Biolabs (Frankfurt a.M.)
ROTI®GelStain Red	Carl Roth GmbH + Co. KG (Karslruhe)
Immobilon Western HRP substrate	Merck KGaA (Darmstadt)
Pierce™ 660 nm Protein Assay Reagent	Thermo Fisher Scientific™, Dreieich
Ionic Detergent Compatibility Reagent for Pierce™ 660nm Protein Assay Reagent	Thermo Fisher Scientific™, Dreieich
Cytiva Amersham™ Protran™ NC Nitrocellulose Membrane	Fisher Scientific GmbH (Schwerte)

Table M 2: Enzymes

Enzyme	**Supplier**
Restriction Endonucleases	New England Biolabs (Frankfurt a.M.)
Antarctic Phosphatase	New England Biolabs (Frankfurt a.M.)
T4 DNA ligase	New England Biolabs (Frankfurt a.M.)
Phusion Green High-Fidelity DNA-Polymerase	Thermo Fisher Scientific™, Dreieich
Taq 2X Master Mix	New England Biolabs (Frankfurt a.M.)
Benzonase	Merck KGaA (Darmstadt)

Table M 3: Kits

Kit	**Supplier**
MasterPure DNA purification kit	Epicentre Biotechnologies (Wisconsin, USA)
NucleoSpin® Gel and PCR Clean-up kit	Macherey & Nagel (Düren)
NucleoSpin® Plasmid kit	Macherey & Nagel (Düren)
Monarch Plasmid Miniprep Kit	New England Biolabs (Frankfurt a.M.)

Table M 4: Equipment

Equipment	Application	Supplier
Mastercycler nexus gradient	Polymerase Chain Reaction	Eppendorf (Hamburg)
Mastercycler nexus X2		
Mastercycler personal		
Thermomixer comfort ThermoMixer C	Incubation of small reaction volumes	Eppendorf (Hamburg)
Centrifuge 5424 R	Centrifugation of small reaction volumes	Eppendorf (Hamburg)
Multifuge X1R	Centrifugation of Falcon tubes	Thermo Fisher Scientific™, Dreieich
Centrifuge Mega Star 1.6R		VWR International GmbH (Darmstadt)
Vortex Genie 2	Mixing of reactions	Fisher Scientific GmbH (Schwerte)
Ultrospec 2100 pro Spectrophotometer	Determination of optical densities	GE Healthcare Europe GmbH (Freiburg)
DS-11 Spectrophotometer	Nucleic acid quantification	DeNovix Inc. (Wilmington, USA)
Multifunktionsreader Infinite M200 Pro	Detection of absorption changes	Tecan Deutschland GmbH (Crailsheim)
Gel Stick "Touch"	Illumination of DNA in agarose gels	Intas Science Imaging Instruments GmbH (Göttingen)
MicroPulser Electroporator	Electroporation of bacterial cells	Bio-Rad (Feldkirchen)
Ultrasonic Lab Homogenizer UP200St	Cell disruption	Hielscher Ultrasonics GmbH (Teltow)
Mini-PROTEAN® 3 cell Mini-PROTEAN® TetraCell	Protein gel electrophoresis	Bio-Rad (Feldkirchen)
TransBlot® Turbo™Transfer System	Western Blotting	Bio-Rad (Feldkirchen)
Fuji Photo Film FPM 100A Luminescent image analyser LAS-4000	Chemiluminescence detection	Fujifilm (Düsseldorf)
M205FA Stereomicroscope with ORCA-Flash4.0 LT+ Digital CMOS camera	Microscopy	Leica (Wetzlar)
DMI6000B inverted microscope with ORCA-Flash4.0 LT+ Digital CMOS camera		
DMi8 inverted microscope with sCMOS camera DFC9000		
DMi8 Inverted microscope with CMOS-Kamera K8		

Table M 5: Software

Software	Application	Supplier
DNASTAR SeqBuilder Pro 17 & SeqMan Pro 17	Bioinformatics tool for *in silico* cloning	DNASTAR, Inc. (Madison, WI, USA)
SnapGene		GSL Biotech LLC (San Diego, CA, USA)
Leica MM AF	image acquisition and data analysis of microscopy pictures	Leica (Wetzlar)
icontrol 1.11	general-purpose software accessory for Tecan reader	Tecan Deutschland GmbH (Crailsheim)
Metamorph® v 7.5	microscopy analysis	Molecular Devices (San José, CA, USA)
Fiji	microscopy analysis	(Schindelin *et al.*, 2012)
MicrobeJ	ImageJ plugin for detection and analysis of bacterial cells	(Ducret *et al.*, 2016)
MATLAB R2020a	automated analyses of fluorescence signals, cell tracking, graph generation	The MathWorks (Natick, MA, USA)
Oufti	automated detection of cells in microscopic pictures	(Paintdakhi *et al.*, 2016)
Prism 9.0	statistical analysis	GraphPad Software (San Diego, CA, USA)

5.2 Media and additives

All media were autoclaved for 20 min at 121°C and 1 bar pressure. Antibiotics and other media additives that could not be autoclaved were filtered using sterile 0.22 µm pore site filters Merck KGaA (Darmstadt). Additives were added to pre-cooled media at around 55°C. Depending on the organism and the purpose, different media were used for cultivation that are listed in tables Table M 6 to Table M 10.

Table M 6: Media and additives used for the growth of *E. coli*.

Medium	Composition	
Luria-Bertani (LB)	1 % (w/v) tryptone, 0.5 % (w/v) yeast extract, 1 % (w/v) NaCl	
LB agar	LB medium 1.5 % (w/v) agar	
Antibtiotic	**Concentration**	**Solvent**
Kanamycin sulfate	50 µg/ml	H_2O
Tetracycline	5 µg/ml	99.99 % EtOH

Table M 7: Media and additives used for the growth of *M. xanthus*.

Medium	**Composition**	
1 % CTT	1% (w/v) BactoTM casitone, 10 mM Tris-HCl pH 8.0, 1 mM potassium phosphate buffer pH 7.6, 8 mM MgSO4	
1 % CTT agar (1.5 %)	1 % CTT medium 1.5 % (w/v) agar	
1 % CTT galactose plates	1 % CTT medium 1.5 % (w/v) agar 2 % - 3 % (w/v) galactose	
Antibiotic	**Concentration**	**Solvent**
Gentamycin sulfate	10 µg/ml	H_2O
Kanamycin sulfate	50 µg/ml	H_2O
Oxytetracycline	10 µg/ml	1M HCl
Vanillate	1µm-5µM	H2O (adjusted to pH 7.6 with KOH)

Table M 8: Media used for the growth of *M. xanthus* in colony-based motility assays

Medium	**Composition**
0.5 % CTT	0,5% (w/v) bactoTM casitone 10 mM Tris, pH 8.0 1 mM K2HPO4/KH2PO4, pH 7.6 8 mM MgSO4
Gliding motility agar (1.5 %) **(Hodgkin & Kaiser, 1977)**	0.5 % CTT medium 1.5% (w/v) select agar
Type-4-pili-dependent motility agar (0.5 %)	0.5 % CTT medium 0.5% (w/v) select agar

Table M 9: Medium used for single-cell gliding motility assay.

Medium	**Composition**
Gliding motility agar	0.5 % CTT medium 1.5% (w/v) SeaKem LE agarose (Lonza, Basel, Switzerland)

Table M 10: Media used for microscopy.

Medium	**Composition**
MC7	10 mM MOPS pH 7.0 1 mM $CaCl_2$
100x chitosan solution	2 M acetic acid 15 mg/ml chitosan

Table M 11: Medium used for washing cells during proximity labelling.

Medium	Composition
TPM	10 mM Tris, pH 7.6 1 mM K2HPO4/KH2PO4 8 mM MgSO4

5.3 Microbiological Methods

5.3.1 *E. coli* strains

Table M 12: *E. coli* strains used in this study

Strain	Genotype	Reference
NEB Turbo	F- proA+B+ lacIq ΔlacZM15 / fhuA2 Δ(lac-proAB) glnV galK16 galE15 R(zgb-210::Tn10)TetS endA1 thi-1 Δ(hsdS-mcrB)5	New England Biolabs (Frankfurt a. M.)

5.3.2 *M. xanthus* strains

Table 5: List of strains used in this study.

Strain	Genotype	Reference
DK1622	WT	(Kaiser, 1979)
DK10410	Δ*pilA*	(Wu & Kaiser, 1997)
SA5239	Δ*aglQ*	(Treuner-Lange *et al.*, 2015)
SA5649	Δ*difE*	Dorota Skotnicka
SA7400	Δ*epsZ*	(Perez-Burgos *et al.*, 2020)
DK10416	Δ*pilB*	(Wu *et al.*, 1997)
SA4420	Δ*mglA*	(Miertzschke *et al.*, 2011)
SA3387	Δ*mglB*	(Leonardy *et al.*, 2010)
SA7300	Δ*mglC*	(McLoon *et al.*, 2016)
SA3300	Δ*romR*	(Keilberg *et al.*, 2012)
SA3683	Δ*romX*	(Szadkowski *et al.*, 2019)
SA5958	Δ*romY*	(Szadkowski *et al.*, 2022)
SA9303	Δ*frzE*	Memduha Muratoglu
SA9543	*frzCD*$^{\Delta 5\text{-}153aa}$	This study
SA9518	Δ*frzX*	This study
SA9525	Δ*frzZ*	This study
SA9542	Δ*frzZ* Δ*frzX*	This study
SA8042	Δ*pixA*	(Kuzmich *et al.*, 2021)
SA9552	Δ*sgmC*	This study
SA12627	Δ*pglH*	This study
SA9967	*frzZ::frzZ-mVenus*	Luís Carreira
SA9527	Δ*frzE frzZ::frzZ-mVenus*	This study
SA9563	*frzCD*$^{\Delta 5\text{-}153aa}$ *frzZ::frzZ-mVenus*	This study
SA9549	Δ*mglA frzZ::frzZ-mVenus*	This study
SA11937	Δ*mglB frzZ::frzZ-mVenus*	This study
SA11912	Δ*mglC frzZ::frzZ-mVenus*	This study
SA11900	Δ*romR frzZ::frzZ-mVenus*	This study

SA11963	Δ*romX frzZ::frzZ-mVenus*	This study
SA11964	Δ*romY frzZ::frzZ-mVenus*	This study
SA9598	Δ*mglA frzCD*$^{\Delta 5\text{-}153aa}$ *frzZ::frzZ-mVenus*	This study
SA11965	Δ*mglB frzCD*$^{\Delta 5\text{-}153aa}$ *frzZ::frzZ-mVenus*	This study
SA11915	Δ*mglC frzCD*$^{\Delta 5\text{-}153aa}$ *frzZ::frzZ-mVenus*	This study
SA9596	Δ*romR frzCD*$^{\Delta 5\text{-}153aa}$ *frzZ::frzZ-mVenus*	This study
SA11934	Δ*romX frzCD*$^{\Delta 5\text{-}153aa}$ *frzZ::frzZ-mVenus*	This study
SA11903	Δ*romY frzCD*$^{\Delta 5\text{-}153aa}$ *frzZ::frzZ-mVenus*	This study
SA11926	Δ*frzE frzZ::frzZ-miniTurbo*	This study
SA11929	*frzCD*$^{\Delta 5\text{-}153aa}$ *frzZ::frzZ-miniTurbo*	This study
SA11975	Δ*frzE att::P*$_{frzZ}$*miniTurbo-FLAG*	This study
SA11976	*frzCD*$^{\Delta 5\text{-}153aa}$ *att::P*$_{frzZ}$*miniTurbo-FLAG*	This study
SA10120	Δ*pixA att::P*$_{nat}$*pixA-flag*	(Kuzmich *et al.*, 2021)
SA10141	Δ*pixA att::P*$_{pilA}$*pixA-flag*	Sofya Kuzmich
SA8054	Δ*frzE* Δ*pixA*	(Kuzmich *et al.*, 2021)
SA8055	*frzCD*$^{\Delta 5\text{-}153aa}$ Δ*pixA*	This study
SA12607	Δ*frzX* Δ*pixA*	This study
SA11984	Δ*frzZ* Δ*pixA*	This study
SA12608	Δ*frzZ* Δ*frzX* Δ*pixA*	This study
SA12619	*frzCD*$^{\Delta 5\text{-}153aa}$ Δ*pixA att::P*$_{pilA}$*pixA-flag*	This study
SA11977	*frzZ::frzZ-mVenus* Δ*pixA*	This study
SA11978	*frzCD*$^{\Delta 5\text{-}153aa}$ *frzZ::frzZ-mVenus* Δ*pixA*	This study
SA8051	*pixA::pixA-mVenus*	Sofya Kuzmich
SA11981	Δ*frzE pixA::pixA-mVenus*	This study
SA11982	*frzCD*$^{\Delta 5\text{-}153aa}$ *pixA::pixA-mVenus*	This study
SA11983	Δ*frzZ pixA::pixA-mVenus*	This study
SA12615	Δ*frzX pixA::pixA-mVenus*	This study
SA12614	Δ*frzZ* Δ*frzX pixA::pixA-mVenus*	This study
SA12612	*frzCD*$^{\Delta 5\text{-}153aa}$ Δ*frzZ pixA::pixA-mVenus*	This study
SA12626	*frzCD*$^{\Delta 5\text{-}153aa}$ Δ*frzX pixA::pixA-mVenus*	This study
SA12613	*frzCD*$^{\Delta 5\text{-}153aa}$ Δ*frzZ* Δ*frzX pixA::pixA-mVenus*	This study
SA12623	*frzCD*$^{\Delta 5\text{-}153aa}$ *pixA::pixA-mVenus ΔmglA*	This study
SA12620	*ΔpixA, att::P*$_{nat}$*pixA-mVenus*	This study
SA12621	*ΔpixA, att::P*$_{pilA}$*pixA-mVenus*	This study
SA12617	*pixA::pixA*^{D180N}*-mVenus*	This study
SA12618	*pixA::pixA*^{D180E}*-mVenus*	This study
SA11985	*pixA::pixA-miniTurbo-FLAG*	This study
SA12629	*18-19::P*$_{van}$*pixA-miniTurbo-FLAG*	This study
SA12632	Δ*frzZ* Δ*pixA 18-19::P*$_{van}$*pixA-miniTurbo-FLAG*	This study
SA12631	*frzCD*$^{\Delta 5\text{-}153aa}$ Δ*pixA 18-19::P*$_{van}$*pixA-miniTurbo-FLAG*	This study
SA12630	Δ*frzE* Δ*pixA 18-19::P*$_{van}$*pixA-miniTurbo-FLAG*	This study
SA12027	*18-19::P*$_{van}$*sfGFP-miniTurbo-FLAG*	Marco Herfurth
SA12611	Δ*frzE 18-19::P*$_{van}$*sfGFP-miniTurbo-FLAG*	This study
SA12610	*frzCD*$^{\Delta 5\text{-}153aa}$ 18-19*::P*$_{van}$*sfGFP-miniTurbo-FLAG*	This study
SA12633	Δ*frzZ 18-19::P*$_{van}$*sfGFP-miniTurbo-FLAG*	This study
SA9587	*frzX::sfGFP-frzX*	This study
SA9585	Δ*frzE frzX::sfGFP-frzX*	This study
SA9590	*frzCD*$^{\Delta 5\text{-}153aa}$ *frzX::sfGFP-frzX*	This study
SA11991	Δ*mglA frzX::sfGFP-frzX*	This study
SA9592	Δ*mglB frzX::sfGFP-frzX*	This study

SA11909	Δ*mglC frzX::sfGFP-frzX*	This study
SA9594	Δ*romR frzX::sfGFP-frzX*	This study
SA11940	Δ*romX frzX::sfGFP-frzX*	This study
SA11906	Δ*romY frzX::sfGFP-frzX*	This study
SA11958	Δ*mglA frzCD*$^{\Delta 5\text{-}153aa}$ *frzX::sfGFP-frzX*	This study
SA11959	Δ*mglB frzCD*$^{\Delta 5\text{-}153aa}$ *frzX::sfGFP-frzX*	This study
SA11960	Δ*mglC frzCD*$^{\Delta 5\text{-}153aa}$ *frzX::sfGFP-frzX*	This study
SA11961	Δ*romR frzCD*$^{\Delta 5\text{-}153aa}$ *frzX::sfGFP-frzX*	This study
SA11962	Δ*romX frzCD*$^{\Delta 5\text{-}153aa}$ *frzX::sfGFP-frzX*	This study
SA11966	Δ*romY frzCD*$^{\Delta 5\text{-}153aa}$ *frzX::sfGFP-frzX*	This study
SA11920	Δ*frzE frzX::flag-miniTurbo-frzX*	This study
SA11921	*frzCD*$^{\Delta 5\text{-}153aa}$ *frzX::flag-miniTurbo-frzX*	This study
SA8185	*mglA::mglA-mVenus*	(Szadkowski *et al.*, 2019)
SA12042	*mglA::mglA-miniTurbo-FLAG*	Marco Herfurth
SA11945	Δ*sgmC att::PnatsgmC*	This study

5.3.3 Cultivation and storage of *E. coli*

E. coli strains were used for cloning and propagation of plasmids. Cells were grown aerobically on LB agar plates, containing selective antibiotics if needed, at 37°C. Liquid cultures were incubated aerobically in LB medium on horizontal shakers at 37°C and 230 rpm in Erlenmeyer flasks in 1/5 of the total flask volume. If necessary, growth was followed by the determination of optical density at 600 nm (OD_{600nm}).

For short-term storage, *E. coli* cultures on solid media were stored at 4°C. For long-term storage, *E. coli* glycerol stocks were prepared from overnight cultures by the addition of 333 µl 40 % (v/v) glycerol to 1 ml of culture in cryo-tubes. The stocks were immediately frozen in liquid nitrogen and then stored at -80°C.

5.3.4 Cultivation and storage of *M. xanthus*

M. xanthus cells were grown aerobically on 1 % CTT agar plates, containing selective antibiotics if needed, at 32°C in the dark. Liquid cultures were grown aerobically in 1 % CTT liquid medium containing antibiotics on horizontal shakers at 32°C and 230 rpm in the dark in Erlenmeyer flasks in 1/5 of the total flask volume. Optical density was determined at 550 nm (OD_{550nm}). All media used for growing *M. xanthus* strains generally contained Gentamycin to prohibit contamination.

For short-term storage, *M. xanthus* cultures on solid media were stored at 18°C in the dark. For long-term storage, *M. xanthus* glycerol stocks were prepared from overnight cultures by adding 333 µl 40 % (v/v) glycerol to 1 ml of culture in cryo-tubes. The stocks were immediately frozen in liquid nitrogen and then stored at -80°C.

5.3.5 Colony-based motility assay

Motility assays were performed to check *M. xanthus* strains for motility phenotypes. Cultures were grown in exponential growth phase for 24 h and harvested at an OD_{550nm} of 0.5 – 1. 2 ml of cultures were centrifuged at 10000 rpm for 5 min at room temperature (RT) and resuspended to an OD_{550nm} of 7 in 1 % CTT medium. 5 µl of each culture was spotted on 0.5 % agar plates for T4P-dependent motility and 1.5% agar plates for gliding motility which were poured 24 h prior to use (composition see Table M 8). After drying the spots, plates were incubated for 24 h at 32°C in the dark. Pictures of colonies of both plates and close-up pictures of 0.5 % plates were acquired using the Leica M205 FA stereomicroscope. Close-up pictures of 1.5 % plates were acquired using the Leica DMi8 Inverted microscope. Settings are described in Table M 13.

Table M 13: Microscope settings for motility assay pictures using Leica M205 FA stereomicroscope and Leica DMi8 Inverted microscope.

0.5 % agar plates		
	Colony	Close-up
Magnification	15	60
Intensity [%]	17	37
Numerical aperture [%]	100	56
Balance [%]	7	7
1.5 % agar plates		
	Colony	Close-up
Magnification	15	
Intensity [%]	27	20x magnification at Leica
Numerical aperture [%]	70	DMi8 Inverted microscope
Balance [%]	-9	

5.3.6 Gliding single-cell motility assay

Single-cell motility assays were performed to check individual cells' reversal frequency, velocity, and overall behavior. For this, an assay performed by Guzzo et al., 2018 was modified. Cultures were grown in exponential growth phase for 24 h and harvested at an OD550nm of 0.5 - 1. 500 µl of cultures were centrifuged at 10000 rpm for 2 min at RT and resuspended to an OD_{550nm} of 2 in 1 % CTT medium. 2 µl of samples were spotted onto a coverslip below a freshly made 0.5 % CTT 1.5% agarose pad (composition see Table M 9). Note, for single-cell motility assay analyzing reversals of a *sgmC* deletion, medium without added CTT was used. After incubation at 32°C in the dark for 30 min, cells were imaged every 30 s for 20 min using a DMi8 inverted microscope with sCMOS camera DFC9000 with a 20x objective. Automated analysis of timelapse movies was then performed using the tracking feature of the ImageJ plugin MicrobeJ. Cells must be tracked for a minimum of 40 frames (the

whole 20 min) by calculating all object distances between two consecutive frames and selecting the nearest object to be considered in the analysis. Directional changes were scored as reversals when cells switched their direction of movement, and the angle between the segments was less than 45°. Trajectories with a "distance mean per frame" of less than 0.3 µm were removed from the data set to remove cells that were not moving. Reversal frequencies were calculated by dividing the number of reversals by track duration and multiplying by 40 to generate a reversal frequency per 20 min. Reversal frequencies were plotted as SuperPlots using MATLAB (Lord *et al.*, 2020). Statistical analysis was performed in GraphPad Prism 9.0 by Kruskal-Wallis-Test.

The gliding single-cell assay in 3.6.1.1 was performed on TPM 1.5 % agarose instead without CTT. Cells were imaged for 1h every 30s instead for 20 min.

5.3.7 Trypan Blue and Congo Red binding assays

Plate assays were carried out to determine the ability of M. xanthus to bind Trypan Blue and Congo Red dyes. Samples were prepared as described in 5.3.5. 20 µl of samples were spotted onto 0.5 % agar plates that contained 20 µl/ml Congo Red or 10 µl/ml Trypan Blue that were poured 24 h prior to use. After drying the spots the plates were incubated upside down for 24 h at 32 °C in the dark. Pictures were acquired using the Epson Perfection V700 Photo scanner.

5.4 Cell biological methods

5.4.1 Fluorophores and filter sets for fluorescence microscopy used in this study

Table M 14: Fluorophores used in this study.

Fluorophore	**Specification**
mVenus	monomeric fluorophore Excitation maximum: 515 nm Emission maximum: 527 nm
sfGFP	weak dimer fluorophore Excitation maximum: 485 nm Emission maximum: 510 nm
mCherry	monomeric fluorophore, codon optimized Excitation maximum: 587 nm Emission maximum: 610 nm

5.4.2 Live cell imaging

To perform fluorescence microscopy with *M. xanthus* strains, liquid cultures were inoculated and grown in 5 ml 1 % CTT medium for 48 h in an exponential growth phase by diluting in the morning and evening to an OD_{550nm} of 0.3 or 0.1, respectively. On day 3, cells were imaged at an OD_{550nm} of 0.5 - 0.9. µ-dishes coated with chitosan were used for microscopy. To this end, a 100 x chitosan stock was prepared by dissolving 30 mg of chitosan in 2 ml 2 M acetic acid (Ducret *et al.*, 2013b). The 100 x chitosan stock solution can be stored at 4 °C until use. A 1 x chitosan solution was prepared by diluting the stock solution in H_2O and gently inverting the tube until mixed. 35 mm glass bottom µ-dishes (ibidi, Gräfelfing) were then coated via incubation of the slide with 1 ml 1 x chitosan solution for 20 min. Dishes were washed with 1 ml H_2O followed by a washing step with 1 ml MC7 buffer. 50 – 150 µl of cell cultures were mixed with 1 ml MC7 buffer and transferred to the slide. Slides were incubated for 1 h (strains expressing FrzZ-mVenus) or 1.5 h (strains expressing sfGFP-FrzX or PixA-mVenus) at 32 °C in the dark. Cells expressing FrzZ-mVenus and sfGFP-FrzX were imaged using a temperature-controlled Leica DMI6000B inverted microscope with ORCA-Flash 4.0 LT+ Digital CMOS camera using the settings listed in Table M 15. Cells expressing PixA-mVenus were imaged using a temperature-controlled Leica DMi8 inverted microscope with a sCMOS camera DFC9000 using the settings listed in Table M 15. IAA was added to the indicated concentrations after incubation of the slide directly before microscopy.

Table M 15: Settings used for live cell imaging.

	Snapshots		**Timelapse movies**	
	Intensity	Exposure time	Intensity	Exposure time
FrzZ-mVenus	100 %	750 ms	10 %	750 ms
sfGFP-FrzX	100 %	1.5 s	10 %	1.2 s
PixA-mVenus	100 %	1.2 s	17 %	1 s

5.4.3 Analysis of fluorescence microscopy images

In order to automatically analyze the fluorescent signal of cells, phase contrast pictures were used to determine cell masks using oufti (Paintdakhi *et al.*, 2016). Next, a custom MATLAB (Mathworks) script used these cell masks to analyze fluorescent microscopy images.

Cells were segmented into two polar regions and the cytoplasmic region, of which the polar regions are defined as the parts of a cell within a distance of 10 pixels, corresponding to 0.65 µm, from the tip of a cell. For spot detection, the background-corrected fluorescence image was first filtered by convolution with a negative Laplacian of Gaussian (LoG) kernel, which enhances spot-like features of the image while compressing the range of pixel intensities in

non-spot regions. This filter is used because of the faint nature of clusters of the examined proteins.

$$L(i,j) = \frac{2\sigma^2 - (i^2 + j^2)}{2\pi\sigma^6} \exp\left(-\frac{i^2 + j^2}{2\sigma^2}\right)$$

The kernel size (L) and width parameter (σ) were chosen to match the detected polar spots with those identified by inspection. Pixels in the LoG-filtered image with intensity greater than a threshold of three standard deviations above the mean of all pixels within the cell mask but outside the two polar search regions were identified. A pole was considered to have a polar spot if a contiguous set of at least three pixels above the threshold intensity was found within the corresponding polar search region. The fluorescence of a polar cluster was defined as the sum of the fluorescence signal of all connected pixels that exceeded the threshold value in that polar region. The total fluorescence of the polar clusters and cytoplasm was recalculated as a percent of the total cell fluorescence. If bipolar clusters were visible, pole 1 always had the higher fluorescent signal. The omega value, which represents the asymmetry between the polar clusters, was calculated from the equation:

$$\omega = \frac{total\ fluorescence\ pole\ 1 - total\ fluorescence\ pole\ 2}{total\ fluorescence\ pole\ 1 + total\ fluorescence\ pole\ 2}$$

The omega value is between 0 and 1. An omega value of ω>0.9 defines a unipolar localization. An omega value of 0.9>ω>0.2 defines asymmetric bipolar, and ω<0.2 defines symmetric bipolar cluster localization. A diffuse signal was detected if no polar cluster was identified.

Table M 16: Parameters used for cluster detection.

	L	**σ**	**threshold**
FrzZ-mVenus	4	1.75	5
sfGFP-FrzX	5	1.7	5
PixA-mVenus	5	1.7	5
PixA-mVenus^{overexpressed}	3	1.7	5

5.5 Molecular biological methods

5.5.1 Oligonucleotides

Oligonucleotides synthesis was performed by Eurofins Genomics Germany GmbH (Ebersberg). Blue sequences indicate indicate recognition sites for restriction endonucleases, red sequences indicate start and stop codons in the primer sequence, grey sequences indicate nucleotides for fusion PCR, green sequences indicate additional nucleotides that were used as linker sequences, and purple sequences indicate additional tags.

Table M 17: List of Oligonucleotides used in this study.

No.	Name	Sequence
	attB left	CGGCACACTGAGGCCACATA
	attB right	GGAATGATCGGACCAGCTGAA
	attP left	GGGAAGCTCTGGGTACGAA
	attP right	GCTTTCGCGACATGGAGGA
	C 18-19 fw	CCCACGGAGAGCTGCGTGAC
	C 18-19 rv	GAGAAGGGTGCCGTCACGTC
	P 18-19 fw	CGCAAGGCGACAAGGTGCTG
	P 18-19 rv	CCCTGGCCGCCATTCGTAAC
	GFP rv	ATCGAAGCTTTTACTTGTACAGCTCGTCCATGCC
	mglA E	GTGGGAAGGGCTCTTTCAG
	mglA F	GACGTCTTCCCCGGCTCC
	mglA G	GGCCCGGGCTCTGCGGGAAG
	mglA H	GCGTGTCGAAGACGCCCACGC
	mglB E	GCGAGAAGCCATAGCCCG
	mglB F	CTTGCCTGTAGGACGTCT
	mglB G	GTTTGCGACCGGCTTACC
	mglB H	GACCCAGCTCCAGGACTG
	romR E	GGAGGCGCTGCCGCACC
	romR F	GGCCCGGTACATCAGGCC
	romR G	AGTCCAACACGATGCCCG
	romR H	GACGCGCGAAGCCACCCG
	romX E	GAGGCTCCGTCCGAGCCGGG
	romX F	CTTCTGGAGCGCCACCAGCGC
	romX G	GCGATTGCCTCGGATATC
	romX H	GAGCGCAGGACGATGTCG
	romY E	GGGCGGATGAGCGCCTTGCCCAGC
	romY F	TCTCGCGCGCCTCCGCGCGG
	romY G	GGCTTCAATCACAACATC
	romY H	GAGGATGACCTCGTCGAG
	mglC E	TTGGTGAAGCCCCCGTAACA
	mglC F	CTTGCCATTGTAGAAGAGGA
FM21	P_{frzX} fw	GCGGATCCAGGGTCCATCTGTCACGGTG
FM22	P_{frzX} rv	AGTTCTTCACCTTTAGACATGGCGACCTTCCTTCACTCCTTTATC
FM23	sfGFP fw	GATAAAGGAGTGAAGGAAGGTCGCCATGAGCAAAGGAGAA
FM24	sfGFP rv	CCTTATGCGTCTGCGCAGCCTAGGCAAGATCCGGCTGGTCTGTTTGTAGAGCTCATCCAT
FM25	frzX fw	GCCTAGGCTGCGCAGACGCATAAGGTCCGAGAAGCGAAGAATCCT
FM26	frzX rv	GCGAATTCTCACCAGAGGATGCTCTGCA
FM27	frzZ A	GCAAGCTTCACGTAGCTGCCCGTGAC
FM28	frzZ B	GGGCATCAGCTCCTTGGCCTCCACCAGCATCGGGCT
FM29	frzZ C	AGCCCGATGCTGGTGGAGGCCAAGGAGCTGATGCCC
FM30	frzZ D	GCGAATTCGGACGTGGAGGCCTCCAT
FM31	frzZ E	GCTTGGAGAAGTTGAGGA
FM32	frzZ F	CAGGCGGGCTCCATCAAC
FM33	frzZ G	CTTGCCAGCCTCGAGCTG
FM34	frzZ H	CTCGACGTTCTCACCCGA

FM35	frzX E	CTCAGCAGAGGAGACACG
FM36	frzX F	CGAAGTCTGCTCCCTGCG
FM37	frzX G	CTCGCGATGGAGAAGGCC
FM38	frzX H	CATGGCTTCCAGTCCGTT
FM39	frzX up fw	GCAAGCTTCTTGCTCAGCGAGCCCAC
FM46	frzCD E	CAATTCCTTGCGCCGGAT
FM47	frzCD F	GTGGCGAGGTTGATGACG
FM48	frzCD G	CAACGAGAAGCCCGCTGG
FM49	frzCD H	GACGAGGACAGCCTCAAC
FM56	sgmC A	GCAAGCTTCCCGCCGCCCAGTGC
FM64	sgmC B2	GCGTCTAGACTCCGCCATGCGCGG
FM65	sgmC C2	GCGTCTAGAAAGAAGTAGGGTGCG
FM59	sgmC D	GCGAATTCGGTGGACTGGGGGA
FM60	sgmC E	GCTACAACTGCGCGA
FM61	sgmC F	GCTGAAGCTGGTGGC
FM62	sgmC G	GGTGTCCGACCCATG
FM63	sgmC H	CTCTTGAGCTCCTCG
FM76	frzZ up fw	GCAAGCTTTCCCCACCGCCGTGCCCG
FM77	frzZ up rv	GCTCCCGCCCCCGCCCTCGTTACCGGTGGG
FM78	turbo fw	GGCGGGGGCGGGAGCATGATCCCGCTCCTG
FM79	turbo rv	CGCGGCCCCTGGGGATCACTTCTCGGCGCT
FM80	frzZ down fw	AGCGCCGAGAAGTGATCCCCAGGGGCCGCG
FM81	frzZ down rv	GCGAATTCGGCCTACTACAAGCCGGT
FM82	frzX up rv	CTTGTCGTCGTCGTCCTTGTAGTCCATGGCGACCTTCCTTCA CTC
FM83	turbo flag fw	ATGGACTACAAGGACGACGACGACAAGATGATCCCGCTC CTGAAC
FM84	turbo rv	GCTCCCGCCCCCGCCCTTCTCGGCGCTGCGCAG
FM85	frzX down fw	GGCGGGGGCGGGAGCGTGTCCGAGAAGCGAAGA
FM86	turbo fw	GCGCTCTAGAATGATCCCGCTCCTG
FM87	turbo rv	GCGCAAGCTTTCACTTGTCGTCGTCGTC
FM90	Pnat frzZ fw	GCGCGAATTCCACGTAGCTGCCCGTGAC
FM91	Pnat frzZ rev	GCGCTCTAGACGTCCTCCTCAAGGGCTT
FM117	pglH A	GCAAGCTTCTGTATCTGGCTGCTCGG
FM118	pglH B	CGTCCCCGCTCAGTTGCCCTTGGCCACGTTCCATGC
FM119	pglH C	GCATGGAACGTGGCCAACGGCAACTGAGCGGGGACG
FM120	pglH D	GCTCTAGAAGGCCTGCACCTCGTAGA
FM121	pglH E	GGTCTTCTTCCGCAAGCG
FM122	pglH F	TGTCATATGCCTCGCCGG
FM123	pglH G	GAGCTGGGACGGCTCAAG
FM124	pglH H	CACTCACCAGCGTCACCT
FM134	pixA start fw	GCGCCATATGATGAACCCGGGTCCAGAGGAC
FM135	turboID rv	GCGCGAATTCTCACTTGTCGTCGTCGTC
SK128	P_{nat}pixA fw	GCGCTCTAGAAGTACCGCACGAGGCCAG
SK188	pixA fw	GCCGTCTAGAATGAACCCGGGTCCAGAGGAC
SK102	pixA E	CTGGGTCAGGCTTTCGTGGTGAT
SK103	pixA F	CATGGCCGAGCGCGAGCT
SK104	pixA G	GGTCCGGCTCGCACTTTCTT
SK105	pixA H	GGACCTCCAGGGGGACCTTT

5.5.2 Plasmids

Table M 18: List of plasmids used in this study.

Plasmid	Description	Reference
pBJ114	vector containing *galK*, used for double homologous recombination at the native site of genes, kanamycin^R	(Julien *et al.*, 2000)
pSWU30	vector containing *Mx8 attP* fragment for integration into genomic *Mx8 attB* site, tetracycline^R	(Wu & Kaiser, 1997)
pSW105	vector containing *Mx8 attP* fragment for integration into genomic *Mx8 attB* site, contains P_{pilA} kanamycin^R	(Jakovljevic *et al.*, 2008)
pMR3690	vector containing P_{van}, used for integration in the *mxan18-19* site, kanamycin^R	(Iniesta *et al.*, 2012)
pDJS102	pBJ114; for generation of an in-frame deletion of *difE*	Dorota Skotnicka
pAP19	pBJ114; for generation of an in-frame deletion of *frzE*	Anna Potapova
pLC68	pBJ114, for generation of an in-fram deletion in *frzCD* deleting 5-153aa	Luís Carreira
pLC46	pBJ114; for generation of an in-frame deletion of *frzX*	Luís Carreira
pFM59	pBJ114; for generation of an in-frame deletion of *frzZ*	This study
pSK41	pBJ114; for generation of an in-frame deletion of *pixA*	(Kuzmich *et al.*, 2021)
pFM61	pBJ114; for generation of an in-frame deletion of *sgmC*	This study
pFM83	pBJ114; for generation of an in-frame deletion of *pglH*	This study
pLC60	pBJ114; for integration of *frzZ-mVenus* at the native site	Luís Carreira
pSL16	pBJ114; for generation of an in-frame deletion of *mglA*	(Miertzschke *et al.*, 2011)
pES2	pBJ114; for generation of an in-frame deletion of *mglB*	(Leonardy *et al.*, 2010)
pAM1	pBJ114; for generation of an in-frame deletion of *mglC*	(McLoon *et al.*, 2016)
pSL37	pBJ114; for generation of an in-frame deletion of *romR*	(Keilberg *et al.*, 2012)
pDK94	pBJ114; for generation of an in-frame deletion of *romX*	(Szadkowski *et al.*, 2019)
pDK95	pBJ114; for generation of an in-frame deletion of *romY*	(Szadkowski *et al.*, 2019)
pFM69	pBJ114; for integration of *frzZ-miniTurbo* at the native site	This study
pFM74	pSW105; for integration of P_{frzZ}*miniTurbo-FLAG* in the Mx8 *attB* site	This study
pSK139	pSWU30, for integration of P_{nat}*pixA-FLAG* in the Mx8 *attB* site	(Kuzmich *et al.*, 2021)
pSK146	pSW105, for integration of P_{pilA}*pixA-FLAG* in the Mx8 *attB* site	Sofya Kuzmich
pSK52	pBJ114; for integration of *pixA-mVenus* at the native site	Sofya Kuzmich
pFM81	pSWU30, for integration of P_{nat}*pixA-mVenus* in the Mx8 *attB* site	This study
pFM82	pSW105, for integration of P_{pilA}*pixA-mVenus* in the Mx8 *attB* site	This study
pSK68	pBJ114; for integration of *pixA*^{D180N}*-mVenus* at the native site	Sofya Kuzmich
pSK69	pBJ114; for integration of *pixA*^{D180E}*-mVenus* at the native site	Sofya Kuzmich
pFM84	pMR3690; for integration of P_{van}*pixA-miniTurbo-FLAG* in 18-19 site	This study
pMH97	pMR3690; for integration of P_{van}*sfGFP-miniTurbo-FLAG* in 18-19 site	Marco Herfurth
pAP37	pBJ114; for integration of *pilQ-sfGFP* at the native site	(Potapova *et al.*, 2020)

pFM65	pSWU30; for integration of *P_{nat}sfGFP-frzX* in the Mx8 *attB* site	This study
pMH52	*miniTurbo* (synthesized)	Marco Herfurth
pMH97	pMR3690; for integration of *P_{van}sfGFP-miniTurbo-FLAG*	Marco Herfurth
pFM71	pSW105; for integration of P_{pilA}miniTurbo-FLAG in the Mx8 *attB* site	This study
pFM67	pBJ114; for integration of *sfGFP-frzX* at the native site	This study
pFM68	pBJ114; for integration of *FLAG-miniTurbo-frzX* at the native site	This study
pFM70	pSWU30; for integration of *P_{nat}sgmC* in the Mx8 *attB* site	This study

5.5.3 Constructionn of plasmids

Purified genomic DNA (gDNA) of the *M. xanthus* WT strain DK1622 as well as plasmids were used as templates to amplify genes and genomic regions. The E. coli strain NEB Turbo was used for all cloning steps. Sequencing of completed plasmids was performed by Eurofins Genomics Germany GmbH (Ebersberg) and Microsynth Seqlab GmbH (Göttingen) using custome made primers.

pFM59 (plasmid for generation of in-frame deletion of *frzZ*): In case of a *frzZ* in-frame deletion the first 15bp and the last 11bp of *frzZ* are left which are fused to each other. Up- (FM27/FM28) and downstream (FM29/FM30) fragments were amplified from *M. xanthus* gDNA and then fused to each other via PCR using the fragments as template and the primers FM27 and FM30. The fusion fragment was digested using EcoRI and HindIII and cloned into pBJ114.

pFM61 (for generation of an in-frame deletion of *sgmC*): In case of a *sgmC* in-frame deletion the first 9 bp and the last 9 bp of *sgmC* are left which are connected with an XbaI restriction site. Up- (FM56/FM64) and downstream (FM65/FM59) fragments were amplified from *M. xanthus* gDNA. Fragments were digested using HindIII and XbaI, and EcoRI and XbaI, respectively, and cloned into pBJ114.

pFM65 (for integration of PnatsfGFP-frzX in the Mx8 *attB* site): The native promoter fragment (FM21/FM22) and *frzX* (FM25/FM26) were amplified from *M. xanthus* gDNA. The *sfGFP* fragment (FM23/FM24) was amplified from pAP37. The thrre fragments were fused to each other via PCR using the fragments as templates and the Primers FM21 and FM26. The fusion fragment was digested using BamHI and EcoRI and cloned into pSWU30.

pFM67 (for integration of *sfGFP-frzX* at the native site): The upstream fragment (FM39/FM22) was amplified from *M. xanthus* gDNA. The downstream fragment (FM23/FM26) containing *sfGFP-frzX* was amplified from pFM65. Fragments were fused to each other via PCR using the fragments as templates and the primers FM39 and FM26. The fusion fragment was digested using EcoRI and HindIII and cloned into pBJ114.

pFM68 (for integration of *FLAG-miniTurbo-frzX* at the native site): The upstream fragment (FM39/FM82) and the downstream fragment (FM85/FM26) were amplified from *M. xanthus* gDNA. The miniTurbo fragment (FM83/FM84) was amplified from pMH97. Fragments were fused to each other via PCR using the fragments as templates and the Primers FM39 and FM26. The fusion fragment was digested using EcoRI and HindIII and cloned into pBJ114.

pFM69 (for integration of *frzZ-miniTurbo* at the native site): The upstream fragment (FM76/FM77) and the downstream fragment (FM80/FM81) were amplified from *M. xanthus* gDNA. The miniTurbo fragment (FM78/FM79) was amplified from pMH97. Fragments were fused to each other via PCR using the fragments as templates and the Primers FM76 and FM81. The fusion fragment was digested using EcoRI and HindIII and cloned into pBJ114.

pFM70 (for integration of P_{nat}*sgmC* in the Mx8 *attB* site): The P_{nat}*sgmC* fragment (FM72/FM was amplified from *M. xanthus* gDNA. The fragment was digested using EcoRI and HindIII and cloned into pSWU30.

pFM71 (for integration of P_{pilA}*miniTurbo-FLAG* in the Mx8 *attB* site): The miniTurbo-FLAG fragment (FM86/FM87) was amplified from pMH52. The fragment was digested using XbaI and HindIII and cloned into pSW105.

pFM74 (for integration of P_{frzZ}*miniTurbo-FLAG* in the Mx8 *attB* site): The P_{frzZ} fragment (FM90/FM91) was amplified from *M. xanthus* gDNA. The fragment was digested using EcoRI and XbaI and cloned into pFM71.

pFM81 (for integration of P_{nat}*pixA-mVenus* in the Mx8 *attB* site): The P_{nat}*pixA-mVenus* fragment (SK128/ GFP rv) was amplified from *M. xanthus* gDNA of the strain SA8051. The fragment was digested using XbaI and HindIII and cloned into pSWU30.

pFM82 (for integration of P_{pilA}*pixA-mVenus* in the Mx8 *attB* site): The *pixA-mVenus* fragment (SK188/ GFP rv) was amplified from *M. xanthus* gDNA of the strain SA8051. The fragment was digested using XbaI and HindIII and cloned into pSW105.

pFM83 (for generation of an in-frame deletion of *pglH*): The upstream fragment (FM117/FM118) and the downstream fragment (FM119/FM120) were amplified from *M. xanthus* gDNA. Fragments were fused to each other via PCR using the fragments as templates and the Primers FM117and FM120. The fusion fragment was digested using XbaI and HindII and cloned into pBJ114.

pFM84 (for integration of P_{van}*pixA-miniTurbo-FLAG* in *18-19* site): The *pixA-miniTurbo-FLAG* (FM134/FM135) was amplified from SA11985 gDNA. The fragment was digested using NdeI and EcoRI and cloned into pMR3690.

5.5.4 Generation of *M. xanthus* in-frame deletion and integrations

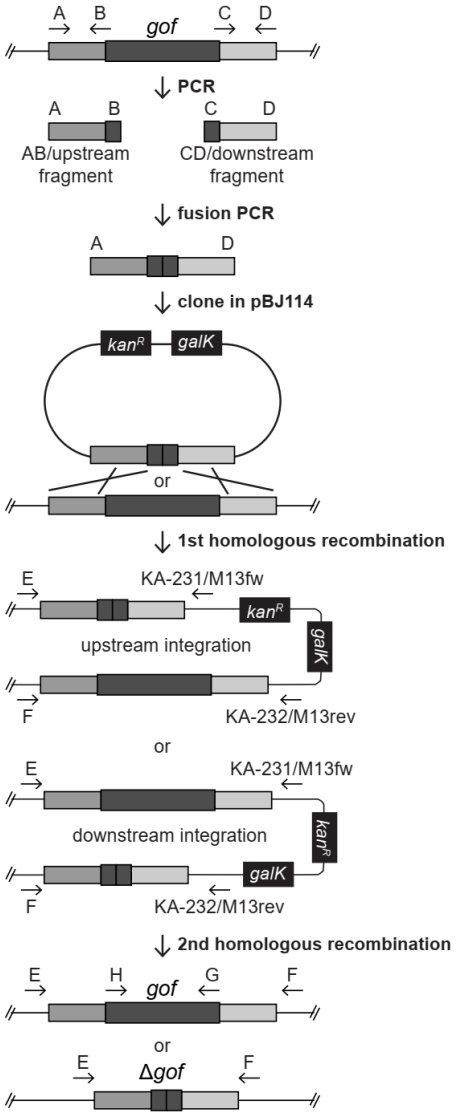

Figure 41: Schematic figure of the method to construct an in-frame deletion.

In-frame deletions and in-frame integrations were generated by two-step homologous recombination (Shi *et al.*, 2008). First, a plasmid is constructed. Upstream and downstream flanking regions (each ≥ 500bp) are amplified from genomic DNA via PCR using the primer pairs "A" and "B" and "C" and "D", respectively. The two fragments are fused via at least 16bp overlapping sequences using fusion PCR to create a deletion cassette. The deletion cassette is fused into the vector pBJ114 via restriction cloning using restriction enzymes as indicated in 5.5.2. The manipulated regions of the created plasmid are checked by sequencing using specific primers to ensure that it carries the correct sequence. Second, *M. xanthus* cells were transformed with the correct plasmid by electroporation using the protocol described in 5.5.10. Cells with a plasmid integration into the native site via homologous recombination grow on CTT-Kanamycin plates. The plasmid can integrate with the upstream fragment (upstream integration) or the downstream fragment (downstream integration). A test PCR was performed using the primer combinations "E" and "F" (which are found on the genome of *M. xanthus*) and the primers "KA-231" and "KA-232" (which are found on the plasmid) to verify the integration. The combinations "E" +" KA-231" (PCR A) and "F" +" KA-231" (PCR B) were used. The PCR was checked for upstream and downstream integration via agarose gel. The PCR of an upstream integration showed a shorter fragment for the A PCR than the B PCR (while a downstream integration showed a shorter fragment for the B PCR than the A PCR). The correct clones (preferably upstream and downstream integration) were then cultivated in CTT-Gm medium overnight for the second homologous recombination called "loop out". The cell cultures were plated on CTT-agar with 2-3% galactose and incubated at 32°C for several days. pBJ114 contains a gene (*galK*) encoding for a galactokinase, which metabolizes galactose to galactose phosphate, which is toxic for the cell at higher levels. Therefore, only cells without the plasmid and the *galK* gene can grow on those plates. To ensure that the colonies found

on the plates were not false positive, the colonies were tested on CTT-Gm-Km and CTT-Gm-Gal plates. The clones in which the plasmid was looped out could only grow on CTT-Gm-Gal plates because they no longer contain a Kanamycin resistance. In the second homologous recombination, two scenarios can happen. First, the recombination into the same fragment that already integrated the plasmid into the chromosome, e.g., after an upstream integration, the upstream "AB" fragment recombines again, resulting in a wildtype situation. Second, the recombination of the other fragment, e.g., after an upstream, the downstream "CD" fragment recombines into its homolog region, resulting in the gene's deletion. To verify that the gene is deleted, another test PCR using the primers "E" + "F" and "G" + "H" was performed. PCR's on cells with a deleted gene show a shorter "EF" fragment than PCRs with wildtype DNA and no "GH" fragment.

Integrations into the native site in the *M. xanthus* genome work similarly. The genomic information added to the *M. xanthus* genome is fused between an upstream and a downstream fragment. Here, the PCR of an upstream integration showed a longer fragment for the A PCR than the B PCR (while a downstream integration showed a longer fragment for the B PCR than the A PCR). The second homologous recombination can lead to integration or the return to wildtype scenario, which is tested via PCR using the primers "E" and "F". Integration results in a longer PCR fragment.

5.5.5 DNA isolation

Genomic DNA from *M. xanthus* was isolated using the "MasterPure DNA preparation Kit" (Epicentre Biotechnologies, Wisconsin, USA)and performed according to the manufacturer's protocol. Plasmid DNA was amplified and extracted from *E. coli* NEB Turbo cells using a NucleoSpin® Plasmid kit (Macherey & Nagel, Düren). The DS-11 Spectrophotometer (DeNovix Inc., Wilmington, USA) was used to determine the quality and concentration of isolated DNA. Crude genomic DNA extracts were obtained by boiling cells in 50 µl H2O for 5 min at 95°C. To sediment cell debris, samples were centrifuged via quick spin before DNA extracts were used

5.5.6 Polymerase chain reaction (PCR)

Polymerase chain reaction (PCR) is performed for the amplification of specific DNA fragments using either Phusion High-Fidelity DNA Polymerase (Thermo Fisher Scientific™, Dreieich) for amplification from genomic or plasmid DNA or Taq 2x Master Mix (New England Biolabs, Frankfurt a.M.) used for test PCRs from crude DNA samples.

Table M 19: General reaction mix for DNA amplification using Phusion polymerase.

Component	Volume
100 ng/µl genomic or plasmid DNA	1 µl
10 µM primer A	0.5 µl
10 µM primer B	0.5 µl
10 mM dNTP Mix	0.4 µl
5x Phusion GC buffer	4 µl
5x enhancer	4 µl
Phusion DNA Polymerase	0.25 µl
HPLC H_2O	9.35 µl

Table M 20: General reaction mix for DNA amplification using Taq 2x Master Mix.

Component	Volume
Template DNA	2 µl
10 µm Primer A	1 µl
10 µm Primer B	1 µl
Taq 2x Master Mix	10 µl
DMSO	2 µl
HPLC H_2O	4 µl

Table M 21: General program for amplification of DNA using Phusion polymerase.

Step	Temperature	Time	
Initial denaturation	95 °C	3 min	
Denaturation	95 °C	30 sec	35 x
Annealing	adjusted to primers	30 sec	
Elongation	72 °C	1000 kb/30 sec	
Final Elongation	72 °C	5 min	

Table M 22: General program for amplification of DNA using Taq 2x Master Mix.

Step	Temperature	Time	
Initial denaturation	95 °C	3 min	
Denaturation	95 °C	30 sec	25 x
Annealing	adjusted to primers	30 sec	
Elongation	72 °C	1000 kb/1 min	
Final Elongation	72 °C	10 min	

DNA fragments were separated by length by running through an agarose gel to check for the correct size. Correct fragments were purified for further processing using the NucleoSpin® Gel and PCR Clean-up kit (Macherey & Nagel, Düren).

5.5.7 Agarose gel electrophoresis

DNA fragments were visualized via agarose gel electrophoresis. Samples were mixed with 6x loading buffer (New England Biolabs, Frankfurt a.M.) and separated in a 1 % agarose gel supplemented with 0.005 % ROTI®GelStain Red (Carl Roth GmbH + Co. KG, Karlsruhe) at 100-140 V. As size standard the 2-log DNA ladder (New England Biolabs, Frankfurt a. M.) was used. Gels were documented with the Gel Stick "Touch" imager (Intas Science Imaging Instruments GmbH, Göttingen).

5.5.8 Restriction and insertion cloning

In this study, plasmids were generated via restriction and insertion cloning. Plasmid backbones were prepared by digesting 2-3 µg of plasmid DNA using endonucleases (New England Biolabs, Frankfurt a. M.) according to manufacturers' instructions for 1 h, at 37 °C in a 50 µl volume. Subsequently, the ends of the digested vectors were dephosphorylated using Antarctic phosphatase (New England Biolabs, Frankfurt a. M.) for 1 h at 37 °C in a total reaction volume of 60 µl. This was followed by separation via agarose gel electrophoresis (5.5.7), after which the DNA fragment was purified from the gel using the NucleoSpin® Gel and PCR Clean-up kit (Macherey & Nagel, Düren). Purified PCR fragments were digested using endonucleases (New England Biolabs, Frankfurt a. M.) according to manufacturers' instructions for 1 h, at 37 °C in a 50 µl volume. The digest was then purified using the NucleoSpin® Gel and PCR Clean-up kit (Macherey & Nagel, Düren). PCR fragment and vector were ligated using T4 DNA ligase (New England Biolabs, Frankfurt a. M.) according to manufacturers' instruction with a ratio of 1:5 (vector to fragment). Ligations were incubated for >2 h at RT. 10 µl of this reaction was used for transformation in *E. coli*.

5.5.9 Preparation and transformation of chemically competent *E. coli* cells

Cells of the *E. coli* strain NEB Turbo were made chemically competent for cloning and amplifying plasmids. An overnight culture was diluted 1:100 into 200 ml LB medium and incubated, shaking at 37 °C to an OD_{600nm} of 0.5-0.6. Cells were harvested in falcon tubes by centrifugation for 10 min at 4700 rpm at 4 °C. Cell pellets were suspended in 100 ml and incubated on ice for 5 min. Cells were harvested again, as described above. Pellets were then resuspended in 4 ml TFB2 buffer and incubated for 1 h on ice. After incubation, 50 µl aliquots of cells were frozen in liquid nitrogen and kept at -80 °C until used.

Table M 23: Composition of TFB buffers for preparation of chemically competent *E. coli* cells.

Buffer	Composition
TFB 1	30 mM potassium acetate 10 mM $CaCl_2$ 10 mM $MnCl_2$ 100 mM RbCl 15 % glycerol (v/v) pH 5.8 (adjusted with 1 M acetic acid)
TFB 2	10 mM MOPS pH 6.5 (adjusted with KOH) 75 mM $CaCl_2$ 10 mM RbCl 15 % glycerol (v/v)

For transformation, 50 µl aliquots of cells were thawed on ice. For transformation, 50 µl of cells were thawed on ice and mixed carefully with 10 µl ligation reaction or 1 µl of plasmid DNA. The mixture was incubated for 15 min on ice and then heat-shocked for 1 min at 42 °C in a water bath. After cooling for 5 min on ice, cells were mixed with 1 ml LB medium and incubated for 1 h at 37 °C, shaking. Then, cells were pelleted for 1 min at 13.000 rpm at RT, resuspended in residual LB medium, and spread on LB agar plates with corresponding antibiotics. Transformations plates were incubated at 37 °C ON. Transformation clones were transferred to fresh LB plates containing antibiotics.

5.5.10 Preparation and transformation of electrocompetent *M. xanthus* cells

M. xanthus cells were inoculated from a single colony in a 5 ml CTT medium as described in 5.3.4. If needed, the volume of cultures was scaled up depending on the number of transformations that ought to be performed. In general, 2 ml of *M. xanthus* culture is needed per transformation. Exponentially growing cultures were harvested in Eppendorf cups at 10000 rpm for 3 min at RT. The pellet was resuspended in sterile ddH_2O to 2 ml. Cells were pelleted and rewashed twice. In the last washing step, cells were resuspended in 50 µl sterile ddH_2O per transformation. 50 µl of washed cells were transferred into a sterile 0.1 cm Gene Pulser® Cuvette (Bio-Rad, München). Cells were mixed with 1 – 2 µg plasmid DNA. The mixture was thne pulsed with 0.65 kV. Subsequently, 1 ml CTT was added to electroporated cells and transferred into 3 ml total volume for recovery. Recovery was performed ON at 32 °C, shaking, in the dark. Cells were harvested at 10000 rpm for 3 min at RT. Cells were resuspended in residual CTT and spread on CTT agar plates containing corresponding antibiotics. Agar plates were incubated at 32 °C in the dark for several days until colonies were visible and could be transferred to fresh CTT agar plates with antibiotics.

5.6 Biochemical methods

5.6.1 Sample preparation for immunoblot analysis

M. xanthus cells were inoculated in 5 ml and incubated at 32 °C, shaking, in the dark. Cells were kept in an exponential growth phase for 48 h by diluting twice daily. After 48 h, 2 ml of cells were pelleted at 13000 rpm at RT for 3 min. The pellet was resuspended in 1x sodium dodecyl sulfate (SDS) loading buffer (prepared from 5x buffer Table M 24) to an OD_{550nm} of 14-20 depending on the protein aimed to detect. Samples were boiled at 95°C, shaking at 1000rpm for 10 min. After boiling, samples were spun down and vortexed. Samples were used directly after preparation or stored at -20 °C until use.

Table M 24: Composition of 5 x SDS loading buffer

Reagent	Amount
Tris pH: 6.8	250 mM
Glycerol	50 %
SDS	10 %
EDTA	10 mM
DTT	500 mM
Bromophenol blue	0,05 % (w/v)

5.6.2 Determination of protein concentrations

Protein concentrations were determined using the Pierce™ 660nm Protein Assay Reagent (Thermo Fisher Scientific™, Dreieich). Samples were obtained as described in 5.6.1. Since samples contained SDS, Ionic Detergent Compatibility Reagent (Thermo Fisher Scientific™, Dreieich was added to 20 ml of the reagent. Protein concentrations were determined in a 96 well cell culture plate (Sarstedt, Nümbrecht). For each measurement assay, a standard curve is measured using 125 µg/ml, 750 µg/ml, and 2000 µg/ml Pierce™ Bovine Serum Albumin Standard Pre-Diluted Set (Thermo Fisher Scientific™, Dreieich) and H_2O as 0 µg/ml. 10 µl for the standard curve and 1:4 diluted samples were added to the plate. 150 µl of protein assay reagent was added to each well and mixed with the sample. The plate was incubated at RT for 5 min. Samples were then measured using the Multifunktionsreader Infinite M200 Pro (Tecan Deutschland GmbH, Crailsheim) at 660nm. Protein concentrations were determined based on the linear slope of the standard curve.

5.6.3 SDS polyacrylamide gel electrophoresis (SDS-PAGE)

SDS polyacrylamide gel electrophoresis (SDS PAGE) was performed to separate proteins under denaturing conditions (Laemmli, 1970). To this end, samples were obtained as

described in 5.6.1 and loaded onto SDS gels with acrylamide concentration of 10 % or 12 % (Table M 25,

Table M 26) or onto Any kD™ Mini-PROTEAN® TGX™ Precast Protein Gels (Bio-Rad, Feldkirchen). Gels were run in a BioRad MiniPROTEAN 3 Cell or MiniPROTEAN TetraCell at 120 V in 1 x Tris Glycin SDS (TGS) buffer (Bio-Rad, Feldkirchen). The size of the proteins was determined by comparison to the protein marker, PageRuler™ Plus Prestained Protein Ladder (Thermo Fisher Scientific™, Dreieich). SDS gels were stained using FastGene® Q-Stain (NIPPON Genetics Europe, Düren).

Table M 25: Composition of SDS gels.

Reagent	**10 %**	**12 %**	**Stacking gel**
Resolving gel buffer	2.5 ml	2.5 ml	-
Stacking gel buffer	-	-	2.5 ml
Acrylamide (30 %)	3.3 ml	4.0 ml	1.1 ml
ddH_2O	4.2 ml	3.4 ml	6.5 ml
TEMED	0.05 ml	0.05 ml	0.05 ml
APS (10 %)	0.05 ml	0.05 ml	0.08 ml
Pyronin Y (in solution)	-	-	100 µl

Table M 26: Compositions of buffers used to prepare SDS gels.

Buffer	**Composition**
Resolving gel buffer	1.5 M Tris-HCl pH: 8.8 0.4 % (w/v) SDS
Stacking gel buffer	0.5 M Tris-HCl pH: 6.8 0.4 % (w/v) SDS

5.6.4 Immunoblot analysis

Immunoblot analysis was performed to detect proteins of interest with specific antibodies. Samples were prepared as described in 5.6.1 and separated by SDS PAGE as described in 5.6.3. Proteins were then transferred to a 0.2 µm nitrocellulose Amersham™ Protran® Western blotting membrane (Merck KGaA, Darmstadt) using the semi-dry TransBlot® Turbo™Transfer System (Bio-Rad, Feldkirchen). For transfer, the blotting buffer or the Towbin buffer (Towbin *et al.*, 1979) was used (Table M 26). The latter is used for blots detecting FrzX and PixA fusions. Transfer was performed at 1.3 A, 25 V for 7 min or at 1.0 A, 25 V for 30 min. Membranes were then blocked in 5 % dried non-fat milk powder (w/v) in 1 x TBS (50 mM Tris-HCl pH:7.5; 150mM NaCl) for 1 h or ON at RT or 4 °C, respectively. After blocking, membranes were incubated in 1 % dried non-fat milk powder (w/v) in 1 x TBS containing primary antibody with a corresponding dilution (Table M 28) ON at 4 °C. After washing 3 x for 5 min with 1 x TBST (50 mM Tris-HCl pH 7.5; 150 mM NaCl; 0.1 % Tween-20 (v/v)) the horseradish peroxidase-coupled goat anti-rabbit or anti-mouse immunoglobulin G secondary antibody was

applied to the blot at a given dilution in 1 % dried non-fat milk powder (w/v) in x TBS for 1 h at 4 °C shaking. Membranes were washed again as described before. Blots were then developed using the luminescent image analyzer LAS-4000 (Fujifilm, Düsseldorf) after applying the Luminata Western HRP Substrate (Millipore Merck, Schwalbach). When using several antibodies on one membrane, the membrane was stripped of the old antibody in between. To this end, membranes were incubated in Restore™ PLUS Western Blot Stripping Buffer (Thermo Fisher Scientific™, Dreieich) for 5 min at RT. Subsequently, the membrane was washed 2x for 5 min using 1 x TBST followed by blocking the membrane for 1 h in 5 % dried non-fat milk powder (w/v) in 1 x TBS at RT. The protocol was then continued as described above.

Table M 27: Transfer buffers used for immunoblot analysis.

Buffer	**Composition**
Blotting Buffer	300 mM Tris 300 mM Glycin 0.5 % (w/v) SDS
Towbin Buffer	25 mM Tris 192 mM Glycin 20 % (v/v) Methanol 0.1 % (w/v) SDS

Table M 28: Antibodies used in this study with their corresponding dilution used for detection.

Antibody	**Dilution**
α-GFP	1:1000
α-FLAG	1:2000
α-FrzZ	1:10000
α-FrzE	1:1000
α -FrzCD	1:5000
α -RomR	1:5000
α-PilA	1:5000
α-PilC	1:2500
α-LonD	1:5000
goat α-rabbit IgG	1:15000
sheep α-mouse IgG	1:2000
Streptactin-HRP	1:4000

5.6.5 Proximity-dependent biotinylation assay

Proximity-dependent biotinylation can be used to study (weak) protein associations. For our studies, we used miniTurbo-based proximity labeling (Branon *et al.*, 2018). To this end, triplicates of each strain were used. *M. xanthus* strains expressing miniTurbo or miniTurbo-fusion proteins were inoculated in 5 ml CTT at 32°C shaking ON. Cultures were then scaled up to get sufficient cells while keeping them in the exponential growth phase by diluting in the

morning and at night to an OD_{550nm} of 0.3 or 0.1, respectively. Subsequently, 40 ml 1 % CTT in Petri dishes (Ø=150 mm) (3 Petri dishes per replicate) were inoculated to an OD_{550nm} of 0.05 in submerged conditions for cells to attach to the bottom of the dish. Petri dishes were incubated at 32 °C in the dark for 24 h. When necessary, vanillate was added ON to induce the expression of miniTurbo proteins. Concentration is indicated in the corresponding chapters in 3. Then, 100 μM biotin (in TRIS pH: 8, titrated) was added to induce labeling for 3 h (for FrzZ, PixA, and FrzX experiments) or 50 μM biotin (in TRIS pH: 8, titrated) was added to induce labeling for 4 h (for MglA experiments) at 32 °C in the dark. After labeling, cells were scraped off the Petri dishes, and cells of the 3 Petri dishes of one sample were combined. Cells were centrifuged at 4500 g for 10 min at RT and washed 3 times with TPM by resuspending the pellet, followed by another centrifugation step. Next, washed cells were resuspended in 600 μl RIPA buffer (Table M 29) and sonicated at 50/60 for 30 s to lyse cells. This was followed by quick spinning the lysates to sediment intact cells. Meanwhile, PD MiniTrap™ G-10 columns (Cytiva, Freiburg) were equilibrated according to the manufacturer's protocol using RIPA buffer. 500 μl of a sample was added to a column and spun down at 1000 g for 2 min to remove free biotin from the sample. 30 μl of Pierce™ Streptavidin Magnetic Beads (Thermo Fisher Scientific™, Dreieich) per sample were equilibrated with 700 µl RIPA buffer. Beads and buffer were separated using a magnetic rack, and RIPA buffer was discarded. This step was repeated once. Protein concentration was determined as described in 0. The same amount of protein was incubated with the beads for 1 h at 4 °C. Following, the supernatant was removed using separation by the magnetic rack. Samples were then washed 2 times with 1 ml RIPA buffer, 2 times with 1 M KCl, and 3 times with 700 µl 50 mM Tris-HCl (pH: 7.6). Beads were then resuspended in 100 µl 50 mM Tris-HCl (pH: 7.6) of which 20 µl were used for quality control. The remaining 80 µl were separated, and the supernatant was discarded while the beads were frozen in liquid nitrogen and stored at -20 °C until further use.

Samples were handed over to the Core Facility for Mass Spectrometry & Proteomics of the Max Planck Institute for Terrestrial Microbiology who performed the analyses described below.

For FrzZ and FrzX experiments, proteins were eluted from the beads using sodium lauryl sulfate (SLS), while PixA and MglA were processed via on-bead digest. Proteins were eluted from the beads by adding 100 µl SLS and incubation at 95 °C for 10 min. The eluted proteins were transferred to a new reaction tube. The elution was repeated by using 50 µl SLS. The two elution fractions were collected in one tube. After elution, proteins were precipitated. To this end, 6-8 x volume ice-cold acetone was added and incubated at -20°C ON. Samples were centrifuged at full speed, at 4 °C for 10 min and Acetone was carefully removed by leaving 50

µl Acetone in the tube not to remove any protein material. 500 µl ice-cold methanol was added without disturbing the pellet, followed by centrifugation at full speed at 4 °C for 5 min. Methanol was removed, and the washing step was repeated once. The sample was heat dried to remove the remaining methanol.

For digestion, samples were incubated with digestion buffer (1µg trypsin in 100 mM ammonium bicarbonate (ABC)) for 30 min at 30 °C, shaking at 1200 rpm. Separate beads from the supernatant if needed. Collect the supernatant in a new tube. Add 100 µl TCEP buffer (2.5 mM Tris-(2-carboxyethyl)-phosphine hydrochloride (TCEP), 100 mM ABC) to the beads. Mix thoroughly, and separate beads again. Add the supernatant to the tube containing the digested sample. Incubate the tryptic digest at 30°C ON. Add alkylation buffer (5 mM iodoacetamide), mix thoroughly, and incubate at RT for 30 min in the dark. The samples were then desalted and prepared for liquid chromatography-massspectrometry (LC-MS) injection using C18 columns. Columns were conditioned with 200 µl acetonitrile and centrifuged at RT at 8 g for 30 s. They were then equilibrated with 400 µl SPE buffer 1 and centrifuged at RT at 15 g for 30 s. Samples were acidified by adding 50 µl 5 % trifluoroacetic acid (TFA), then loaded onto the equilibrated C18 columns and centrifuged at RT at 8 g for 1 min. The columns were washed with 400 µl SPE buffer 1 and centrifuged at RT at 15 g for 30 s. The columns are transferred to a new tube. 400 µl SPE buffer 2 was added, and columns were centrifuged at RT at 15 g for 30 s. In order to concentrate the eluted peptides, samples were dried under a vacuum in a SpeedVac for 2 h. Reconstitute peptides in 50 µl SPE buffer 1, vortex, and transfer the sample into an LC vial.

LC-MS analysis of the peptide samples was carried out on an Ultimate 3000 RSLC system connected to an Exploris 480 Orbitrap mass spectrometer using a data-dependent acquisition MS strategy for label-free protein quantification. 5 µl peptide material is loaded onto the Pre-column with 10 µl/min flow LC buffer A (0.15 % formic acid). A self-packed C18 column (42 cm length, 75 µm ID x 360 µM OD, 60 °C heated) was used for peptide separation. Peptide separation was performed at a constant flow rate of 300 nl/min using a 40 min gradient from 6-35% LC buffer B (99.85% acetonitrile/0.15 % formic acid) on a 42 cm self-packed analytical. Eluted peptides are ionized with a spray voltage of 2.3 kV in positive mode, and the capillary temperature was set to 300 °C. The MS1 survey scan (scan range m/z 350-1, 650) was acquired by setting the Orbitrap resolution to 600, the AGC target setting to 300 %, and max fill to,e to 25 ms, and the RF lens to 40 %. The MS7MS fragment spectra in data-dependent acquisition (DDA) mode were acquired with the following parameters: Quadrupole isolation window m/z 1.5, for fragmentation include ions with charge states 2-6, set Orbitrap resolution to 15,000, AGC target setting to 200% and max fill time set to “Auto”, HCD normalized collision

energy 27, dynamic exclusion 20 s, Set cycle time for MS/MS sequencing attempts to 1 s. The MS raw data is analyzed with MaxQuant for protein label-free quantification (LFQ).

Cell lysate, flow through, and eluate samples were examined via Immunoblot analysis (see 5.6.3 and 5.6.4) using Streptactin-HRP for quality control of the assay.

Table M 29: Composition of RIPA buffer used for cell lysis.

Reagent	**Amount**
Tris pH: 7	50 mM
NaCl	150 mM
Triton X-100	1 % (v/v)
sodium deoxycholate (SDC)	0.5 % (v/v)
SDS	0.2 % (v/v)
Benzonase	0.05 % (v/v)
cOmplete™ Mini Protease Inhibitor Cocktail (Merck KGaA (Darmstadt))	1 per 10 ml

6 Literature

Adams, D.W., Pereira, J.M., Stoudmann, C., Stutzmann, S., and Blokesch, M. (2019) The type IV pilus protein PilU functions as a PilT-dependent retraction ATPase. *PLoS Genet* **15**: e1008393.

Almawi, A.W., Matthews, L.A., and Guarne, A. (2017) FHA domains: Phosphopeptide binding and beyond. *Prog Biophys Mol Biol* **127**: 105-110.

Astling, D.P., Lee, J.Y., and Zusman, D.R. (2006) Differential effects of chemoreceptor methylation-domain mutations on swarming and development in the social bacterium Myxococcus xanthus. *Mol Microbiol* **59**: 45-55.

Balchin, D., Hayer-Hartl, M., and Hartl, F.U. (2016) In vivo aspects of protein folding and quality control. *Science* **353**: aac4354.

Balish, M.F. (2006) Subcellular structures of mycoplasmas. *Front Biosci* **11**: 2017-2027.

Banani, S.F., Lee, H.O., Hyman, A.A., and Rosen, M.K. (2017) Biomolecular condensates: organizers of cellular biochemistry. *Nat Rev Mol Cell Biol* **18**: 285-298.

Bautista, S., Schmidt, V., Guiseppi, A., Mauriello, E.M.F., Attia, B., Elantak, L., Mignot, T., and Mercier, R. (2023) FrzS acts as a polar beacon to recruit SgmX, a central activator of type IV pili during *Myxococcus xanthus* motility. *EMBO J* **42**: e111661.

Behmlander, R.M., and Dworkin, M. (1994) Biochemical and structural analyses of the extracellular matrix fibrils of *Myxococcus xanthus*. *J Bacteriol* **176**: 6295-6303.

Berg, P., Bergmann, F.H., Ofengand, E.J., and Dieckmann, M. (1961) The Enzymic Synthesis of Amino Acyl Derivatives of Ribonucleic Acid: I. THE MECHANISM OF LEUCYL-, VALYL-, ISOLEUCYL-, AND METHIONYL RIBONUCLEIC ACID FORMATION. *J Biol Chem* **236**: 1726-1734.

Berleman, J.E., Vicente, J.J., Davis, A.E., Jiang, S.Y., Seo, Y.E., and Zusman, D.R. (2011) FrzS regulates social motility in Myxococcus xanthus by controlling exopolysaccharide production. *PLoS One* **6**: e23920.

Bernal-Bernal, D., Abellon-Ruiz, J., Iniesta, A.A., Pajares-Martinez, E., Bastida-Martinez, E., Fontes, M., Padmanabhan, S., and Elias-Arnanz, M. (2018) Multifactorial control of the expression of a CRISPR-Cas system by an extracytoplasmic function sigma/anti-sigma pair and a global regulatory complex. *Nucleic Acids Res* **46**: 6726-6745.

Bernhardt, J., (2022) Characterization of MXAN_4666 and MXAN_4667, two MshEN domain containing proteins of *Myxococcus xanthus*. In: Department of Ecophysiology, Max Planck Institute for Terrestrial Microbiology. Marburg: Philipps-Universität Marburg, pp.

Bertrand, J.J., West, J.T., and Engel, J.N. (2010) Genetic analysis of the regulation of type IV pilus function by the Chp chemosensory system of *Pseudomonas aeruginosa*. *J Bacteriol* **192**: 994-1010.

Bhat, S., Boynton, T.O., Pham, D., and Shimkets, L.J. (2014) Fatty acids from membrane lipids become incorporated into lipid bodies during Myxococcus xanthus differentiation. *PLoS One* **9**: e99622.

Bhaya, D., Bianco, N.R., Bryant, D., and Grossman, A. (2000) Type IV pilus biogenesis and motility in the cyanobacterium Synechocystis sp. PCC6803. *Mol Microbiol* **37**: 941-951.

Bhaya, D., Takahashi, A., and Grossman, A.R. (2001) Light regulation of type IV pilus-dependent motility by chemosensor-like elements in Synechocystis PCC6803. *Proc Natl Acad Sci U S A* **98**: 7540-7545.

Biberfeld, G., and Biberfeld, P. (1970) Ultrastructural features of *Mycoplasma pneumoniae*. *J Bacteriol* **102**: 855-861.

Bischoff, D.S., Bourret, R.B., Kirsch, M.L., and Ordal, G.W. (1993) Purification and characterization of *Bacillus subtilis* CheY. *Biochemistry* **32**: 9256-9261.

Black, W.P., Schubot, F.D., Li, Z., and Yang, Z. (2010) Phosphorylation and dephosphorylation among Dif chemosensory proteins essential for exopolysaccharide regulation in *Myxococcus xanthus*. *J Bacteriol* **192**: 4267-4274.

Black, W.P., Wang, L., Davis, M.Y., and Yang, Z. (2015) The orphan response regulator EpsW is a substrate of the DifE kinase and it regulates exopolysaccharide in Myxococcus xanthus. *Sci Rep* **5**: 17831.

Black, W.P., Xu, Q., and Yang, Z. (2006) Type IV pili function upstream of the Dif chemotaxis pathway in Myxococcus xanthus EPS regulation. *Mol Microbiol* **61**: 447-456.

Black, W.P., and Yang, Z. (2004) *Myxococcus xanthus* chemotaxis homologs DifD and DifG negatively regulate fibril polysaccharide production. *J Bacteriol* **186**: 1001-1008.

Blackhart, B.D., and Zusman, D.R. (1985) "Frizzy" genes of Myxococcus xanthus are involved in control of frequency of reversal of gliding motility. *Proc Natl Acad Sci U S A* **82**: 8767-8770.

Bonner, P.J., Xu, Q., Black, W.P., Li, Z., Yang, Z., and Shimkets, L.J. (2005) The Dif chemosensory pathway is directly involved in phosphatidylethanolamine sensory transduction in Myxococcus xanthus. *Mol Microbiol* **57**: 1499-1508.

Bourret, R.B. (2010) Receiver domain structure and function in response regulator proteins. *Curr Opin Microbiol* **13**: 142-149.

Bowden, M.G., and Kaplan, H.B. (1998) The Myxococcus xanthus lipopolysaccharide O-antigen is required for social motility and multicellular development. *Mol Microbiol* **30**: 275-284.

Branon, T.C., Bosch, J.A., Sanchez, A.D., Udeshi, N.D., Svinkina, T., Carr, S.A., Feldman, J.L., Perrimon, N., and Ting, A.Y. (2018) Efficient proximity labeling in living cells and organisms with TurboID. *Nat Biotechnol* **36**: 880-887.

Bretl, D.J., Ladd, K.M., Atkinson, S.N., Muller, S., and Kirby, J.R. (2018) Suppressor mutations reveal an NtrC-like response regulator, NmpR, for modulation of Type-IV Pili-dependent motility in Myxococcus xanthus. *PLoS Genet* **14**: e1007714.

Bretl, D.J., Muller, S., Ladd, K.M., Atkinson, S.N., and Kirby, J.R. (2016) Type IV-pili dependent motility is co-regulated by PilSR and PilS2R2 two-component systems via distinct pathways in Myxococcus xanthus. *Mol Microbiol* **102**: 37-53.

Bulyha, I., Lindow, S., Lin, L., Bolte, K., Wuichet, K., Kahnt, J., van der Does, C., Thanbichler, M., and Søgaard-Andersen, L. (2013) Two small GTPases act in concert with the bactofilin cytoskeleton to regulate dynamic bacterial cell polarity. *Dev Cell* **25**: 119-131.

Burrows, L.L. (2012) Pseudomonas aeruginosa twitching motility: type IV pili in action. *Annu Rev Microbiol* **66**: 493-520.

Bustamante, V.H., Martinez-Flores, I., Vlamakis, H.C., and Zusman, D.R. (2004) Analysis of the Frz signal transduction system of Myxococcus xanthus shows the importance of the conserved C-terminal region of the cytoplasmic chemoreceptor FrzCD in sensing signals. *Mol Microbiol* **53**: 1501-1513.

Cai, Q., Li, Z., Ouyang, Q., Luo, C., and Gordon, V.D. (2016) Singly Flagellated *Pseudomonas aeruginosa* Chemotaxes Efficiently by Unbiased Motor Regulation. *mBio* **7**: e00013.

Campbell, E.L., Hagen, K.D., Chen, R., Risser, D.D., Ferreira, D.P., and Meeks, J.C. (2015) Genetic analysis reveals the identity of the photoreceptor for phototaxis in hormogonium filaments of *Nostoc punctiforme*. *J Bacteriol* **197**: 782-791.

Carreira, L.A.M., Szadkowski, D., Lometto, S., Hochberg, G.K.A., and Søgaard-Andersen, L. (2023) Molecular basis and design principles of switchable front-rear polarity and directional migration in Myxococcus xanthus. *Nat Commun* **14**: 4056.

Carreira, L.A.M., Tostevin, F., Gerland, U., and Søgaard-Andersen, L. (2020) Protein-protein interaction network controlling establishment and maintenance of switchable cell polarity. *PLoS Genet* **16**: e1008877.

Carter, T., Buensuceso, R.N., Tammam, S., Lamers, R.P., Harvey, H., Howell, P.L., and Burrows, L.L. (2017) The Type IVa Pilus Machinery Is Recruited to Sites of Future Cell Division. *mBio* **8**.

Chang, Y.W., Rettberg, L.A., Treuner-Lange, A., Iwasa, J., Søgaard-Andersen, L., and Jensen, G.J. (2016) Architecture of the type IVa pilus machine. *Science* **351**: aad2001.

Cho, K., Treuner-Lange, A., O'Connor, K.A., and Zusman, D.R. (2000) Developmental aggregation of *Myxococcus xanthus* requires frgA, an frz-related gene. *J Bacteriol* **182**: 6614-6621.

Cho, Y.W., Gonzales, A., Harwood, T.V., Huynh, J., Hwang, Y., Park, J.S., Trieu, A.Q., Italia, P., Pallipuram, V.K., and Risser, D.D. (2017) Dynamic localization of HmpF regulates type IV pilus activity and directional motility in the filamentous cyanobacterium Nostoc punctiforme. *Mol Microbiol* **106**: 252-265.

Christen, M., Kulasekara, H.D., Christen, B., Kulasekara, B.R., Hoffman, L.R., and Miller, S.I. (2010) Asymmetrical distribution of the second messenger c-di-GMP upon bacterial cell division. *Science* **328**: 1295-1297.

Craig, L., Forest, K.T., and Maier, B. (2019) Type IV pili: dynamics, biophysics and functional consequences. *Nat Rev Microbiol* **17**: 429-440.

Cyr, D.M., Langer, T., and Douglas, M.G. (1994) DnaJ-like proteins: molecular chaperones and specific regulators of Hsp70. *Trends Biochem Sci* **19**: 176-181.

D'Costa, V.M., Coyaud, E., Boddy, K.C., Laurent, E.M.N., St-Germain, J., Li, T., Grinstein, S., Raught, B., and Brumell, J.H. (2019) BioID screen of Salmonella type 3 secreted

effectors reveals host factors involved in vacuole positioning and stability during infection. *Nat Microbiol* **4**: 2511-2522.

Darnell, C.L., Wilson, J.M., Tiwari, N., Fuentes, E.J., and Kirby, J.R. (2014) Chemosensory regulation of a HEAT-repeat protein couples aggregation and sporulation in *Myxococcus xanthus*. *J Bacteriol* **196**: 3160-3168.

Darzins, A. (1993) The pilG gene product, required for *Pseudomonas aeruginosa* pilus production and twitching motility, is homologous to the enteric, single-domain response regulator CheY. *J Bacteriol* **175**: 5934-5944.

Davis, N.J., Cohen, Y., Sanselicio, S., Fumeaux, C., Ozaki, S., Luciano, J., Guerrero-Ferreira, R.C., Wright, E.R., Jenal, U., and Viollier, P.H. (2013) De- and repolarization mechanism of flagellar morphogenesis during a bacterial cell cycle. *Genes Dev* **27**: 2049-2062.

Dogra, G., Purschke, F.G., Wagner, V., Haslbeck, M., Kriehuber, T., Hughes, J.G., Van Tassell, M.L., Gilbert, C., Niemeyer, M., Ray, W.K., Helm, R.F., and Scharf, B.E. (2012) *Sinorhizobium meliloti* CheA complexed with CheS exhibits enhanced binding to CheY1, resulting in accelerated CheY1 dephosphorylation. *J Bacteriol* **194**: 1075-1087.

Ducret, A., Fleuchot, B., Bergam, P., and Mignot, T. (2013a) Direct live imaging of cell-cell protein transfer by transient outer membrane fusion in *Myxococcus xanthus*. *Elife* **2**: e00868.

Ducret, A., Quardokus, E.M., and Brun, Y.V. (2016) MicrobeJ, a tool for high throughput bacterial cell detection and quantitative analysis. *Nat Microbiol* **1**: 16077.

Ducret, A., Theodoly, O., and Mignot, T. (2013b) Single cell microfluidic studies of bacterial motility. *Methods Mol Biol* **966**: 97-107.

Ducret, A., Valignat, M.P., Mouhamar, F., Mignot, T., and Theodoly, O. (2012) Wet-surface-enhanced ellipsometric contrast microscopy identifies slime as a major adhesion factor during bacterial surface motility. *Proc Natl Acad Sci U S A* **109**: 10036-10041.

Ellison, C.K., Fei, C., Dalia, T.N., Wingreen, N.S., Dalia, A.B., Shaevitz, J.W., and Gitai, Z. (2022) Subcellular localization of type IV pili regulates bacterial multicellular development. *Nat Commun* **13**: 6334.

Errington, J. (2015) Bacterial morphogenesis and the enigmatic MreB helix. *Nat Rev Microbiol* **13**: 241-248.

Faure, L.M., Fiche, J.B., Espinosa, L., Ducret, A., Anantharaman, V., Luciano, J., Lhospice, S., Islam, S.T., Treguier, J., Sotes, M., Kuru, E., Van Nieuwenhze, M.S., Brun, Y.V., Theodoly, O., Aravind, L., Nollmann, M., and Mignot, T. (2016) The mechanism of force transmission at bacterial focal adhesion complexes. *Nature* **539**: 530-535.

Ferre, A., De La Mora, J., Ballado, T., Camarena, L., and Dreyfus, G. (2004) Biochemical study of multiple CheY response regulators of the chemotactic pathway of *Rhodobacter sphaeroides*. *J Bacteriol* **186**: 5172-5177.

Fink, J.M., and Zissler, J.F. (1989) Characterization of lipopolysaccharide from *Myxococcus xanthus* by use of monoclonal antibodies. *J Bacteriol* **171**: 2028-2032.

Friedrich, C., Bulyha, I., and Søgaard-Andersen, L. (2014) Outside-in assembly pathway of the type IV pilus system in *Myxococcus xanthus*. *J Bacteriol* **196**: 378-390.

Fulcher, N.B., Holliday, P.M., Klem, E., Cann, M.J., and Wolfgang, M.C. (2010) The Pseudomonas aeruginosa Chp chemosensory system regulates intracellular cAMP levels by modulating adenylate cyclase activity. *Mol Microbiol* **76**: 889-904.

Gegner, J.A., Graham, D.R., Roth, A.F., and Dahlquist, F.W. (1992) Assembly of an MCP receptor, CheW, and kinase CheA complex in the bacterial chemotaxis signal transduction pathway. *Cell* **70**: 975-982.

Gosink, K.K., Kobayashi, R., Kawagishi, I., and Hase, C.C. (2002) Analyses of the roles of the three cheA homologs in chemotaxis of *Vibrio cholerae*. *J Bacteriol* **184**: 1767-1771.

Goy, M.F., Springer, M.S., and Adler, J. (1977) Sensory transduction in Escherichia coli: role of a protein methylation reaction in sensory adaptation. *Proc Natl Acad Sci U S A* **74**: 4964-4968.

Guiseppi, A., Vicente, J.J., Herrou, J., Byrne, D., Barneoud, A., Moine, A., Espinosa, L., Basse, M.J., Molle, V., Mignot, T., Roche, P., and Mauriello, E.M.F. (2019) A divergent CheW confers plasticity to nucleoid-associated chemosensory arrays. *PLoS Genet* **15**: e1008533.

Gumerov, V.M., Andrianova, E.P., and Zhulin, I.B. (2021) Diversity of bacterial chemosensory systems. *Curr Opin Microbiol* **61**: 42-50.

Guzzo, M., Agrebi, R., Espinosa, L., Baronian, G., Molle, V., Mauriello, E.M., Brochier-Armanet, C., and Mignot, T. (2015) Evolution and Design Governing Signal Precision and Amplification in a Bacterial Chemosensory Pathway. *PLoS Genet* **11**: e1005460.

Guzzo, M., Murray, S.M., Martineau, E., Lhospice, S., Baronian, G., My, L., Zhang, Y., Espinosa, L., Vincentelli, R., Bratton, B.P., Shaevitz, J.W., Molle, V., Howard, M., and Mignot, T. (2018) A gated relaxation oscillator mediated by FrzX controls morphogenetic movements in Myxococcus xanthus. *Nat Microbiol* **3**: 948-959.

Han, Y., Jakob, A., Engel, S., Wilde, A., and Schuergers, N. (2022) PATAN-domain regulators interact with the Type IV pilus motor to control phototactic orientation in the cyanobacterium Synechocystis. *Mol Microbiol* **117**: 790-801.

Hartzell, P., and Kaiser, D. (1991) Function of MglA, a 22-kilodalton protein essential for gliding in *Myxococcus xanthus*. *J Bacteriol* **173**: 7615-7624.

Harwood, T.V., Zuniga, E.G., Kweon, H., and Risser, D.D. (2021) The cyanobacterial taxis protein HmpF regulates type IV pilus activity in response to light. *Proc Natl Acad Sci U S A* **118**.

Herfurth, M., Müller, F., Søgaard-Andersen, L., and Glatter, T. (2023a) A miniTurbo-based proximity labeling protocol to identify conditional protein interactomes *in vivo* in *Myxococcus xanthus*. *STAR Protocols*.

Herfurth, M., Perez-Burgos, M., and Sogaard-Andersen, L. (2023b) The mechanism for polar localization of the type IVa pilus machine in *Myxococcus xanthus*. *mBio*: e0159323.

Hess, J.F., Bourret, R.B., and Simon, M.I. (1988a) Histidine phosphorylation and phosphoryl group transfer in bacterial chemotaxis. *Nature* **336**: 139-143.

Hess, J.F., Oosawa, K., Kaplan, N., and Simon, M.I. (1988b) Phosphorylation of three proteins in the signaling pathway of bacterial chemotaxis. *Cell* **53**: 79-87.

Hess, J.F., Oosawa, K., Matsumura, P., and Simon, M.I. (1987) Protein phosphorylation is involved in bacterial chemotaxis. *Proc Natl Acad Sci U S A* **84**: 7609-7613.

Hodgkin, J., and Kaiser, D. (1977) Cell-to-cell stimulation of movement in nonmotile mutants of Myxococcus. *Proc Natl Acad Sci U S A* **74**: 2938-2942.

Hodgkin, J., and Kaiser, D. (1979) Genetics of Gliding Motility in *Myxococcus xanthus* (Myxobacterales): Two Gene Systems Control Movement. *Molecular and General Genetics MGG* **171**: 167-176.

Huitema, E., Pritchard, S., Matteson, D., Radhakrishnan, S.K., and Viollier, P.H. (2006) Bacterial birth scar proteins mark future flagellum assembly site. *Cell* **124**: 1025-1037.

Inclan, Y.F., Vlamakis, H.C., and Zusman, D.R. (2007) FrzZ, a dual CheY-like response regulator, functions as an output for the Frz chemosensory pathway of Myxococcus xanthus. *Mol Microbiol* **65**: 90-102.

Iniesta, A.A., Garcia-Heras, F., Abellon-Ruiz, J., Gallego-Garcia, A., and Elias-Arnanz, M. (2012) Two systems for conditional gene expression in *Myxococcus xanthus* inducible by isopropyl-beta-D-thiogalactopyranoside or vanillate. *J Bacteriol* **194**: 5875-5885.

Islam, S.T., and Mignot, T. (2015) The mysterious nature of bacterial surface (gliding) motility: A focal adhesion-based mechanism in Myxococcus xanthus. *Semin Cell Dev Biol* **46**: 143-154.

Islam, S.T., Vergara Alvarez, I., Saidi, F., Guiseppi, A., Vinogradov, E., Sharma, G., Espinosa, L., Morrone, C., Brasseur, G., Guillemot, J.F., Benarouche, A., Bridot, J.L., Ravicoularamin, G., Cagna, A., Gauthier, C., Singer, M., Fierobe, H.P., Mignot, T., and Mauriello, E.M.F. (2020) Modulation of bacterial multicellularity via spatio-specific polysaccharide secretion. *PLoS Biol* **18**: e3000728.

Jain, R., Sliusarenko, O., and Kazmierczak, B.I. (2017) Interaction of the cyclic-di-GMP binding protein FimX and the Type 4 pilus assembly ATPase promotes pilus assembly. *PLoS Pathog* **13**: e1006594.

Jakob, A., Nakamura, H., Kobayashi, A., Sugimoto, Y., Wilde, A., and Masuda, S. (2020) The (PATAN)-CheY-Like Response Regulator PixE Interacts with the Motor ATPase PilB1 to Control Negative Phototaxis in the Cyanobacterium Synechocystis sp. PCC 6803. *Plant Cell Physiol* **61**: 296-307.

Jakovljevic, V., Leonardy, S., Hoppert, M., and Søgaard-Andersen, L. (2008) PilB and PilT are ATPases acting antagonistically in type IV pilus function in *Myxococcus xanthus*. *J Bacteriol* **190**: 2411-2421.

Jones, C.E., Brook, J.M., Buck, D., Abell, C., and Smith, A.G. (1993) Cloning and sequencing of the Escherichia coli panB gene, which encodes ketopantoate hydroxymethyltransferase, and overexpression of the enzyme. *J Bacteriol* **175**: 2125-2130.

Julien, B., Kaiser, A.D., and Garza, A. (2000) Spatial control of cell differentiation in Myxococcus xanthus. *Proc Natl Acad Sci U S A* **97**: 9098-9103.

Kaimer, C., and Zusman, D.R. (2013) Phosphorylation-dependent localization of the response regulator FrzZ signals cell reversals in Myxococcus xanthus. *Mol Microbiol* **88**: 740-753.

Kaimer, C., and Zusman, D.R. (2016) Regulation of cell reversal frequency in Myxococcus xanthus requires the balanced activity of CheY-like domains in FrzE and FrzZ. *Mol Microbiol* **100**: 379-395.

Kaiser, D. (1979) Social gliding is correlated with the presence of pili in Myxococcus xanthus. *Proc Natl Acad Sci U S A* **76**: 5952-5956.

Karatan, E., Saulmon, M.M., Bunn, M.W., and Ordal, G.W. (2001) Phosphorylation of the response regulator CheV is required for adaptation to attractants during Bacillus subtilis chemotaxis. *J Biol Chem* **276**: 43618-43626.

Kato, J., Nakamura, T., Kuroda, A., and Ohtake, H. (1999) Cloning and characterization of chemotaxis genes in *Pseudomonas aeruginosa*. *Biosci Biotechnol Biochem* **63**: 155-161.

Kazmierczak, B.I., and Hendrixson, D.R. (2013) Spatial and numerical regulation of flagellar biosynthesis in polarly flagellated bacteria. *Mol Microbiol* **88**: 655-663.

Kearns, D.B., Campbell, B.D., and Shimkets, L.J. (2000) Myxococcus xanthus fibril appendages are essential for excitation by a phospholipid attractant. *Proc Natl Acad Sci U S A* **97**: 11505-11510.

Keilberg, D., Wuichet, K., Drescher, F., and Søgaard-Andersen, L. (2012) A response regulator interfaces between the Frz chemosensory system and the MglA/MglB GTPase/GAP module to regulate polarity in Myxococcus xanthus. *PLoS Genet* **8**: e1002951.

Khayatan, B., Meeks, J.C., and Risser, D.D. (2015) Evidence that a modified type IV pilus-like system powers gliding motility and polysaccharide secretion in filamentous cyanobacteria. *Mol Microbiol* **98**: 1021-1036.

Khursigara, C.M., Wu, X., Zhang, P., Lefman, J., and Subramaniam, S. (2008) Role of HAMP domains in chemotaxis signaling by bacterial chemoreceptors. *Proc Natl Acad Sci U S A* **105**: 16555-16560.

Kimmel, J., Kehrer, J., Frischknecht, F., and Spielmann, T. (2022) Proximity-dependent biotinylation approaches to study apicomplexan biology. *Mol Microbiol* **117**: 553-568.

Kirby, J.R. (2009) Chemotaxis-like regulatory systems: unique roles in diverse bacteria. *Annu Rev Microbiol* **63**: 45-59.

Kirby, J.R., and Zusman, D.R. (2003) Chemosensory regulation of developmental gene expression in Myxococcus xanthus. *Proc Natl Acad Sci U S A* **100**: 2008-2013.

Kirsch, M.L., Peters, P.D., Hanlon, D.W., Kirby, J.R., and Ordal, G.W. (1993a) Chemotactic methylesterase promotes adaptation to high concentrations of attractant in Bacillus subtilis. *J Biol Chem* **268**: 18610-18616.

Kirsch, M.L., Zuberi, A.R., Henner, D., Peters, P.D., Yazdi, M.A., and Ordal, G.W. (1993b) Chemotactic methyltransferase promotes adaptation to repellents in Bacillus subtilis. *J Biol Chem* **268**: 25350-25356.

Kobe, B., and Kajava, A.V. (2001) The leucine-rich repeat as a protein recognition motif. *Curr Opin Struct Biol* **11**: 725-732.

Konovalova, A., Petters, T., and Søgaard-Andersen, L. (2010) Extracellular biology of *Myxococcus xanthus*. *FEMS Microbiol Rev* **34**: 89-106.

Kühn, M.J., Macmillan, H., Tala, L., Inclan, Y., Patino, R., Pierrat, X., Al-Mayyah, Z., Engel, J.N., and Persat, A. (2023) Two antagonistic response regulators control *Pseudomonas aeruginosa* polarization during mechanotaxis. *EMBO J* **42**: e112165.

Kühn, M.J., Tala, L., Inclan, Y.F., Patino, R., Pierrat, X., Vos, I., Al-Mayyah, Z., Macmillan, H., Negrete, J., Jr., Engel, J.N., and Persat, A. (2021) Mechanotaxis directs Pseudomonas aeruginosa twitching motility. *Proc Natl Acad Sci U S A* **118**.

Kuzmich, S., Skotnicka, D., Szadkowski, D., Klos, P., Perez-Burgos, M., Schander, E., Schumacher, D., and Søgaard-Andersen, L. (2021) Three PilZ Domain Proteins, PlpA, PixA, and PixB, Have Distinct Functions in Regulation of Motility and Development in *Myxococcus xanthus*. *J Bacteriol* **203**: e0012621.

Laemmli, U.K. (1970) Cleavage of structural proteins during the assembly of the head of bacteriophage T4. *Nature* **227**: 680-685.

Lam, H., Schofield, W.B., and Jacobs-Wagner, C. (2006) A landmark protein essential for establishing and perpetuating the polarity of a bacterial cell. *Cell* **124**: 1011-1023.

Larsen, S.H., Reader, R.W., Kort, E.N., Tso, W.W., and Adler, J. (1974) Change in direction of flagellar rotation is the basis of the chemotactic response in Escherichia coli. *Nature* **249**: 74-77.

Leonardy, S., Freymark, G., Hebener, S., Ellehauge, E., and Søgaard-Andersen, L. (2007) Coupling of protein localization and cell movements by a dynamically localized response regulator in *Myxococcus xanthus*. *EMBO J* **26**: 4433-4444.

Leonardy, S., Miertzschke, M., Bulyha, I., Sperling, E., Wittinghofer, A., and Søgaard-Andersen, L. (2010) Regulation of dynamic polarity switching in bacteria by a Ras-like G-protein and its cognate GAP. *EMBO J* **29**: 2276-2289.

Li, Y., Sun, H., Ma, X., Lu, A., Lux, R., Zusman, D., and Shi, W. (2003) Extracellular polysaccharides mediate pilus retraction during social motility of Myxococcus xanthus. *Proc Natl Acad Sci U S A* **100**: 5443-5448.

Lord, S.J., Velle, K.B., Mullins, R.D., and Fritz-Laylin, L.K. (2020) SuperPlots: Communicating reproducibility and variability in cell biology. *J Cell Biol* **219**.

Luciano, J., Agrebi, R., Le Gall, A.V., Wartel, M., Fiegna, F., Ducret, A., Brochier-Armanet, C., and Mignot, T. (2011) Emergence and modular evolution of a novel motility machinery in bacteria. *PLoS Genet* **7**: e1002268.

Lupas, A., and Stock, J. (1989) Phosphorylation of an N-terminal regulatory domain activates the CheB methylesterase in bacterial chemotaxis. *J Biol Chem* **264**: 17337-17342.

Makarova, K.S., Koonin, E.V., Haselkorn, R., and Galperin, M.Y. (2006) Cyanobacterial response regulator PatA contains a conserved N-terminal domain (PATAN) with an alpha-helical insertion. *Bioinformatics* **22**: 1297-1301.

Masduki, A., Nakamura, J., Ohga, T., Umezaki, R., Kato, J., and Ohtake, H. (1995) Isolation and characterization of chemotaxis mutants and genes of *Pseudomonas aeruginosa*. *J Bacteriol* **177**: 948-952.

Mauriello, E.M., Mouhamar, F., Nan, B., Ducret, A., Dai, D., Zusman, D.R., and Mignot, T. (2010) Bacterial motility complexes require the actin-like protein, MreB and the Ras homologue, MglA. *EMBO J* **29**: 315-326.

May, D.G., and Roux, K.J. (2019) BioID: A Method to Generate a History of Protein Associations. *Methods Mol Biol* **2008**: 83-95.

McBride, M.J., Kohler, T., and Zusman, D.R. (1992) Methylation of FrzCD, a methyl-accepting taxis protein of *Myxococcus xanthus*, is correlated with factors affecting cell behavior. *J Bacteriol* **174**: 4246-4257.

McBride, M.J., Weinberg, R.A., and Zusman, D.R. (1989) "Frizzy" aggregation genes of the gliding bacterium Myxococcus xanthus show sequence similarities to the chemotaxis genes of enteric bacteria. *Proc Natl Acad Sci U S A* **86**: 424-428.

McCleary, W.R., McBride, M.J., and Zusman, D.R. (1990) Developmental sensory transduction in *Myxococcus xanthus* involves methylation and demethylation of FrzCD. *J Bacteriol* **172**: 4877-4887.

McCleary, W.R., and Zusman, D.R. (1990) Purification and characterization of the *Myxococcus xanthus* FrzE protein shows that it has autophosphorylation activity. *J Bacteriol* **172**: 6661-6668.

McLoon, A.L., Wuichet, K., Hasler, M., Keilberg, D., Szadkowski, D., and Søgaard-Andersen, L. (2016) MglC, a Paralog of *Myxococcus xanthus* GTPase-Activating Protein MglB, Plays a Divergent Role in Motility Regulation. *J Bacteriol* **198**: 510-520.

Mercier, R., Bautista, S., Delannoy, M., Gibert, M., Guiseppi, A., Herrou, J., Mauriello, E.M.F., and Mignot, T. (2020) The polar Ras-like GTPase MglA activates type IV pilus via SgmX to enable twitching motility in Myxococcus xanthus. *Proc Natl Acad Sci U S A* **117**: 28366-28373.

Merz, A.J., So, M., and Sheetz, M.P. (2000) Pilus retraction powers bacterial twitching motility. *Nature* **407**: 98-102.

Miertzschke, M., Koerner, C., Vetter, I.R., Keilberg, D., Hot, E., Leonardy, S., Søgaard-Andersen, L., and Wittinghofer, A. (2011) Structural analysis of the Ras-like G protein MglA and its cognate GAP MglB and implications for bacterial polarity. *EMBO J* **30**: 4185-4197.

Mignot, T., Attia, B., My, L., Castaing, J.P., Dinet, C., Le Guenno, H., Schmidt, V., Espinosa, L., Anantharaman, V., Aravind, L., Sebban-Kreuzer, C., Nouailler, M., Bornet, O., Viollier, P., and Elantak, L. (2023) A novel molecular switch controls assembly of bacterial focal adhesions. *PREPRINT (Version 1) available at Research Square*.

Moak, P.L., Black, W.P., Wallace, R.A., Li, Z., and Yang, Z. (2015) The Hsp70-like StkA functions between T4P and Dif signaling proteins as a negative regulator of exopolysaccharide in Myxococcus xanthus. *PeerJ* **3**: e747.

Mukherjee, T., Elmas, M., Vo, L., Alexiades, V., Hong, T., and Alexandre, G. (2019) Multiple CheY Homologs Control Swimming Reversals and Transient Pauses in *Azospirillum brasilense*. *Biophys J* **116**: 1527-1537.

Mukherjee, T., Kumar, D., Burriss, N., Xie, Z., and Alexandre, G. (2016) *Azospirillum brasilense* Chemotaxis Depends on Two Signaling Pathways Regulating Distinct Motility Parameters. *J Bacteriol* **198**: 1764-1772.

Nakane, D., Enomoto, G., Bahre, H., Hirose, Y., Wilde, A., and Nishizaka, T. (2022) *Thermosynechococcus* switches the direction of phototaxis by a c-di-GMP-dependent process with high spatial resolution. *Elife* **11**.

Nakane, D., and Miyata, M. (2007) Cytoskeletal "jellyfish" structure of Mycoplasma mobile. *Proc Natl Acad Sci U S A* **104**: 19518-19523.

Nolan, L.M., McCaughey, L.C., Merjane, J., Turnbull, L., and Whitchurch, C.B. (2020) ChpC controls twitching motility-mediated expansion of Pseudomonas aeruginosa biofilms in response to serum albumin, mucin and oligopeptides. *Microbiology (Reading)* **166**: 669-678.

O'Connor, K.A., and Zusman, D.R. (1991) Development in *Myxococcus xanthus* involves differentiation into two cell types, peripheral rods and spores. *J Bacteriol* **173**: 3318-3333.

Okajima, K., Yoshihara, S., Fukushima, Y., Geng, X., Katayama, M., Higashi, S., Watanabe, M., Sato, S., Tabata, S., Shibata, Y., Itoh, S., and Ikeuchi, M. (2005) Biochemical and functional characterization of BLUF-type flavin-binding proteins of two species of cyanobacteria. *J Biochem* **137**: 741-750.

Paintdakhi, A., Parry, B., Campos, M., Irnov, I., Elf, J., Surovtsev, I., and Jacobs-Wagner, C. (2016) Oufti: an integrated software package for high-accuracy, high-throughput quantitative microscopy analysis. *Mol Microbiol* **99**: 767-777.

Perez-Burgos, M., Garcia-Romero, I., Jung, J., Schander, E., Valvano, M.A., and Søgaard-Andersen, L. (2020) Characterization of the Exopolysaccharide Biosynthesis Pathway in *Myxococcus xanthus*. *J Bacteriol* **202**.

Perez-Burgos, M., Garcia-Romero, I., Jung, J., Valvano, M.A., and Søgaard-Andersen, L. (2019) Identification of the lipopolysaccharide O-antigen biosynthesis priming enzyme and the O-antigen ligase in Myxococcus xanthus: critical role of LPS O-antigen in motility and development. *Mol Microbiol* **112**: 1178-1198.

Persat, A., Inclan, Y.F., Engel, J.N., Stone, H.A., and Gitai, Z. (2015) Type IV pili mechanochemically regulate virulence factors in Pseudomonas aeruginosa. *Proc Natl Acad Sci U S A* **112**: 7563-7568.

Poggio, S., Abreu-Goodger, C., Fabela, S., Osorio, A., Dreyfus, G., Vinuesa, P., and Camarena, L. (2007) A complete set of flagellar genes acquired by horizontal transfer coexists with the endogenous flagellar system in *Rhodobacter sphaeroides*. *J Bacteriol* **189**: 3208-3216.

Pogue, C.B., Zhou, T., and Nan, B. (2018) PlpA, a PilZ-like protein, regulates directed motility of the bacterium Myxococcus xanthus. *Mol Microbiol* **107**: 214-228.

Porter, S.L., and Armitage, J.P. (2002) Phosphotransfer in Rhodobacter sphaeroides chemotaxis. *J Mol Biol* **324**: 35-45.

Porter, S.L., and Armitage, J.P. (2004) Chemotaxis in Rhodobacter sphaeroides requires an atypical histidine protein kinase. *J Biol Chem* **279**: 54573-54580.

Porter, S.L., Wadhams, G.H., Martin, A.C., Byles, E.D., Lancaster, D.E., and Armitage, J.P. (2006) The CheYs of Rhodobacter sphaeroides. *J Biol Chem* **281**: 32694-32704.

Potapova, A., Carreira, L.A.M., and Søgaard-Andersen, L. (2020) The small GTPase MglA together with the TPR domain protein SgmX stimulates type IV pili formation in M. xanthus. *Proc Natl Acad Sci U S A* **117**: 23859-23868.

Rao, C.V., Glekas, G.D., and Ordal, G.W. (2008) The three adaptation systems of Bacillus subtilis chemotaxis. *Trends Microbiol* **16**: 480-487.

Reisenauer, A., Quon, K., and Shapiro, L. (1999) The CtrA response regulator mediates temporal control of gene expression during the *Caulobacter* cell cycle. *J Bacteriol* **181**: 2430-2439.

Risser, D.D., Chew, W.G., and Meeks, J.C. (2014) Genetic characterization of the hmp locus, a chemotaxis-like gene cluster that regulates hormogonium development and motility in *Nostoc punctiforme*. *Mol Microbiol* **92**: 222-233.

Rosario, M.M., and Ordal, G.W. (1996) CheC and CheD interact to regulate methylation of Bacillus subtilis methyl-accepting chemotaxis proteins. *Mol Microbiol* **21**: 511-518.

Ryjenkov, D.A., Tarutina, M., Moskvin, O.V., and Gomelsky, M. (2005) Cyclic diguanylate is a ubiquitous signaling molecule in bacteria: insights into biochemistry of the GGDEF protein domain. *J Bacteriol* **187**: 1792-1798.

Santin, Y.G., Doan, T., Lebrun, R., Espinosa, L., Journet, L., and Cascales, E. (2018) In vivo TssA proximity labelling during type VI secretion biogenesis reveals TagA as a protein that stops and holds the sheath. *Nat Microbiol* **3**: 1304-1313.

Sarkar, M.K., Paul, K., and Blair, D. (2010) Chemotaxis signaling protein CheY binds to the rotor protein FliN to control the direction of flagellar rotation in Escherichia coli. *Proc Natl Acad Sci U S A* **107**: 9370-9375.

Schindelin, J., Arganda-Carreras, I., Frise, E., Kaynig, V., Longair, M., Pietzsch, T., Preibisch, S., Rueden, C., Saalfeld, S., Schmid, B., Tinevez, J.Y., White, D.J., Hartenstein, V., Eliceiri, K., Tomancak, P., and Cardona, A. (2012) Fiji: an open-source platform for biological-image analysis. *Nat Methods* **9**: 676-682.

Schmidt, F., (2022) Characterization of Mxan_1131 and further investigation of the MshEN protein FrgA in *Myxococcus xanthus*. In: Department of Ecophysiology, Max Planck Institute for Terrestrial Microbiology. Marburg: Philipps-Universität Marburg, pp.

Schroder, H., Langer, T., Hartl, F.U., and Bukau, B. (1993) DnaK, DnaJ and GrpE form a cellular chaperone machinery capable of repairing heat-induced protein damage. *EMBO J* **12**: 4137-4144.

Schuhmacher, J.S., Thormann, K.M., and Bange, G. (2015) How bacteria maintain location and number of flagella? *FEMS Microbiol Rev* **39**: 812-822.

Scott, A.E., Simon, E., Park, S.K., Andrews, P., and Zusman, D.R. (2008) Site-specific receptor methylation of FrzCD in Myxococcus xanthus is controlled by a tetra-trico peptide repeat (TPR) containing regulatory domain of the FrzF methyltransferase. *Mol Microbiol* **69**: 724-735.

Shi, W., Kohler, T., and Zusman, D.R. (1993) Chemotaxis plays a role in the social behaviour of Myxococcus xanthus. *Mol Microbiol* **9**: 601-611.

Shi, X., Wegener-Feldbrugge, S., Huntley, S., Hamann, N., Hedderich, R., and Søgaard-Andersen, L. (2008) Bioinformatics and experimental analysis of proteins of two-component systems in *Myxococcus xanthus*. *J Bacteriol* **190**: 613-624.

Siewering, K., Jain, S., Friedrich, C., Webber-Birungi, M.T., Semchonok, D.A., Binzen, I., Wagner, A., Huntley, S., Kahnt, J., Klingl, A., Boekema, E.J., Søgaard-Andersen, L., and van der Does, C. (2014) Peptidoglycan-binding protein TsaP functions in surface assembly of type IV pili. *Proc Natl Acad Sci U S A* **111**: E953-961.

Skotnicka, D., Petters, T., Heering, J., Hoppert, M., Kaever, V., and Søgaard-Andersen, L. (2016a) Cyclic Di-GMP Regulates Type IV Pilus-Dependent Motility in *Myxococcus xanthus*. *J Bacteriol* **198**: 77-90.

Skotnicka, D., Smaldone, G.T., Petters, T., Trampari, E., Liang, J., Kaever, V., Malone, J.G., Singer, M., and Søgaard-Andersen, L. (2016b) A Minimal Threshold of c-di-GMP Is Essential for Fruiting Body Formation and Sporulation in Myxococcus xanthus. *PLoS Genet* **12**: e1006080.

Smith, I.W. (1954) Flagellation and motility in *Aerobacter cloacae* and *Escherichia coli*. *Biochim Biophys Acta* **15**: 20-24.

Søgaard-Andersen, L., and Kaiser, D. (1996) C factor, a cell-surface-associated intercellular signaling protein, stimulates the cytoplasmic Frz signal transduction system in Myxococcus xanthus. *Proc Natl Acad Sci U S A* **93**: 2675-2679.

Sourjik, V., and Schmitt, R. (1996) Different roles of CheY1 and CheY2 in the chemotaxis of Rhizobium meliloti. *Mol Microbiol* **22**: 427-436.

Sourjik, V., and Schmitt, R. (1998) Phosphotransfer between CheA, CheY1, and CheY2 in the chemotaxis signal transduction chain of *Rhizobium meliloti*. *Biochemistry* **37**: 2327-2335.

Springer, W.R., and Koshland, D.E., Jr. (1977) Identification of a protein methyltransferase as the cheR gene product in the bacterial sensing system. *Proc Natl Acad Sci U S A* **74**: 533-537.

Stamatakis, A. (2014) RAxML version 8: a tool for phylogenetic analysis and post-analysis of large phylogenies. *Bioinformatics* **30**: 1312-1313.

Steinböck, F.A., and Wiche, G. (1999) Plectin: a cytolinker by design. *Biol Chem* **380**: 151-158.

Stock, A.M., Robinson, V.L., and Goudreau, P.N. (2000) Two-component signal transduction. *Annu Rev Biochem* **69**: 183-215.

Stock, J.B., and Koshland, D.E., Jr. (1978) A protein methylesterase involved in bacterial sensing. *Proc Natl Acad Sci U S A* **75**: 3659-3663.

Sutherland, I.W., and Thomson, S. (1975) Comparison of polysaccharides produced by Myxococcus strains. *J Gen Microbiol* **89**: 124-132.

Szadkowski, D., Carreira, L.A.M., and Søgaard-Andersen, L. (2022) A bipartite, low-affinity roadblock domain-containing GAP complex regulates bacterial front-rear polarity. *PLoS Genet* **18**: e1010384.

Szadkowski, D., Harms, A., Carreira, L.A.M., Wigbers, M., Potapova, A., Wuichet, K., Keilberg, D., Gerland, U., and Søgaard-Andersen, L. (2019) Spatial control of the GTPase MglA by localized RomR-RomX GEF and MglB GAP activities enables Myxococcus xanthus motility. *Nat Microbiol* **4**: 1344-1355.

Szurmant, H., Muff, T.J., and Ordal, G.W. (2004) Bacillus subtilis CheC and FliY are members of a novel class of CheY-P-hydrolyzing proteins in the chemotactic signal transduction cascade. *J Biol Chem* **279**: 21787-21792.

Tanaka, K., Nakasone, Y., Okajima, K., Ikeuchi, M., Tokutomi, S., and Terazima, M. (2012) Time-resolved tracking of interprotein signal transduction: *Synechocystis* PixD-PixE complex as a sensor of light intensity. *J Am Chem Soc* **134**: 8336-8339.

Taylor, B.L., and Zhulin, I.B. (1999) PAS domains: internal sensors of oxygen, redox potential, and light. *Microbiol Mol Biol Rev* **63**: 479-506.

Thormann, K.M., Beta, C., and Kuhn, M.J. (2022) Wrapped Up: The Motility of Polarly Flagellated Bacteria. *Annu Rev Microbiol* **76**: 349-367.

Tostevin, F., Wigbers, M., Søgaard-Andersen, L., and Gerland, U. (2021) Four different mechanisms for switching cell polarity. *PLoS Comput Biol* **17**: e1008587.

Towbin, H., Staehelin, T., and Gordon, J. (1979) Electrophoretic transfer of proteins from polyacrylamide gels to nitrocellulose sheets: procedure and some applications. *Proc Natl Acad Sci U S A* **76**: 4350-4354.

Treuner-Lange, A., Chang, Y.W., Glatter, T., Herfurth, M., Lindow, S., Chreifi, G., Jensen, G.J., and Søgaard-Andersen, L. (2020) PilY1 and minor pilins form a complex priming the type IVa pilus in Myxococcus xanthus. *Nat Commun* **11**: 5054.

Treuner-Lange, A., Macia, E., Guzzo, M., Hot, E., Faure, L.M., Jakobczak, B., Espinosa, L., Alcor, D., Ducret, A., Keilberg, D., Castaing, J.P., Lacas Gervais, S., Franco, M., Søgaard-Andersen, L., and Mignot, T. (2015) The small G-protein MglA connects to the MreB actin cytoskeleton at bacterial focal adhesions. *J Cell Biol* **210**: 243-256.

Treuner-Lange, A., and Søgaard-Andersen, L. (2014) Regulation of cell polarity in bacteria. *J Cell Biol* **206**: 7-17.

Vetter, I.R., and Wittinghofer, A. (2001) The guanine nucleotide-binding switch in three dimensions. *Science* **294**: 1299-1304.

Vlamakis, H.C., Kirby, J.R., and Zusman, D.R. (2004) The Che4 pathway of Myxococcus xanthus regulates type IV pilus-mediated motility. *Mol Microbiol* **52**: 1799-1811.

Wadhams, G.H., Warren, A.V., Martin, A.C., and Armitage, J.P. (2003) Targeting of two signal transduction pathways to different regions of the bacterial cell. *Mol Microbiol* **50**: 763-770.

Wall, D., and Kaiser, D. (1999) Type IV pili and cell motility. *Mol Microbiol* **32**: 1-10.

Wang, Y.C., Chin, K.H., Tu, Z.L., He, J., Jones, C.J., Sanchez, D.Z., Yildiz, F.H., Galperin, M.Y., and Chou, S.H. (2016) Nucleotide binding by the widespread high-affinity cyclic di-GMP receptor MshEN domain. *Nat Commun* **7**: 12481.

Webb, B.A., Helm, R.F., and Scharf, B.E. (2016) Contribution of Individual Chemoreceptors to Sinorhizobium meliloti Chemotaxis Towards Amino Acids of Host and Nonhost Seed Exudates. *Mol Plant Microbe Interact* **29**: 231-239.

Wehbi, H., Portillo, E., Harvey, H., Shimkoff, A.E., Scheurwater, E.M., Howell, P.L., and Burrows, L.L. (2011) The peptidoglycan-binding protein FimV promotes assembly of the *Pseudomonas aeruginosa* type IV pilus secretin. *J Bacteriol* **193**: 540-550.

Welch, M., Oosawa, K., Aizawa, S., and Eisenbach, M. (1993) Phosphorylation-dependent binding of a signal molecule to the flagellar switch of bacteria. *Proc Natl Acad Sci U S A* **90**: 8787-8791.

Willett, J.W., and Kirby, J.R. (2011) CrdS and CrdA comprise a two-component system that is cooperatively regulated by the Che3 chemosensory system in Myxococcus xanthus. *mBio* **2**.

Wireman, J.W., and Dworkin, M. (1977) Developmentally induced autolysis during fruiting body formation by *Myxococcus xanthus*. *J Bacteriol* **129**: 798-802.

Wu, S.S., and Kaiser, D. (1997) Regulation of expression of the pilA gene in *Myxococcus xanthus*. *J Bacteriol* **179**: 7748-7758.

Wu, S.S., Wu, J., and Kaiser, D. (1997) The Myxococcus xanthus pilT locus is required for social gliding motility although pili are still produced. *Mol Microbiol* **23**: 109-121.

Wuichet, K., and Søgaard-Andersen, L. (2014) Evolution and diversity of the Ras superfamily of small GTPases in prokaryotes. *Genome Biol Evol* **7**: 57-70.

Wuichet, K., and Zhulin, I.B. (2010) Origins and diversification of a complex signal transduction system in prokaryotes. *Sci Signal* **3**: ra50.

Xu, Q., Black, W.P., Ward, S.M., and Yang, Z. (2005) Nitrate-dependent activation of the Dif signaling pathway of *Myxococcus xanthus* mediated by a NarX-DifA interspecies chimera. *J Bacteriol* **187**: 6410-6418.

Yamaichi, Y., Bruckner, R., Ringgaard, S., Moll, A., Cameron, D.E., Briegel, A., Jensen, G.J., Davis, B.M., and Waldor, M.K. (2012) A multidomain hub anchors the chromosome segregation and chemotactic machinery to the bacterial pole. *Genes Dev* **26**: 2348-2360.

Yang, R., Bartle, S., Otto, R., Stassinopoulos, A., Rogers, M., Plamann, L., and Hartzell, P. (2004) AglZ is a filament-forming coiled-coil protein required for adventurous gliding motility of *Myxococcus xanthus*. *J Bacteriol* **186**: 6168-6178.

Yang, Z., Geng, Y., Xu, D., Kaplan, H.B., and Shi, W. (1998) A new set of chemotaxis homologues is essential for Myxococcus xanthus social motility. *Mol Microbiol* **30**: 1123-1130.

Yang, Z., and Li, Z. (2005) Demonstration of interactions among *Myxococcus xanthus* Dif chemotaxis-like proteins by the yeast two-hybrid system. *Arch Microbiol* **183**: 243-252.

Yoshihara, S., and Ikeuchi, M. (2004) Phototactic motility in the unicellular cyanobacterium Synechocystis sp. PCC 6803. *Photochem Photobiol Sci* **3**: 512-518.

Youderian, P., and Hartzell, P.L. (2006) Transposon insertions of magellan-4 that impair social gliding motility in *Myxococcus xanthus*. *Genetics* **172**: 1397-1410.

Yu, R., and Kaiser, D. (2007) Gliding motility and polarized slime secretion. *Mol Microbiol* **63**: 454-467.

Zeytuni, N., and Zarivach, R. (2012) Structural and functional discussion of the tetra-trico-peptide repeat, a protein interaction module. *Structure* **20**: 397-405.

Zhang, Y., Franco, M., Ducret, A., and Mignot, T. (2010) A bacterial Ras-like small GTP-binding protein and its cognate GAP establish a dynamic spatial polarity axis to control directed motility. *PLoS Biol* **8**: e1000430.

Zhou, T., and Nan, B. (2017) Exopolysaccharides promote Myxococcus xanthus social motility by inhibiting cellular reversals. *Mol Microbiol* **103**: 729-743.

Zusman, D.R., Scott, A.E., Yang, Z., and Kirby, J.R. (2007) Chemosensory pathways, motility and development in Myxococcus xanthus. *Nat Rev Microbiol* **5**: 862-872.

7 Supplementary Information

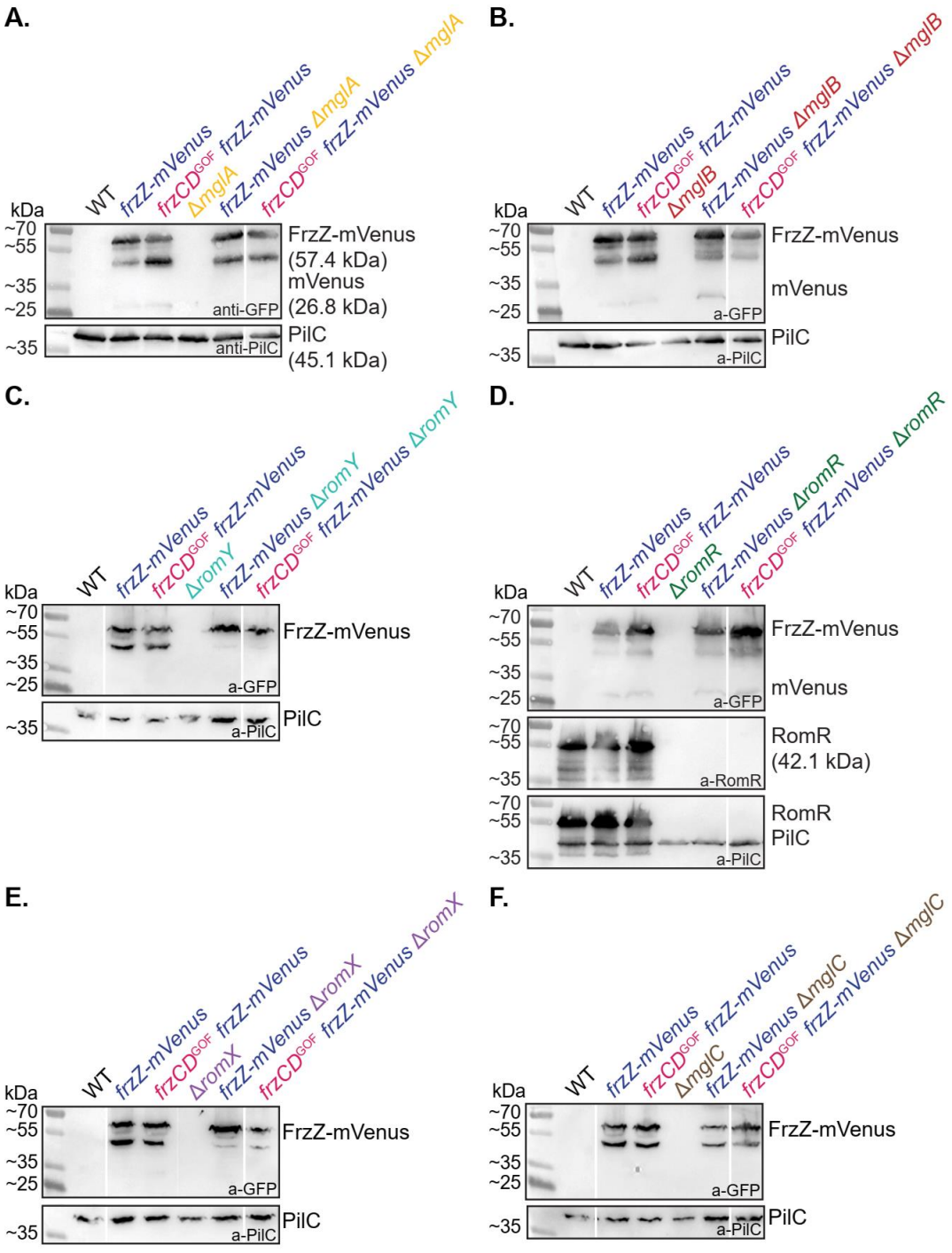

Supplementary Figure 1: **Accumulation of FrzZ-mVenus (A-B)** in WT, Δ*frzE*, and *frzCD*^{GOF} strains and **(C-H)** in WT and *frzCD*^{GOF} strains also containing one of the Δ*mglA*, Δ*mglB*, Δ*romR*, Δ*romX*, Δ*romY* and Δ*mglC* mutations. Immunoblot analysis of cell lysates of exponentially grown cells expressing *frzZ-mVenus* from the native site using anti-GFP and anti-PilC antibodies as a loading control. WT was used as a control. Cell lysate from the same number of cells was loaded per lane.

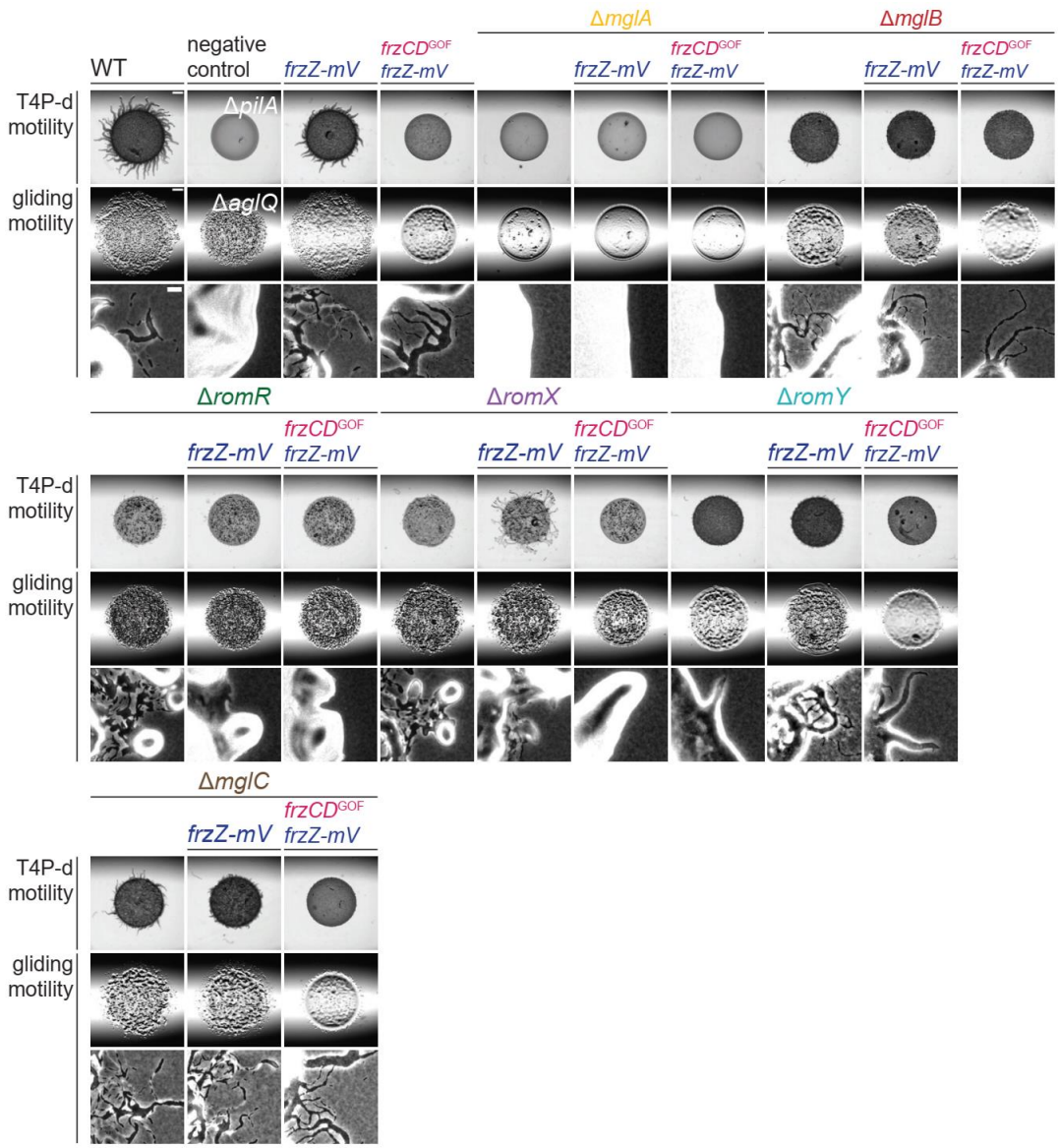

Supplementary Figure 2: **Motility phenotypes of strains expressing *frzZ-mVenus*.** Motility assay of indicated strains containing *frzZ-mVenus*. T4P-dependent motility was tested on 0.5 % agar. Gliding motility was tested on 1.5 % agar. Scale bars from top to bottom: 1 mm, 0.5 mm, 1 mm, and 50 µm.

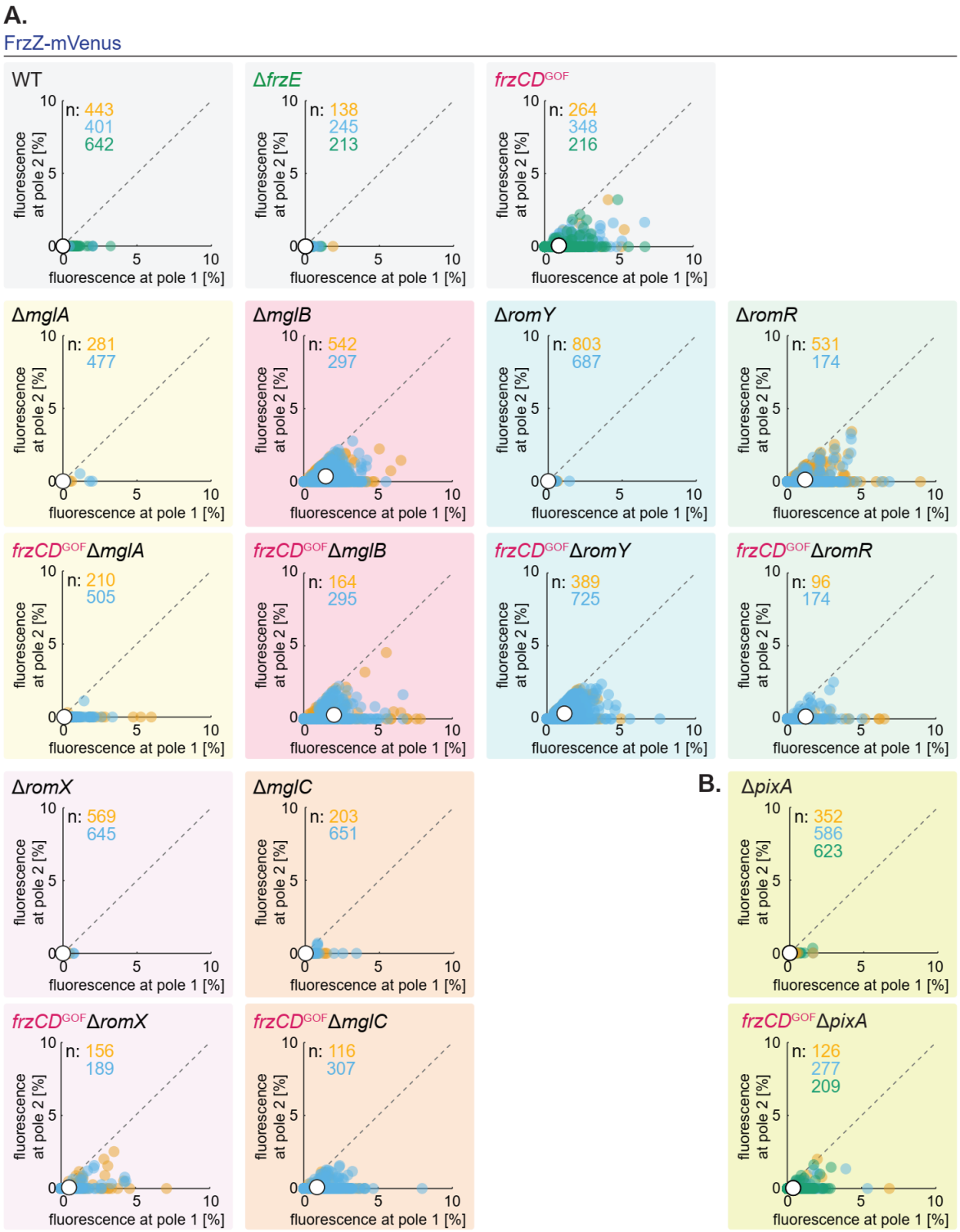

Supplementary Figure 3: **Scatterplots depicting the fluorescent polar signals of FrzZ-mVenus strains.** In the scatter plot, the percentage of total fluorescence at pole 2 is plotted against the percentage of total fluorescence at pole 1. Pole 1 is per definition the pole with the highest fluorescence. Individual cells are color-coded according to replicate. Grey dashed lines are symmetry lines, white spots with black outline show the mean and numbers in the upper left corner number of cells analyzed (n) of each replicate. Replicates are shown in orange, blue and green.

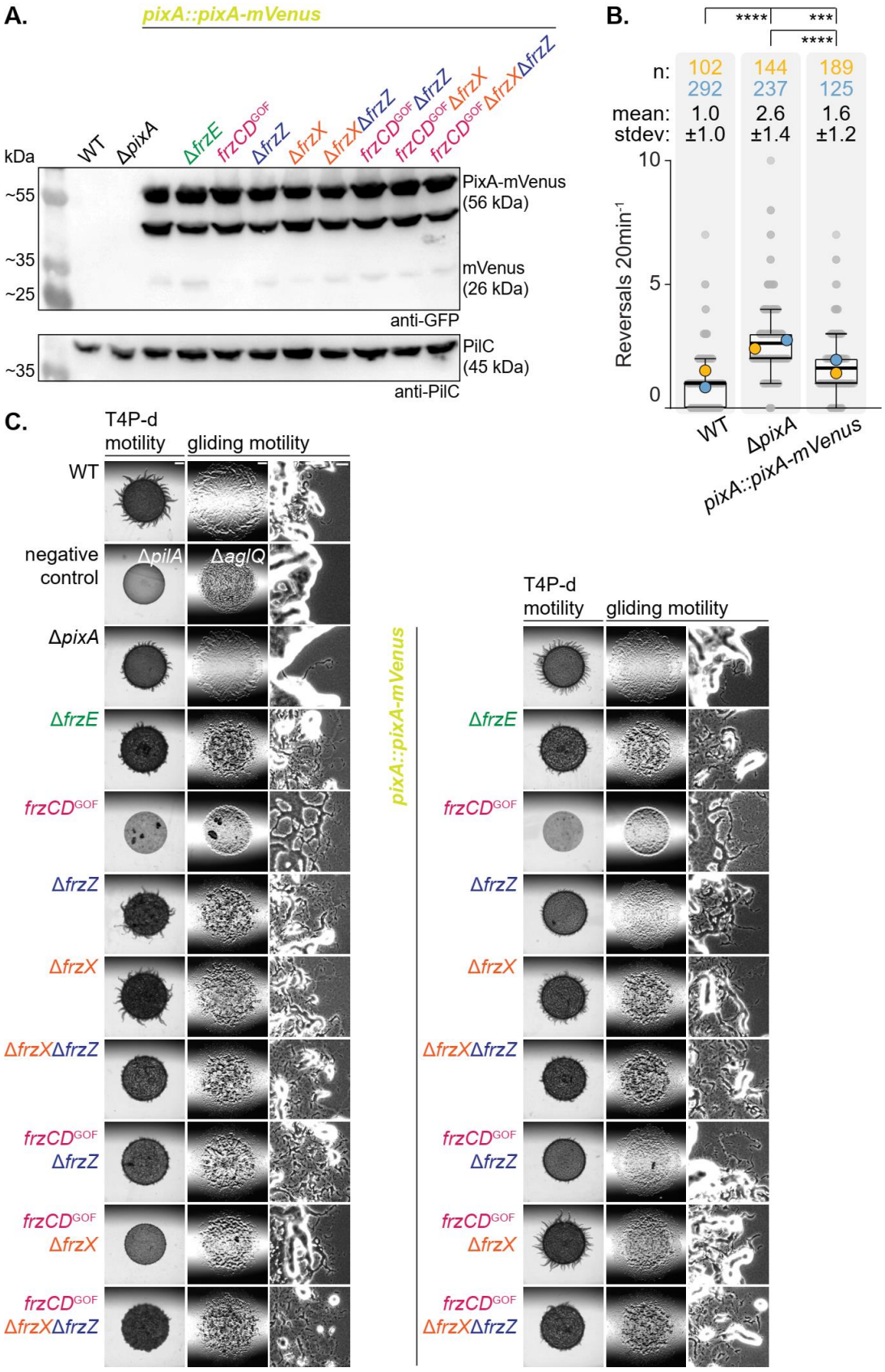

Supplementary Figure 4: **Accumulation and functionality of PixA-mVenus. (A)** Accumulation of PixA-mVenus in *frz* mutants (Δ*frzE*, *frzCD*^{GOF}, Δ*frzZ*, Δ*frzX*, Δ*frzZ*Δ*frzX*, *frzCD*^{GOF}Δ*frzZ*, *frzCD*^{GOF}Δ*frzX*, *frzCD*^{GOF}Δ*frzX*Δ*frzZ*). Immunoblot analysis of cell lysates of exponentially grown cells expressing *pixA-mVenus* from the native were performed using anti-GFP and anti-PilC antibodies as a loading control. WT was used as a control. Cell lysate from the same number of cells was loaded per lane. One

representative clone for each strain is shown. It was tested for the presence of PixA-mVenus (56 kDa), and PilC (45 kDa). **(B)** Single-cell gliding reversal assay on 0.5 % CTT 1.5% agarose of Δ*pixA frz* mutant strains. Scatterplots show the measured reversal frequency monitored as the number of directional changes per 20 min. Each dot in the scatterplot represents the reversal frequency of one cell. Boxes enclose the 25th and 75th percentile. Whiskers enclose the 5th and 95th percentile. The median is shown as a thin line in the box. The overall mean is shown as thick black line. The mean of each replicate is shown as a symbol in orange, blue, and green. The number of trajectories analyzed per replicate (n) and mean reversal frequencies for each strain are shown above the graph. Reversal frequencies of one representative clone for each strain are shown. Kruskal-Wallis test was used for statistical analysis using GraphPad Prism 9.0.2. "***" indicates p≤0.001, "****" indicates p<0.0001. Analysis of strains are the same as in Figure 22. **(C)** Motility assay of strains expressing *pixA-mVenus* from the native sites in *frz* mutants. T4P-dependent motility was tested on 0.5 % agar. Gliding motility was tested on 1.5 % agar. Scale bars from left to right: 1 mm, 1 mm, and 50 µm. One representative clone of each strain is shown.

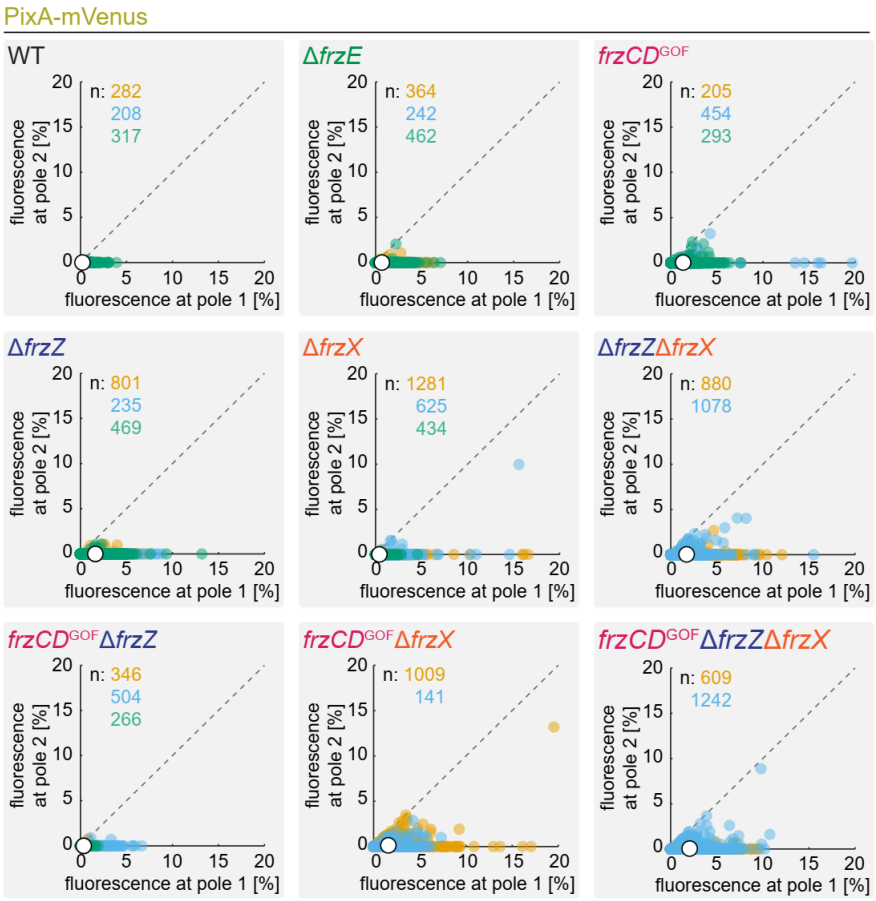

Supplementary Figure 5: **Scatterplots depicting the fluorescent polar signals of PixA-mVenus.** In the scatter plot, the percentage of total fluorescence at pole 2 is plotted against the percentage of total fluorescence at pole 1. Pole 1 is per definition the pole with the highest fluorescence. Individual cells are color-coded according to replicate. Grey dashed lines are symmetry lines, white spots with black outline show the mean and numbers in the upper left corner number of cells analyzed (n) of each replicate. Replicates are shown in orange, blue and green.

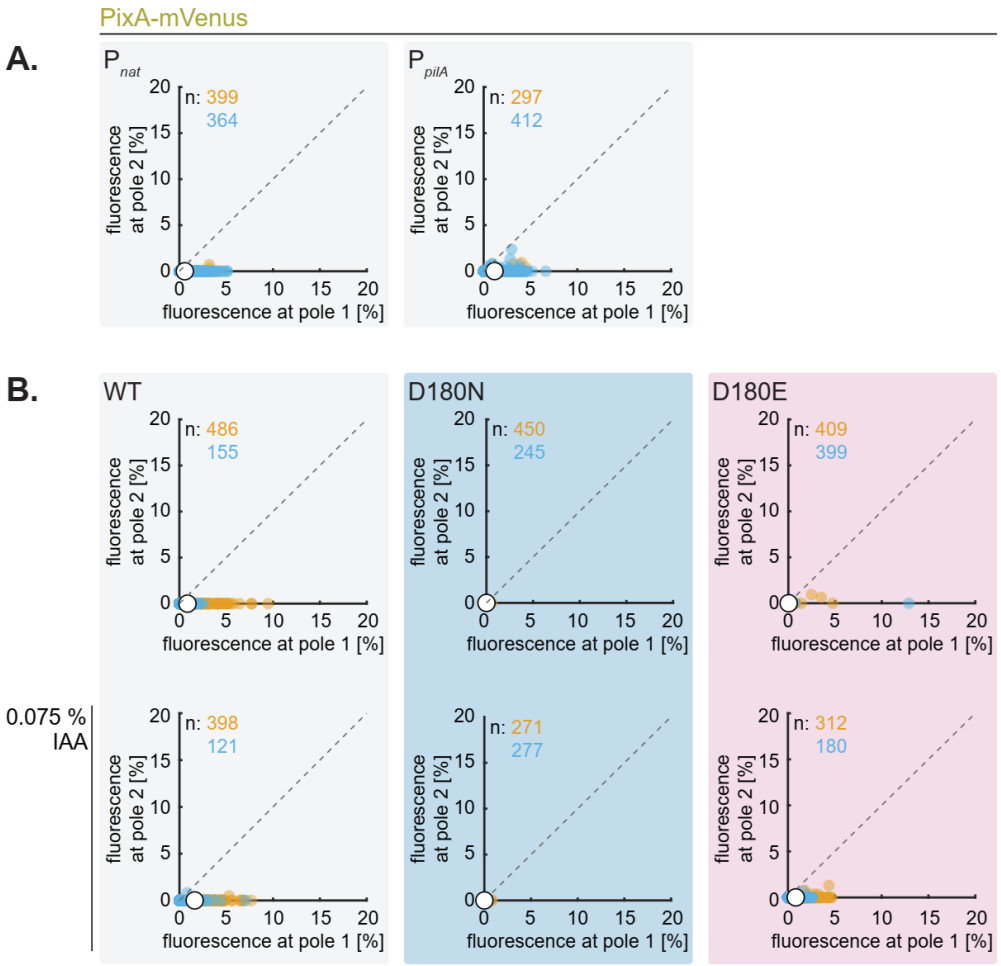

Supplementary Figure 6: **Scatterplots depicting the fluorescent polar signals of PixA-mvenus. (A)** Scatterplots of complementation strains. **(B)** Scatterplots of D180 mutant analyses. In the scatter plot, the percentage of total fluorescence at pole 2 is plotted against the percentage of total fluorescence at pole 1. Pole 1 is per definition the pole with the highest fluorescence. Individual cells are color-coded according to replicate. Grey dashed lines are symmetry lines, white spots with black outline show the mean and numbers in the upper left corner number of cells analyzed (n) of each replicate. Replicates are shown in orange, blue and green.

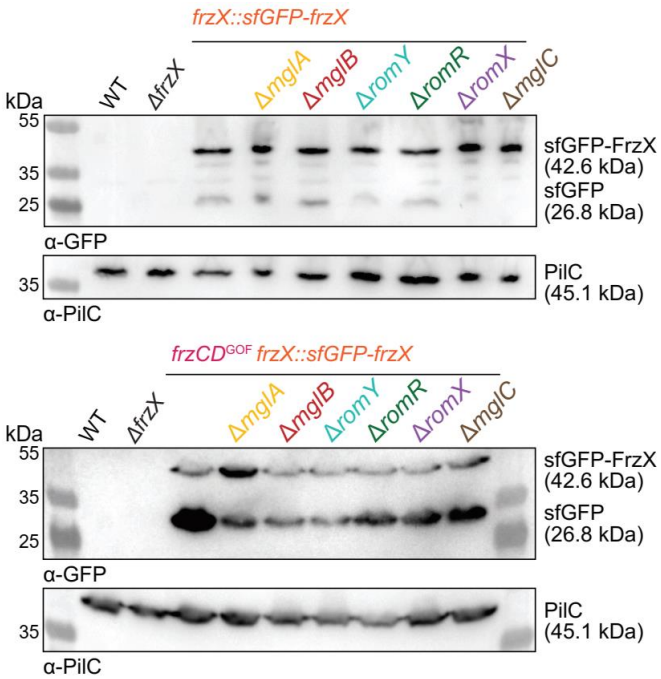

Supplementary Figure 7: **Accumulation of sfGFP-FrzX** in WT and *frzCD*^{GOF} strains also containing one of the Δ*mglA*, Δ*mglB*, Δ*romR*, Δ*romX*, Δ*romY* and Δ*mglC* mutations. Immunoblot analysis of cell lysates of exponentially grown cells expressing *sfGFP-frzX* from the native were performed using anti-GFP and anti-PilC antibodies as a loading control. WT was used as a control. Cell lysate from the same number of cells was loaded per lane. One representative clone for each strain is shown. It was tested for the presence of sfGFP-FrzX (42.6 kDa), and PilC (45.1 kDa).

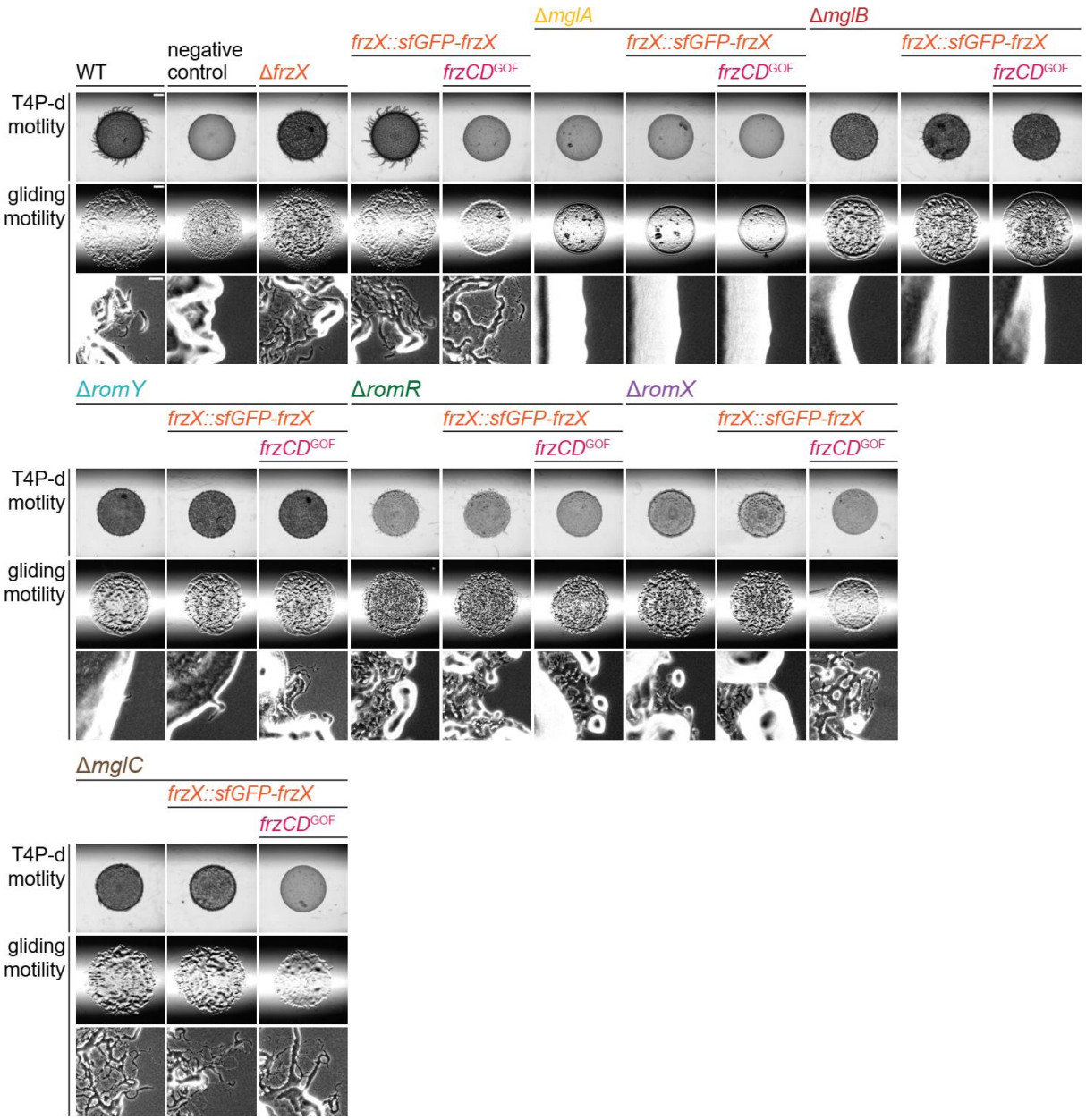

Supplementary Figure 8: **Motility phenotypes of strains expressing *sfGFP-FrzX***. Motility assay of indicated strains containing *sfGFP-frzX*. T4P-dependent motility was tested on 0.5 % agar. Gliding motility was tested on 1.5 % agar. Scale bars from top to bottom: 1 mm, 1 mm, 1 mm, and 50 µm. One representative clone of each strain is shown.

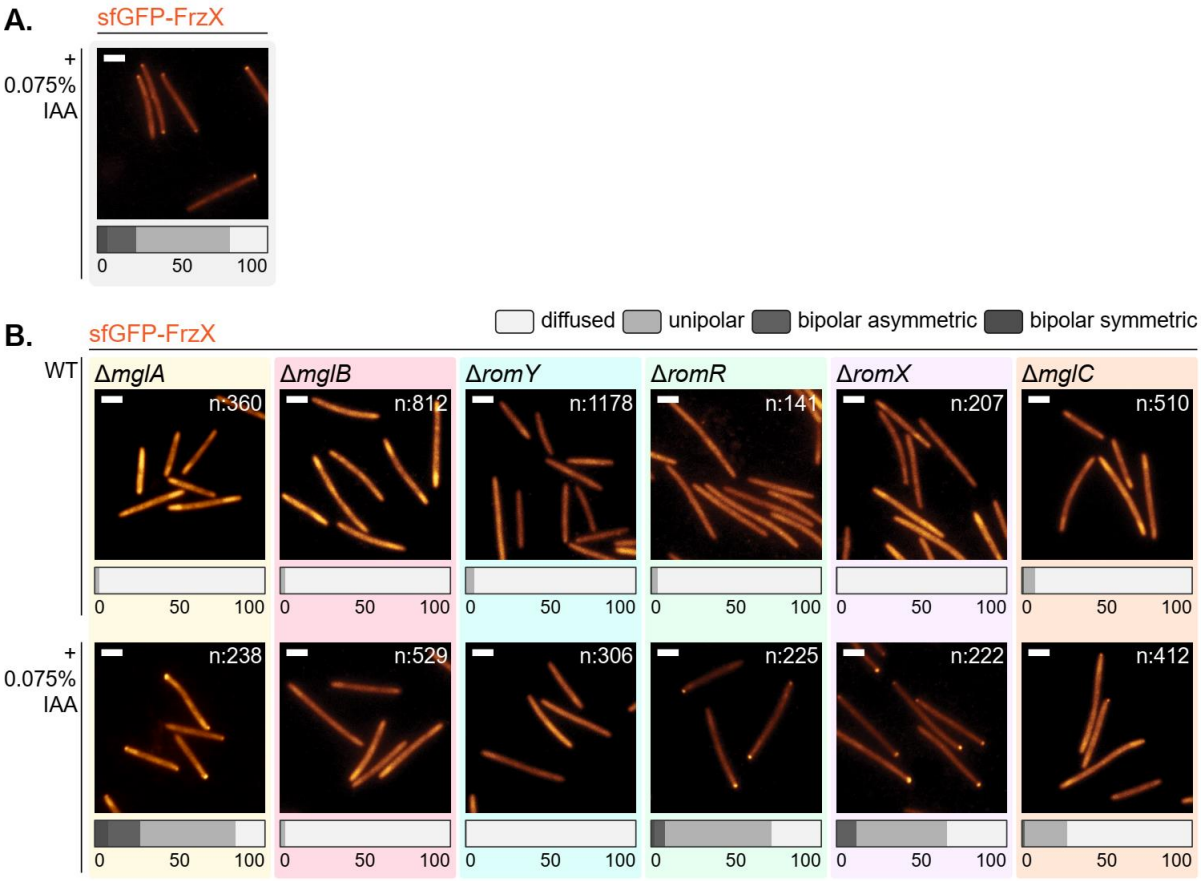

Supplementary Figure 9: **Localization of sfGFP-FrzX. (A)** Fluorescence microscopic analysis of *sfGFP-frzX* mutants in the presence of 0.075 % IAA. **(B)** Fluorescence microscopic analysis of sfGFP-frzX in ppolarity mutants. Cells were analyzed for the presence of polar localization. Pictures show representative cells of each strain in exponential growth phase. Cells were imaged on chitosan-coated slides in MC7 buffer for 1.5 h. Number of cells analyzed (n) is shown in the right top corner of microscopy images for each strain. The polar regions are defined as the parts of a cell within a distance of 0.65 µm, from a tip of a cell. A pole was considered to have a polar cluster if a contiguous set of at least three pixels above the threshold intensity was found in the polar region. Horizontal bars show the percentage of cells with a polar localization pattern and diffuse localization according to the color code. Scale bar, 2 µm.

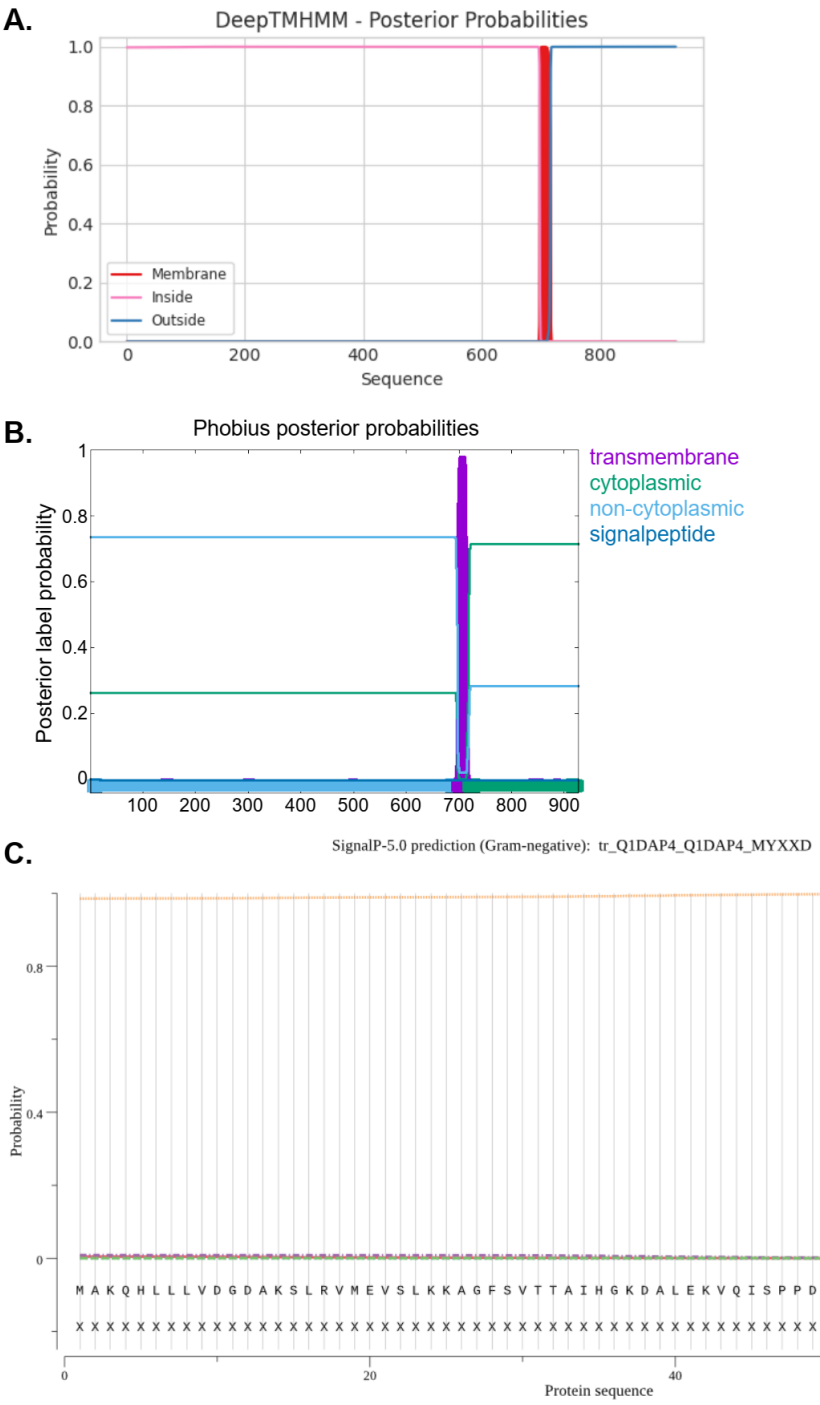

Supplementary Figure 10: **Prediction of subcellular localization of PglH. (A)** Prediction based on DeepTMHMM. Red shows probability for a transmembrane domain while pink and blue lines indicate the probability for cytoplasmic or periplasmic localization. **(B)** Prediction based on Phobius. Violet shows probability of a transmembrane domain. Green and lightblue indicate probability for cytoplasmic or non-cytoplasmic localization. Blue indicates probability for a signal peptide. **(C)** Signal peptide prediction by SignalP 5.0. Red Line shows probability for a Sec signal peptide, violet for TAT signal peptide, blue for a lipo signal peptide, and orange for no detected signal peptide. Green marks predicted cleavage sites.

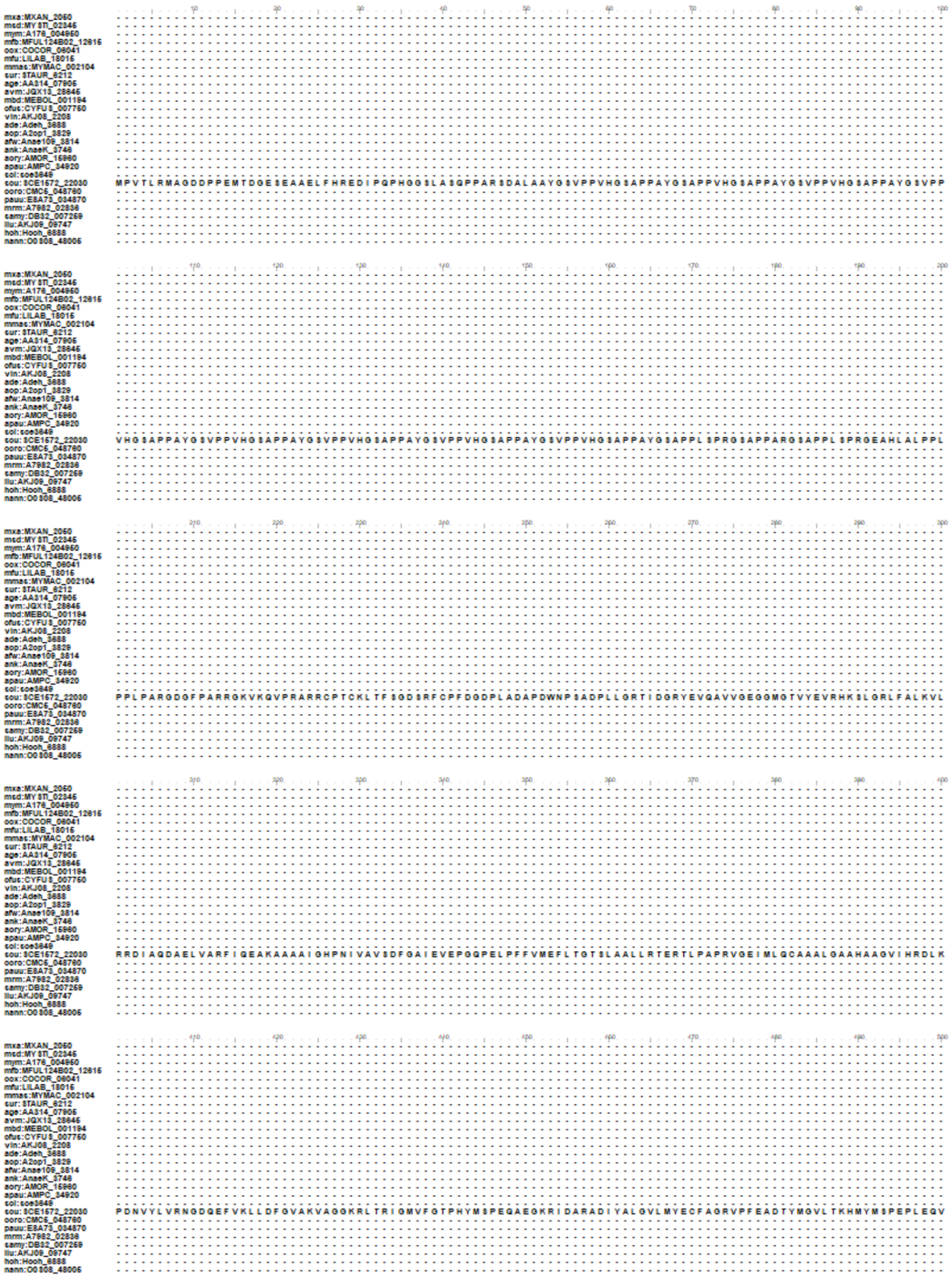
mxa:MXAN_2060
msd:MYSTI_02345
mym:A176_004960
mfb:MFUL124B02_12815
oox:COCOR_06041
mfu:LILAB_18015
mmas:MYMAC_002104
sur:STAUR_6212
age:AA314_07905
avm:JQX13_28645
mbd:MEBOL_001194
ofu:CYFUS_007750
vin:AKJ08_2208
ade:Adeh_3888
aop:A2cp1_3829
afw:Anae109_3814
ank:AnaeK_3748
aory:AMOR_16980
apau:AMPC_34920
sol:soe3849
sou:SCE1572_22030
ooro:CMC5_048780
psuu:E8A73_034870
mrm:A7982_02838
samy:DB32_007269
llu:AKJ09_09747
hoh:Hooh_6888
nann:O0S08_48005

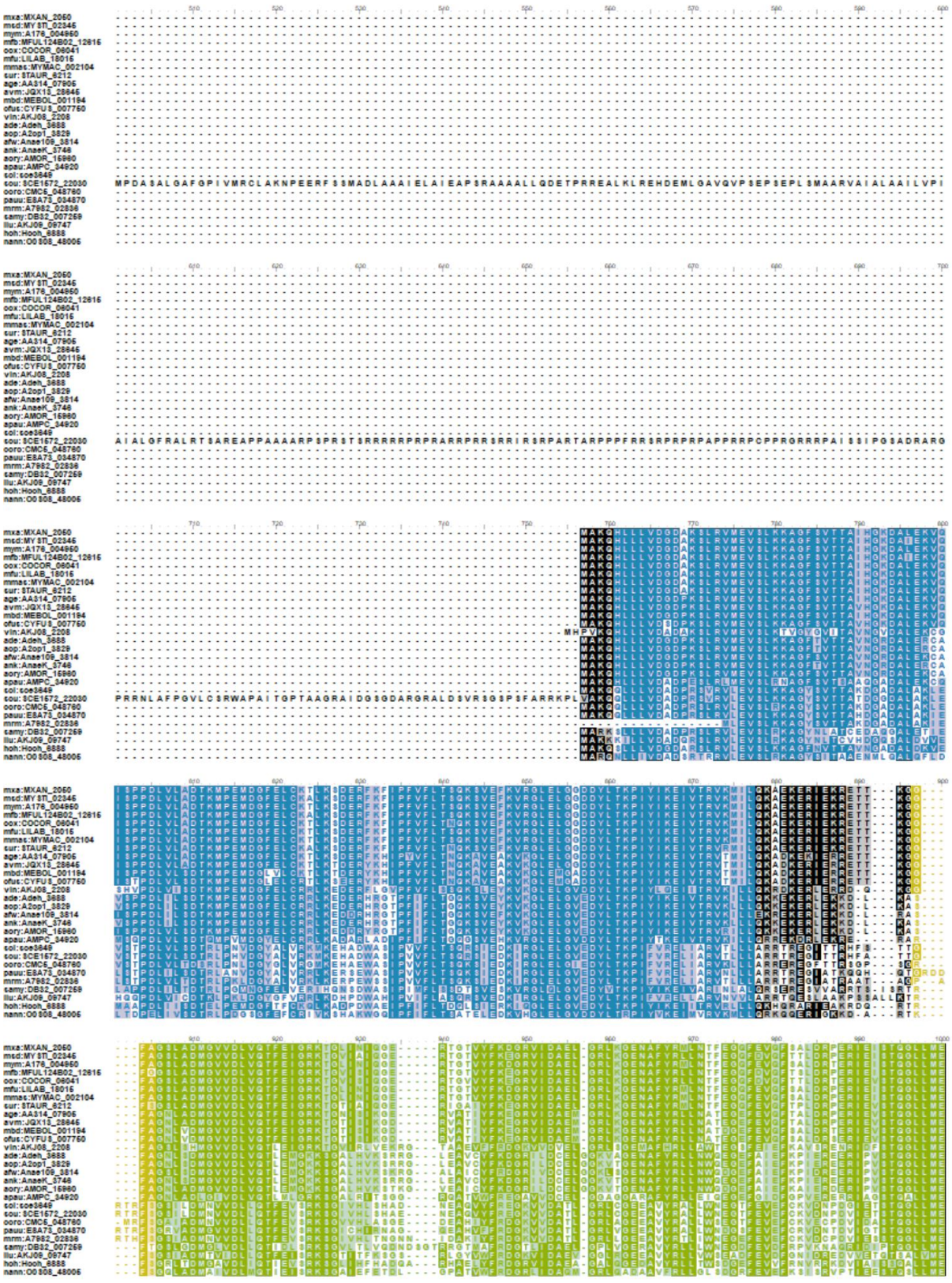

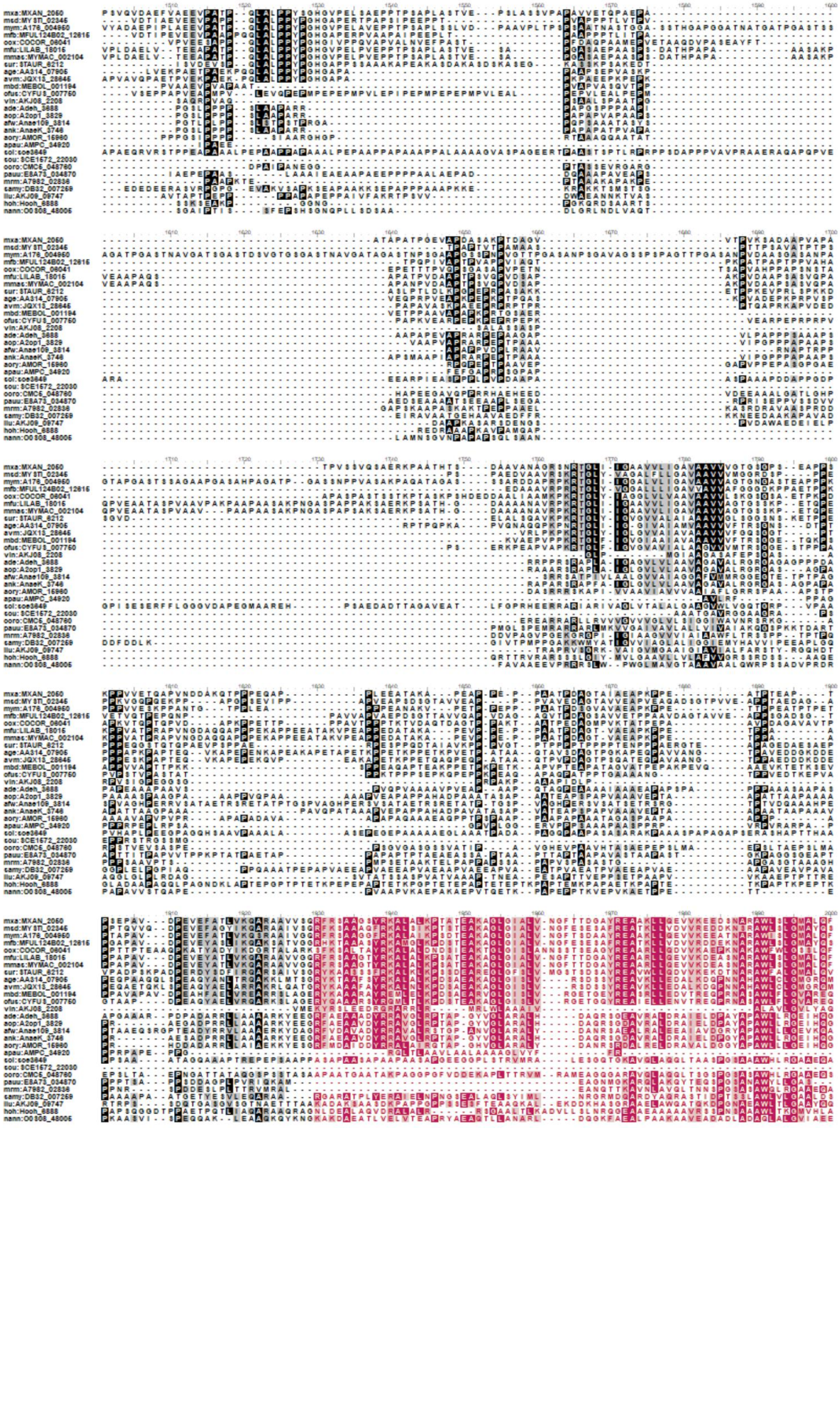

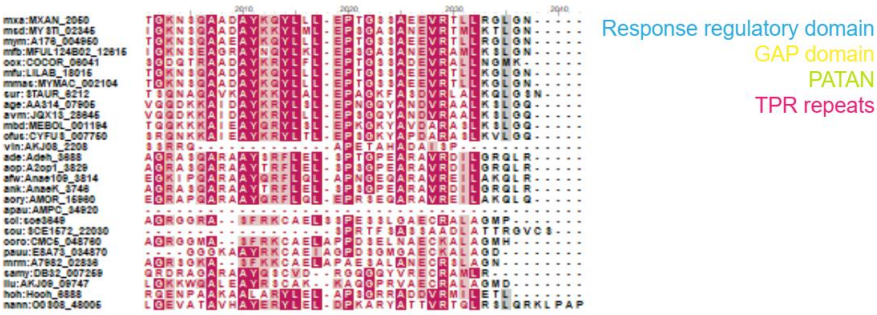

Supplementary Figure 11: **Alignment of PglH homologs found in Myxococcota.** The numbers on top indicate aa residues. Black and grey backgrounds indicate identical and similar aa residues, respectively. Colors show the conserved domains. Blue indicates the RR domain, yellow the GAP protein domain, green the PATAN domain, and pink the TPR repeats.

Supplementary Table 1: **Pulled down biotinylated proteins in the proximity of PixA [5].**

	WT		***ΔfrzE***		***frzCD*^{GOF}**	
Protein	Log2ratio	-LOG(p-value)	Log2ratio	-LOG(p-value)	Log2ratio	-LOG(p-value)
PixA	5.85	3.89	5.49	2.29	7.31	4.20
PglH	6.07	2.77	8.69	3.08	7.13	7.27
MXAN_5199	7.20	4.09	6.91	4.29	6.88	6.60
PilS2	4.86	3.91	5.60	5.23	5.21	4.22
FrzZ	3.91	4.12	4.38	2.11	4.08	4.21
MXAN_5812	3.37	1.80	3.64	3.13	4.47	3.48
MXAN_6866	4.86	3.29	4.87	2.89	5.44	3.73
RomY	2.63	2.43	3.67	2.41	3.80	3.46
MXAN_4841	-1.00	1.76	5.33	2.55	-0.68	1.72
MXAN_1234	-0.87	2.12	3.94	2.43	-0.65	2.55
MXAN_2386	1.08	0.44	3.45	2.38	1.85	2.88
topA	5.27	2.48	0.29	0.05	3.71	2.59
MXAN_4279	-3.14	1.81	-1.49	2.11	4.25	3.05
MXAN_4280	-1.70	1.10	-0.61	0.99	4.64	3.65
MXAN_4535	-2.41	1.35	-2.01	0.93	4.43	2.47
MXAN_4514	-2.19	1.37	-0.08	0.08	6.43	4.88
MXAN_4513	-3.35	1.72	-1.04	1.67	7.43	4.36
devR	-1.22	1.44	-0.81	1.17	5.78	2.73
devS	-1.94	1.44	-1.19	1.93	4.76	3.06
cas3	-1.92	0.86	0.36	0.11	5.02	3.81
MXAN_0010	2.97	3.67	2.50	0.89	3.14	3.36
pheS	3.31	3.45	2.91	3.17	3.33	3.56
pheT	2.32	3.05	3.77	2.62	3.04	1.44
def	2.98	1.59	3.74	3.33	0.94	2.34
MXAN_4601	0.33	0.28	3.52	2.82	-0.48	0.28
MXAN_4402	0.12	0.04	3.26	2.55	4.14	1.64

[5] **[5].** Black text indicates proteins enriched above the set threshold. Grey text indicates proteins enriched below the threshold.

MXAN_5404	0.92	0.26	3.21	2.89	-0.40	0.33
MXAN_7089	4.22	3.65	3.19	1.96	0.22	0.15
MXAN_0572	4.22	4.13	3.02	2.13	0.44	0.37
MXAN_5086	2.57	4.72	3.24	1.93	3.46	2.68
MXAN_6732	2.05	2.31	4.22	2.99	0.89	2.34
MXAN_3183	-0.44	0.49	3.38	2.86	-0.27	0.64
MXAN_7298	3.11	2.15	2.23	1.48	3.25	3.66
MXAN_4511	-3.43	2.72	-2.38	0.93	5.02	3.23
MXAN_2060	4.58	3.73	4.88	3.21	0.67	0.13
MXAN_1907	-1.21	0.76	1.97	0.94	4.89	2.92
MXAN_2229	-2.85	1.02	0.09	0.07	8.25	4.21
MXAN_6707	1.81	1.23	3.46	2.64	0.55	0.87
ubiE	1.50	0.39	4.31	3.58	0.72	0.71
MXAN_2659	4.70	3.96	3.74	2.66	2.93	1.50
MXAN_3129	6.67	2.25	3.07	1.30	0.96	0.43
MXAN_7040	6.01	3.24	2.79	1.52	4.05	1.10
MXAN_0543	5.22	3.68	2.88	1.78	2.66	1.22
MXAN_6196	5.10	3.61	1.28	1.66	1.36	0.52
MXAN_4727	4.94	3.67	2.85	1.38	2.32	0.80
MXAN_5025	4.83	3.66	2.51	1.50	1.70	0.74
sodC	4.66	2.94	2.69	0.98	1.33	0.52
MXAN_4947	4.55	2.97	1.95	0.78	1.88	0.72
MXAN_0962	4.42	3.15	1.65	1.02	-1.30	0.57
MXAN_6884	4.41	2.84	2.53	1.78	0.61	0.25
cglB	4.38	2.92	2.75	1.78	0.05	0.03
MXAN_6601	4.23	2.84	2.40	1.13	-0.06	0.01
MXAN_5136	4.23	2.34	2.08	0.94	0.61	0.38
MXAN_0659	4.23	3.40	2.24	1.83	0.24	0.13
atpH	4.16	3.19	0.16	0.05	2.09	1.15
MXAN_6849	4.12	3.61	2.13	1.09	1.01	0.30
hemB	4.07	2.48	2.05	0.82	0.63	0.39
MXAN_6483	4.06	3.69	2.16	2.98	0.09	0.06
MXAN_5297	3.99	4.75	1.14	0.95	0.71	0.46
MXAN_4860	3.96	2.33	2.04	0.94	1.26	0.48
agmO	3.92	3.29	2.36	1.45	1.07	0.38
MXAN_5743	3.89	3.08	1.62	0.67	2.08	0.94
MXAN_2382	3.87	3.16	1.39	0.41	1.34	1.18
MXAN_7112	3.84	2.61	1.50	0.72	0.65	0.57
MXAN_6184	3.74	4.52	-0.13	0.04	1.18	0.59
MXAN_5164	3.68	2.32	2.13	1.37	0.39	0.09
MXAN_4966	3.60	3.98	1.37	1.33	0.59	0.50
MXAN_6878	3.58	3.08	2.23	0.91	2.42	1.23
MXAN_7039	3.51	3.74	0.81	0.61	0.46	0.83
MXAN_5558	3.51	2.51	-0.19	0.11	-0.19	0.05
MXAN_1450	3.46	2.95	1.16	0.75	1.63	2.11
MXAN_4866	3.37	2.41	1.35	0.45	0.35	0.08

MXAN_5315	3.33	3.68	0.84	0.28	0.44	0.13
MXAN_6665	3.17	3.49	-0.20	0.22	-0.03	0.03
MXAN_0290	3.16	2.72	0.75	0.29	0.54	0.31
MXAN_2837	3.14	3.92	0.24	0.05	1.62	1.16
MXAN_4431	3.13	2.86	1.93	0.81	2.69	2.75
MXAN_0199	3.13	2.83	1.52	0.51	1.01	0.64
trxB	3.12	2.56	1.99	1.53	1.80	1.15
sdhB	3.10	3.33	-0.49	0.44	1.37	1.44
MXAN_5981	3.10	2.70	-0.60	0.51	1.65	1.17
MXAN_4706	3.09	2.32	-1.06	0.64	1.15	0.53
MXAN_6518	3.08	2.60	1.58	0.93	0.82	0.34

Supplementary Table 2: **Pulled down biotinylated proteins in the proximity of MglA.**

Protein	**log2ratio**	**-log(p-value)**	**potential Function**
MglA	1.98	3.56	bait
MglB	2.95	3.87	polarity module
RomR	5.02	3.04	
AglZ	2.51	2.62	gliding motility
GltJ	4.17	6.32	
FrzS	3.60	5.23	T4P-d motility
SgmX	4.15	4.68	
Mxan_6705	2.00	2.44	
Mxan_1995	2.09	3.89	
Mxan_3083	2.07	1.55	
MXAN_1142	7.21	6.18	Plectin
ValS	6.00	6.53	tRNA-ligase
MXAN_4627	8.23	2.92	MshEN
FrgA	2.03	2.41	
MXAN_4666	4.59	4.52	
MXAN_4436	3.05	3.33	
SgnC	3.86	3.95	RR-PATAN
PglH	2.24	3.62	
MXAN_5052	2.25	1.61	
NmpS	2.19	1.57	signaling
MXAN_6865	2.42	2.77	
MXAN_3202	2.56	1.69	
MXAN_3203	2.78	3.54	FHA
MXAN_1423	2.58	2.26	TPR
MXAN_1948	2.78	3.78	
MXAN_1942	2.05	4.46	
MXAN_1145	3.05	2.32	DnaJ-TPR
MXAN_2049	3.47	1.69	
MXAN_5804	2.57	3.25	Dnak
MXAN_5765	2.50	3.37	secretion pathway A protein
iorA	2.42	3.05	iron sulfur domain

MXAN_0791	2.93	3.81	Peptidase, M16 (Pitrilysin) family
MXAN_1527	2.37	1.33	NAD dependent epimerase/dehydratase family protein
MXAN_1560	2.02	1.30	Aminotransferase, class I
MXAN_2642	2.36	1.57	dTTP/UTP pyrophosphatase
MXAN_2754	2.05	2.34	Peptidase, M4 (Thermolysin) family
MXAN_3550	2.11	1.91	SmC protein
MXAN_3645	2.18	1.46	2,3-dihydroxybenzoate-AMP ligase
MXAN_4001	3.06	3.28	Non-ribosomal peptide synthase/polyketide synthase
MXAN_4186	2.42	5.65	Metallo-dependent phosphatase-like
MXAN_5137	2.80	1.78	Aminopeptidase N
MXAN_5667	2.17	2.34	Hydrolase
MXAN_5740	3.33	3.36	Glycosyl transferase, group 2
MXAN_6541	2.14	1.86	NAD+ kinase
MXAN_6732	2.67	3.37	Class II aldolase/adducin domain protein

Supplementary Table 3: **Genomic neighborhood of *frz* homologs in *V. incomptus* with homologous proteins found in *M. xanthus*[6].**

V. incomptus	AKJ08_2784	AKJ08_2785	AKJ08_2786	AKJ08_2787	AKJ08_2788	AKJ08_2789	AKJ08_2790-AKJ08_2797	AKJ08_2798	AKJ08_2799	AKJ08_2800	AKJ08_2801
M. xanthus		MXAN_7040 (*fadL*)	MXAN_3707		MXAN_7288 (*ddvA*)	MXAN_5507	***frzZ - frzX***		MXAN_6745	MXAN_6948	MXAN_4214

Supplementary Table 4: Genomic neighborhood of *frz* homologs in Anaeromyxobacter species with homologous proteins found in *M. xanthus*. Grey boxes indicate that no homolog was found. The orange column encapsulates the eight proteins encoded in the *frz* cluster.

A. dehalogenans 2CP-C	Adeh_0605	Adeh_0606	Adeh_0607	Adeh_0608	Adeh_0609 - Adeh_0616		Adeh_0617	Adeh_0618
M.xanthus	MXAN_7002	Mxan_6956 (*dotR*)	MXAN_1131	MXAN_1106 *(sgmC)*	***frzZ-frzX***		MXAN_5710	MXAN_6386
A. dehalogenans 2CP-1	A2cp1_0630	A2cp1_0631	A2cp1_0632	A2cp1_0633	A2cp1_0634 - A2cp1_0641		A2cp1_0651	A2cp1_0652
M.xanthus	MXAN_5849	Mxan_6956 (*dotR*)	MXAN_1131	MXAN_2746	***frzZ-frzX***		MXAN_5710	MXAN_6386
Anaeromyxobacter sp. K	AnaeK_0639	AnaeK_0640	AnaeK_0641	AnaeK_0642	AnaeK_0643 - AnaeK_0650		AnaeK_0651	AnaeK_0652
M. xanthus	MXAN_7002	Mxan_6956 (*dotR*)	MXAN_1429	MXAN_2746	***frzZ-frzX***		MXAN_5710	MXAN_6386
Anaeromyxobacter sp. Fw109-5	Anae109_0649	Anae109_0650	Anae109_0651	Anae109_0652	Anae109_0653 - Anae109_0660	Anae109_0661	Anae109_0662	Anae109_0663
M. xanthus	MXAN_7002	Mxan_6956 (*dotR*)	MXAN_0907	MXAN_6472	***frzZ-frzX***	MXAN_4974	MXAN_5710	MXAN_6386

[6] Grey boxes indicate that no homolog was found in *M. xanthus*. The orange column encapsulates the eight proteins encoded in the *frz* cluster.

Danksagung/Acknowledgments

Thank you to Prof. Dr. Lotte Søgaard-Andersen, who allowed me to work on my project in her group. I grew a lot in the past years. Thank you to my Thesis Advisory Committee members, Prof. Dr. Martin Thanbichler, Dr. Andreas Diepold and Prof. Dr. Simon Ringgaard, for reading my TAC report(s) and the helpful discussions during our meetings. I would also like to thank Prof. Dr. Martin Thanbichler (again), Prof. Dr. Victor Sourjik and Prof. Dr. Hans-Ulrich Mösch for being members of my thesis committee. I would also like to thank Dr. Dominik Schumacher, Dr. Luis Carreira and Dr. Michael Seidel for proofreading this thesis.

Danke an Memduha, Jana und Michel. Wir haben diese akademische Reise zusammen begonnen und bis zu diesem Punkt auch zusammen bestritten und uns dabei ungemein weiterentwickelt (*slay*, ich bin so stolz auf euch!). Und darum (und unsere gemeinsame Zeit im Computerraum) bin ich auch sehr froh. Ohne unsere gegenseitige Motivation, wäre ich oft an dem Punkt gewesen einfach alles hinzuschmeißen. Ich hoffe wir sehen uns irgendwann in Roßlau, auf der documenta oder in irgendeiner Kneipe in Marburg wieder.

Danke Michael, für die Motivation und Hilfe während unserer Zeit in der Spätschicht in Labor 3 während Covid und dann später in einer Bay in Labor 1. Aber du weißt selbst, dass mein Dank viel weiter darüber hinaus gilt, da wir unsere Seelenverwandschaft über Drag Race, die Superbowl Halftime Show und cupcakKe entdeckt haben. Love u (platonically).

Dominik, auch du hast mich seit meinem ersten Tag als kleine Bachelor-Studentin begleitet. Du hast mich in meiner wissenschaftlichen Entwicklung stark geprägt und ich habe viel von dir gelernt. Dabei habe ich dich auch als Menschen sehr zu schätzen gelernt. Danke für alles.

Philipp, lass dich nicht von den Orcas angreifen oder den Kampfdelfinen ausspionieren! Thank you, Luis, expert of the polarity module. You're a brilliant scientist and a great person. Thanks for the helpful discussions about my project. Ozan, you will manage those last few months with a lot of cat support by Leia. Johannes, bleib so diszipliniert, aber verletze dich bitte nicht mehr so oft beim Fußball. Maria, thank you for all your scientific support and for introducing me to Zumba with Christine and the other girls. Marco, danke für die vielen Stunden in denen du mir bei Skripten und Bioinformatik geholfen hast und dafür dass wir das mit dem Proximity Labeling durchgezogen haben. Andrea, Steffi und Yvonne, ohne euch würde diese Gruppe untergehen. Danke Andrea, für die vielen wissenschaftlichen Tipps seit meiner Bachelorarbeit und dafür, dass du nicht ausgerastet bist als Memduha und ich geschmolzenen Agar im Autoklav verteilt haben. Danke Steffi, für die Hilfe, die Gespräche und Gänge zum Mensa Mobil. Ein Teil der faulen Bande dankt nun ab. Danke Yvonne, für deine Arbeit und die witzigen Pausen. Durch dich weiß ich was der OHG ist. I would also like to thank the rest of AG LSA

(present and past), for nice scientific and non-scientific discussions and the help with everyday issues.

Danke an Timo für unsere Kollaboration und die gemeinsame Arbeit. Ohne Proximity Labeling wäre mein Projekt im Nichts verlaufen.

Thank you for your work as the IMPRS coordinator and for you as a person, Dusica. Also, a huge shoutout to my IMPRS peers. I think we really only got to know each other in the past months leading up to our belated retreat. This shared experience bonds us.

Mein größter Dank gilt meiner Familie und meinen Freunden. Danke für eure Liebe und eure Perspektiven, ohne die ich diese schwierige Zeit nicht überstanden hätte. Worte würden dem nicht gerecht werden.

Curriculum Vitae

Erklärung

Ich versichere, dass ich meine Dissertation mit dem Titel „Regulation of dynamic front-rear cell polarity by the Frz chemosensory system in *Myxococcus xanthus*“ selbstständig ohne unerlaubte Hilfe angefertigt und mich dabei keiner anderen als der von mir ausdrücklich bezeichneten Quellen und Hilfsmittel bedient habe.

Diese Dissertation wurde in der jetzigen oder einer ähnlichen Form noch bei keiner anderen Hochschule eingereicht und hat noch keinen sonstigen Prüfungszwecken gedient.

Marburg, den 26.10.2023

Franziska Müller

Einverständniserklärung

Ich erkläre mich damit einverstanden, dass die vorliegende Arbeit:

- in Bibliotheken allgemein zugänglich gemacht wird. Dazu gehört, dass sie von der Bibliothek der Einrichtung, in der ich meine Arbeit angefertigt habe, zur Benutzung in ihren Räumen bereitgehalten wird;
- in konventionellen und maschinenlesbaren Katalogen, Verzeichnissen und Datenbanken verzeichnet wird;
- der UB für die lokale Nutzung und für Fernleihzwecke zur Verfügung steht;
- im Rahmen der urheberrechtlichen Bestimmungen für Kopierzwecke genutzt werden kann.

_____

Marburg, den

_____

Unterschrift des Autors